Wobbly winds in an ice age: the mutual interaction between the great continental ice sheets and atmospheric stationary waves

by

Gerard Hugh Roe

B.A., Oriel College, Oxford Univeristy
(1992)

Submitted to the Department of Earth, Atmospheric, and Planetary Sciences
in partial fulfillment of the requirements for the degree of

Doctor of Philosophy

at the

MASSACHUSETTS INSTITUTE OF TECHNOLOGY

June 1999

Signature of Author .....
Department of Earth, Atmospheric, and Planetary Sciences
26 February, 1999

Certified by .....
Richard S. Lindzen
Alfred P. Sloan Professor of Meteorology
Thesis Supervisor

Accepted by .....
Ronald G. Prinn
Chairman, Department of Earth, Atmospheric, and Planetary Sciences

Wobbly winds in an ice age: the mutual interaction between the great continental ice sheets and atmospheric stationary waves

by

Gerard Hugh Roe

B.A., Oriel College, Oxford Univeristy
(1992)

Submitted to the Department of Earth, Atmospheric, and Planetary Sciences
on 26 February, 1999, in partial fulfillment of the
requirements for the degree of
Doctor of Philosophy

Abstract

The ice sheets of the last glacial maximum (about 21 thousand years ago) covered a significant fraction of the high latitude land mass, reached up to $3km$ in height, and had length scales of thousands of kilometers. They represented significant obstacles to the westerly flow of the atmosphere. As the atmospheric flow is forced to deviate around such topographic features, stationary waves—large scale standing patterns in the winds and temperatures—are established within the atmosphere. The largest of the ice sheets, the Laurentide (over North America), was approximately equal in both horizontal extent and height to the Tibetan Plateau, which is known to be a significant contributor to the stationary wave pattern in today's climate. As the ice sheet evolves, the patterns of temperature and winds due to the stationary wave change, and therefore the distribution of precipitation and ablation (melting) is altered over the ice sheet. These altered distributions will, in turn, change the shape of the ice sheet itself, given sufficient time over which to act.

It is not possible to integrate full dynamical climate models for the long time scales appropriate to ice sheet dynamics ($> 10^3 yrs$). Previous studies have typically either used general circulation models (GCMs) for 'snapshot' climate simulations with prescribed ice age insolation and boundary conditions, or used long integrations of energy balance models (EBMs), which do not account for atmospheric dynamics. We aim for an intermediate approach—including some of the important dynamical features of the climate within a framework which is nonetheless simple enough to do long term calculations with. In the most reduced approach, an ice sheet is treated as a perfectly

plastic material, lying in the north-south direction. Simple representations of ablation and accumulation show that in equilibrium the southern margin of the ice sheet is tied quite strongly to a particular annually averaged isotherm. For a topographically forced stationary wave of reasonable amplitude, this implies that the potential effect of the stationary wave is to double the extent of the ice sheet over and above that which would exist without the stationary wave.

The effects explored above in the rather restrictive two-dimensional approach are further studied using a fully three-dimensional ice sheet model coupled to a β-plane channel stationary wave model, which is quasi-geostrophic, steady state, and linear. The two components of the model interact via the accumulation and ablation parameterizations which are, of necessity, very simplified representations. The ablation parameterization is the positive degree day model which has been used to model the modern ice sheets. The accumulation parameterization places particular emphasis on the topographic influence on precipitation. This more sophisticated approach shows that, in an idealized rectangular geometry, the height, shape, and orientation of the ice sheet are all dependent on the stationary wave that it creates. The fundamental competing balance is between the enhanced precipitation on the windward slopes, and the cold temperatures due to the atmospheric flow in the lee of the ice sheet, which allows the ice there to flow to lower latitudes than it otherwise could.

When the stationary wave model is applied to a reconstruction of the topography at the last glacial maximum, the results suggest that the stationary wave patterns due to Tibet and the Rockies may have played a role in preconditioning different regions for ice sheet initiation. Once established, the Laurentide ice sheet exerted a strong influence on the climate over the Fennoscandian ice sheet (over northern Europe) due to the downstream propagation of the stationary wave it created. Simulations with the ice sheet model over North America show that the atmospheric stationary wave creates a tendency for the ice sheet to have the shape of the Laurentude at the last glacial maximum. However, the simplicity of the model, together with the lack of knowledge about the glacial atmosphere, means it is not possible to conclude that the interaction was sufficient to create the observed configuration.

Thesis Supervisor: Richard S. Lindzen
Title: Alfred P. Sloan Professor of Meteorology

Acknowledgments

The process of getting a PhD is an odd one; the rules are largely unwritten, different in each case, and acquired along the way. It is not always an easy path, and therefore not possible without the help, support and understanding of many good souls. To any who I have overlooked here, my apologies and thank you.

Firstly, I am indebted to my advisor, Dick Lindzen. Without his guidance and insight, my research would never have got off the ground or survived through the lean periods. Dick gave generously of his time throughout, and taught me that nature should come first, and equations second. His perspective on science and his ability to launch into any topic with something interesting to say are qualities I will long keep with me.

I thank also the members of my committee, Maureen Raymo, Reginald Newell, and Edmund Chang, who were always available and patiently endured my naive ramblings. I am grateful for their advice, balance, and occasional pastoral care. I also gained much insight from conversations with Kerry Emanuel, Peter Stone, Myles Allen, and Doug MacAyeal, as well as many others. Ralph Greve generously gave me his ice sheet model and readily answered my questions. Thanks also to Veronique Bugnion, not only for the fondues, but also for teaching me about ice.

I am grateful to Linda Meinke, Will Heres, Tom Yates, and Michael Batchelder, all of whom helped me overcome my confusion with all things silicon. Thanks also to Jane McNabb, Tracey Stanelun, and Mary Elliff, who not only dealt efficiently with all manner of requests, but have also given the department a heart. Joel Sloman's musings, poetic and otherwise, added a necessary note of the surreal.

I have been fortunate to have had friends too numerous to mention, in an environment which can otherwise be quite cold. Ian Loveless, Nick Rees, and Mark Burnett kept me in touch with my roots, and the pleasures of aimless rambling, in both senses. The 'old guard' at MIT, Michael Morgan, James Risbey, Lars Schade, Chris Forest, Francoise Robe, and Marja Bister took me under their collective wing and showed me how to survive via advice, example, and diversion. Louis Kaye, the maddest maven of them all (a significant achievement) protected me from the dreaded Harkonnen during my first years here. Thanks to Eddie Nelson for trading puns admirably, and to Constantine Giannitsis for sharing his favorite 'Ask Beths'. I am lucky to have crossed paths with my classmate, Adam Sobel, whose friendship and debating endurance I am the better for. I thank also Amy Solomon, Natalie Mahowald, Bonnie Souter, and John Mulquiney for wings, movies, bikes, and chess, among other enduring memories. Sarah Samuel and Gavin Esler reminded me in the best possible way of why I miss home. Mark van der Helm, Dave ('left') Grundy , and Dave ('right') Glass have been challenging drinking companions, and were it not for them I would have finished much sooner.

My house-mates, Danny, Heather, Paul and Isaac Kirk-Davidoff, John Olsen, and Kara Osborne have been an oasis of domesticity for me. Moreover their kindness and

close friendship have given me a home–thank you. Marcus, Donna, James, and Harriet Weldon provided a valuable escape hatch, and supplied all the blarney and Barney I could want. Nili Harnik has been a soul-mate and a shoulder, without whom I would long ago have packed my bags. I am deeply grateful to Nili and her husband, Boaz Nehmet, for seeing me through. Lastly, I want especially to thank Rebecca Morss for being herself and being there, for rescuing me from some of my less impressive tendencies, and for showing me the female dead frog.

Lastly, I come to my family. My sister, Natasha, showed me the path from adolescence. My parents Philip and Susan Roe have given me so much, each in very different ways. Without you and your love and support, I could not be who I am. I am very grateful for that precious gift.

Contents

1 Introduction **17**

1.1 General properties of ice sheets 18

1.2 The last glacial maximum 18

1.3 Milankovitch cycles 19

1.4 Paleoclimate modeling 23

1.5 Stationary waves 24

1.6 Mass balance of an ice sheet 28

1.7 Approach and outline 30

2 Simplified representation of ice sheets **33**

2.1 Two-dimensional ice sheet model 35

2.1.1 Ablation rate 38

2.2 Equilibrium ice sheets 41

2.2.1 The effects of a stationary wave 44

2.3 Time dependence of ice sheets 47

2.4 Stability of the ice sheet 52

3 The stationary wave response to an ice sheet **59**

3.1 Stationary wave model equations 60

3.1.1 Canonical form of the wave equation 64
3.1.2 Barotropic stationary waves 65
3.1.3 Meaning of thermal damping 66
3.2 Response of stationary wave model 67
3.2.1 Basic state, parameters choices, and channel configuration 68
3.2.2 Response to uniform forcing as function of wavenumber 71
3.2.3 Test case ice sheet 75
3.2.4 General shape of stationary wave response in standard case 80
3.2.5 Nonlinearities 83
3.2.6 Baroclinicity in standard case 87
3.2.7 Poleward heat transport 90
3.3 Testing of model parameter choices 93
3.3.1 Basic state surface velocity 93
3.3.2 Basic state shear 95
3.3.3 Lapse rate 95
3.3.4 Latitude of β, f_0 calculation 97
3.3.5 Boundary layer damping times 99
3.3.6 Free atmosphere damping times 103
3.3.7 Output fields at different heights close to the surface 104
3.3.8 Different numbers of wavenumbers 105
3.3.9 Different cut-off thresholds 105
3.4 Sensible heating 105

4 Ice sheets, accumlation, ablation, and the seasonal cycle 111

4.1 Ice sheet modeling 112

4.1.1 Shallow ice approximation 114
4.1.2 Ice sheet boundary conditions 116
4.2 Ablation parameterization 117
4.3 Accumulation parameterization 119
4.4 Zonally symmetric climate forcing 125
4.4.1 Equilibrium ice sheet 126
4.4.2 Mass balance of an ice sheet 127
4.4.3 Ice sheet modeling assumptions 129
4.5 Seasonal cycle 131
4.5.1 Precipitation 134
4.5.2 Ablation 135

5 Results for an idealized geometry **139**

5.1 Equilibrium ice sheets 141
5.1.1 Precipitation feedback 141
5.1.2 Stationary wave feedback 143
5.1.3 Combined feedbacks 147
5.2 Results for different basic states 153
5.3 Background stationary wave 154
5.4 Growth phase of ice sheet 156
5.4.1 Growth from isolated plateau with gradual climate cooling 161
5.5 Decay phase of an ice sheet 164
5.6 Periodic forcing of the basic state 168
5.6.1 Varying basic state temperature 169
5.6.2 Varying basic state shear 175

5.6.3 Varying background stationary wave 176

5.6.4 Ice sheet response to beating of precessional frequencies 180

6 Application to Pleistocene climates **185**

6.1 Stationary waves for interglacial topography 186

6.1.1 Separation of topography into eastern and western hemispheres 187

6.1.2 Initiation of the Laurentide 189

6.2 Stationary waves for LGM topography 193

6.3 Evolution of North American ice sheets 198

6.3.1 Zonally symmetric forcing 201

6.3.2 Stationary wave feedback 201

6.3.3 Current precipitation patterns 206

6.3.4 Combined feedbacks 209

7 Summary and discussion **217**

A Moisture budget **225**

B Moisture integral **229**

List of Figures

1.1 LGM reconstruction and current topography 20

1.2 $\delta^{18}O$ record for the last $2300kyr$ from deep sea core 607 21

1.3 Comparison of Laurentide and Tibetan Plateau 25

1.4 Observed January stationary wave pattern 26

1.5 Schematic illustration of processes involved in the stationary wave/ice sheet interaction 31

2.1 Schematic of 2-D ice sheet for Pleistocene 34

2.2 Infinitesimal segment through 2-D ice sheet 36

2.3 Accumulation and ablation rates as a function of halfwidth 43

2.4 Halfwidth versus mean accumulation 44

2.5 Halfwidth versus mean accumulation, including feedbacks 48

2.6 Profiles of ice sheets including feedbacks 49

2.7 Growth of ice sheets including feedbacks 51

2.8 Response of ice sheets to imposed $5^{o}C$ climate change 54

2.9 Response to temporary warming 57

3.1 Standard atmospheric basic state 69

3.2 Damping time vertical profiles 70

3.3 Spectrum of $1km$ response to uniform forcing 72

3.4 Vertical structure of solution for different wavenumbers 73
3.5 Test ice sheet topography and spectral decomposition 75
3.6 Stationary wave response to test ice sheet 77
3.7 Longitudinal section at $60N$ of response to test ice sheet 78
3.8 Height-longitude section for geopotential perturbation 79
3.9 Separation of response into small and large scale components 82
3.10 Perturbation velocities and potential vorticity gradients for response test ice sheet 85
3.11 Comparison of linear and nonlinear terms in standard case 86
3.12 Local growth rate for baroclinic eddies for standard case 89
3.13 EP fluxes for standard case 91
3.14 Poleward heat flux in standard case 92
3.15 Sensitivity to basic state surface velocity 94
3.16 Sensitivity to basic state wind shear 96
3.17 Sensitivity to basic state lapse rate 97
3.18 Sensitivity to latitude taken for β and f_0 98
3.19 Sensitivity to boundary layer momentum damping time 99
3.20 Sensitivity to boundary layer thermal damping time 100
3.21 WKB amplitude factor for different thermal damping times 102
3.22 Sensitivity to free troposphere damping time 103
3.23 Sensitivity to model output height 104
3.24 Model response to imposed cooling of $15Wm^{-2}$ 107

4.1 Precitation rate as function of vertical velocity 124
4.2 Ice sheet fields for zonally symmetric climate forcing 128
4.3 Profiles for different ice modeling assumptions 130

4.4 Seasonal atmospheric basic states 133

4.5 Atmospheric response to seasonal basic states 134

4.6 Seasonal precipitation rates 137

5.1 Contours, fluxes, and 3-D view for equilibrium ice sheet in zonally symmetric climate 142

5.2 As for Figure 5.1, but including topographic precipitation feedback only . 144

5.3 Forcing climate fields for Figure 5.2 145

5.4 As for Figure 5.1, but including stationary wave feedback only 146

5.5 Forcing climate fields for Figure 5.2 148

5.6 Cross sections through ice sheet in Figure 5.4 149

5.7 As for Figure 5.1, but including stationary wave and precipitation feedbacks 150

5.8 Forcing climate fields for Figure 5.2 152

5.9 Equilibrium ice sheets for strong and weak atmospheric basic states . . . 155

5.10 Background stationary wave, geopotential heights and temperatures . . . 157

5.11 Equilibrium ice sheet for climate including background stationary wave . 158

5.12 Ice sheet growth to equilibrium for different cases 160

5.13 Contour time sequence of growth from initial plateau 163

5.14 Response for different cases to imposed 5^oC warming 166

5.15 Contour time sequence of response to 5^oC warming for two cases 167

5.16 Time series of response to imposed $20kyr$ and $40kyr$ oscillation in basic state temperature 171

5.17 Contour time sequence for response to $40kyr$ oscillation in basic state temperature 173

5.18 Time series of response to imposed $20kyr$ and $40kyr$ oscillation in basic state shear 177

5.19 Contour time sequence for response to $40kyr$ oscillation in basic state shear 178

5.20 Time series of response to imposed $20kyr$ and $40kyr$ oscillation in background stationary wave 179

5.21 Response to $19kyr$ and $23kyr$ forcing in basic state temperature 182

6.1 Stationary wave for current topography 188

6.2 Stationary wave for current eastern topography only 190

6.3 As for Figure 6.2 but for current western topography only 191

6.4 Stationary wave response for $21kbp$ reconstruction topography 194

6.5 As for Figure 6.2 but for $21kbp$ eastern topography only 196

6.6 As for Figure 6.2 but for $21kbp$ western topography only 197

6.7 Mask and surface topography for ice sheet model integrations 200

6.8 Equilibrium ice sheet over North America evolved in a zonally symmetric climate 202

6.9 Equilibrium ice sheet over North America evolved including stationary wave feedback 204

6.10 Cross section through Rockies topography at two latitudes 205

6.11 Equilibrium ice sheet over North America evolved including stationary wave feedback and using current precipitation patterns 207

6.12 Comparison of accumulation rates from model parameterization and from current patterns 208

6.13 Equilibrium ice sheet over North America using both stationary wave and precipitation feedbacks 210

6.14 Forcing climate fields for Figure 6.13 211

6.15 As for Figure 6.13 but for strong stationary wave forcing 213

A.1 Terms in the moisture budget equation. 228

List of Tables

5.1 Ice sheet parameters for integrations with different feedbacks 151

Chapter 1

Introduction

The waxing and waning of the great continental ice sheets over the last two million years is one of the major puzzles of the climate system. At the peak of the last ice age, the Laurentide and Cordilleran ice sheets covered most of what is now Canada, and to a depth of about two miles. The Fennoscandian was smaller in both extent and elevation but nonetheless enveloped a large part of northern Europe and northwestern Russia. Combined with changes to the Antarctic and Greenland ice sheets, they enclosed a volume of ice of $33 \times 10^6 km^3$, sufficient to cause a drop in global sea level of $105m$ (Peltier, 1994). These immense bodies of ice formed significant topographic obstacles to the prevailing westerly winds in midlatitudes. The response of the atmosphere to surface topography is a classic problem in dynamical meteorology (e.g. Charney and Eliassen, 1949): if the length scale exceeds a few hundred kilometers then the deviation of the atmospheric flow around the topography establishes planetary scale stationary waves—standing patterns in the winds and temperatures—within the atmosphere. Associated with the reorganization of the circulation are altered patterns of snowfall and melting over the ice sheets. Thus in a very direct way the atmospheric stationary waves, created in part by the evolving ice sheets themselves, acted to sculpt the great ice sheets over many thousands of years. It is this interaction that is the focus of this thesis.

1.1 General properties of ice sheets

Given sufficient time, an ice sheet behaves as a viscous fluid, slowly spreading under its own weight. Accumulation of snow in the interior is gradually compressed into ice by subsequent years' snowfall, and incorporated into the main body of the ice sheet. In the interior, the ice surface is too cold (in part because of its elevation) for any melting. The increasing ice load builds up stresses within the ice, which responds by gradually redistributing its mass. The ice flows towards the margins, and if it encounters a coastline most of the ice will calve (shed icebergs) into the ocean (although it may form a floating ice shelf before doing so). At a land based ice margin there must be, in equilibrium, enough melting during the summer to balance the flux of ice from within the interior. Ice sheets are also characterized by steep sides: the large stresses within the ice are created either by a large ice depth or a large surface slope, so as the depth tends to zero towards the margin, the surface slope increases: an ice sheet typically rises to $1km$ in height within $100km$ of the margin. The steep sides means the surface temperature decreases rapidly away from the margins and therefore the zone of melting is confined to a narrow band around the edge.

1.2 The last glacial maximum

The last ice age reached its peak around $21kbp$ (thousands of years before present), at the last glacial maximum (LGM). Having evolved over the the previous $100kyr$ (thousands of years), the ice sheets rapidly collapsed, with most of the ice disappearing over the $5kyr$ interval between 14 and $9kbp$, leaving Greenland as the only major body of ice in the northern hemisphere. The history of land ice since the LGM can be reconstructed from several paleoclimate indicators, and utilizing the known physical properties of ice. As it advances, an ice sheet scours the surface beneath it, making it difficult to determine its progress (or the presence of previous ice sheets). On the other hand when it retreats, dated terminal moraines record the ice sheet's margin. For a given margin the ice sheet's volume can be estimated from ice flow models or bedrock depression. A large ice sheet is massive enough to partly displace the bedrock upon which it sits. Although the bedrock rebounds once the ice is removed, the surface depressions from the last great ice sheets are still measurable (Simons and Hager, 1997).

Peltier (1994) derived the history of land ice over the last $20kyr$, accounting for dynamic bedrock rebound, and using relative sea level histories since the LGM. His estimate for the northern hemisphere ice coverage at $21kbp$ is shown in Figure 1.1a. For comparison the current topography is plotted in Figure 1.1b. The Laurentide and Cordilleran formed a continuous body of ice across North America (hereafter we will generally refer to the combined body as the Laurentide), reaching a maximum height of $3.2km$. Over Europe and northwest Russia, the Fennoscandian ice sheet dominated the landscape. Greenland has changed comparatively little since the LGM. Large climate changes accompanied the presence of the ice sheets (e.g. Crowley and North, 1991). Annually averaged midlatitude temperatures were about 10^oC cooler, with the differences larger in winter than in summer. Mammoths, arctic foxes and lemming roamed the areas south of the ice sheet margins in arctic tundra. The temperatures in the tropics are less certain, but are now thought to have been about 3 to 5^oC colder than present (e.g. Anderson and Webb, 1994).

Figure 1.1 shows some interesting features to the ice cover. Why were Alaska and Siberia largely ice free, despite being more than 20^o north of areas with permanent ice cover? There might be several explanations for this: low snowfall; high melting rates removing any accumulation or ice flux; weak flow of ice in these directions from the main ice sheets; or highly variable topography with high peaks and deep valleys preventing the development of large areas of ice cover. In this thesis we will develop a model which is able to look at the relative importance of these different factors.

1.3 Milankovitch cycles

Much of the work on glacial climates has centered on trying to explain the cyclic behavior of the global ice volume over the last two million years (the Pleistocene). The record of these great ice ages is perhaps best seen in drill cores from the deep ocean bed (e.g. Crowley and North, 1991). Because of fractionation during condensation, ice sheets lock up a smaller proportion of heavy oxygen isotopes than exists generally, so the ocean becomes enriched in ^{18}O; when the ice melts the isotopic ratio is restored. This ratio is recorded in the shells of living foraminifera when oxygen is incorporated into the carbonates of which their shells are comprised. When the foraminifera die they settle on the ocean floor, where they are gradually buried by succeeding layers. They

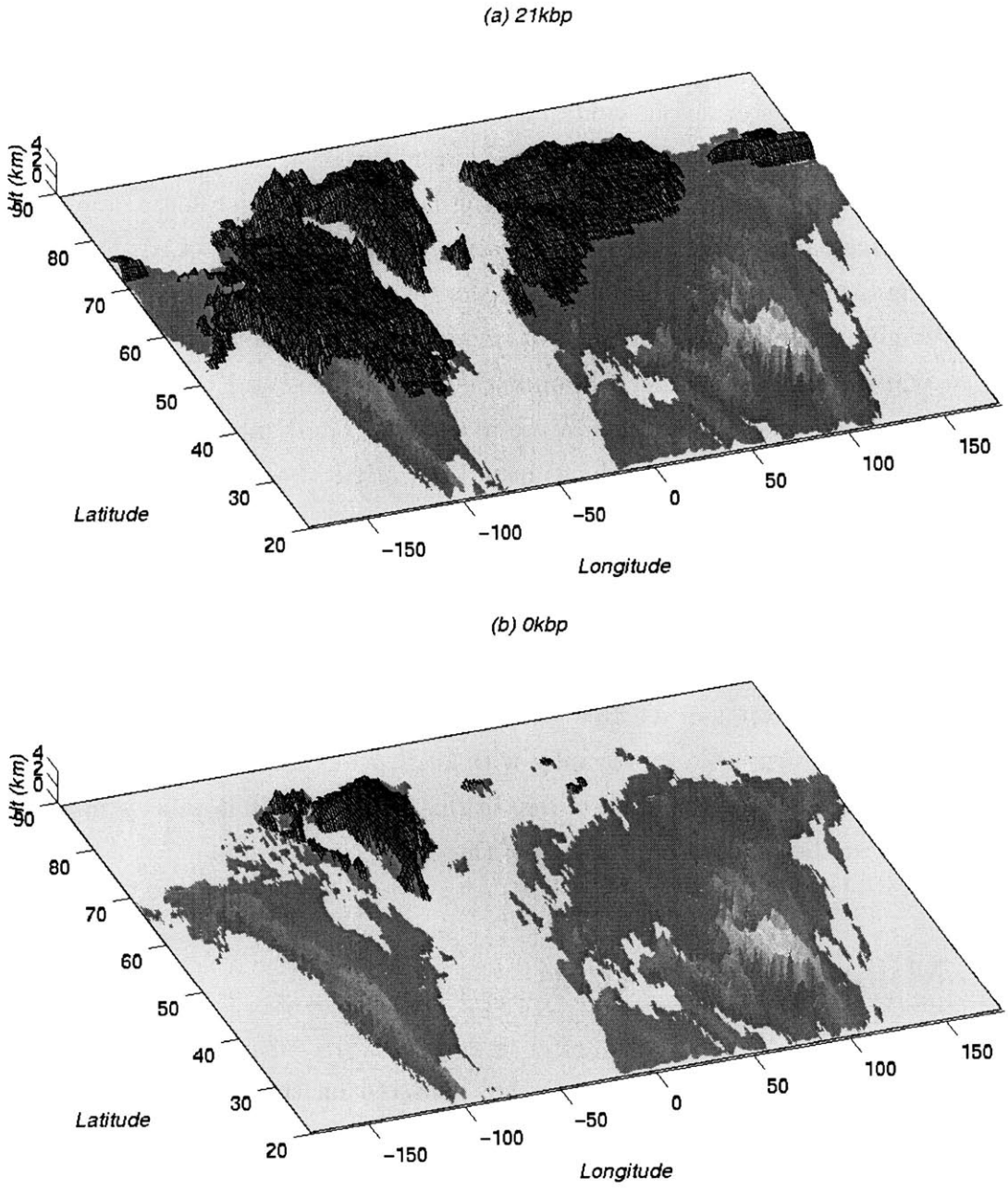

Figure 1.1: Land ice and topography from Peltier (1994). (a) $21kbp$ reconstruction, and (b) current. Land ice is shown as a meshed grid. Elsewhere the height of topography is inversely proportional to the intensity of the shading.

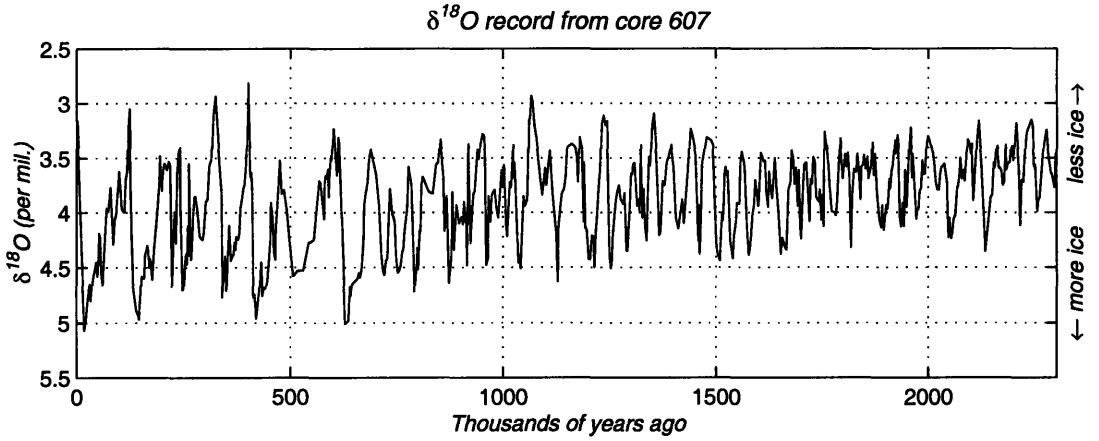

Figure 1.2: $\delta^{18}O$ record for the last $2300kyr$ from deep sea core 607.

thus form a stratified record of global ice volume, stretching back, in some cases, more than 10 million years.

Figure 1.2 shows the isotopic ratio from one core (site 607, from the central North Atlantic) for the last $2300kyr$ (Raymo et al., 1989). The isotope ratio also records the local temperature of the foraminifera's environment, but this makes up a small part for the signal (Shackleton and Opdyke, 1973). The record shows increasing glaciation over the last two million years. Before $850kbp$ there are clear oscillations in global ice volume, with a dominant period of about $40kyr$.

Since about $850kbp$, the dominant period has become $100kyr$, with $20kyr$ and $40kyr$ variability also in the record. Generally, but by no means uniformly, the cycle has a saw-toothed shape, with growth occurring for $80kyr$ or more, followed by a rapid deglaciation taking place within about $10kyr$.

There is general agreement about the cause of the variability on time scales of 20 and $40kyr$, and the theory stems from the work of Milankovitch (1941). Due to the gravitational influence of other planetary bodies, the earth's orbit is not constant but undergoes periodic changes. Three parameters are required to describe the earth's orbit. They are (with their dominant periods of oscillation), the precession (19 and $23kyr$), the obliquity ($41kyr$), and the eccentricity (90, 105, and $400kyr$) (e.g. Berger, 1978). These variations in the orbital configuration change the sunlight (insolation) incident on the earth with the effect varying in magnitude in different locations and seasons. The amplitude of the variation is significant. Midlatitude insolation at the summer

solstice varies by up to $65 W m^{-2}$, or 13% of its mean value. Based on energy balance model calculations, Short et al. (1990) calculated that the precessional variations were equivalent to a temperature forcing maximizing in the continental interiors at around $10^{o}C$. The effects of obliquity variations are felt most strongly at the poles; Short et al. determine the maximum equivalent temperature to be about $4^{o}C$. These do not equate to the actual climate response because energy balance models contain no fluid dynamics and therefore have poor representations of any redistribution of the heating by the atmosphere. On its own, the eccentricity does little to change the incident insolation, but it does strongly modulate the amplitude of the precessional forcing.

The $20kyr$ and $40kyr$ periodicity recorded in the global ice volume can be modeled as a linear response to the precessional parameters (Imbrie et al. 1993a). The variation in ice volume is most likely a direct response due to variations in high latitude summer insolation—the original Milankovitch hypothesis. However, since a given combination of orbital parameters can represent insolation for a range of latitudes and times of the year (Imbrie and Imbrie, 1980), the attribution also rests on physical theory.

The climate response at $100kyr$ is much more mysterious. Although the oscillation period lies close those of the eccentricity, the physical link is not obvious. The insolation has much more power at 20 and $40kyr$ than at $100kyr$, and yet for the last $850kyr$, the climate response has been larger at $100kyr$. Various explanations have been sought to explain the dominant climate response at this period. Generally efforts have been directed at investigating whether the climate system can sustain a $100kyr$ oscillation whose phase is determined by the insolation, or whether plausible nonlinear climate processes can extract sufficient power from the $100kyr$ modulating envelope of the precession to drive the ice ages. Imbrie et al. (1993b) contains a good review of the various contending theories, but as yet none are completely satisfactory from the standpoint of their physics, and none perform better statistically, as explanations of the global ice volume, than the others (Roe and Allen, 1999).

The effect on the ice sheets of varying the climate on Milankovitch time scales is considered in chapter 5. While this thesis does not attempt to explain the $100kyr$ cycle directly, a study of how the atmosphere and the ice sheets interacted on the time scales of the ice ages contributes to an understanding the whole ice-age climate system.

1.4 Paleoclimate modeling

The extensive body of Pleistocene climate data has motivated a large modeling effort to understand the physics of the ice ages. The approaches can be broadly divided into two categories.

The first approach is 'snapshot' simulations of a particular climate state (e.g. Gates, 1976; Manabe and Broccoli, 1985; Hall et al. 1996). A general circulation model (GCM) of the atmosphere and/or ocean is run to equilibrium with appropriate boundary conditions and insolation. The advantage of such an approach is that the GCM contains representations of many physical processes which simpler models do not have. This allows for the interactions and feedbacks associated with those processes to be examined. The modeled atmospheric circulation is important not only because it has to be reconciled with the paleoclimate data, but because it may also suggest what new data would be useful to gather. However, the computational expense of running such models is a major drawback in their use. Simulations are restricted to only a small number of model parameter sets. Moreover, the model cannot be run for anything like the tens of thousands of years appropriate to ice sheet dynamics. Because the surface topography must necessarily be fixed in these simulations, there is no ability to assess how the ice sheets respond to the modeled climate. It is not clear either, whether GCMs are not so highly tuned for today's climate that they can reasonably model a climate with such drastically different conditions.

The second approach is to perform long integrations with very simplified climate models (e.g. Pollard, 1978; Suarez and Held, 1979; Berger et al., 1990; Tarasov and Pelter, 1997). The climate is stripped down to what is believed to be the important physical processes, and simplified representations of them are constructed. The big advantage of this approach is that it allows the ice physics to be included, and the feedbacks between the ice sheets and the climate can thus be studied. A lot of work has used energy balance climate models (EBMs) which, as the name suggests, involve balancing the terms in a conservation of energy equation. The atmosphere and ocean are typically assumed to provide a diffusive heat flux. The main variable in such models is the surface temperature, from which accumulation and melting (ablation) fields must be diagnosed. EBMs have been used to simulate the ice age cycle and to assess the importance of various hypothesized climate processes (e.g. Peltier and Marshall, 1995).

The disadvantage of these models is their inherent simplicity. Reduced parameterizations tuned to reproduce the current climate may not effectively represent the desired process in a different climate. In addition, the processes included in such models are those chosen by the modeler and so the results often amount only to a numerical exploration of a physically based verbal argument (this is also true of this thesis). There is no guarantee that additional processes do not arise in a different climate, or that those considered unimportant in today's climate do not become significant. EBMs omit atmospheric dynamics and as, we shall argue in this thesis, this leaves out an important feedback which arises as the ice sheet develops.

1.5 Stationary waves

The work in this thesis is pitched somewhere between the two approaches outlined above. We want to be able to look at ice dynamics, but also include the relevant atmospheric dynamics. That is, if the presence of the ice sheet changes the atmospheric circulation, how does that altered circulation then change the climate seen by the evolving ice sheet? We will have to use a simplified representation of the atmosphere, and we wish therefore to isolate the physical processes which we believe will be important to the interaction. There are several ways an ice sheet might affect the atmosphere. The most obvious is that once an ice sheet is established, the atmosphere has to go around it. The Laurentide ice sheet was approximately the same scale and height as the Tibetan Plateau, which is the largest topographic feature on the earth's surface today. They are compared in Figure 1.3.

Observations from the current climate highlight the effect of stationary waves. Figure 1.4 shows the typical winter $500mb$ geopotential heights, and also the accompanying lower tropospheric temperature perturbations (calculated by equating the $1000mb - 500mb$ thickness to a mean vertical mean temperature (e.g. Holton, 1979)). The data was taken from the NCEP reanalysis (Kalnay et al., 1996). The influence of the surface topography is clearly seen. The Rockies are second to the Tibetan Plateau in scale, and together they are the two major northern hemisphere mountain complexes. A high pressure ridge lies over, or slightly to the west of, each mountain range, generating an anticyclonic circulation. In both cases the perturbation from the zonal mean (maximum minus minimum) is about $300gpm$ (geopotential meters). Also noticeable is that

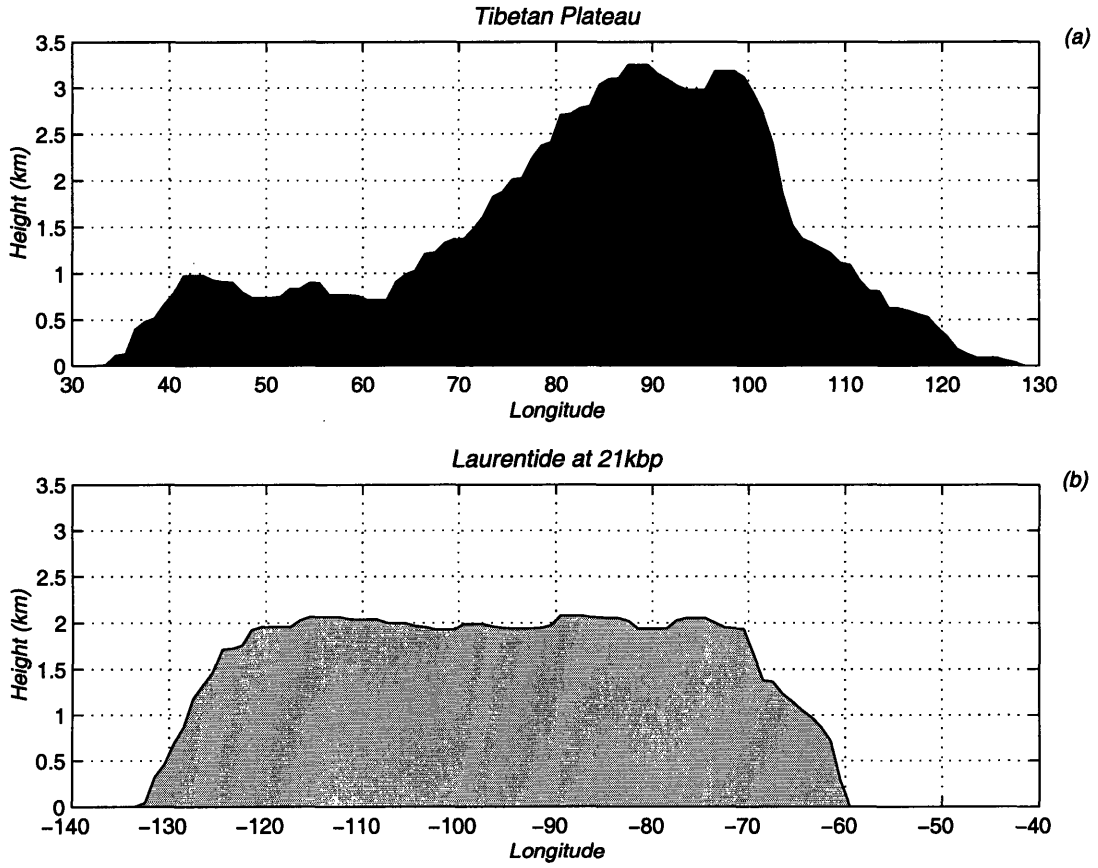

Figure 1.3: (Comparison of (a) Tibetan Plateau and (b) the Laurentide at $21kbp$ (Peltier, 1994). Both figures have the same span of longitude, and both are means over 20^o of latitude: for the Tibetan plateau, $25N$ to $45N$, for the Laurentide, $45N$ to $65N$.

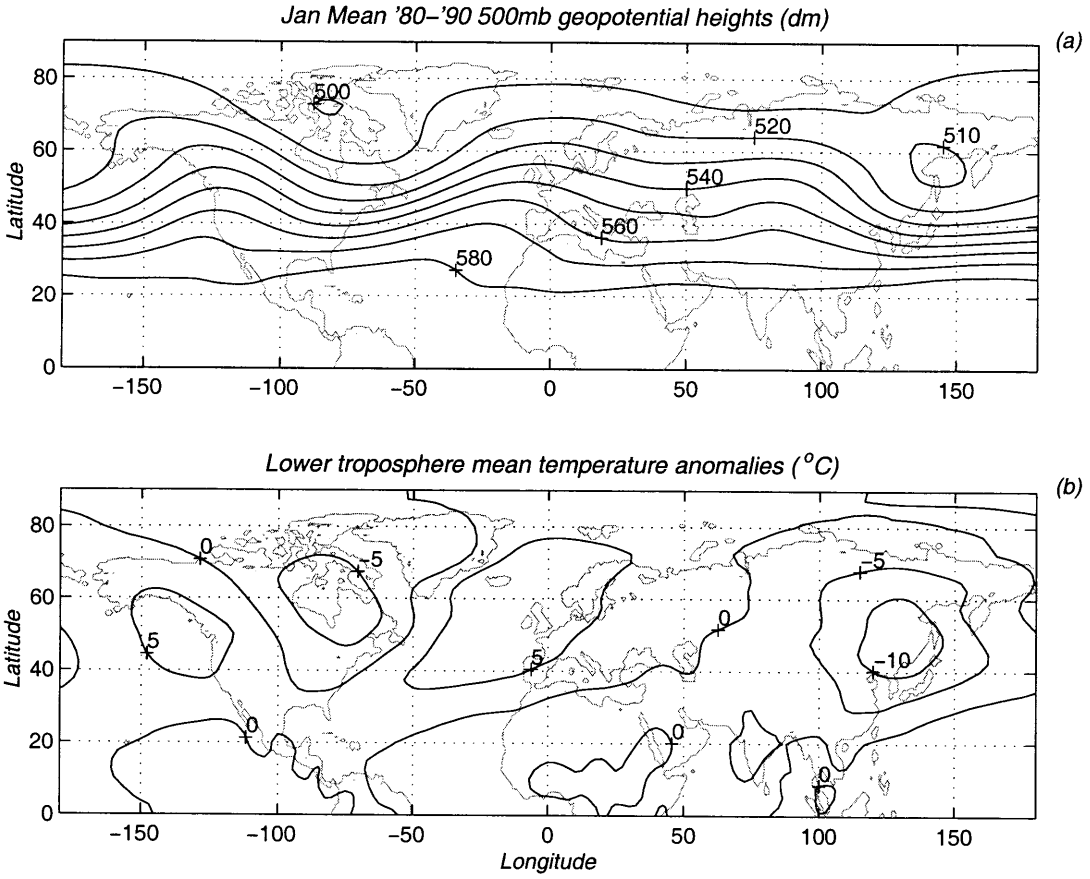

Figure 1.4: Observed January stationary wave. NCEP reanalysis data, average from 1980 to 1990. (a) $500mb$ geopotential heights (dm), and (b) lower tropospheric temperature (^oC).

the atmospheric response is not localized to the mountain ranges but extends around the globe. This implies a climate teleconnection: changes to the stationary waves will affect climates remote from the forcing. The strong low pressure trough in the lee of each range produces increased local temperature gradients; these are associated with the atmospheric storm tracks, which are locations of enhanced storminess in the climate.

The lower tropospheric temperatures (Figure 1.4) are associated very closely with the direction and strength of the wind. The east-west temperature difference over each range is slightly more than 10^oC. The highest temperature perturbations occur at the end of long southerly fetches of air, and the coldest at the end of long northerly fetches. The relationship is straightforward: prevailing northerlies (southerlies) bring with them colder (warmer) air. Given that the Laurentide ice sheet was of the same scale as the Tibetan Plateau, we expect it also must have created a significant stationary wave pattern.

It was likely even more important to the climate; in summer today, the northern hemisphere stationary wave decreases substantially because the subtropical jet (the winds forcing the stationary wave) moves northwards away from the Tibetan plateau (Nigam and Lindzen, 1989). In contrast, the Laurentide sat year round in the middle of the midlatitude westerlies. If we take 10^oC as a plausible amplitude for the stationary wave, then the stationary wave represents a forcing as large as Milankovitch insolation cycles. Taking a typical midlatitude meridional temperature gradient of $-6.5^oC/1000km$, that cooling of 10^oC across the continent is equivalent to a climate about $1500km$ further north. This emphasizes an important motivation for this thesis, namely that east-west temperature differences can be as important to the climate as north-south differences. It is not correct to think of a glacial climate as one in which the temperatures are merely uniformly colder, but rather it is also necessary to account for the redistribution of temperature patterns arising from the altered planetary stationary waves. The climate forcing that the stationary wave represents is an important one for the ice sheets. The reorganization of the winds and temperatures over an ice sheet will change the patterns of accumulation and melting. Therefore the stationary waves they created must have acted as a powerful feedback on the evolution of the ice sheets.

The theory of atmospheric flow around topography has been developed in many studies (see Smith, 1979 for a comprehensive review). If the topography exceeds a few hundred kilometers in scale then the effect of the earth's rotation begins to be felt by the atmosphere as it is forced to deviate around the topography. In steady state, topography forces stationary Rossby waves, which propagate against the restoring force created by the background vorticity gradient due to the earth's rotation and due to the structure of the zonal mean atmospheric flow. The Rossby waves have fully balanced winds and temperature fields. The physics of these these waves is reviewed in Chapter 3, and they can account reasonably well for the observed patterns (e.g. Hoskins and Karoly, 1981). Planetary scale stationary waves can be created by any zonal asymmetries in the atmospheric forcing. The forcing may be either topographic (mountains), thermal (land-sea temperature contrast), or it can be the convergence of the heat and momentum fluxes of transient eddies, such as occurs within the storm tracks (Valdes and Hoskins, 1989). There is disagreement about the relative importance of these different forcings (e.g. Jacqmin and Lindzen, 1985; Valdes and Hoskins, 1989). The modeling ambiguity arises because much of the contributing non-topographic forcing comes from within the atmospheric storm tracks and its effect is such that the patterns tend to overlay each

other. We shall argue, consistent with the results of Cook and Held (1988), that the stationary waves associated with the ice sheets, especially local to the topography, were largely forced topographically.

1.6 Mass balance of an ice sheet

An ice sheet feels the climate mainly through the accumulation and melting of snow and ice. There is an additional influence in that ice flow is temperature dependent. The temperature (and therefore flow) profile within an ice sheet is a record of the climate history at the surface of the ice sheet (e.g. Calov and Hutter, 1996). We shall show however, that the temperature dependence of the flow is much less important to the ice sheets shape than are the changes caused to the mass balance.

Many climate variables affect the melting of snow and ice. Shortwave and longwave radiation, air and surface temperatures, cloudiness, surface albedo, atmospheric humidity, and surface wind speeds all affect the rate of melting. Melting does not necessarily remove ice from the ice sheet; refreezing of meltwater occurs within the overlying snow pack. Ablation is the term used to describe all processes which lead to removal of snow and ice from the ice sheet (which includes calving).

For the purpose of modeling large scale ice sheets, where local details are not the concern, a melting parameterization expressed in terms of temperature can be used. If the summer temperature rises much above freezing, then melting rates of several meters a year are observed and the rates increase rapidly with temperature. These rates are comparable with the expected mass flux from within the interior of the ice sheet, and so on large scales the ice cannot exist at locations where the summer temperature significantly exceeds 0^oC.

We have seen in the current climate that the atmospheric stationary waves are responsible for large variations in the temperature around a latitude circle. We will demonstrate that the stationary waves due to the development of an ice sheet also cause significant temperature perturbations, and via the ablation patterns, exert a strong influence of the shape of an ice sheet. This confirms the suggestion of Lindemann and Oerlemans (1987) who argued for the importance of stationary waves to an ice sheet's mass balance.

Accumulation is an even more complicated process to model than melting, and any

simple model obviously cannot account for all the processes involved. One point to emphasize is that an ice sheet is quite insensitive to the patterns of accumulation in the interior. An ice sheet behaves diffusively; by the time accumulation deep in the interior has flowed to the margin (which can take tens of thousand of years) the details of the precipitation distribution have been smeared out. The exception to this is at the ice sheet margin where topography has a big effect on precipitation. The influence of topography on precipitation in today's climate is readily observed. On the windward side of mountain ranges (e.g. the Rockies) there are high rainfall rates, due to the convergence of moisture in the air column as the air is forced to rise. Conversely, in the lee of the range, descent and warming dries the air column and rainfall is suppressed (often the region is called the 'rain shadow') (Smith, 1979).

The important additional factor for an ice sheet is that, provided it is sufficiently cold, the topographic precipitation will be incorporated into the ice and will therefore contribute to its overall shape. We expect the high accumulation rates to track the evolving windward margin of the ice sheet. Where the prevailing winds result in downslope flow, accumulation will be diminished.

The Laurentide and Fennoscandian were significant topographic features and therefore they must have experienced the effects of topographic precipitation. In the current climate, for example, the average accumulation over Antarctica is $0.18myr^{-1} \pm 0.04$. There are interior regions where the accumulation is less than $0.05myr^{-1}$, but in places where the prevailing winds are generally upslope and at the coast, accumulation can exceed $1myr^{-1}$ (Ohmura et al., 1996). Sanberg and Oerlemans (1983) showed that the effects of upslope precipitation had a marked effect on the growth and extent of a simulated Fennoscandian ice sheet. We find results consistent with theirs and demonstrate also that the precipitation reduction in the lee of the ice sheet also contributes to its shape.

An ice sheet may affect the climate in other ways. The high albedo of ice reflects much of the incident insolation. Over Antarctica and Greenland this produces significant temperature inversions. The ice sheet therefore acts to cool the overlying atmosphere, and so is a source of thermal stationary waves. We will try to assess the importance of this possibility.

1.7 Approach and outline

To summarize, we expect a topographic obstacle in midlatitudes like the ice sheets, to induce a high pressure, anticyclonic atmospheric circulation over, or slightly to the west of, the peak topography (why this is so is explained in Chapter 3). This means that warm, moist air is brought up over the southwestern flank of the ice sheet, which gives rise to two possible consequences. First, the air is warmer and so may cause enhanced melting. Second, we expect more precipitation both because the warmer air holds more moisture, and because the flow will tend to be upslope. The first process acts to reduce the size of the ice sheet, the second acts to build it up. Conversely in the lee of the ice sheet, cold (and hence dry) air flows down the ice. Colder air means less melting, but low precipitation and downslope flow mean less accumulation, so again the processes have an opposite tendency. These mechanisms are illustrated schematically in Figure 1.5 We want to understand first how the ice sheet changes the atmospheric circulation, and then how these competing feedback processes play off against each other to create the final configuration of the ice sheet.

Detailed simulations of any particular climate state tend to involve the interaction between numerous modeled processes making it confusing to diagnose the cause of any particular feature. We choose to start by studying the feedbacks between the atmosphere and the ice sheet in an idealized geometry and isolating the separate mechanisms of the interaction. The results are then extended to more realistic configurations. The principal questions addressed in this thesis are the following:

- How do the stationary waves and topographic precipitation control the ice sheet's equilibrium configuration and size?
- How do these feedbacks affect the growth and decay of ice sheets?
- How might insolation forcing on Milankovitch time scales affect the interaction between the ice sheets and the stationary waves?
- To what extent can the answers to the above questions account for the actual ice sheets of the Pleistocene?

Chapter 2 takes the most reduced approach and considers a two-dimensional ice sheet (height and latitude). The ice sheet is represented as a perfectly plastic material,

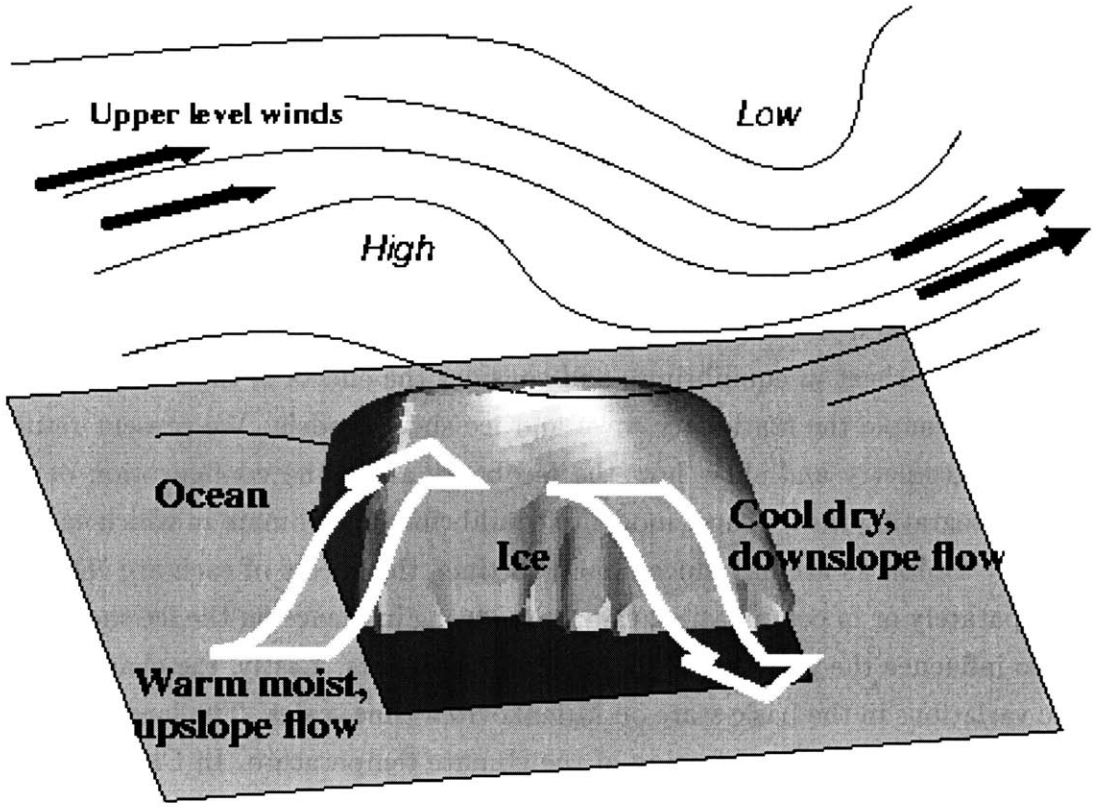

Figure 1.5: Schematic illustration of processes involved in the stationary wave/ice sheet interaction. The length scale of the ice sheet is $2 - 3000km$, and the height scale is $2 - 3km$.

and very simple melting and accumulation parameterizations are used. Even such a basic model illustrates several important aspects of ice sheet behavior. We allow the temperature at the southern margin to be linked to the height of the ice sheet, which demonstrates the potential power of the stationary waves to affect the size of the ice sheet, and also suggests that the feedback might exert an influence of the growth and decay of ice sheets. In Chapters 3 and 4, a framework is developed to examine the extent to which the conclusions carry over to a three-dimensional world. Chapter 3 develops a linear quasigeostrophic stationary wave model to look at the atmospheric response to a topographic feature characteristic of an ice sheet. We address the relative magnitudes of stationary waves caused by different forcings, and also what aspects of the climate the stationary wave is most sensitive to. The basic physics needed for ice sheet modeling is reviewed in Chapter 4, and we introduce and justify parameterizations for accumulation and melting. Using these parameterizations, we illustrate the basic balance in an ice sheet in equilibrium, and consider the effects of the seasonal cycle. In Chapter 5 we couple the stationary wave and ice sheet models. We present results for an idealized geometry and show how the feedbacks affect the configuration of the ice sheet. By integrating the ice sheet model to equilibrium in a climate in which each of the atmospheric feedbacks are introduced one at a time, the effects of each are clearly seen. Acting separately or in combination, they have strong influence on the ice sheet's shape. They also influence the growth and decay of the ice sheets. Lastly, the chapter looks at periodic variations in the basic state on Milankovitch time scales. The largest impact on the ice sheet is through direct forcing of the climate temperature. In Chapter 6 we use the current and reconstructed LGM topography to look at the influence the stationary waves had on the remote climate. In particular we suggest that the climate over the Fennoscandian was strongly influenced by the stationary wave due to the Laurentide ice sheet, 3000 miles upstream. In integrations of the coupled stationary wave/ice sheet model over North America, we show that the stationary wave likely contributed to the deglaciation of Alaska and the extension of the ice over New England. The results of the thesis are summarized and discussed in Chapter 7.

Chapter 2

Simplified representation of ice sheets

In this chapter we introduce a very simplified representation of an ice sheet in order to illustrate some basic features of ice sheet behavior. The ice sheet is two-dimensional (height and latitude). Given this assumption, a relevant configuration for the Pleistocene ice sheets is shown in Figure 2.1. The northern edge of the ice sheet is grounded by the Arctic Sea. The southern margin however is free to vary, and its location is therefore determined by where the climate is warm enough for the summer melting to balance the southward spreading of the ice as it flows under its own weight. By using this reduced approach we can demonstrate what the important parameters are that determine the ice sheet configuration in equilibrium.

We also demonstrate, albeit in a very ad hoc way, the effects on the ice sheet of the induced atmospheric stationary wave. We allow the ice sheet to modify the surrounding climate by creating a temperature perturbation. This temperature perturbation is representative of that caused by the deviation of the atmospheric flow around the ice sheet. This feedback alters the equilibrium size, and in time dependent calculations, the model suggests that the inclusion of the stationary wave effect should destabilize the eastern slopes of the ice sheet, while stabilizing the western slopes.

The ice sheet behaviors we find here are modeled more comprehensively in later chapters.

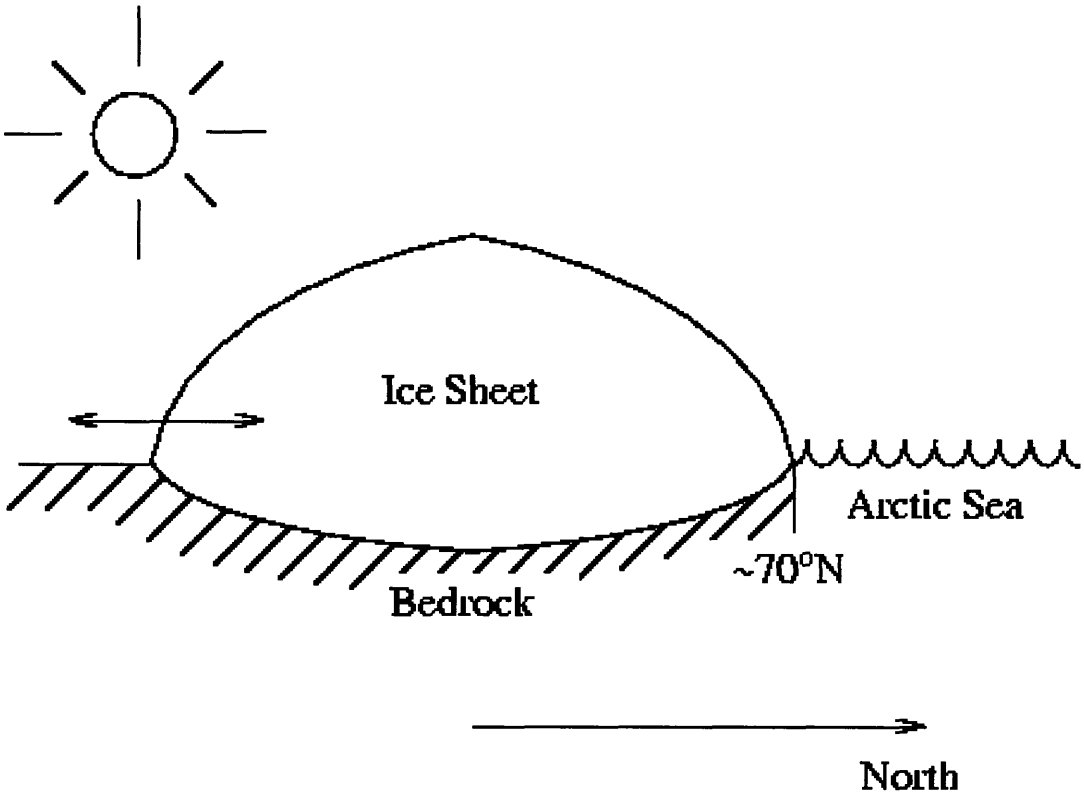

Figure 2.1: Schematic of relevant ice sheet configuration for the Pleistocene ice sheets. Ice is grounded by the Arctic Sea at $70N$, and the southern margin is free to vary. The ice depresses the underlying bedrock.

2.1 Two-dimensional ice sheet model

On sufficiently long time scales, a body of ice as large as the great continental ice sheets of the Pleistocene will flow under its own weight. Snowfall in the interior is gradually compressed into ice by succeeding overlying layers. The build up of this new ice creates stresses within the ice sheet to which it responds over time. The manner of this response is governed by the constitutive relation relating the strain rates to the applied stresses. Glen's Flow law (e.g. Paterson, 1994) suggests that the strain rate, $\dot{\epsilon}$, is related to the applied stress, τ by the following relation:

$$\dot{\epsilon} = C(\tau/\tau_0)^n \tag{2.1}$$

where C, τ_0, and n are constants. The value of n usually taken to be 3, based on a combination of empirical measurements and observations (e.g. Paterson, 1994). The constitutive relation can be combined with the laws of conservation of mass, energy, and momentum to give the equations of motion governing ice flow. These are detailed in Chapter 4, when a fully three-dimensional ice sheet model is introduced.

A simpler approach, which nonetheless gives some mileage in qualitatively describing an ice sheet's behavior, is to treat the ice sheet as a perfectly plastic material. This means that there is no deformation of the ice until the threshold (or yield) stress is reached, at which point there is instantaneous adjustment. In equilibrium therefore, all of the ice is at the yield stress. This assumption is equivalent to taking the value of n in Equation (2.1) to be infinity (Paterson, 1994).

The assumption of a perfectly plastic material allows us to derive the profile of the ice sheet. In equilibrium, the integral of the forces acting on the boundary of a segment through the ice sheet must be zero. To a good approximation, the normal stress at a point within the ice sheet is given by the pressure head of the overlying ice (e.g. Paterson, 1994). We can also assume a stress free surface. So, considering the infinitesimal segment depicted in Figure 2.2, and resolving the boundary forces acting in the y direction, we can write:

$$\tau_0 \delta y = \int_0^{h(y+\delta y)} \rho g(h-z)dz - \int_0^{h(y)} \rho g(h-z)dz \tag{2.2}$$

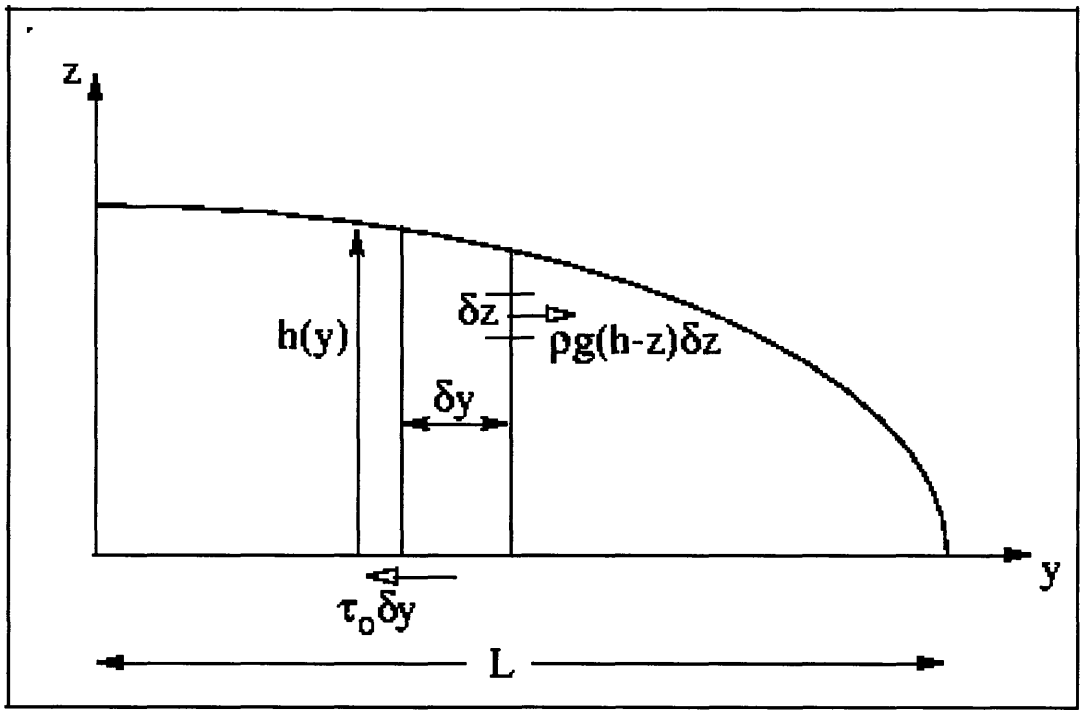

Figure 2.2: Schematic of an infinitesimal segment through a two-dimensional ice sheet. Horizontal forces are shown by arrows with unfilled heads. τ_0 is the yield stress of the ice sheet, and ρ is the density of the ice.

where y is the distance from the middle of the ice sheet, τ_0 is the yield stress of the ice sheet, ρ is the density of ice, and g is taken as $9.8ms^{-2}$. Using a first order Taylor expansion on first term on the right hand side of Equation (2.2), we can simplify to

$$\tau_0 \delta y = \frac{d}{dy}(\frac{1}{2}\rho g h^2)\delta y \tag{2.3}$$

therefore,

$$h^2 = \int_0^L \frac{2\tau_0}{g} dy \tag{2.4}$$

L is the halfwidth of the ice sheet, which is defined as the distance from the southern (or northern) margin to the middle of the ice sheet, which because of symmetry is also the highest point of the ice sheet. Up to this point, we have assumed a flat lower boundary. In fact, continental ice sheets are massive enough to depress the underlying bedrock. Assuming that in equilibrium we can say that hydrostatic balance applies, a correction factor of $(1 - \rho/\rho')$ is needed on the right hand side of Equation (2.4), where ρ' is the density of the bedrock (e.g. Paterson, 1994). The ratio of densities is about $1 : 3$. So, allowing for the bedrock depression, (2.4) gives

$$h = \lambda(L - |y|)^{1/2} \tag{2.5}$$

with $\lambda = 4\tau_0/3\rho g$, which we call the the yield stress coefficient. Integrating over y, the volume of southern half of the ice is given by

$$V = \lambda L^{3/2} \tag{2.6}$$

Measurements from existing ice sheets suggest that the observed range of yield stresses is between $0.5 - 1.0 \times 10^5 Pa$ which means λ can reasonably take values between 2.65 and 3.74 (Weertman, 1976). Equation (2.5) describes the profile of ice sheets existing in today's climate reasonably well, and has been used by Weertman among others to study ice sheet growth and response to Milankovitch cycles (Weertman 1963, 1976).

The application of the perfectly plastic ice sheet assumption to time evolving prob-

lems is inappropriate on time scales shorter than a few thousand years. The perfectly plastic assumption implies that an ice sheet whose profile is given by Equation (2.5) instantaneously redistributes accumulation over the whole ice sheet in order to maintain that profile. We have also assumed that the bedrock adjusts instantly to changes in the overlying ice sheet. In reality, both of these processes have time scales of several thousand years (e.g. Paterson, 1994). Equation (2.5) is however a very useful qualitative description of the way a large body of ice will reorganize itself under its own weight.

2.1.1 Ablation rate

For the type of problem we are looking at, we do not need a very detailed representation of melting (ablation) at the ice sheet's surface. In reality ablation is the consequence of many complicated and competing processes (reviewed in Chapter 4). Here we employ a very straightforward parameterization of ablation rate which is essentially an adaptation of the work of Pollard (1980). Pollard took the ablation rate, where melting occurs, to be linearly related to monthly mean surface air temperature, T, and insolation, Q. This can be expressed as $ablation = max(0, a + bT + cQ)$. For the sake of simplicity we take Q constant at $334 W m^{-2}$, and subsume the cQ term into the constant a. Pollard's results suggest taking values of $a = 6 myr^{-1}$, and $b = 1.2 myr^{-1}$. These values are not well constrained by measurements from glaciers, reflecting the significance of local meteorological conditions other than temperature on the melting. Pollard's parameterization and similar forms have been used in models which have been used to simulate past and present ice sheets (e.g. Sanberg and Oerlemanns, 1983; Abe-Ouchi, 1993; Peltier and Marshall, 1995). This ablation rate formulation is essentially a simple version of a positive degree day (PDD) model (Braithwaite and Oleson, 1989), which is described in detail in Chapter 4. More sophisticated ablation treatments have a different melting rate for snow and ice (due to their different albedos), and allow for some refreezing within the snow pack. The PDD approach and that of Pollard are an improvement over earlier parameterizations (e.g Weertman, 1963), which did not allow for a temperature dependence in the ablation rate.

In order to pin down the total ablation over the year, we need to have a representation of the seasonal cycle in temperature at the southern margin of the ice sheet. An obvious choice to take is a sinusoidal cycle, $T = T_0 + T_a \sin(2\pi t)$, where T_0 is the annually

averaged temperature, T_a is the amplitude of the annual cycle and t is measured in years. However, because of the abrupt cut-off in melting if $T < -b/a$, the integration of the ablation rate over a year does not yield a particularly clean expression. We therefore choose to approximate the annual cycle by a square wave:

$$\begin{aligned} T &= T_0 + 2 \cdot T_a/\pi \text{ for } 0 \leq \mathrm{t} < 0.5 \\ T &= T_0 - 2 \cdot T_a/\pi \text{ for } 0.5 \leq \mathrm{t} < 1 \end{aligned} \tag{2.7}$$

The factor of $2/\pi$ preserves the same integral of temperature over each half year as the sinusoidal variation. Taking $T_s(y)$ to be the annually average surface temperature on the ice sheet at latitude y, then the melting model we choose is then given by the following conditions:

- if $T_s + 2T_a/\pi < -a/b$ then no melting occurs.
- if $T_s + 2T_a/\pi > -a/b > T_s - 2T_a/\pi$ then melting occurs for half a year at a rate $a + b(T_s + 2T_a/\pi)$.
- if $T - 2T_a/\pi > -a/b$ then melting occurs for half a year at a rate $a + b(T_s + 2T_a/\pi)$ and half a year at a rate $a + b(T_s - 2T_a/\pi)$.

If we take $T_a = 15^oC$ it means that the annually averaged temperature at y would have to exceed 5.5^oC for the third condition to apply. This does not happen in practice for reasonable values for the accumulation rate. Melting therefore occurs for half a year at most. Because of the choice of the annual temperature cycle, the snow line (the elevation above which there is no melting) will be lower than for a sinusoidal temperature cycle (which would allow for a few melting days at higher elevations), and the ablation rate at the ice margin will be slightly underestimated due to the greater number of melting days under the sine curve than the square wave. All melt-water is assumed to run off the ice sheet.

We can now calculate the total annual ablation over an ice sheet whose profile is given by Equation (2.5). Defining T_0 as the annually averaged temperature at the southern margin of the ice sheet, then T_s may be written:

$$T_s(y) = T_0 + \Gamma h(y) + \overline{T}_y \cdot y \tag{2.8}$$

where Γ is the atmospheric lapse rate (which we take as -6.5^oCkm^{-1}), and $\overline{T}_y$ is the meridional temperature gradient (taken to be $-6.0^oC/1000km$). Ablation only takes place within a couple of hundred kilometers of an ice sheet margin. Within this distance the ice sheet rises to a height of around $1.5km$. Therefore, in comparison to the vertical variation in temperature over the ablating zone, the meridional variation can be neglected.

By the above condition for melting, and using Equations (2.8) and (2.5), the snow line, y_0, will be where:

$$a + b(T_0 + 2T_a\pi + \Gamma\lambda(L - y_0)^{1/2}) = 0 \tag{2.9}$$

from which

$$L - y_0 = \left(\frac{a + 2bT_a/\pi + bT_0}{b\Gamma\lambda}\right)^2 \tag{2.10}$$

The width of the ablating zone is thus quadratic in the margin temperature. This a simple consequence of the parabolic shape of the ice sheet. The above equation also implies that the lower the yield stress of the ice sheet, the greater the ablation rate will be. An ice sheet with lower yield stress has more gently sloping margins, increasing the width of the ablating zone. For the values we have already stated and taking $T_a = 15^oC$, $T_0 = -5^oC$, and $\lambda = 3.4m^{1/2}$, Equation (2.10) gives the width of the ablating zone as $187km$. Letting ψ be the distance from the ice margin, and assuming that at all times and all locations on the ice sheet that $T_0 - 2T_a/\pi > -a/b$, (which may be checked a posteriori), then melting takes place for half a year only, and the total annual ablation, A, over the ice sheet can be found:

$$A = \frac{1}{2} \cdot \int_0^{\psi_0} (a + b(T_0 + 2T_a/\pi) - b\Gamma\lambda\psi^{1/2})d\psi \tag{2.11}$$

which, after some manipulation, can be written as

$$A = \frac{(a + 2bT_a/\pi + bT_0)^3}{6(b\Gamma\lambda)^2} \tag{2.12}$$

So, the total annual ablation is independent of the size of the ice sheet (except to the extent that the size of the ice sheet determines the temperature of the southern margin). This is because the ablation rate is dependent on the surface temperature which only depends on the distance from the edge of the ice sheet and not on its size. A is a cubic function of the ice margin temperature because of two effects: the ablation rate at any given point depends linearly on temperature, and, as noted above, the area over which that ablation is occurring increases as the square of the margin temperature. This strong functional dependence of A on T_0 suggests that the ice margin will be tied quite strongly to a particular isotherm: a change in accumulation rate in the interior of the ice sheet can be compensated for by only a small change in T_0, or equivalently, a small change in the southern margin of the ice sheet.

2.2 Equilibrium ice sheets

A relevant configuration for the late Pleistocene ice sheets is shown in Figure 2.1. The northern edge of both the Laurentide and Fennoscandian ice sheets were grounded at the edge of the Arctic Ocean, and any flux of ice across that margin calved into the ocean. Since all ice polewards of the peak of the ice sheet will flow northwards, all accumulation in the northern half of the ice sheet depicted in Figure 2.1 is assumed to calve into a polar ocean, which we take to lie polewards of $70N$. This is the approach of Weertman (1963), although he treated the ablation rate as independent of temperature, and dependent only on the area of the ice sheet below the snow line. If T_n is the temperature at the edge of the polar sea, then T_0 can be expressed as:

$$T_0 = T_n - 2\overline{T}_y \cdot L \tag{2.13}$$

Let $\overline{p}$ be the average accumulation rate in the interior. We might more properly take the accumulation rate at a specific latitude and height as proportional to the local saturation mixing ratio, which via the Claussius-Clapeyron equation (e.g. Emanuel, 1994), is an exponential function of surface temperature. However, the results presented below

show that the equilibrium halfwidth is in fact rather insensitive to the mean interior accumulation rate. In addition, because of the assumption of perfect plasticity, the ice sheet adjusts instantly everywhere and so the details of the accumulation distribution do not affect the ice sheet response.

In equilibrium the southern margin is determined by where there is a balance between accumulation rate over southern half of the ice sheet interior and the ablation rate at the southern margin. This gives a cubic equation for the equilibrium halfwidth of an ice sheet:

$$\overline{p}L = \frac{(a + 2bT_a/\pi + b(T_n - 2\overline{T}_y L))^3}{(b\Gamma\lambda)^2} \tag{2.14}$$

Figure 2.3 shows the accumulation rate and ablation rate curves with the parameter values already stated, plus $T_n = -15^oC$, $T_a = 15^oC$, $\lambda = 3.4m^{1/2}$, and $\overline{p} = 0.3myr^{-1}$. The intersection of the ablation curve with the horizontal axis is at positive L, so the two curves only intersect once for positive L and there is therefore only one equilibrium solution. However, the cubic nature of the ablation rate function does though allow for the possibility of more than one equilibrium solution, if we use a different set of parameters. If, for example, the accumulation rate is increased and T_n raised, then there can be two equilibrium solutions: for $\overline{p} = 1myr^{-1}$, and $T_n = -10^oC$, then the possible equilibrium halfwidths are around $40km$ and $530km$. The smaller ice cap is, however, unstable to small perturbations. The ice cap will either collapse to nothing or grow to the larger ice sheet, depending in the direction of the initial change.

As mentioned above, the halfwidth is relatively insensitive to changes in the accumulation rate. Figure 2.4 shows the equilibrium halfwidth as a function of mean interior accumulation rate for three different values of the yield stress coefficient, λ. For $\lambda = 3.4m^{1/2}$, a doubling of mean interior accumulation rate from $0.3myr^{-1}$ to $0.6myr^{-1}$ only changes the halfwidth by about 40%, or equivalently, T_0 changes by only 1.6^oC. Figure 2.4 also demonstrates that the size of the equilibrium ice sheet decreases as the basal yield stress decreases, a result which at first sight appears counter-intuitive. The lower the value of λ, the greater the halfwidth for a given volume of ice (see Equation (2.6)). We might therefore expect a more spread out equilibrium ice sheet. However, the slopes at the edge of the ice sheet decrease for decreasing yield stress and so the area of the ablating zone increases as the inverse square of the yield stress (Equation (2.10)), leading

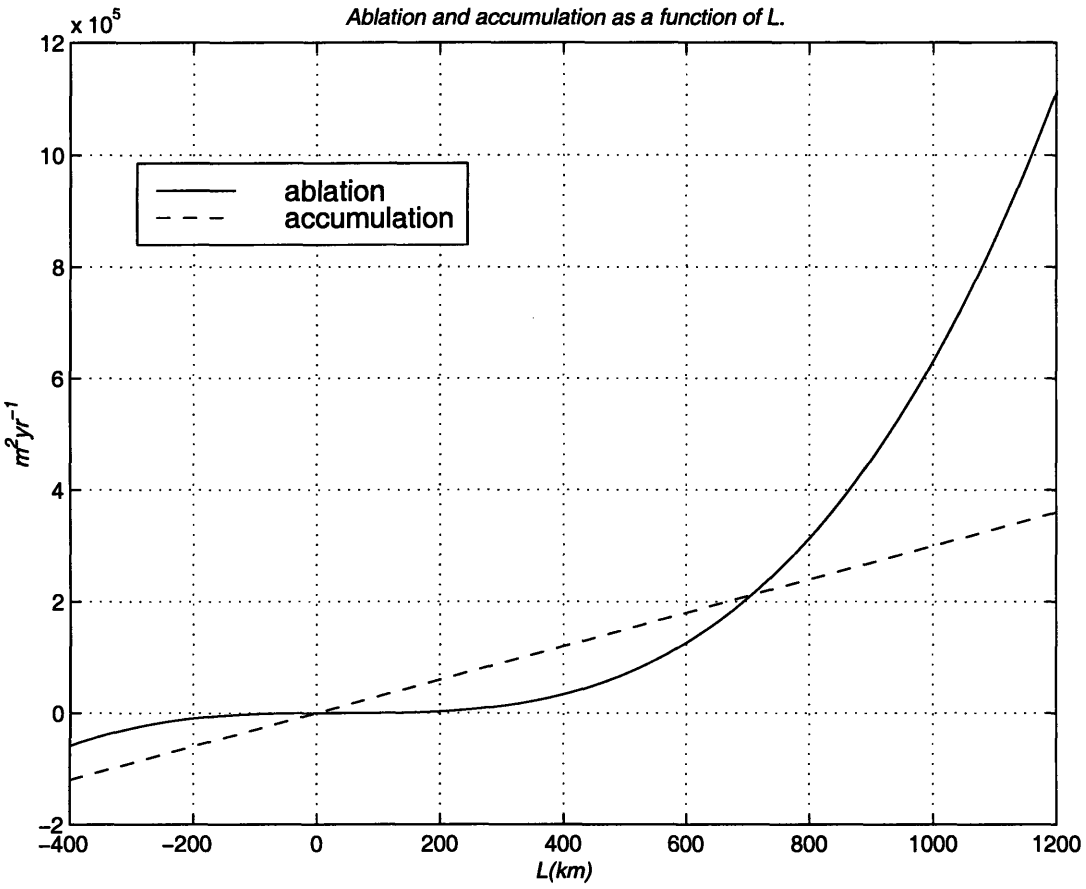

Figure 2.3: Accumulation and ablation rates integrated over the ice sheet (m^2yr^{-1}) as a function of ice sheet halfwidth, L. The negative values of L have no physical meaning and are plotted to show the functional dependence of the mass budget. The accumulation is linear in L because a constantant average accumulation has been defined.

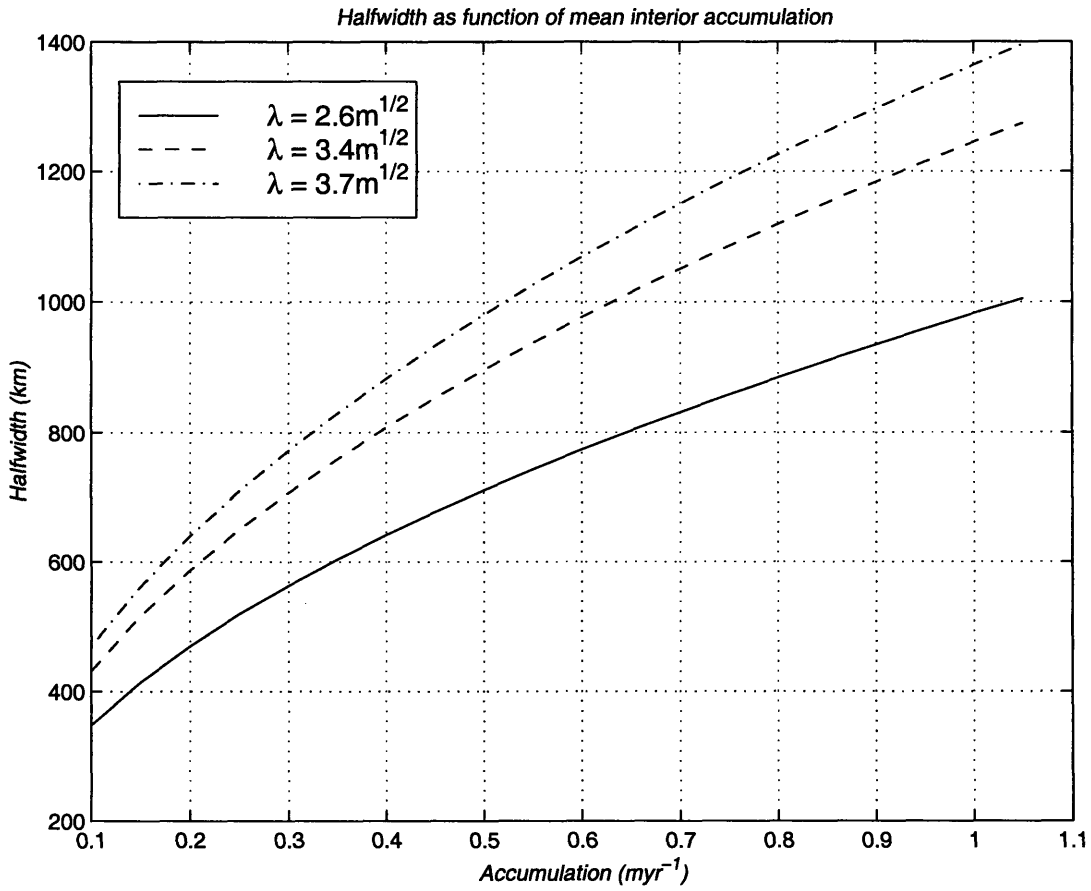

Figure 2.4: Equilibrium halfwidth as a function of mean accumulation rate, for different value of the yield stress.

to a much increased ablation rate. Therefore a perfectly plastic ice sheet has a smaller equilibrium profile on a soft bed, or a base which is temperate (i.e. a mixture of ice and water), than if it has a frozen bed.

2.2.1 The effects of a stationary wave

As reviewed in the introduction, the great continental ice sheets of the last Pleistocene were large enough to be significant obstacles to the westerly flow at midlatitudes. In today's climate the Tibetan Plateau and the Rockies, which are of equivalent size to the continental ice sheets, force large scale stationary patterns in the time mean winds and temperatures, as the flow is forced to deviate around the topography. An obvious feedback on the ice sheet is created by including the effects of a stationary wave. The

changing patterns of temperature and winds due to the stationary wave alter the distribution of precipitation and ablation over the ice sheet (in Equation (2.12)). These altered distributions will, over time, change the shape of the ice sheet itself.

The classic solution for a planetary scale topographically forced stationary wave in midlatitudes is a high pressure ridge over the western slopes of the forcing mountain and a low pressure trough over the eastern slopes. The amplitude and phase of the wave depend on the details of the zonally averaged climate, as well as the size and location of the mountain. But as a generality, the western slopes of the mountain experience warmer temperatures than the zonally averaged basic state, and the eastern slopes colder temperatures. In the linear regime the magnitude of these temperature perturbations is proportional to the height of the mountain. Cook and Held (1988) simulate the LGM winter stationary wave pattern using a GCM, and find that the temperature perturbations in the GCM can be explained largely by the linear response to the topographic forcing of the Laurentide ice sheet. The nature of the stationary wave solution for a topographic feature the size of an ice sheet is explored in much more detail in the next chapter.

The two-dimensional model introduced in this chapter can be used to investigate the effects of a stationary wave if we allow for some further approximations. The assumption has to be made that the longitudinal flux of ice is a negligible part of the mass budget. In other words, the ice adjusts to the climate by flowing meridionally. This will clearly hold best on a longitudinally broad ice sheet, and away from the latitudinal boundaries where the effects of calving into an ocean would be significant. For an ice sheet like the Laurentide, which is approximately as wide as it is long, the longitudinal adjustment could be significant.

In studying the response to stationary waves in this section, we consider the model to be a north-south slice through the ice sheet at a particular longitude. The effect of the topographically forced stationary wave at that longitude can then be included in the model equations. Due to the uncertainty about any east-west spreading of the ice sheet, the results are best thought of as the upper limit on the latitudinal response of the ice sheet to the stationary wave feedbacks. The extent to which the conclusions drawn here can be carried over to the three-dimensional case depends on the phase and magnitude of the stationary wave generated by the ice sheet.

We model the effect of the stationary wave on the ice sheet by assuming that it creates

a temperature perturbation over the ablating zones which is linearly proportional to the maximum height of the ice sheet, h_{max}:

$$T'_{sw} = \gamma h_{max} = \gamma \lambda L^{1/2} \tag{2.15}$$

The actual temperature perturbation induced in response to the ice sheet will also depend on the east-west extent of the ice sheet, which we do not account for here. However, all we are trying to do at this point is qualitatively include the effect that the topographic influence of the ice sheet might make the surrounding climate warmer or colder. A linear dependence is the easiest way to introduce the effect.

For our purposes, the magnitude of γ need only be approximate. For a $2km$ mountain a reasonable amplitude for a stationary wave would be a change in the $1000mb - 500mb$ thickness of $100gpm$, corresponding to a change in the mean temperature in the lower troposphere of 5^oC (consistent with Figure. 1.4). Therefore we consider two values of γ of $\pm 5^oC/2km$, representing the effects of both a warm temperature ridge on the western slopes of the ice sheet, and a cold temperature trough on the eastern slopes. Obviously the stationary wave temperature field varies smoothly between these values over the real ice sheet. The extension of the results for other sections of the ice sheet is direct. For ease of notation we call the cold temperature trough the CTT feedback, and the warm temperature ridge the WTR feedback.

It is possible that one or other of the feedbacks could dominate over the full three-dimensional ice sheet, depending on the phase of the stationary wave. If, for example, the cold temperatures extended over most of the ice sheet then only a small region will feel the WTR feedback. In this case we then might expect that the CTT feedback would determine the behavior of the whole ice sheet.

T'_{sw} can be incorporated directly into the ablation rate parameterization in Equation (2.12), and it is straightforward to solve for the equilibrium halfwidths. Figure 2.5 shows the results for the different stationary wave feedbacks as a function of mean interior accumulation. λ was taken to be $3.4m^{1/2}$. Otherwise all the same parameters were kept as for Figure 2.4. The effect of the CTT feedback is to more than double the halfwidth for all accumulation rates considered. For an ice sheet of halfwidth $1000km$, which has a height of $3.4km$, the CTT feedback gives cooling of 8.5^oC (Equation (2.15)). Using the meridional temperature gradient, this means the same isotherm is located $1400km$

further south (a halfwidth change of $700km$). There is also the additional effect of extra accumulation over the extended ice sheet, which pushes the margin even further south. The WTR feedback is equally striking; the size of the ice sheet is strongly limited to only a few hundred kilometers. The ice sheet is prevented from pushing very far south by the warm temperatures that the stationary wave generates. An ice sheet of halfwidth $200km$ has a height of $1.5km$, so the warming effect of the stationary wave is already quite pronounced at these scales. The two-dimensional results for such small ice sheets have to be treated skeptically: for ice sheets which are of limited north-south extent, the magnitude of the induced stationary wave will depend mostly on the ice sheets east-west extent (the more extended it is, the larger the stationary wave). The north-south profiles of the ice sheets, using $\overline{p} = 0.3myr^{-1}$, are shown in Figure 2.6, illustrating the dramatic differences in the ice sheet size and volume, depending on which of the feedbacks is included.

The above results only take into account the effect of the stationary wave on temperatures. There will also be some change in the moisture supply to the interior of the ice sheet. We expect a high pressure ridge to bring warmer, moist air up onto the western sector of the ice sheet, and the upslope flow would create enhanced precipitation on the western slopes. The consequent increased accumulation rate in the western interior of the ice sheet would lead to more ice spreading southward and would tend therefore to partially off-set the higher ablation rate at the southern margin due to the the warm temperatures there. Conversely on the eastern sector of the ice sheet where dry northerly air and downslope flow predominate, we would expect to find decreased precipitation. This would again tend to counteract the effect of the stationary wave temperatures. These moist processes are not easy to include well in the two-dimensional formulation, but from the results shown in Figure 2.4, we expect their effects to be secondary: the ice margin is relatively insensitive to interior accumulation rate and is more or less tied to a particular annually averaged isotherm. This would suggest that the temperature effects of the ice sheet induced stationary wave will dominate over the precipitation effects.

2.3 Time dependence of ice sheets

There are some important insights to be gained from looking at how the two-dimensional model attains equilibrium or responds to imposed climate changes. The

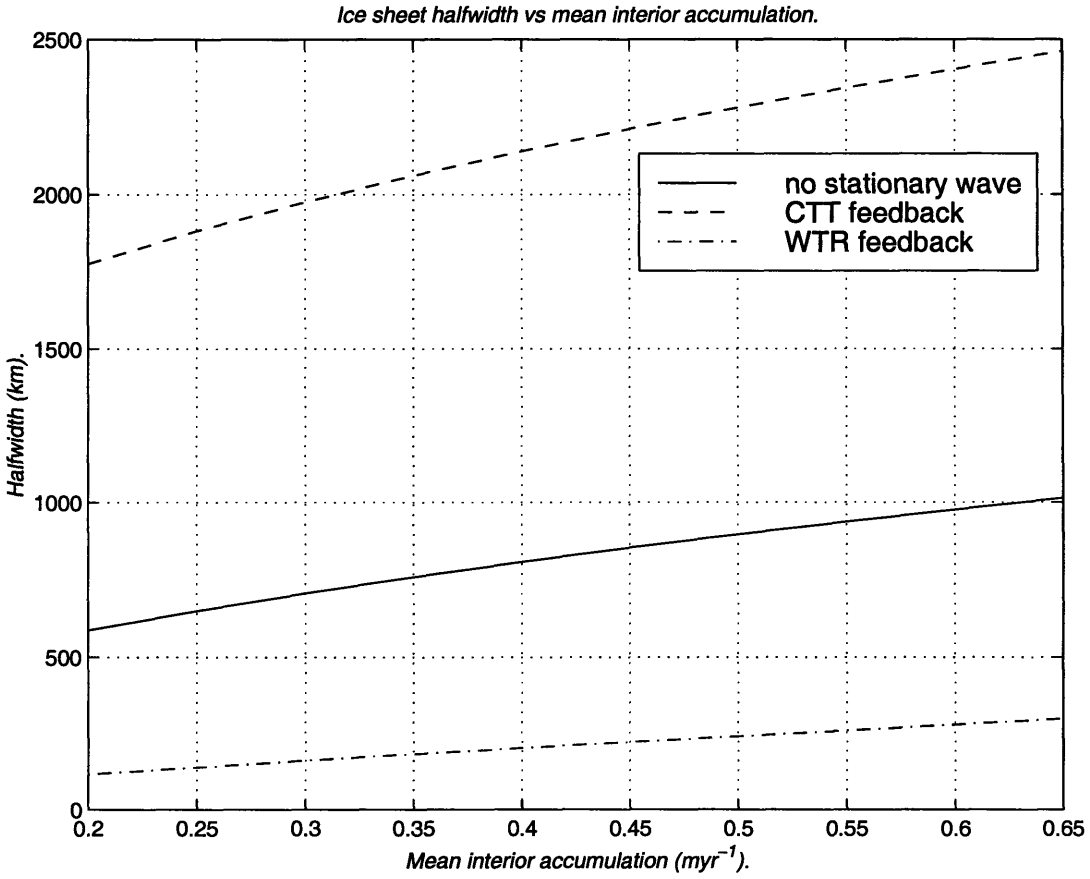

Figure 2.5: Equilibrium halfwidth as a function of mean interior accumulation for runs including stationary wave feedback described in text. CTT is the cold temperature trough feedback, WTR is the warm temperature feedback.

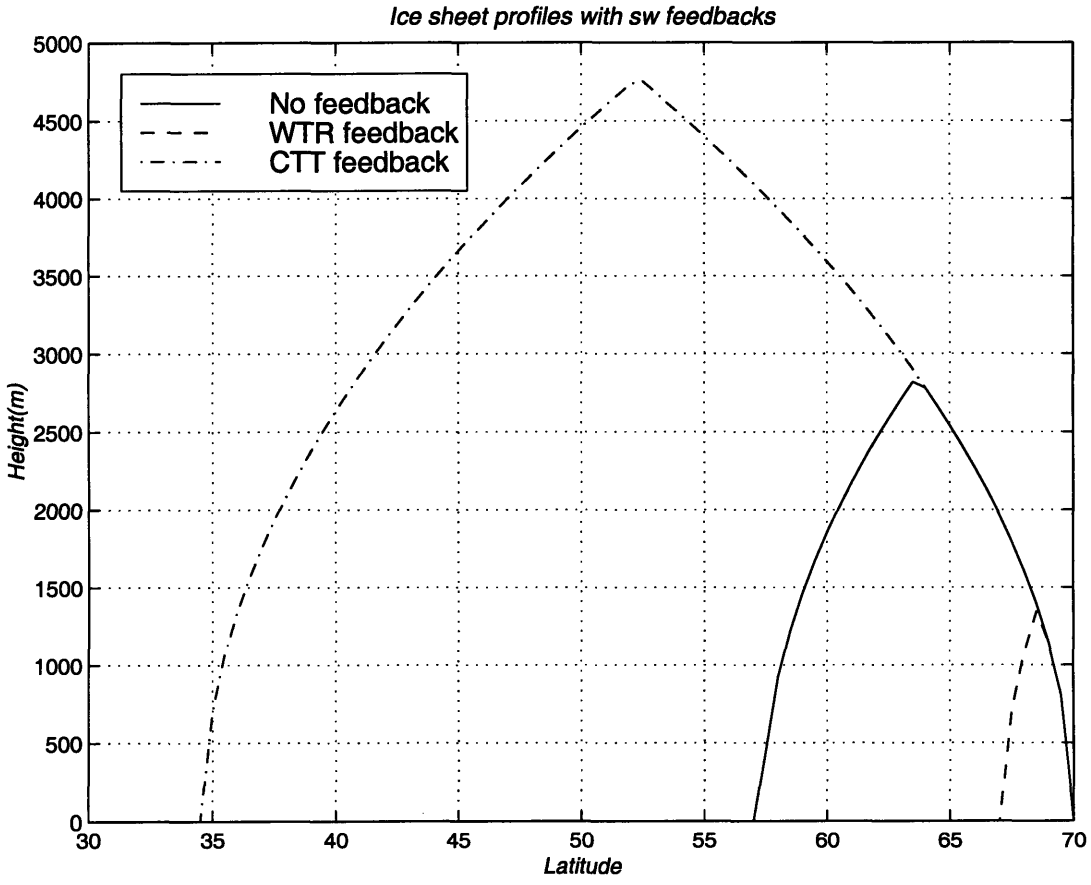

Figure 2.6: North-south profiles for ice sheets with the different feedbacks. The mean accumulation rate is set at $0.3myr^{-1}$. Feedbacks labeled as for Figure 2.5.

model is readily expressed in time dependent form:

$$\frac{dV}{dt} = \frac{3}{2}\lambda L^{1/2}\frac{dL}{dt} = \text{accumulation rate} - \text{ablation rate} \tag{2.16}$$

where accumulation and ablation refer to the integrated totals over the ice sheet. Hence for an active ice sheet with both accumulating and ablating regions,

$$\frac{dL}{dt} = \frac{2}{3\lambda}L^{-1/2}\left[\overline{p}L - \frac{1}{6}\frac{(a + 2bT_a/\pi - 2b\overline{T}_y L + bT_n - b\gamma\lambda L^{1/2})^3}{(b\Gamma\lambda)^2}\right] \tag{2.17}$$

Note that we still assume that at all times the ice sheet is described by its equilibrium profile; that is, the process of adjustment to changes in accumulation is instantaneous. In talking about deviation from equilibrium we really mean that the ice sheet is not in equilibrium with the surrounding forcing climate, or in other words, the growth rate dL/dt is non-zero.

If the ablation rate term is neglected in Equation (2.17) (the second term inside the square brackets on the right hand side), then the time to reach halfwidth L can be shown to be:

$$t = 3\lambda/\overline{p}(L(t)^{1/2} - L(t=0)^{1/2}) \tag{2.18}$$

It is only as the ice sheet approaches equilibrium size that the ablation at the southern margin begins to be significant (Weertman, 1963). Equation (2.18) gives a useful rule of thumb, therefore, for the growth time scale of ice sheets. More generally it means that the ice sheet growth time is determined by how long it takes for sufficient snow to accumulate, rather than by any balance with the ablation. This conclusion is restricted to ice sheets where the growth is not limited by the rate of cooling of the climate.

Equation (2.17) was integrated forward in time from an ice sheet of initial halfwidth $200km$, without including the stationary wave term in the ablation rate (i.e. setting γ equal to zero). Values of $\lambda = 3.4m^{1/2}$ and $\overline{p} = 0.3myr^{-1}$ were used (and also for all ice sheets hereafter in this chapter). The growth curve is shown in Figure 2.7. Equation (2.18) would give a growth time of $13.2kyr$ to get to the final size of $700km$. After $13kyr$, the halfwidth is actually about $550km$. The final size of $700km$ is reached after about $25kyr$. These numbers are consistent with Weertman's time scale of between

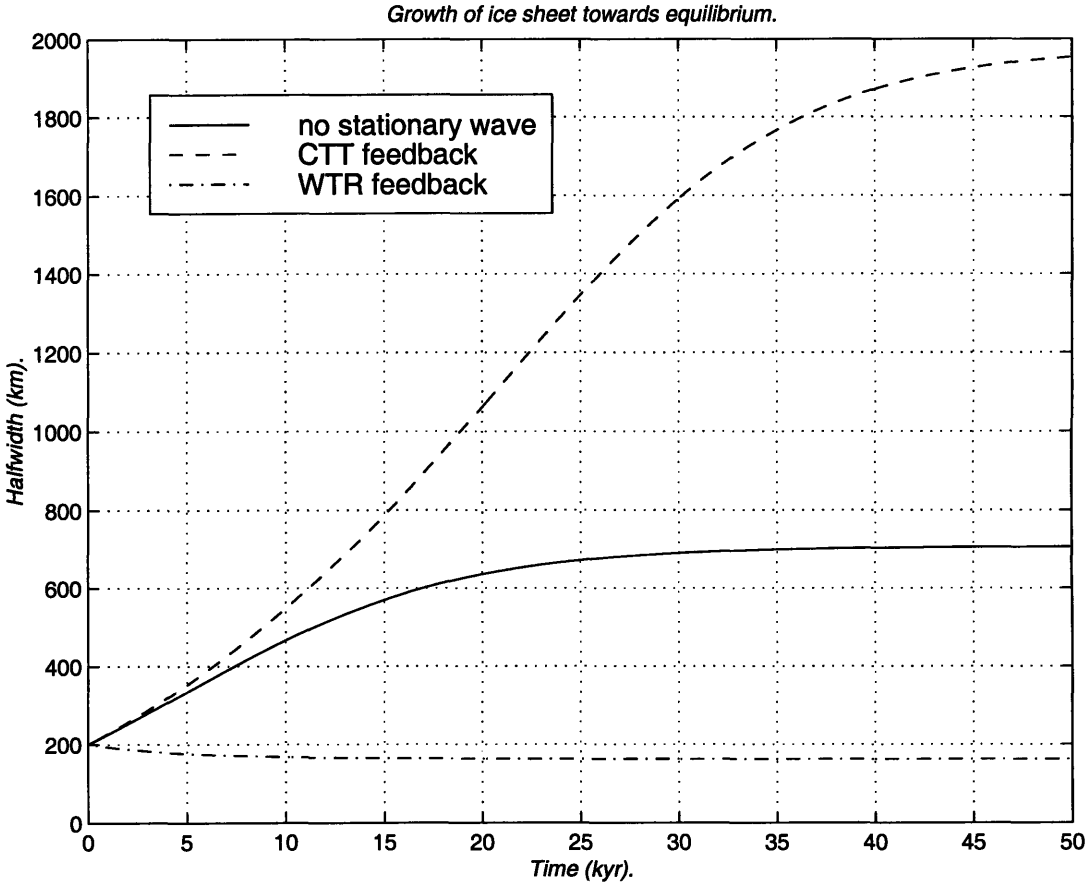

Figure 2.7: Growth of ice sheets from an initial L of $200km$. Feedbacks labeled as for Figure 2.5.

$15kyr$ and $30kyr$ for an ice sheet to develop (Weertman, 1963).

The inclusion of the stationary wave feedback in the ablation rate has a marked effect on the growth of the ice sheet (Figure 2.7). The warm temperature ridge causes the ice sheet to actually shrink a little but the initial size is close to its equilibrium value, which it attains quickly. The CTT feedback leads to a much larger equilibrium size and it takes about $45kyr$ before the ice sheet gets close to equilibrium. In contrast to the no stationary wave case, this is enough time to see that the growth rate increases slightly with time, as given by Equation (2.17). The $45kyr$ time scale to equilibrium is due mainly to the size of the ice sheet that forms for the parameters we have chosen here. The inclusion of the stationary wave changes the time taken to attain equilibrium by changing what that equilibrium size is. The growth is determined by the length of time it takes for sufficient accumulation to produce a given ice sheet. This can be seen from

the growth rates over the first few thousand years for the no stationary wave and CTT feedback cases. Since their sizes differ so little at that stage, the integrated accumulation rates are very similar, and the growth rates are therefore also approximately equal.

2.4 Stability of the ice sheet

We can ask how the inclusion of a stationary wave might affect the stability of an ice sheet. For instance, paleodata show Heinrich events in which large deglaciations have occurred in relatively short intervals of time (e.g. Crowley and North, 1991), and the terminations at the end of most of the ice ages take place in only a few thousand years. Both of these facts suggest that significant collapses of the ice sheets are possible on short time scales. These events are generally attributed to changes in the bottom boundary conditions of the ice sheet (MacAyeal, 1993), or to positive feedbacks on the ablation process such as melting into pro-glacial lakes (Pollard, 1983), or snow ageing (Gallee et al., 1992). We can use the two-dimensional model to investigate how the inclusion of a stationary wave response to the collapsing ice sheet might influence the decay. The initiation of the great ice sheet is also an unresolved problem. General circulation models (GCMs) and energy balance models (EBMs) are generally unable to reproduce the initiation of the last ice age cycle at $122kbp$ by just changing the insolation at the top of the model and the atmospheric CO_2 concentration. There is enough freedom in the behavior of an ice sheet-induced stationary wave to allow for the possibility of a positive feedback on the ice sheet growth. As the ice sheet grows, the induced stationary wave might modify the surrounding climate in a way that allows the ice sheet to grow faster than it would in the absence of the stationary wave. Again, we can use the simplified two-dimensional model to explore the range of possibilities.

For a fixed climate, Figure 2.6 shows that the inclusion of a stationary wave feedback changes what the equilibrium halfwidth is. This is not true though for all possible climates. We shall show below that the inclusion of the CTT feedback prevents even the existence of an equilibrium ice sheet for some climate changes. In general however, if we take an ice sheet initially in equilibrium and ask how it will evolve if small climate changes are imposed, we can say that the ice sheet will tend towards a new equilibrium, and that what that new equilibrium is will depend both on whether a stationary wave feedback is included, and what the strength of that feedback is. Because the strength

of the stationary wave feedback goes as $L^{1/2}$, the power of the feedback to change the climate at the southern margin decreases as L increases. Including the feedback will not, therefore, lead to runaway growth. In talking about the stability in this section, we refer to changes to the time tendency of the ice sheet. If the growth rate is increased by the inclusion of a feedback we say it has been destabilized; similarly, if the growth rate is decreased, it is stabilized.

For the case of the CTT feedback, which we expect over the eastern slopes of an ice sheet, the effect of the stationary wave would appear to be destabilizing. The southern margin there is maintained partly by the colder temperature caused by the stationary wave. For example, in response to a climate warming, the ice would begin to melt, thereby reducing the height of the ice sheet. This in turn reduces the amplitude of the cold temperatures due to stationary wave, and therefore increases the amount of melting. Likewise, a climate cooling will lead to an enlargement of the ice sheet, which will increase the stationary wave amplitude, creating more cooling over the region, and further increasing the ice sheet size.

On the western slopes, a WTR feedback will tend to make the ice sheet resist changes in climate: a retreat (growth) of the ice reduces (increases) the height of the ice sheet and the amplitude of the stationary wave. That implies a cooling (warming), which is in opposition to further changes in ice sheet size.

The stability of ice sheets with and without the stationary wave feedbacks can be tested using the two-dimensional model. As mentioned earlier, the application of the perfectly plastic ice sheet model cannot really be justified on time scales of less than a few thousand years. Therefore the measure we take for the stability of the ice sheet is not the initial growth rate at the time of an imposed climate change, but the difference in halfwidth after $3kyr$ (i.e. a $3kyr$ integration of the growth rate). In this approach we are again neglecting the effect of the possible longitudinal redistribution of ice.

We compare three runs for ice sheets starting from equilibrium and with the same initial size. In the first run, there is no stationary wave feedback. A 5^oC warming is imposed and the model integrated forward in time. The change in the halfwidth after $3kyr$ is noted. In the second and third runs the stationary wave is included as a WTR feedback and a CTR feedback respectively. When the feedbacks are included, the climate (i.e. T_n) in those runs has to be adjusted so as to be able to start from equilibrium with the same initial ice sheet size as for the first run. Again a 5^oC is imposed, and the

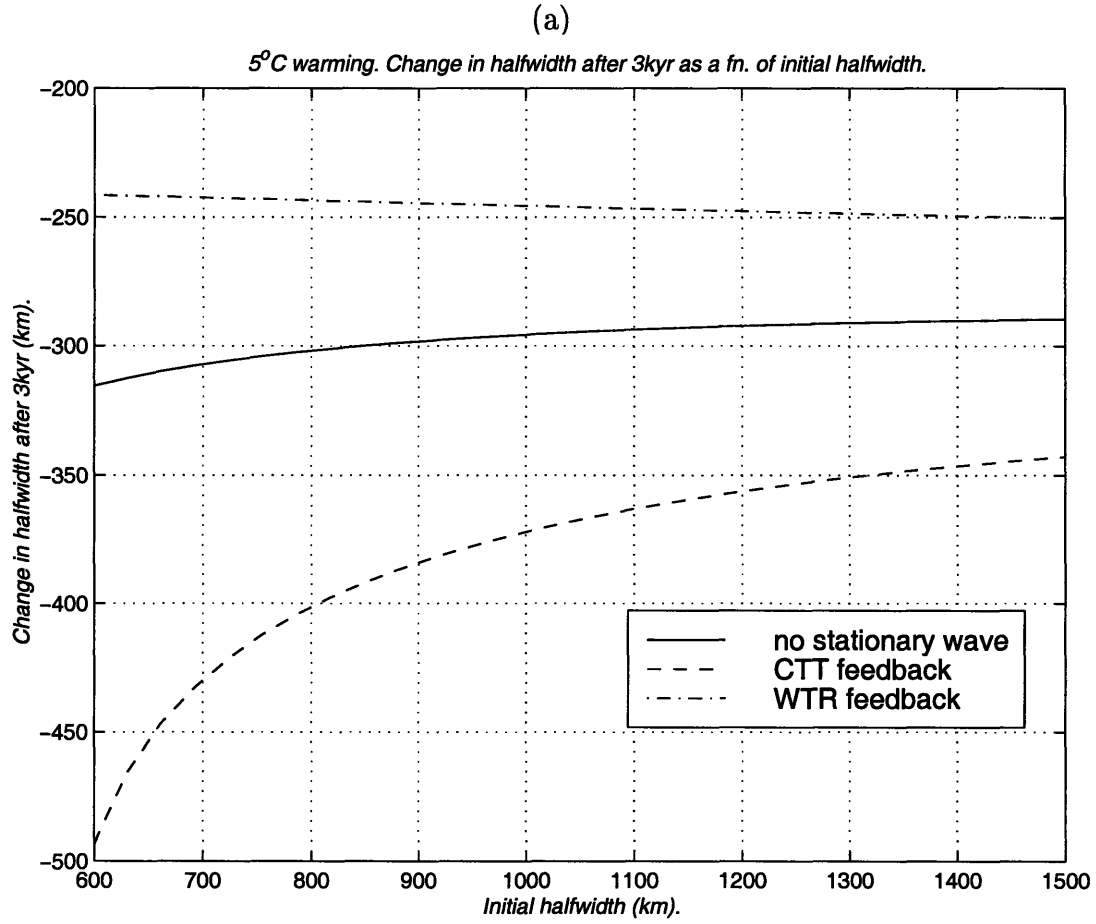

Figure 2.8: Response of ice sheets to imposed climate change as a function of initial halfwidth. (a) a 5^oC warming, and (b) a 5^oC cooling. Graph plots change from the initial size after $3kyr$. Ice sheets start from same equilibrium size. The climate is adjusted so all ice sheets start from equilibrium with the same initial size. Feedbacks labeled as for Figure 2.5.

changes in the halfwidth of the ice sheet are compared after $3kyr$.

The results are shown in Figure 2.8a as a function of initial ice sheet size. For all starting sizes the change after 3kyr is greater for the CTT feedback and smaller for the WTR feedback, consistent with expectations from the above reasoning.

The CTT feedback has destabilized the ice sheet. For a large ice sheet the effect is proportionately quite small; about $50km$ difference over $3kyr$ in the edge of the ice sheet. The size of the difference increases however, as the initial size decreases. For an initial halfwidth of $600km$, the ice sheet has almost completely disappeared after $3kyr$ when the CTT feedback is included, whereas without any feedbacks the halfwidth is still

(b)

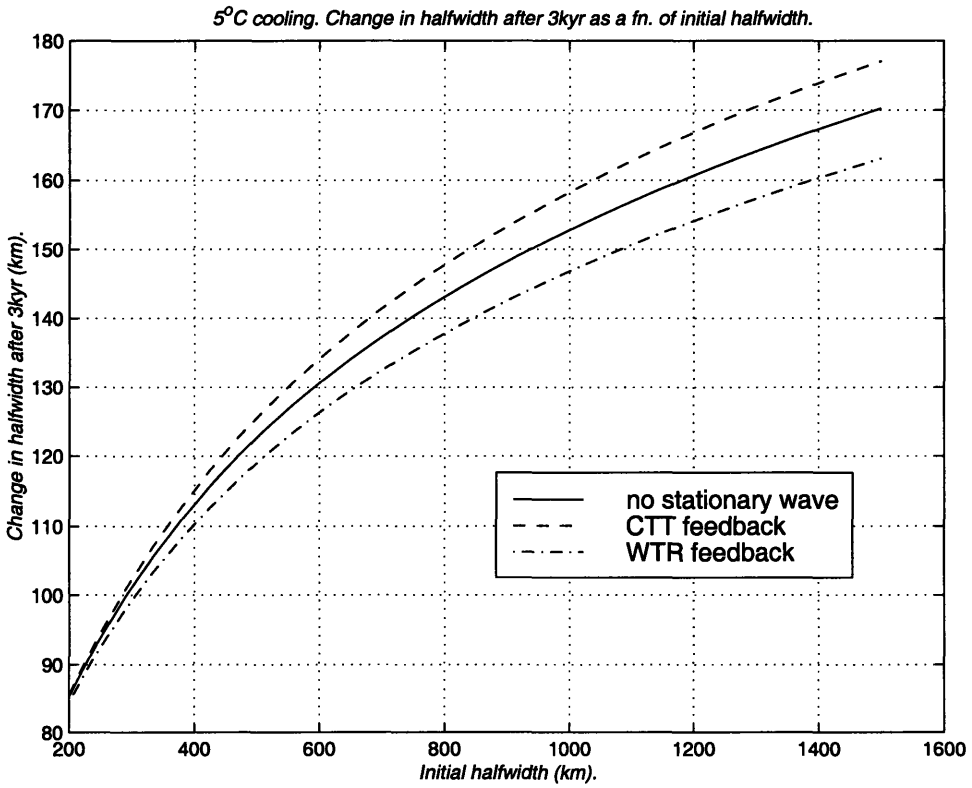

Figure 2.8, continued.

around $300km$ after that time. Figure 2.8b shows the results for a cooling of 5^oC instead of a warming. The effect of the feedbacks are relatively small although qualitatively in the expected direction. The small difference between the different feedbacks shows that the growth of the ice sheet is basically limited by the accumulation rate.

The results in Figure 2.8 suggest that because of the CTT feedback, smaller ice sheets ($L < 400km$) may be less able to withstand prolonged warmings of a few thousand years. Conversely, the WTR feedback might allow an ice sheet to resist a temporary warming and survive until the temperature fell again. It is not possible to say to whether this could happen in practice without a three-dimensional model to see how the ice redistributes itself longitudinally. Nevertheless we can demonstrate this effect; Figure 2.9 shows runs made for the three cases (no feedback, CTT feedback, WTR feedback). All three runs start with an ice sheet of halfwidth $500km$ in equilibrium. As with the stability runs, an adjustment is made to T_n in the two runs with feedbacks to ensure that each ice sheet starts off in equilibrium. At $t = 1kyr$, the climate is warmed by 5^oC and held steady until $t = 3kyr$, when it is returned to its original value. For the no feedback case, the ice sheet undergoes strong melting, and reaches a minimum halfwidth of around $250km$. When the climate returns to its original state at $3kyr$, the ice sheet slowly grows back towards its original size. For the WTR feedback case, the ice sheet is stabilized to change. The reduction in size is less than for no feedback, and the ice sheet returns faster towards it equilibrium size, consistent with the notion that the ice sheet is being stabilized. For the CTR feedback there is very strong ablation between $1kyr$ & $3kyr$. After the climate returns to its previous state however, the ice sheet is now too small to be sustained. This is because the stationary wave that it creates is now no longer large enough to support sufficiently cold temperatures for the ice sheet to exist. Therefore the ice sheet continues to collapse down towards zero. In this CTT case, a further cooling of around 7^oC is necessary to initiate a new ice sheet. This would lead to a sort of hysterisis loop in the ice age cycle with a large cooling required to get the ice sheet to initiate, and a smaller temperature increase needed to bring about a collapse.

Summary

The two-dimensional modeling results have illustrated some basic features of ice sheet behavior. The ice sheet exists because of a balance between accumulation in the interior

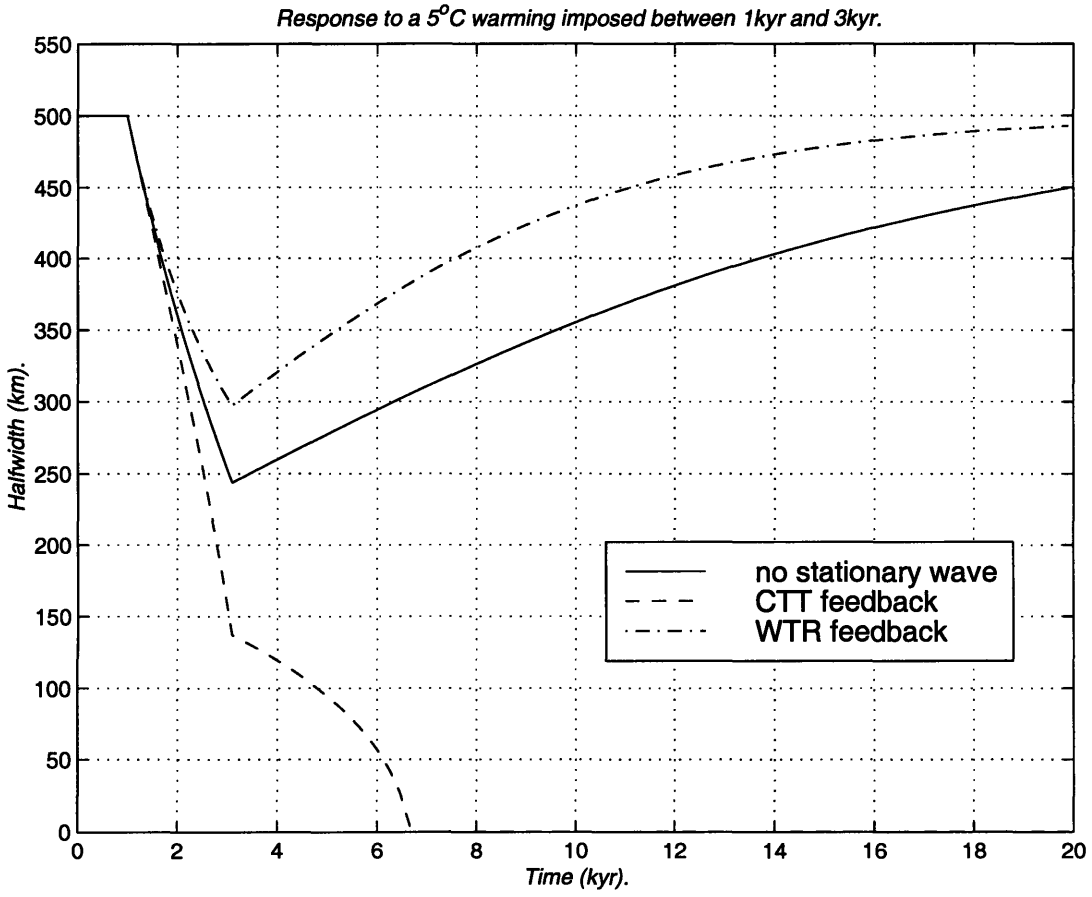

Figure 2.9: Response of ice sheets to temporary warming. A 5^oC is imposed between $1kyr$ and $3kyr$. The climate is adjusted so all ice sheets start from equilibrium with the same initial size. Feedbacks labeled as for Figure 2.5.

and melting at the margin. The size of the ice sheet is quite insensitive to interior accumlation because of the strong dependence of the ablation on the temperature of the southern margin.

We have also shown that the changes to the atmospheric flow induced by the ice sheet can potentially have a large effect on its size: an induced stationary wave that creates cold temperatures at the southern margin increases the ice sheet size considerably. The stationary wave also affects the time dependent behavior of the ice sheet.

The conclusions reached in this chapter must be weighted by the simplicity of the two-dimensional modeling. We have not included any variation in the precipitation, and the behavior of the coupled stationary wave – ice sheet system (especially the time dependent behavior) is dependent on the rather arbitrary functional choice for the feedback. The rest of this thesis takes a more realistic (and complex) modeling approach, using these results as suggestive of possible regimes of behavior. In the next chapter, we examine the atmospheric response to a characteristically shaped ice sheet and assess the relevance of the feedbacks presented here.

Chapter 3

The stationary wave response to an ice sheet

This chapter explores how the atmosphere responds to the presence of an ice sheet. The main tool we use for this is a linear, quasigeostrophic, channel stationary wave model. Such an approach has some limitations and we aim to emphasize how the response might change in a more comprehensive treatment. The model shows that a topographic obstacle the size of the Laurentide induces a high pressure, anticyclonic circulation over it. The temperature perturbations associated with the altered atmopsheric flow are of the order of 10^oC, consistent with observations (Figure 1.4), and also with modeling results (Cook and Held, 1988).

We discuss how a nonlinear calculation might modify the linear solution and how plausible changes in the atmospheric basic state (the zonally averaged time-mean atmosphere) change the atmospheric response. We find that changes in the response can largely be understood through the changes that are made to the quasigeostrophic potential vorticity gradients. We also find that the low level temperature perturbations in our model are sensitive to the choice of the boundary layer thermal damping time.

Observations of the current climate show that the air temperatures immediately above the ice sheets in Greenland and Antarctica are generally warmer than the underlying surface temperatures. On average therefore, the air above an ice sheet is being cooled. We look at the atmospheric response to a realistic cooling imposed over the ice sheet. We conclude, in agreement with Cook and Held (1988), that the thermal forcing

creates a much smaller atmospheric response than the topographic forcing.

3.1 Stationary wave model equations

We first derive the equations used in the stationary wave model. Although the model we use is very similar to that in Lindzen (1994), and the derivation of the equations is only slightly different from standard ones in textbooks (e.g. Pedlosky, 1992), it is worth reviewing here because some of the behavior of the stationary wave model that is relevant to the ice sheet problem is most clearly seen from an inspection of the equations. In particular, we use them to explain why different thermal and momentum damping times in the boundary layer proves to be very important to the model response.

The atmospheric fields are linearized about a zonally symmetric basic state that is independent of latitude. An overbar denotes a basic state field and a prime denotes the perturbation fields. That is to say, $u(x,y,z) = \overline{U}(z) + u'(x,y,z)$, and $\phi(x,y,z) = \overline{\phi}(z) + \phi'(x,y,z)$, where u is the zonal wind, and ϕ is the geopotential height. x and y are the eastward and northward distances respectively, and z is a scaled log-pressure coordinate given by

$$z = -Hln(p/p_0), \tag{3.1}$$

where H is a constant which is chosen to be close to the atmospheric scale height, and p_0 is a reference pressure.

Consistent with quasigeostrophic scaling, the vorticity equation can be written as

$$\frac{D_G}{Dt}\left(\frac{{\nabla_h}^2\phi}{f_0} + f\right) + \frac{1}{\tau_m(z)}\frac{{\nabla_h}^2\phi}{f_0} + f_0\nabla_h \cdot \vec{u} = 0. \tag{3.2}$$

f is the Coriolis parameter where $f = f_0 + \beta y$. β is the planetary vorticity gradient (assumed linear in a β-plane approximation). Linear damping has been included on relative vorticity with a time scale of τ_m, which is allowed to be a function of height. ∇_h is the gradient operator containing horizontal derivatives only, $\vec{u}$ is the horizontal velocity vector, and D_G/Dt is the quasigeostrophic total derivative, given by

$$\frac{D_G}{Dt} = \frac{\partial}{\partial t} + u_G \frac{\partial}{\partial x} + v_G \frac{\partial}{\partial y}. \tag{3.3}$$

Here u_G and v_G are the geostrophic velocities: $u_G = \overline{U} - 1/f_0 \partial\phi'/\partial y$, and $v_G = 1/f_0 \partial\phi'/\partial x$. We also need the continuity equation:

$$\nabla_h \cdot \vec{u} + e^{z/H} \frac{\partial}{\partial z} \left(e^{-z/H} w \right) = 0. \tag{3.4}$$

$w = \frac{dz}{dt}$ and is the vertical velocity in the vertical coordinate that we are using. The first law of thermodynamics gives the thermodynamic equation:

$$\frac{D_G}{Dt} \left(\frac{\partial\phi}{\partial z} \right) + wN^2 = -\frac{1}{\tau_r} \frac{\partial\phi'}{\partial z} + \frac{g}{c_p T} \dot{Q} \tag{3.5}$$

T is the basic state temperature, N^2 is the square of the Brunt-Vaisala frequency, g is the earth's gravitational acceleration ($= 9.81 ms^{-2}$), and c_p is the specific heat capacity of air at constant volume ($= 1004 J^o C^{-1} kg^{-1}$). Linear damping is applied to the temperature perturbation. The temperature relaxes back to the basic state with a time scale, τ_r, which, like the momentum damping time scale, is allowed to be a function of height. $\dot{Q}$ is the rate of heating per unit volume.

Linear damping is a crude representation of the physics of the exchange of sensible and latent heat between the atmosphere and the surface, and we discuss what linear damping means in this context in Section 3.1.3.

The Brunt-Vaisala frequency is given by

$$N^2 = \frac{g}{T} \left(\frac{dT}{dz} + \frac{g}{c_p} \right). \tag{3.6}$$

We will also need to make use of both the hydrostatic relationship

$$\frac{\partial\phi}{\partial z} = \frac{RT}{H} \tag{3.7}$$

where R is the gas constant for air ($= 287 J kg^{-1o} C^{-1}$), and also the thermal wind balance:

$$\frac{\partial u}{\partial z} = -\frac{R}{f_0 H}\frac{\partial T}{\partial y} \tag{3.8}$$

For the sake of clarity, we will develop the equations without including the diabatic heating term, $\dot{Q}$, but it is straightforward to carry it through with the rest of the calculations. Equation (3.5) may be rearranged as an expression for w. Combining that expression with Equations (3.4) and (3.2) gives:

$$\frac{D_G}{Dt}\left(\frac{{\nabla_h}^2\phi}{f_0} + f\right) + \frac{1}{\tau_m}\frac{{\nabla_h}^2\phi'}{f_0} + f_0 e^{z/H}\frac{\partial}{\partial z}\left[\frac{e^{-z/H}}{N^2}\left(\frac{D_G}{Dt}\left(\frac{\partial\phi}{\partial z}\right) + \frac{1}{\tau_r}\frac{\partial\phi'}{\partial z}\right)\right] = 0 \tag{3.9}$$

In quasigeostrophy, it is possible to permute the D_G/Dt and the $\partial/\partial z$ operators, which means the above can be rearranged as

$$\frac{D_G}{Dt}\left[\frac{{\nabla_h}^2\phi}{f_0} + f + f_0 e^{z/H}\frac{\partial}{\partial z}\left(\frac{e^{-z/H}}{N^2}\frac{\partial\phi}{\partial z}\right)\right] + \frac{1}{\tau_m}\frac{{\nabla_h}^2\phi'}{f_0} + f_0 e^{z/H}\frac{\partial}{\partial z}\left(\frac{e^{-z/H}}{N^2}\frac{1}{\tau_r}\frac{\partial\phi'}{\partial z}\right) = 0 \tag{3.10}$$

This is the full quasigeostrophic potential vorticity (PV) equation. For stationary wave solutions we set $\partial/\partial t = 0$. We now linearize the equation by expanding out the quasigeostrophic total derivative and taking only first order terms. This gives the linear PV equation:

$$\overline{U}\frac{\partial q'}{\partial x} + v'\overline{q}_y + \frac{1}{\tau_m}\frac{{\nabla_h}^2\phi'}{f_0} + f_0 e^{z/H}\frac{\partial}{\partial z}\left(\frac{e^{-z/H}}{N^2}\frac{1}{\tau_r}\frac{\partial\phi'}{\partial z}\right) = 0. \tag{3.11}$$

q' is the perturbation PV,

$$q' = \frac{1}{f_0}{\nabla_h}^2\phi' + f_0 e^{z/H}\frac{\partial}{\partial z}\left(\frac{e^{-z/H}}{N^2}\frac{\partial\phi'}{\partial z}\right) = 0, \tag{3.12}$$

and $\overline{q}_y$ is the background basic state PV gradient:

$$\overline{q}_y = \beta - e^{-z/H}\frac{d}{dz}\left(\frac{f_0^2}{N^2}e^{-z/H}\frac{dU}{dz}\right), \tag{3.13}$$

where use has been made of the thermal wind balance, Equation (3.8).

The lower boundary condition arises out of the thermodynamic equation together with the vanishing of the vertical velocity at the surface. We need to be careful about the vertical coordinates we are using. In steady state, the actual vertical velocity, W is related to w by

$$W = \vec{u} \cdot \nabla_h z_s = \frac{RT}{gH} w \tag{3.14}$$

where $z_s(x, y)$ is the actual surface height. If we take the constant H as $H = RT^*/g$, where T^* is a typical mean temperature close to the surface then w and W only differ from each other by a factor of T/T^*. Since the variations in T are much less than its magnitude, we can equate w with W. This leads to an effective error in the forcing vertical velocity about 10% at most.

Linearizing the steady state version of Equation (3.5) and using Equation (3.8), we can express the lower boundary condition as

$$\overline{U} \frac{\partial}{\partial x} \left(\frac{\partial \phi'}{\partial z} \right) - \frac{\partial \phi'}{\partial x} \left(\frac{\partial \overline{U}}{\partial z} \right) + \frac{1}{\tau_r} \frac{\partial \phi'}{\partial x} = -N^2 \overline{U} \frac{\partial z_s}{\partial x}. \tag{3.15}$$

There is some ambiguity about what is the appropriate forcing wind to use on the right hand side of Equation (3.15). The boundary condition should be strictly applied at the surface, but the linearization has implicitly assumed that the mountain does not stick out into the fluid domain. In reality the wind impinging on the mountain side will be larger than the surface wind. Linear simulations of the stationary wave pattern in the current climate have used analyzed winds taken from anywhere between the surface and $1.5km$. We shall use the $1km$ wind (denoted as $\overline{U}_f$). This is somewhat a matter of tuning. Since the basic state we are using is arbitrary to some extent, we could obtain the same forcing by using a larger surface wind, and taking the effective forcing wind to be at a lower level. The results would be qualitatively similar. A consequence of the linearity assumption is that the atmospheric fields exist at all levels, even within the topography. Because the fields change only slowly with height, this rather unphysical situation is not fatal to the calculation.

For the upper boundary condition, we employ a radiation condition (e.g. Lindzen,

1990) such that no wave energy propagates downwards from the top of the model domain.

If the topography is expressible in the form

$$z_s(x,y) = \sum_{k,l} h_{kl} sin(ly) e^{ikx} \tag{3.16}$$

then solutions exist for Equations (3.11) and (3.15) of the form

$$\phi' = \sum_{k,l} \phi_{kl} sin(ly) e^{ikx} \tag{3.17}$$

Substituting the above into Equation (3.11) gives a vertical structure equation for each mode which, after a little rearrangement, can be expressed as

$$-(k^2+l^2)\phi_{kl} + f_0^2 e^{z/H} \frac{\partial}{\partial z}\left(\frac{e^{-z/H}}{N^2}\frac{\partial \phi_{kl}}{\partial z}\right) + \frac{\overline{q}_y}{\overline{U}}\phi_{kl} + \frac{i}{\tau_m k \overline{U}}(k^2+l^2)\phi_{kl} - \frac{i}{k\overline{U}} f_0^2 e^{z/H} \frac{\partial}{\partial z}\left(\frac{e^{-z/H}}{N^2}\frac{1}{\tau_r}\frac{\partial \phi_{kl}}{\partial z}\right) = 0. \tag{3.18}$$

The lower boundary condition becomes

$$\left(\overline{U} - \frac{i}{k\tau_r}\right)\frac{d\phi_{kl}}{dz} - \frac{d\overline{U}}{dz}\phi_{kl} = -N^2 \overline{U}_f h_{kl}. \tag{3.19}$$

The solution to Equations (3.18) and (3.19), and the radiation condition for the upper boundary condition is readily expressed in finite difference form as a tri-diagonal matrix equation. We employ an LU decomposition algorithm (e.g. Press et al., 1990) to solve it. The separate ϕ_{kl}s are summed to give the total response to the topographic forcing, z_s.

3.1.1 Canonical form of the wave equation

It is useful to manipulate Equation (3.18) a little further to get it into the canonical form of the wave equation. We will look at the simplified case where N^2, τ_m, and τ_r are

independent of height. In this case Equation (3.18) becomes

$$\left[\frac{\overline{q}_y}{\overline{\overline{U}}} - \left(1 - \frac{i}{\tau_m k \overline{\overline{U}}}\right)(k^2 + l^2)\right]\phi_{kl} + \left(1 - \frac{i}{\tau_r k \overline{\overline{U}}}\right)\frac{f_0^2}{N^2}\frac{\partial}{\partial z}\left(e^{-z/H}\frac{\partial \phi_{kl}}{\partial z}\right) = 0 \qquad (3.20)$$

We now make the transformation $\phi_{kl} = \phi^*_{kl} exp(z/2H)$ which, after some rearranging, yields

$$\frac{\partial^2 \phi^*_{kl}}{\partial z^2} + \phi^*_{kl}\underbrace{\left\{\frac{1}{(1 - \frac{i}{\tau_r k \overline{\overline{U}}})}\frac{N^2}{f_0^2}\left[\frac{\overline{q}_y}{\overline{\overline{U}}} - \left(1 - \frac{i}{\tau_m k \overline{\overline{U}}}\right)(k^2 + l^2)\right] - \frac{1}{4H^2}\right\}}_{=\lambda^2(z)} = 0 \qquad (3.21)$$

$\lambda^2(z)$ is the refractive index, and is a useful diagnostic for the nature of the wave propagation in the basic state: λ is the vertical wavenumber for the transformed ϕ^* equation. The real part of λ represents a propagating wave, while the imaginary part represents the component of the wave that is either growing or decaying with height.

3.1.2 Barotropic stationary waves

We will frequently refer to the barotropic solution for stationary waves. The following is taken from Holton (1979). For a homogenous fluid of variable depth with a fixed upper boundary at a fixed height, D, and a bottom boundary at a variable height, h_b, the linearized quasigeostrophic barotropic vorticity equation on a β-plane gives

$$\overline{u}\frac{\partial}{\partial x}\zeta' + \beta v' = -f_0\frac{f_0}{D}\overline{u}\frac{\partial h_b}{\partial x} \qquad (3.22)$$

where $\overline{u}$ is the basic state wind, and ζ' is the relative vorticity. For topography of the form $h_b = h_0 cos(kx)cos(ly)$, the solution for the stream function, ψ is

$$\psi = \frac{f_0 h_0}{[D(K^2 - K_c^2]} \qquad (3.23)$$

where and K is the total wavenumber, and K_c^2 is the critical wavenumber given by

$$K_c = \beta/\overline{u} \tag{3.24}$$

For $K < K_c$ the streamfuction is in phase with the forcing topography. For $K < K_c$ it is in antiphase. At exactly $K = K_c$ the wavelength of the forcing equals the wavelength of the free Rossby waves in the fluid. There is resonance and, in the absence of damping, the amplitude of the response is infinite.

We can relate a lot of the results that follow in this chapter to Equation (3.24); changes to the vertical structure of the basic state alter the basic state PV gradient, equivalent to changing β in Equation (3.24). This therefore changes the dominant wavelength (i.e. the resonant wavelength) of the atmospheric response.

3.1.3 Meaning of thermal damping

The linear damping in Equation 3.5 acts to try to restore the atmospheric temperature to the zonal mean value, and it does so with a characteristic time scale, τ_r. In actuality the atmosphere exchanges sensible and latent heat with the surface directly underlying it, which may be colder or warmer that the zonal mean. Over most of an ice sheet, it is too cold for melting, and sensible heating is the dominant term. Sensible heat exchange depends on the nature of the surface (e.g. Emanuel, 1994), so the damping time scale appropriate to each is different. Unfortunately, the model linearity does not hold if τ_r is a function of (x, y). However in a spectral model, the damping acts on each mode, all of which 'feel' the entire model domain. Since most of the model domain introduced in the next section is ocean, we might take a damping time scale appropriate to the ocean. However it is the atmosphere's local reponse over the ice which is most important for the ice sheet's development, so we consider a time scale appropriate to sensible heat exchange over ice.

Parameterizations of the sensible heat flux from a snow or ice surface have been studied in the context of energy balance melting models for glaciers and snow packs, often for the purpose of avalanche forecasting (e.g. Brun et al., 1989). The sensible heat flux, SH, at the surface is usually modeled in terms of a bulk aerodynamic formula where $SH = \alpha\Delta T$. ΔT is the temperature difference between the ice surface and the air

immediately above it, and α is a parameter which absorbs all the effects of stability and turbulence (Kuhn, 1979). Bader and Weilenman (1991) suggest the range of plausible values for α as between about 4 and $12 W m^{-2} K^{-1}$. Oerlemans and Hoogendoorn (1989), for example, use $\alpha = 10 W m^{-2} K^{-1}$. The damping term on the LHS of Equation (3.5) can be related to sensible heat flux at the surface via a scaling relationship. If the sensible heat flux is assumed to be mixed quickly within the boundary layer, then the flux at the surface is equivalent to an interior heating (or cooling) rate, $\dot{Q}'$, acting over the boundary layer depth, δz. Therefore, we can write:

$$SH = \alpha \Delta T = \rho \dot{Q}' \delta z = \frac{\delta z \rho c_p \Delta T}{\tau_r} \tag{3.25}$$

where τ_r is the damping time appropriate for the layer δz. This is equivalent to assuming that the response is limited by the surface fluxes, rather than by the mixing time within the boundary layer. For the $1500m$ boundary layer used in our standard basic state, the above range of αs implies that the damping time should be between $2.1 days$ and $6.5 days$. We have taken $5 days$ for the standard case.

3.2 Response of stationary wave model

The purpose of this next section is to explore the response of the stationary wave model to an ice sheet. We first discuss the model's general behavior, and then show that there is a characteristic response to a realistically shaped ice sheet. The consequences of using a linear model are discussed, as is the effect that the modeled stationary wave might have on the transient eddies and the poleward heat flux. Most of the discussion is based on standard theory (e.g. Smith, 1979, Held, 1983), but we will focus on the relevant aspects for the atmosphere—ice sheet interaction. The ice sheet is affected by the atmosphere through its surface mass balance, and also through sensible and latent heat fluxes. The mass balance (accumulation and ablation) is dependent largely on the low level winds and temperatures, since these determine the direction of upslope precipitation, how much moisture the air is able to hold, and whether it is cold enough for snow or warm enough to melt.

3.2.1 Basic state, parameters choices, and channel configuration

Recall that the atmospheric basic state is the zonal mean climate, which in this model is imposed and fixed constant. The basic state appropriate to a climate under full glacial conditions is not known. Moreover we expect that basic state will vary on time scales of around $20kyr$ and $40kyr$ due to the redistribution of incident insolation as the earth's orbit changes (Milankovitch forcing). GCM and EBM simulations can provide only a rough basis for choosing an atmospheric basic state. We must therefore explore how the stationary wave response varies for a plausible range of atmospheric basic states. First though, we define a standard basic state, which will be used as a bench-mark against which to test model sensitivities.

The great continental ice sheets of the Northern Hemisphere existed roughly between $50N$ and $70N$ so we take the parameters f_0 and β to be calculated at $60N$. The scale height is taken as $7.5km$ (equivalent to a mean tropospheric temperature of $256K$). The basic state fields used in the model are shown in Figure 3.1. The surface wind is $3ms^{-1}$, and the jet has a $10km$ strength of about $23ms^{-1}$, which is larger than the jet at $60N$ in today's climate, but GCM simulations show increased baroclinicity at last glacial maximum conditions. The shear in the troposphere of $2.0 \times 10^{-3}s^{-1}$ corresponds to a meridional temperature gradient of $-6.6^oC/1000km$. For the surface velocity and vertical shear used in this standard basic state, the forcing velocity at $1km$, $\overline{U}_f$, is $5ms^{-1}$. The tropospheric lapse rate is -6.5^oCkm^{-1}. The 0^oC isotherm is taken lie at $45N$. Unless stated otherwise this is the atmospheric basic state that will be used.

The top of the model domain is taken at $20km$ and 100 grid points are used in the vertical in finite differencing of Equation (3.18). The details of the basic state above $10km$, while important for the local solution, are not important to the response at the surface. This is because there is very little downward reflection of wave activity for most plausible basic states. Using the same basic state as used in Lindzen (1994), which has a $60km$ vertical domain and realistic variation in the stratosphere, did not produce any difference in the surface response. The more realistic stratospheric basic state does create additional internal modes (Lindzen and Roe, 1997), but the maximum amplitudes of these modes are in the stratosphere, and they do not appear to be excited sufficiently for the response at the surface to be significantly affected.

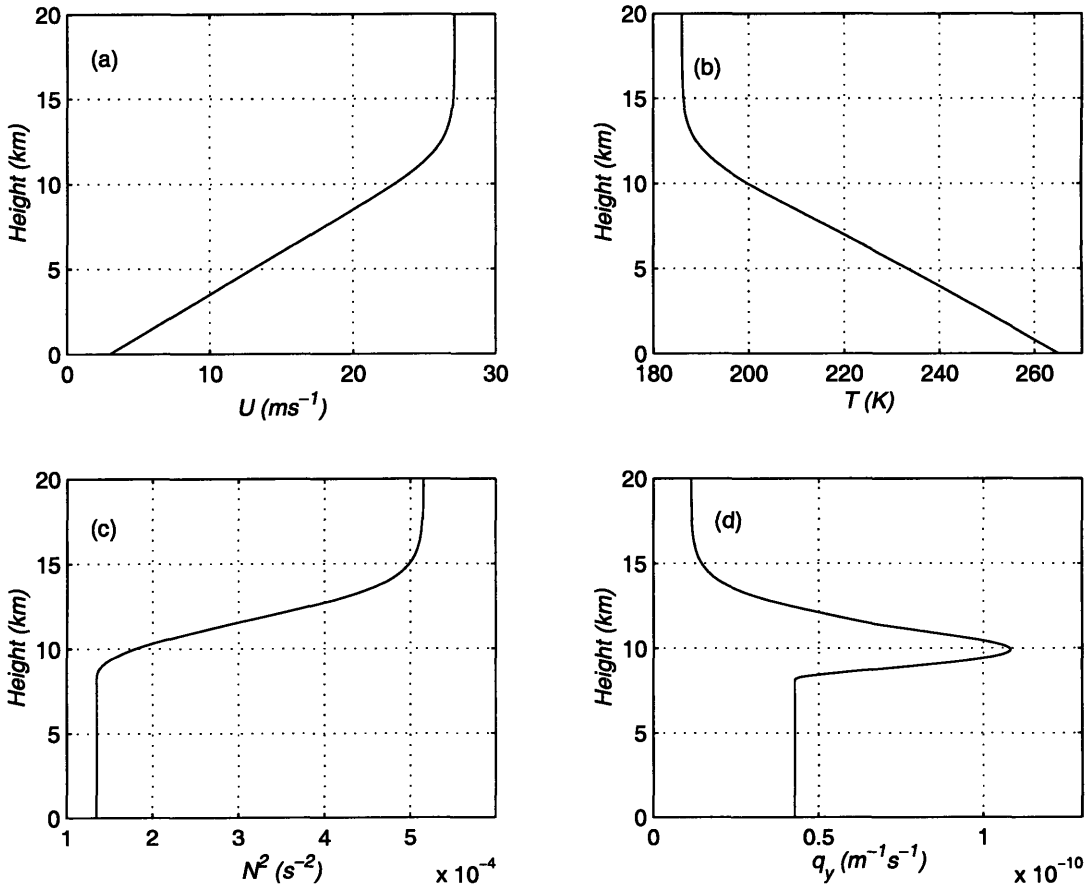

Figure 3.1: Vertical profiles of the standard atmopsheric basic state. Fields shown are (a) zonal wind, (b) temperature, (c) square of Brunt-Vaisala frequency, and (c) potential vorticity gradient.

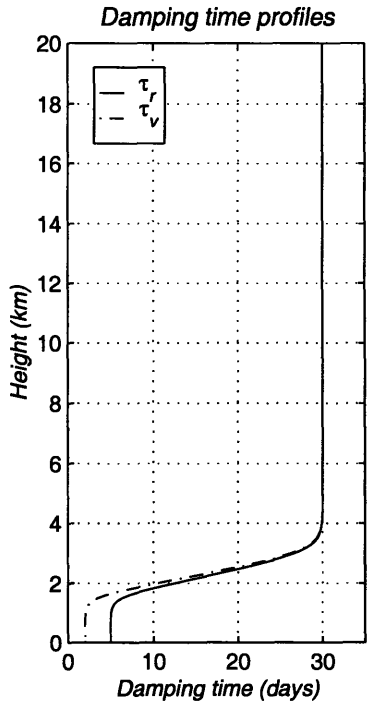

Figure 3.2: Vertical profiles of the standard damping time scales used.

The damping time profiles used are shown in Figure 3.2. Both the momentum and thermal damping times in the free troposphere are set to $30days$. The damping times have a smooth transition from free troposphere values above $3km$ to values more appropriate for the boundary layer below $1.5km$. We use $2days$ for the momentum damping time, and $5days$ for the thermal damping time (see Section 3.1.3). As we will show in Section 3.3 below, only the value chosen for the thermal boundary layer damping time is really important for the atmospheric response at the surface. Both the damping time profiles and the basic state are generated using *tanh* functions, using the same method as Lindzen (1994).

The length of the channel is taken to be that of a longitude circle at $60N$ because of our interest mainly in the high latitude response. The northern wall of the channel is taken to be at $90N$. We place the southern boundary of the channel sufficiently far south that, with the light linear damping applied, the reflections from the southern boundary are largely dissipated before returning to the northern high latitudes. We find that a southern wall at a distance equivalent to $90S$ acts effectively as a 'poor man's sponge'.

Given these channel dimensions we can define nondimensional wavenumbers k' and

l':

$$k = \frac{k'}{acos60} \qquad l = \frac{2l'}{a}$$

where a is the earth's radius.

3.2.2 Response to uniform forcing as function of wavenumber

To demonstrate the behavior of the stationary wave model, we first show the response to a uniform forcing at all wavenumbers. We take $h_{kl} = 100m$ for all k, l. This is an amplitude which is typical of the spectral decomposition at low wavenumbers of the northern hemisphere topography. For k' greater than 5 or 6 however this is a much larger forcing than for the real earth.

Figure 3.3 shows a quasi-resonant maximum in the geopotential response occurring along a line of constant total wavenumber, K (a constant K line is an ellipse in the nondimensional wavenumber space in Figure 3.3). The response is quite sharply peaked around the resonant wavenmuber, and for wavenumber pairs greater than about (5,10) the response is an order of magnitude less than the maximum.

The resonance is directly related to the barotropic resonance in Section 3.1.2. The baroclinic basic state supports a free mode, referred to as the external Rossby wave (also called the equivalent barotropic mode). There is resonance when the wavelength of the forcing is the same as the wavelength of the external Rossby wave. We see from Figure 3.3 that the equivalent barotropic mode is close to (k',l') = (2,3). This is equivalent to a total wavenumber of $7.8 \times 10^{-7} m^{-1}$. Following Held (1983) we can find the equivalent barotropic level, z_R, defined from the resonance condition: $U(z_R) = \beta/K_s^2$ where K_s is the total wavenumber at resonance. z_R turns out to be $7.8km$, close to Held's value.

The barotropic resonance condition can be used to understand how changes in the basic state that we use will affect the atmospheric response. If the PV gradients (equivalent to β in Equation (3.24)) increase, we expect the wavelength of the external mode to decrease. Similarly, a decrease in the tropospheric wind should lead to an increase in the wavelength of the external Rossby wave.

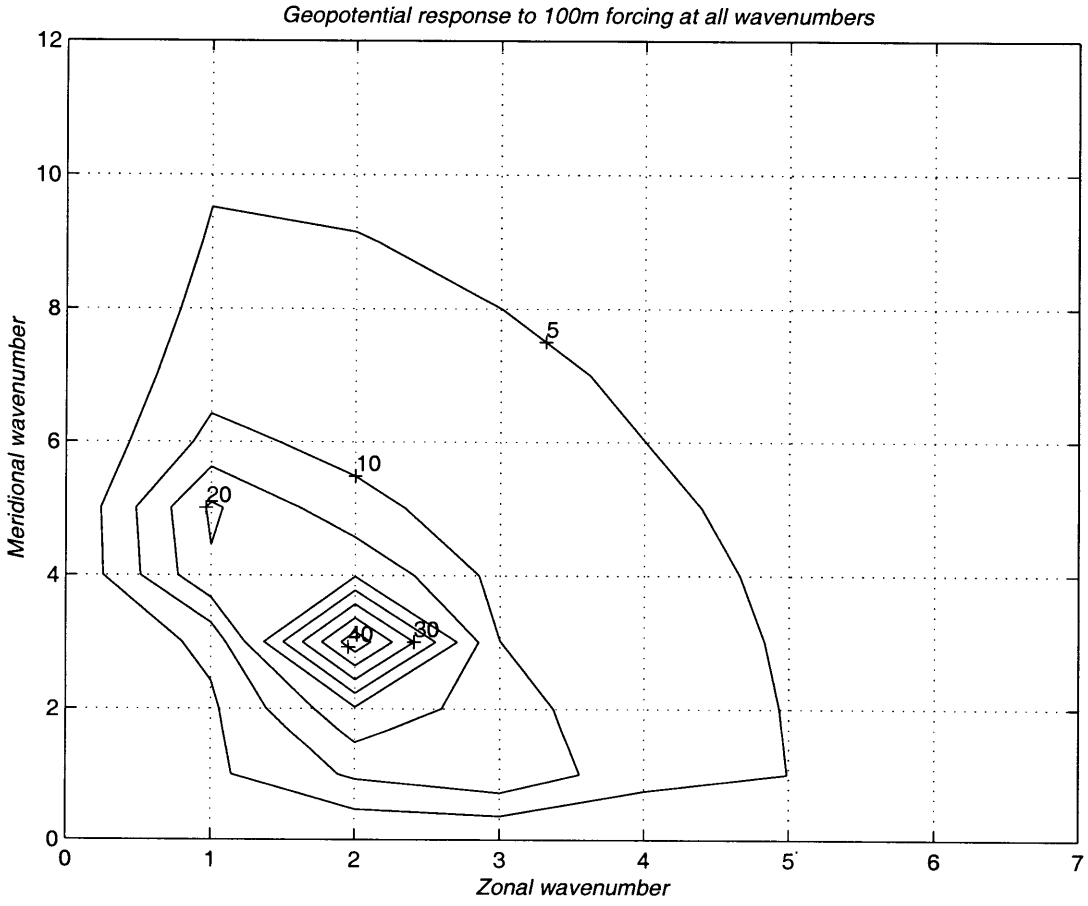

Figure 3.3: Spectrum of perturbation geopotential response at $1km$ to topographic forcing of $100m$ at all wavenumbers. Contours are in units of geopotential meters.

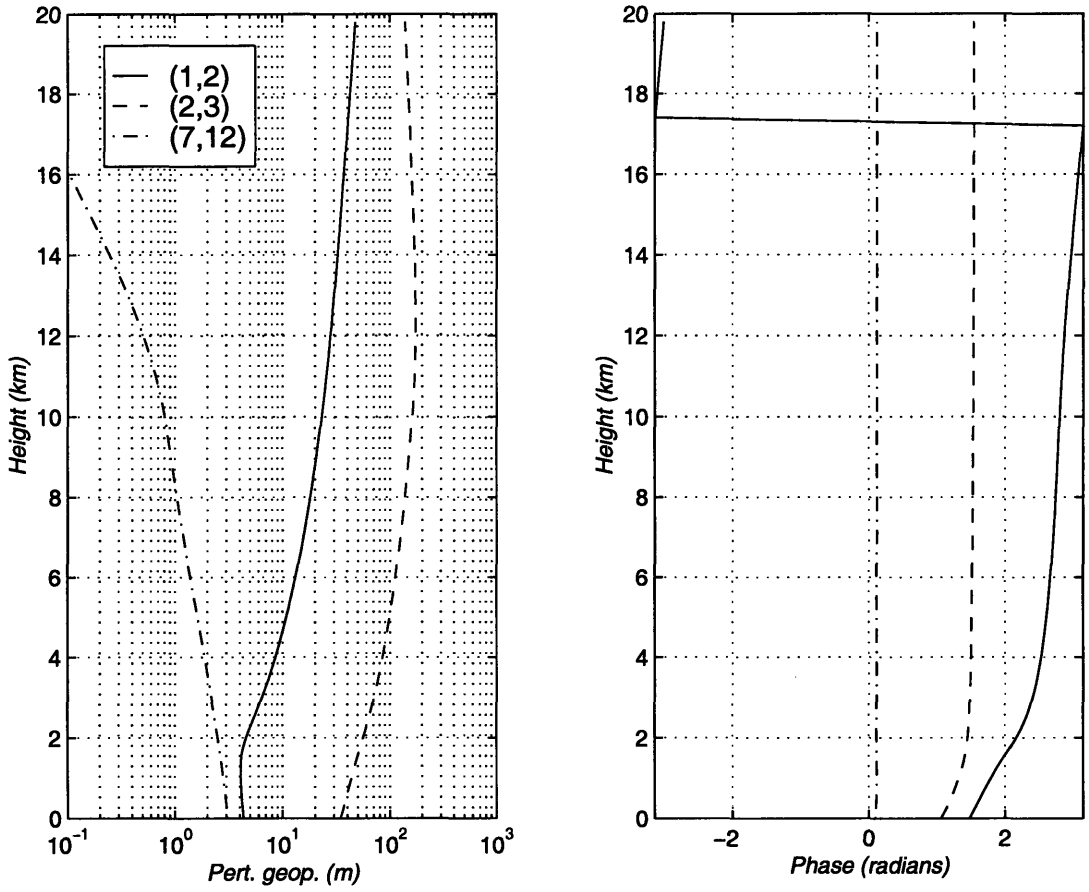

Figure 3.4: Vertical structure of amplitude and phase for several modes with topographic forcing of $100m$. The (k', l') pairs for each mode are given in the legend.

Figure 3.4 shows the vertical structure of the amplitude and phase for several wavenumber pairs, again for a forcing topography of $h_{kl} = 100m$. For sufficiently low wavenumber modes the refractive index (Equation (3.21)) is positive everywhere (Lindzen and Roe (1997)). The $(k',l') = (1,2)$ mode grows slowly and has a phase increasing with height, corresponding to a vertically propagating solution.

The external Rossby wave mode is close to the $(k',l') = (2,3)$ wavenumber pair, which has a barotropic structure with little phase change with height. The amplitude of this mode grows towards the tropopause and then decays in the stratosphere where the refractive index for this mode becomes negative.

The high wavenumber mode $(k',l') = (7,12)$, also shown in Figure 3.4, is strongly confined to the surface. The refractive index is negative almost everywhere in the do-

main. There however is a slight westward phase tilt with height in a small region very close to the surface, where this mode propagates in a region of positive refractive index. Above this though, the mode is purely exponentially decaying.

The (1,2) mode shows a change in $\partial\phi_{kl}/\partial z$ at around $1.5km$. This is because of the transition from the boundary layer damping to the free troposphere damping as shown in Figure 3.2. The temperature response will be especially affected at these levels, since temperature is directly related to $\partial\phi/\partial z$ (Equation (3.7)). A more gradual change in the vertical profile of the damping time would result in a smoother transition between the boundary layer response and the free troposphere response.

The existence of a pure resonance in a channel model is an artefact of having a perfectly reflecting southern boundary. This allows the undamped modes to become established (Held, 1983). In the real atmosphere the meridional variation in the basic state means the presence of a zero wind line - a transition from westerlies to easterlies in the tropics. In the case of simple linear damping this would imply complete absorption and therefore no resonance.

Since the channel model is dominated by the response at the resonant wavenumber, and moreover has no meridional variation in the basic state, it is not obvious that the channel model is a relevant one for the atmosphere. There are several points to be made in favor of its use in this thesis however. The channel model provides a qualitatively correct picture of the atmospheric response to topography (e.g. Charney and Eliasen, 1949), and its simplicity allows for a ready understanding of the physical balances involved. Also, absorption at the zero wind line does not mean that the response will not be peaked at a particular wavenumber: even in more complicated and realistic flows in spherical geometry, the response downwind of the topography is dominated by a pattern which has the structure of an external Rossby wave (e.g. Held, 1983). We have imitated the effects of a zero wind line by applying damping and allowing the southern boundary to be sufficiently far south that any wave propagating southwards will be damped before it returns to interfere with emanating waves. The northern channel boundary is a wall which also generates complete reflection. In spherical coordinates the existence of a $1/cos(\theta)$ term in the meridional refractive index (e.g. Hoskins and Karoly, 1981), where θ is latitude, means all wave trains are reflected before reaching the pole. There is therefore a smooth transition in behavior from a channel mode to more realistic flows on a sphere.

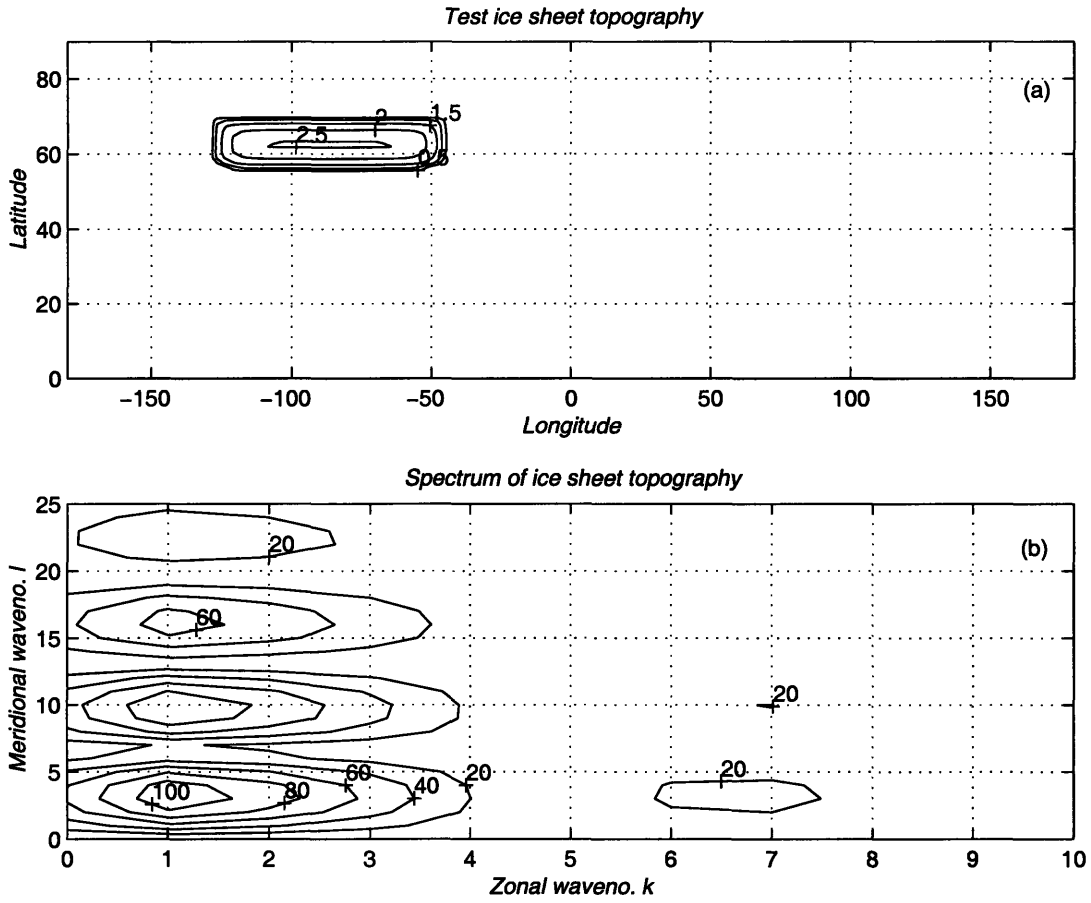

Figure 3.5: (a) Test ice sheet topography. Contours in units of km. (b) Fourier decomposition of test ice sheet topography. Contours in units of m.

3.2.3 Test case ice sheet

We next consider the total stationary wave response to realistically scaled topography placed in the channel. We will use the topography shown in Figure 3.5. This is an ice sheet grown using the SICOPOLIS ice sheet code which will be explained in detail in Chapter 4. The ice sheet was grown on a rectangular continent with boundaries at approximately $40N$, $70N$, $130W$, and $50W$, roughly representing North America. It is about the height the continental ice sheets reached at the last glacial maximum ($\sim 2.5km$). If the ice sheet reaches the side of the continent, it is assumed to calve into the ocean and the height there is set to zero. The test ice sheet we are using therefore has very steeps sides, characteristic of ice sheets in general. We will be able to attribute some of the shape of the atmosphere's response to this steepness.

The ice sheet is interpolated from the $40km$ grid, onto a 128×128 grid the size of the channel model domain. A cubic spline interpolation routine is used (Press et. al., 1990), which preserves both the value and the slope at the interpolated grid points. An FFT algorithm (Press et al., 1990) is used to decompose the topography into its spectral components, also shown in Figure 3.5. The Fourier transform of a general bump shape will look roughly like a $sinc(x)$ function, with the forcing maximizing at the lowest wavenumbers. Because the domain is much larger relative to the ice sheet size in the north-south direction than in the east-west direction, there is relatively more spectral power at the higher meridional waveumbers.

For the standard run, we retain 15 zonal and 25 meridional wavenumbers. In order to speed up computation a little, we keep only those wavenumbers at which the amplitude of h_{kl} is more than 5% of the maximum h_{kl}. We can do this because the forcing is spread broadly enough around the wavenumber of the resonant response that there is no danger of a small forcing projecting onto the resonant mode and dominating the response. We address the reasonableness of the above assumptions in succeeding sections.

Figure 3.6 shows the response to the test ice sheet topography. We are concerned principally with the low level atmospheric response, so we show the model fields at $1km$. Only the part of the channel domain north of $30N$ is plotted. The forcing topography is outlined with a dashed line. The perturbation temperature field (upper panel) shows a maximum temperature perturbation of about -8^oC centered over the eastern slopes of the ice sheet at about $60N$. Using the basic state meridional temperature gradient, a -8^oC temperature perturbation is equivalent to that point being $1200km$ further north in the zonally averaged climate. There is a small positive temperature perturbation on the western slopes of about 2^oC.

The perturbation velocities u' and v' are largely confined to the forcing region and decay quickly away from the ice sheet. The maximum perturbation velocity is about $8ms^{-1}$. There are strong southerlies on the western slopes; warm air is advected from the south to compensate for the cooling of the air as it is forced up over the ice sheet. Conversely the downslope warming is balanced by advection of cold air from the north on the eastern slopes. Consistent with this, the geopotential response is dominated by a ridge sitting over the western slopes and extending over most of the ice sheet. There is a trough in the geopotential immediately downstream of the ice sheet. The amplitude of the ridge minus the trough is about $300gpm$ (geopotential meters), which is reasonable

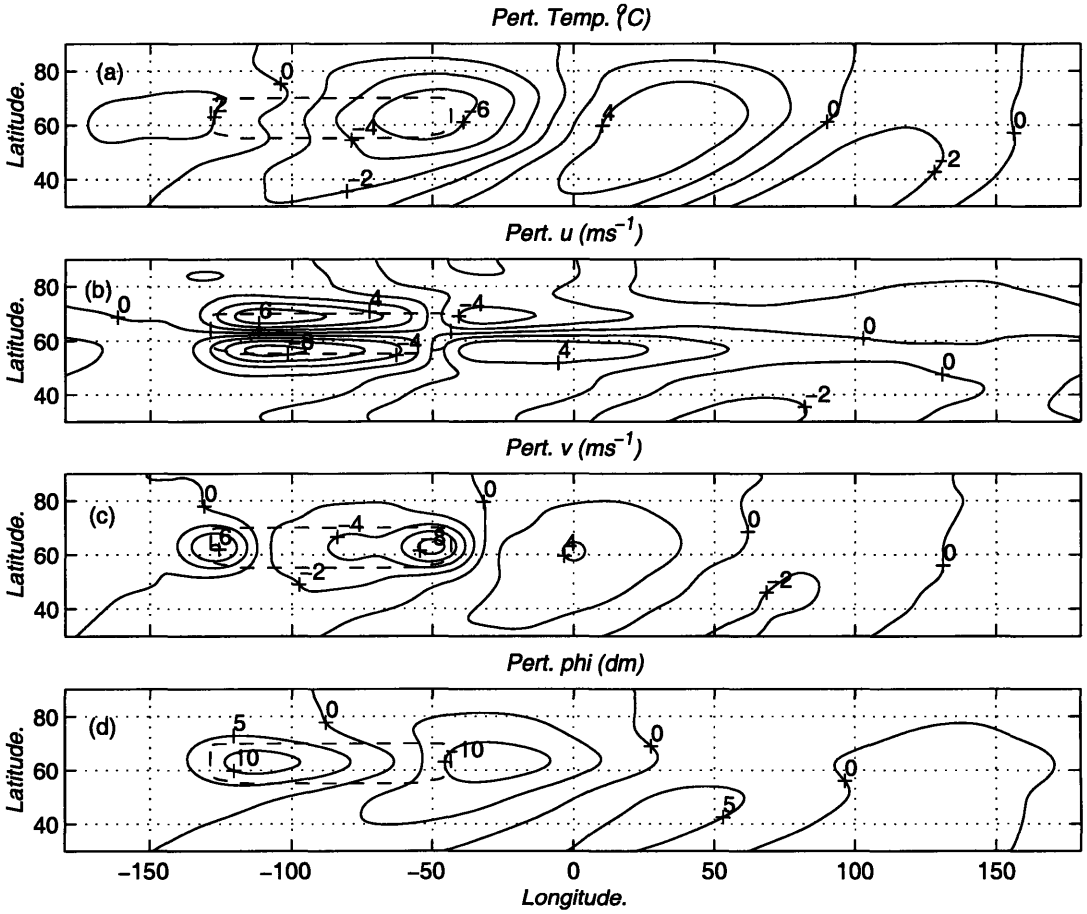

Figure 3.6: Stationary wave response to the test ice sheet. Standard basic state used. All fields are taken at $1km$. (a) perturbation temperature (^oC), (b) Perturbation zonal velocity ms^{-1}, (c) perturbation meridional velocity ms^{-1}, and (d) perturbation geopotential (dm). The outline of the forcing ice sheet is shown by the dashed line.

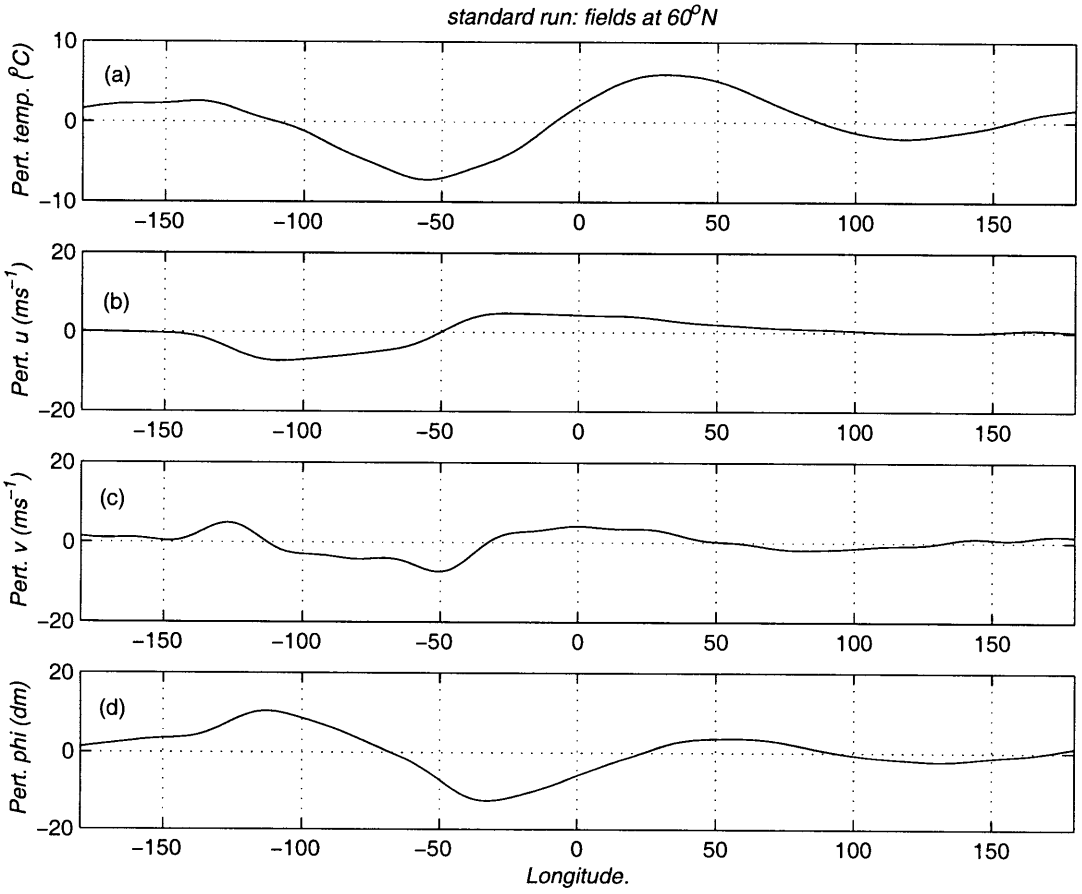

Figure 3.7: Longitudinal section at $60N$ of stationary wave response at $1km$ to the test ice sheet. (a) perturbation temperature (^oC), (b) Perturbation zonal velocity ms^{-1}, (c) perturbation meridional velocity ms^{-1}, and (d) perturbation geopotential (dm). The test ice sheet lies between $130W$ and $50W$.

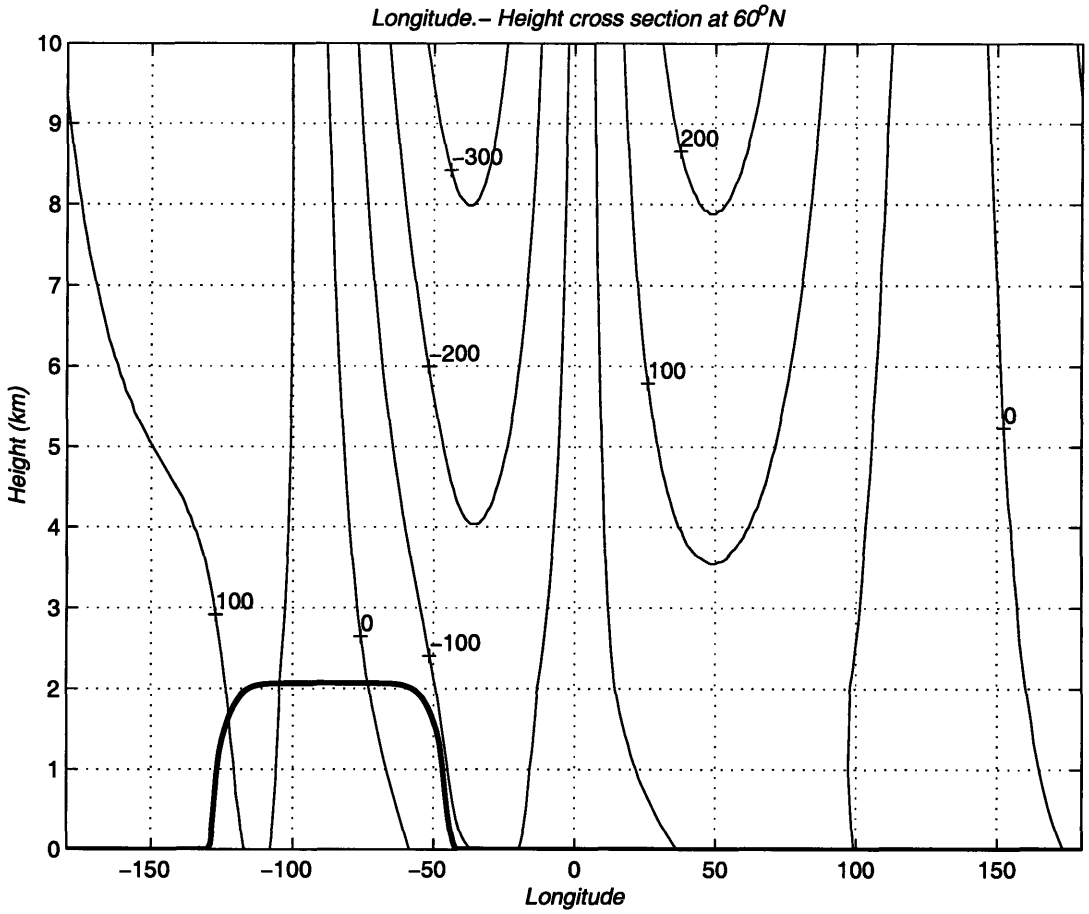

Figure 3.8: Longitude-height cross section at 60N of stationary wave response to test ice sheet. Outline of test ice sheet shown with bold line. Contours are in units of geopotential meters.

for a topographic feature of this size. The high at the surface is equivalent to a mean sea level pressure of about $1030mb$.

Looking at the longitude-height cross-section at $60N$ in Figure 3.8, the far field response is dominated by what looks like the equivalent barotropic mode; there is very little phase variation with height away from the ice sheet. There is slight westward tilting of the phase lines above the ice sheet, which is an indication of the presence of the vertically propagating modes. The amplitude of the trough immediately downstream of the ice sheet reaches $300gpm$ at the tropopause.

3.2.4 General shape of stationary wave response in standard case

As seen in Figure 3.6, there are northerly velocities over most of the ice sheet except for a small region on the western slopes. Balanced with this velocity field is a high pressure ridge which has an asymmetric shape with tight pressure gradients to the west of the maximum and weaker ones to the east. We want to understand the shape of this response. If v' is negative over most of the ice sheet this implies, in the absence of sufficiently warm temperature anomalies ahead of the ice sheet, that cold air is being brought down from the north and that a cold temperature perturbation will overlay most of the ice sheet. It seems therefore that for the test ice sheet at least, the CTT (cold temperature trough) feedback described in Chapter 2 will dominate the interaction between the ice sheet and atmosphere. It is important to understand the range of basic states and other parameters that this will hold for.

The standard baroclinic response to topography is well described by Hoskins and Karoly (1981). At small spatial scales the response to topography is dominated by the advection of the mean temperature gradient by the perturbation velocity field (the $v'd\overline{T}/dy$ term, or the second term on the left hand side of Equation (3.15)). Advection of warm air from the south balances the cooling due to the upslope flow on the western slopes. Conversely, downslope warming on the lee side is balanced by northerly winds. The result is a high pressure ridge sitting over the topographic feature. Since high wavenumber modes are not propagating, and in addition the damping acts preferentially on the modes with the sharpest gradients, the response will be mainly localized to the vicinity of the topography. At larger scales some of the western slope cooling can be balanced by advection of warm perturbation temperatures ahead of the topography. The warm temperature perturbation implies positive v' ahead of the ice sheet, and therefore the ridge is phase shifted to the west of the topography. The inclusion of damping also contributes to a phase shift of the ridge westwards.

As shown in Chapter 2 the characteristic shape of ice sheets means that although the spatial scale of the ice sheet as a whole can be large, the sides rise very steeply over only a very short distance. Within $100km$ of the edge, an ice sheet rises to over $1km$ in height. This compares to an overall length scale of maybe $3000km$ and a maximum height of 2 or $3km$). We can examine the effect of these different forcing scales on the atmosphere

by separating the topography into slowly varying and fast varying components.

The top panel in Figure 3.9 shows an arbitrarily chosen, steeply sided topographic feature described by the function $exp(-((x-x_0)/L_0)^{20}) * sin(ly)$, where x_0 is chosen to center the topography at $100W$ and L_0 is equivalent to a halfwidth of 40^o. We split this topography into a smoothly varying part given by $exp(-((x-x_0)/L_0)^2) * sin(ly)$, and the remainder, representing the fast varying component. Taking a meridional wavenumber equivalent to $l' = 4$, we calculate the response of the stationary wave model using the standard basic state parameters. This is shown in the remaining panels of Figure 3.9. The far field response is dominated by the large scale forcing. The peak in the geopotential perturbation is phase shifted to the west of the topographic maximum by about 20^o longitude. It is this phase shift which is largely responsible for the northerly winds over most of the ice sheet. In the linear model, this phase shift is a consequence of both the applied damping and also the non-zero surface velocity - there is partial compensation of the topographic forcing by advection of temperature perturbations by the basic state zonal wind at the lower boundary. For zero surface wind and no damping, the ridge would sit directly over the topography and there would be equal areas of southerlies and northerlies over the ice sheet.

The response of the small scale component of the topography is predominantly localized to the vicinity of the topography. There is only a slight projection onto a propagating mode, seen from the small far field response. Over the ice sheet, the geopotential perturbation is in phase with the small scale topography, and when this perturbation is added to the more gradually varying response due to the large scale forcing, it creates the asymmetric high pressure ridge that we have noted in the total geopotential perturbation. In addition, the region of northerly winds over the topography is extended a little further to the west.

We have used an arbitrarily chosen topographic shape, but any realistic ice sheet could be divided up into small scale and a large scale components. Figure 3.9 demonstrates that the basic response of the atmosphere, even over the topography, is dictated by the large scale forcing. The small scale forcing (i.e. the steep ice sheet sides) adds some details to the resulting flow.

The main influence on how the stationary waves affect the ice sheet is the presence of low level winds and damping which, by the balance described above, creates cold perturbation temperatures over most of the ice sheet.

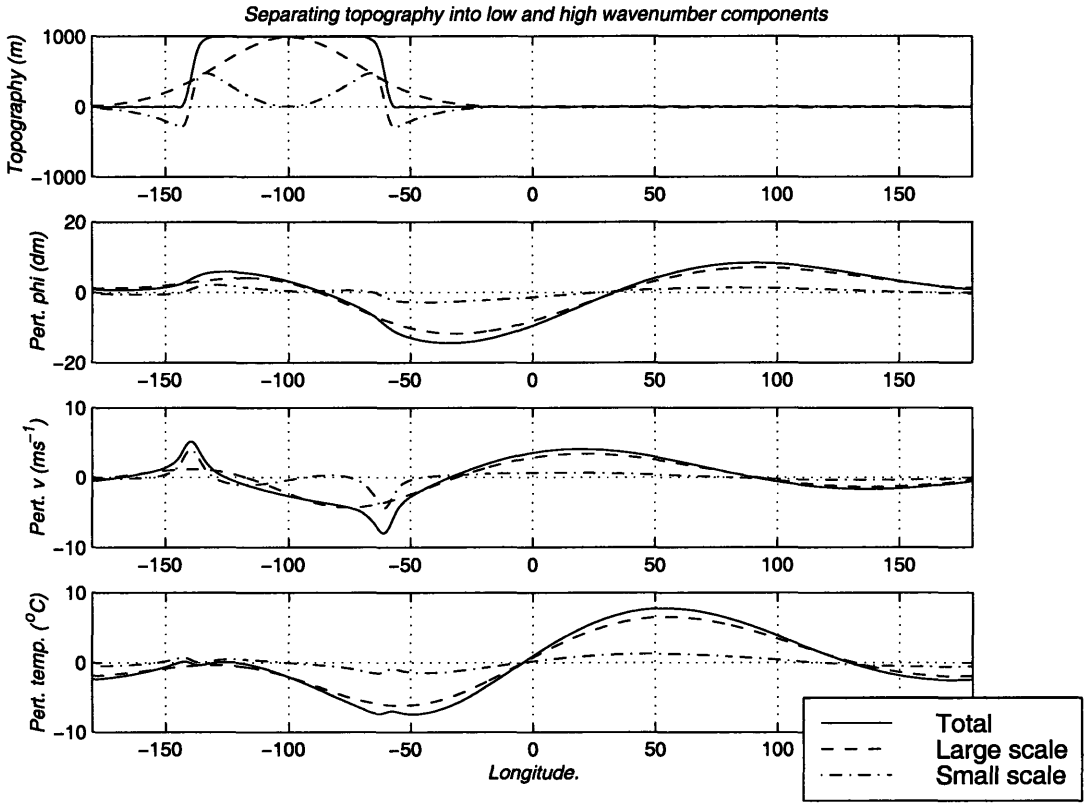

Figure 3.9: Separation of arbitrary topography into small scale and large scale components. (a) the topography, (b) perturbation geopotential, (c) meridional velocity, and (d) perturbation temperatures. Fields at $1km$ are plotted Details are described in the text.

3.2.5 Nonlinearities

We have chosen to use a linear stationary wave model both for simplicity and for ease of understanding the balances of the terms involved. Previous research has examined in some detail the validity of the linear solution for a topographic obstacle of this size (e.g. Trenberth and Chen, 1988; Cook and Held 1992). Strictly speaking, the linear solution is valid for a regime in which the first order linear forcing, $\overline{U}_f \partial z_s / \partial x$, is much greater than the second order forcing, $\vec{u'} \cdot \nabla_h z_s$. The linear forcing is an implicit assumption that the flow is constrained to go over the topography, and does not allow for the possibility that the flow might go around the topography instead. Trenberth and Chen conclude that for the Tibetan Plateau in today's climate, the 'around' component of the flow dominates the 'over' component, and that linearity does not hold for mountain ranges of a size similar to the Tibetan Plateau. An important factor in this result is the steepness of the slopes, since the nonlinear terms involve the products of gradients. The great continental ice sheets, however, were of the size of the Tibetan plateau (Figure 1.3), and so the use of a linear model must be justified.

A result that is worth keeping in mind is that in the absence of meridional shear the linear solution is, mode by mode, also the full nonlinear solution (Pedlosky, 1992). The second order term in Equation (3.10) is of the form $\vec{u'} \cdot \nabla q'$. Expanding out the advective operator for the perturbation fields gives $u' \partial / \partial x + v' \partial / \partial y$. This is identically zero for each mode taken in turn. This can be seen easily by substituting in the geostrophic relationships for u' and v'. The nonlinearities, then, arise only from cross terms multiplying different wavenumbers. This result is sometimes cited as the reason why linear stationary wave simulations perform well compared to nonlinear calculations, even beyond the domain of strict linear validity (Cook and Held, 1988).

Cook and Held (1992) looked at the validity of the linear approximation using an idealized nonlinear GCM. The model had 7.5^o zonal and 4.5^o meridional resolution, a treatment of moisture, and a Gaussian shaped mountain situated at $45N$. They compared the linear and GCM responses to topographic forcing for different heights of mountains. The geopotential response in the linear case had the same pattern as the GCM calculations, but the amplitude of the geopotential perturbations are overestimated in the linear calculations by up to a factor of 2 for a $2km$ mountain. For larger mountains there was a gradual change in the stationary wave pattern. The location of the main ridge shifted progressively northeastwards as the height of the mountain increased, and

the main trough retrogressed southwestwards. The winds therefore had a more easterly component over the mountain than in the linear case. For a $4km$ mountain the high sat over the northeastern slopes and the trough over the southern slopes, and the predominant flow was southeasterly.

These nonlinear results may be thought of qualitatively as an iteration of the linear solution. The linear solution generates northerlies over most of the mountain as explained in Section 3.2.4 above. These northerlies then create a secondary forcing. The flow is now upslope on the northern flank of the mountain, which will force a negative vorticity anomaly (equivalent to a geopotential ridge). Conversely, the response to the downslope flow on the southern flank is a positive anomaly (equivalent to a trough). The sum of these patterns added to the linear response is roughly the pattern of the nonlinear results described above.

Given that the Laurentide and Fennoscandian ice sheets reached up to $3km$ in height, they were topographic obstacles at the limit of the applicability of the linear approximation. We can look at how we would expect a nonlinear calculation to modify our linear solution. The linear calculation has neglected the $\vec{u'} \cdot \nabla q'$ term. We show the perturbation winds overlain on a contour plot of the perturbation PV for the standard case in Figure 3.10. Wherever there is cross-contour flow, there will be advection of perturbation PV by the perturbation winds and a contribution, therefore, to the nonlinear term. From the plot it is clear that the largest nonlinearity will be over the eastern flank of the ice sheet. We can compare the size of the linear and nonlinear terms in the equation. Figure 3.11 shows the advection of the planetary vorticity by the perturbation winds, $v'\partial\overline{q}/\partial y$ in the top panel, together with the advection of the perturbation vorticity by the perturbation winds, $\vec{u'} \cdot \nabla q'$ in the lower panel. For consistency the linear approximation would require that the former be much larger than the latter. Figure 3.11 shows that this is not the case on the eastern flank of the ice sheet, which indicates that the linear results will be modified by the full nonlinear solution.

The $\vec{u} \cdot \nabla q'$ term can also be interpreted as a tendency on the PV equation. For example, where it is positive, there is an effective advection of positive perturbation vorticity into that region. Figure 3.11 therefore implies that there is a tendency for our linear calculation to be modified by the nonlinear terms in the same way as the results of Cook and Held (1992) (i.e. the main ridge extending northeastwards, and the trough retrogressing southwestwards).

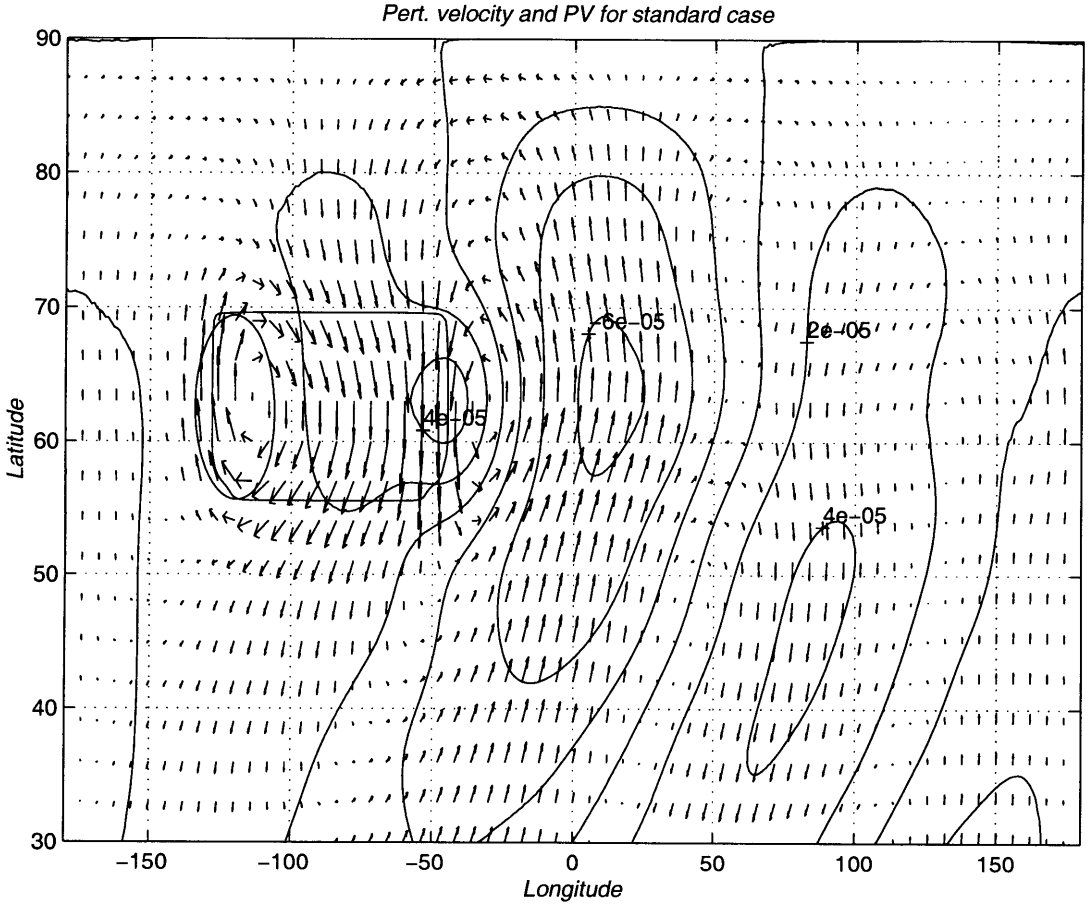

Figure 3.10: Perturbation velocity and perturbation potential vorticity at $1km$ for test ice sheet and standard basic state. Where there are cross PV-contour wind vectors, there is a contribution to the nonlinear terms in the PV equation. The maximum wind vector is $9ms^{-1}$. PV units are s^{-1}.

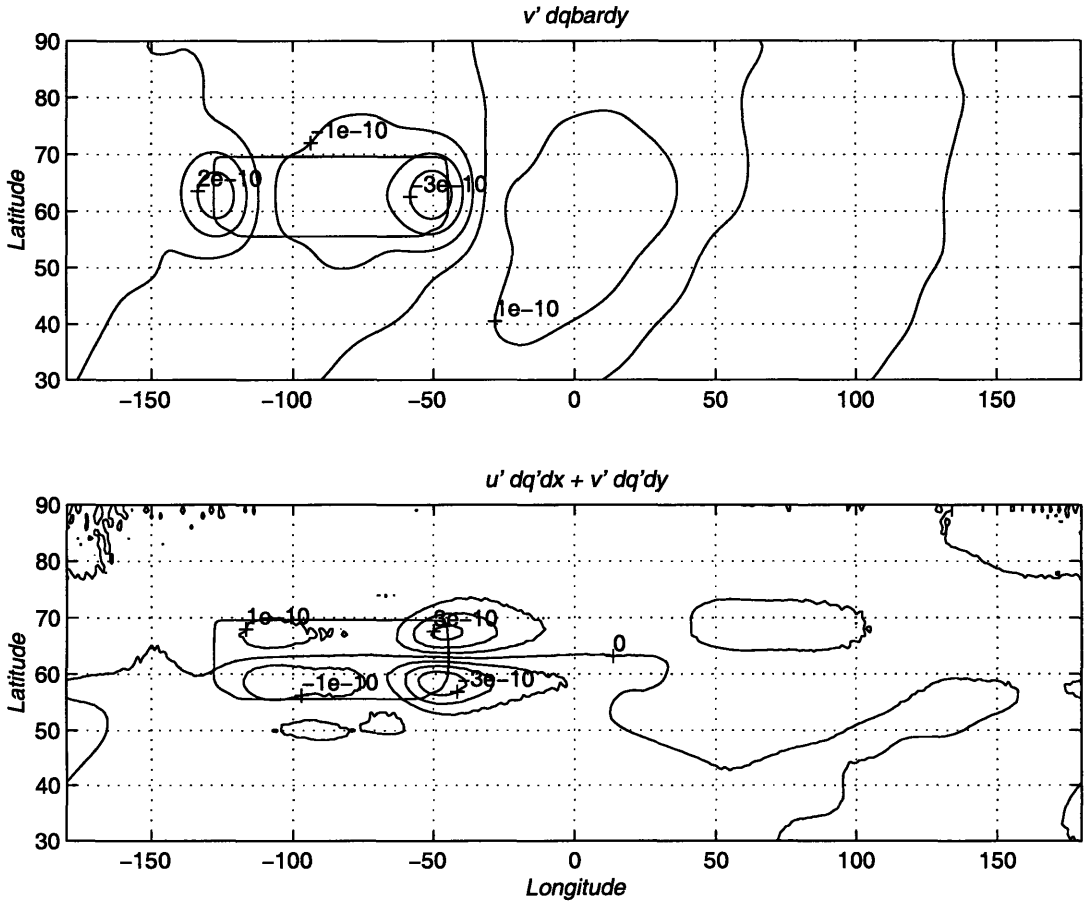

Figure 3.11: Comparison of magnitude of linear and nonlinear terms in PV equation. Top panel is $v' \frac{\partial \overline{q}}{\partial y}$ (a linear term), and the lower panel is $v' \frac{\partial q'}{\partial y}$ (the non linear term. Units are s^{-1} and fields are taken at $1km$.

Without doing the full nonlinear calculation, it is not possible to say exactly the extent to which the results from our linear model would be modified. Of course, a consistent nonlinear calculation would require keeping all terms of the same order, and in such a calculation it might not be possible to discard the wave-mean flow interaction. However, some support for the linear model's use can be taken from Cook and Held (1988) who showed that in a GCM run with imposed boundary conditions from the last glacial maximum, the linear topographic response accounted for most of the stationary wave pattern. Comparing their linear and nonlinear calculations there is some indication from their figures of the retrogressing southwestward of the trough in the full nonlinear solution, but the basic pattern is well captured by the linear model.

When taken as a whole, the above picture suggests that the overall pattern of the linear stationary model is correct. The exact amplitude and phase of the response will however be modified by a nonlinear treatment of the stationary wave forcing. But while even small changes in phase and amplitude have very significant consequences for the details of local climate, we are aiming only to explore the nature of the feedbacks between the stationary wave and the ice sheet. Since this purpose requires only a qualitatively correct response, a linear calculation is adequate.

3.2.6 Baroclinicity in standard case

The role of transient eddies in the climate is potentially important for the ice sheet—climate interaction for several reasons. For example, the moisture supply to the ice sheet will come largely from transient weather systems precipitating over the ice. Another factor is how any zonal asymmetry in the convergence of transient eddy heat and momentum fluxes might force the stationary wave pattern. Valdes and Hoskins (1989), for example, conclude that in today's climate heating due to transients is an important factor in the forcing of the Aleutian and Icelandic lows.

In using the linear steady state equations to solve for the topographically forced stationary wave solutions, there is an implicit assumption that the presence of transient eddies does not change the calculated time-mean pattern. This would be true if either the time-mean pattern were absolutely stable to small perturbations, or if the dissipation rate in the atmosphere were such that the transients eddies are damped quickly before they modify the time-mean pattern much. In today's climate in the northern hemisphere,

the Pacific and Atlantic storm tracks, are regions of enhanced baroclinicity (equivalent to enhanced vertical shear), and are consequently the focus for a lot of transient eddy activity. Precipitation is enhanced over these regions, and the transient eddies in these storm tracks are responsible for a large part of the northward flux of moisture (e.g. Peixoto and Oort, 1992). If the storm tracks change position in a glacial climate, then the distribution of precipitation and moisture transport will change.

A feature common to many of the GCM simulations of the last glacial maximum climate is an enlarged Atlantic storm track which extends further to the southeast than in the current climate (e.g. Kutzbach and Guetter, 1986). This brings enhanced precipitation over the southeastern slopes of the Laurentide ice sheet.

With a simple model such as the one we are using, we cannot model the effects of an ice sheet on the transients directly. We can however investigate qualitatively the changes in the transients that might be expected by looking at a rough local measure for the growth time of baroclinic eddies. We use the measure developed in Lindzen and Farrell (1980), which is a general formula for the maximum growth rate for baroclinic instabilities, applicable to flow on a β-plane, characterized by constant vertical shear. The maximum growth rate for baroclinic eddies turns out to be proportional to the meridional temperature gradient. The formula was derived for eddy growth rates on a zonally symmetric basic state, whereas we are interested in the growth rate of eddies on the time-mean flow including stationary wave pattern. Since we are only looking for a rough measure of growth rate we replace the basic state meridional temperature gradient in the growth rate expression with the local temperature gradient at $1km$. Provided that the local temperature gradient applies over a length scale which is large compared to the scale of the eddies, the physics of the instability is basically the same, and so we expect the growth rate to scale with the temperature gradient with roughly the same constant of proportionality. The growth rate of Lindzen and Farrell is given by:

$$(kc_i)_{max} = -8.6 \times 10^4 \nabla_h T|_{z=1km}\, mK^{-1}day^{-1} \tag{3.26}$$

where c_i is the imaginary part of the phase speed. The growth rate given by (3.26) has to be treated cautiously. Niehaus (1980) showed that the growth rate of normal modes developing in regions of enhanced baroclinicity was not governed completely by the local shear, indicating that the modes are constrained to some extent by the global properties

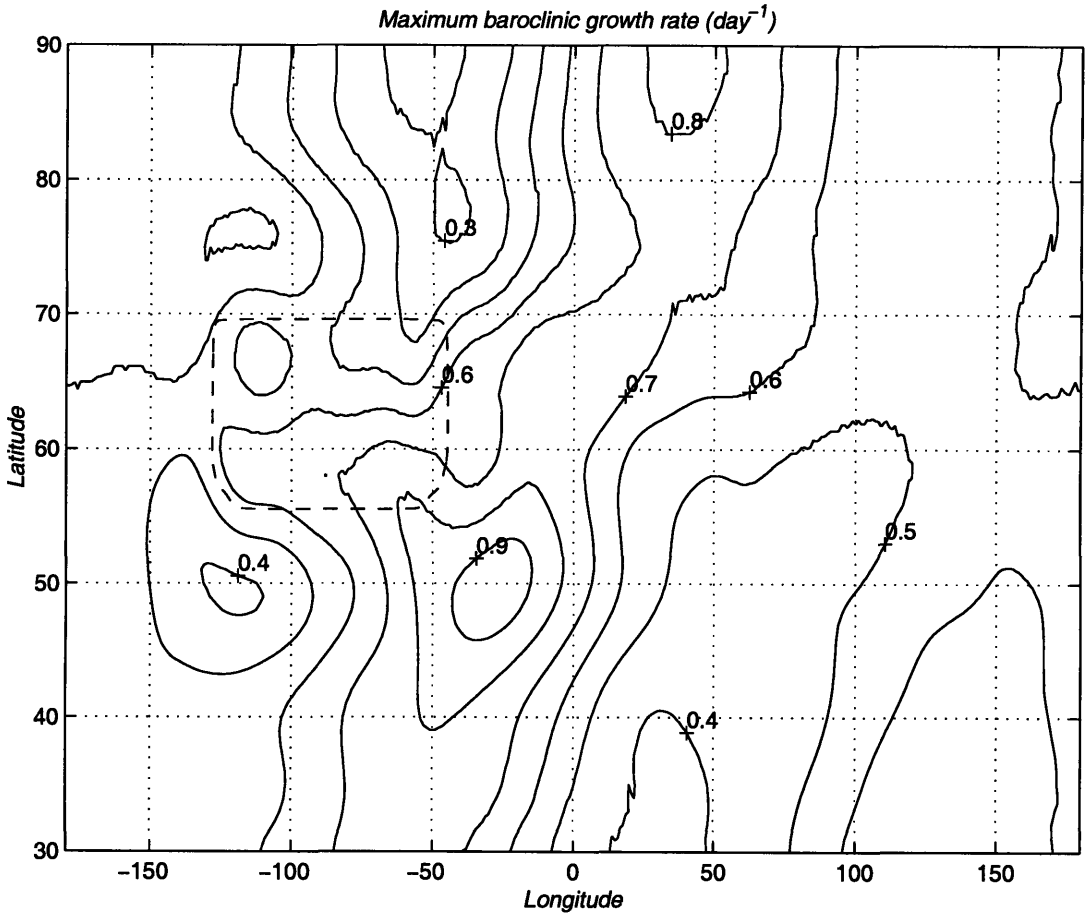

Figure 3.12: Measure of growth rate of baroclinic eddies for standard basic state response to test ice sheet. Details are described in the text. Units are day^{-1}. The growth rate for the zonally averaged basic state in the absence of a stationary wave is $0.57 day^{-1}$. The small scale irregularities are numerical.

of the background flow.

Figure 3.12 shows the results of applying Equation (3.26) to the standard case temperature field. For reference, the growth rate calculated using the basic state meridional temperature gradient, which would be the growth rate in the absence of the stationary wave, is $0.57 day^{-1}$. There is a region of increased baroclinicity running along the axis of the low geopotential trough (which is consistent with the thermal wind balance). This increased baroclinicity extends over the southeastern slopes of the ice sheet, and is consistent with the LGM GCM simulations referred to above. We will return to the effects of the changing position of the storm tracks in discussing the results in Chapter 6.

3.2.7 Poleward heat transport

The Eliassen-Palm (EP) flux is a standard measure of wave activity (e.g. Andrews et al., 1987), and is defined for this coordinate system and geometry, as

$$\vec{F} = \left\{ -e^{-z/H}\overline{u'v'}, e^{-z/H}\frac{f_0 R}{N^2 H}\overline{v'T'} \right\} \tag{3.27}$$

The overbar denotes that a zonal average has been taken. The EP flux for the response of the standard basic state to the test ice sheet is shown in Figure 3.13. There is overall upward propagation of wave activity and also a slight turning equatorward. This equatorward turning is due to the asymmetric positioning of the topography in the model domain; there is a larger region of dissipation to the south of the ice sheet than to the north. In the real atmosphere, the equatorward propagation of the EP flux is much more pronounced: the strength of the westerlies decreases southwards, and so the refractive index for the waves Equation (3.21) increases with decreasing latitude. The wave activity is therefore refracted towards that direction.

In steady state, the divergence (convergence) of the EP flux represents source (dissipation) regions for wave activity. Figure 3.14 shows that there is convergence throughout most of the domain, and therefore dissipation. The largest convergence is found within the lowest $2km$ of the model domain, where the highest damping is applied (Figure 3.2). The source of the wave activity lies on the $z = 0$ boundary. This is a consequence of the linear model assuming that the topography is small ($z_s << H$).

The divergence of the EP fluxes can be used to calculate the resulting local atmospheric heating. It takes into account not only the eddy heat transports by the wave, but also the large scale regions of subsidence or ascent due to the induced ageostrophic circulation. This local heating implies a net meridional heat flux which is shown in Figure 3.14. Because we have made an assumption of steady state, there is an implicit and balancing diabatic heating/cooling in the model, due to radiative imbalance or other processes.

The maximum heat flux of $\sim 0.75PW$ ($= 10^{15}$) is not small. The total heat transport in today's climate is $2PW$ in summer and $8PW$ in winter (Peixoto and Oort, 1992). The poleward heat transport suggests that the stationary wave produced by the ice sheet compensates to some degree for the cooling effect at high latitudes due to increased

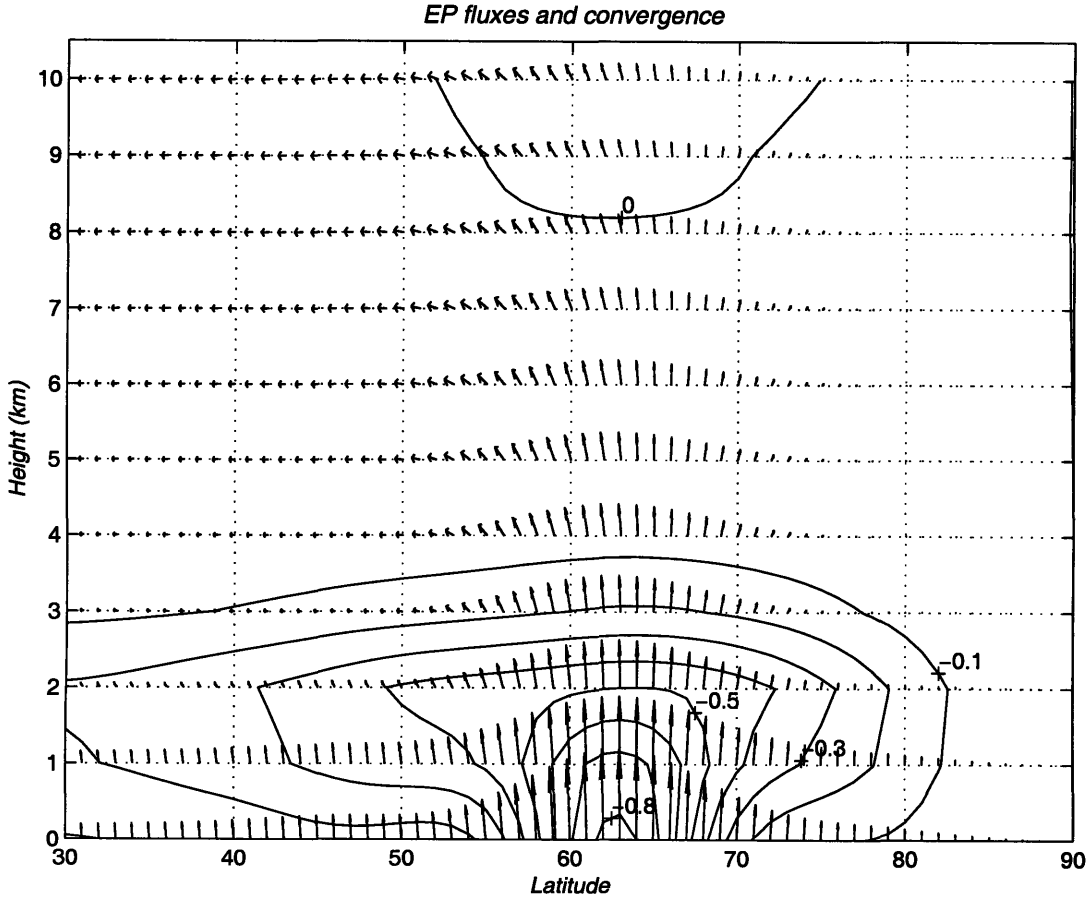

Figure 3.13: EP fluxes and convergence for standard case. The vertical component of the EP fluxes has been exagerated by a factor of 50. The units of the EP convergence are $10^{-4} ms^{-2}$.

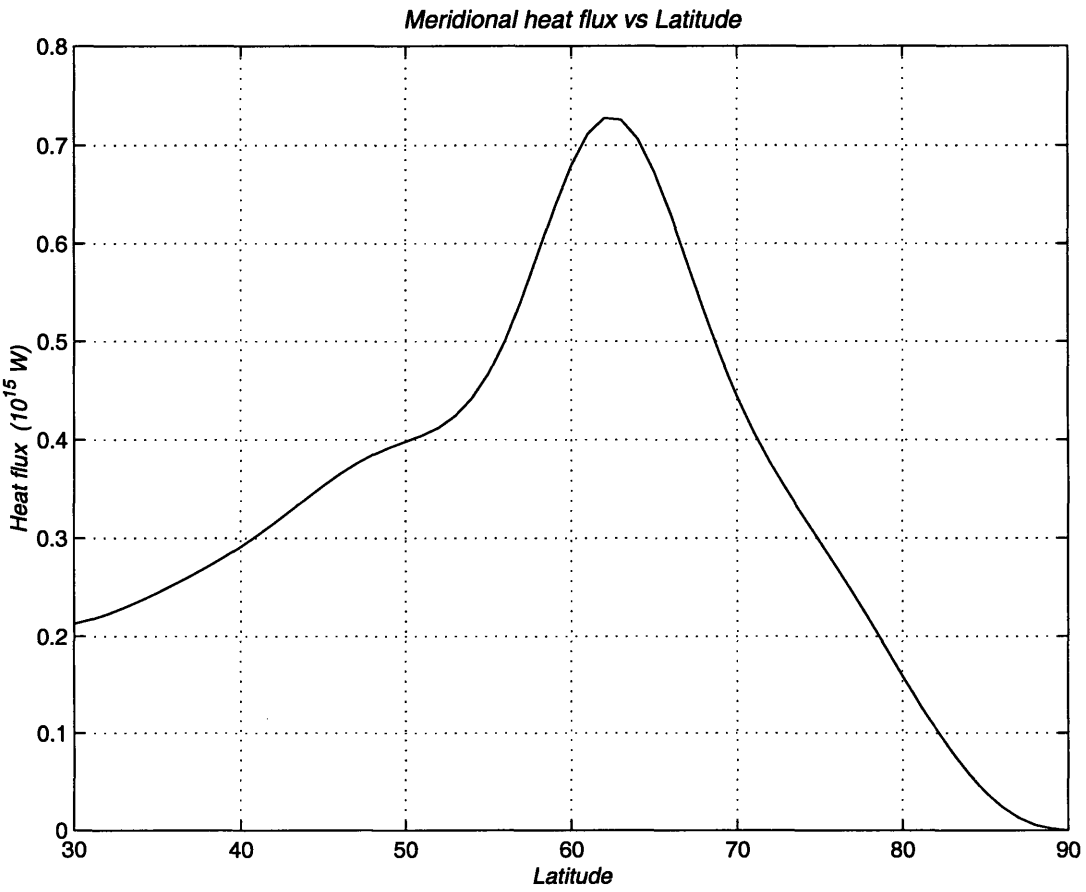

Figure 3.14: Poleward heat flux in PW due to the standard case stationary wave, taking into account the residual mean circulation

albedo. However, this should be taken only as suggestive of a tendency. The channel geometry becomes most unrealistic at high latitudes, where it must have a strong effect on the convergence of the heat flux. Also, in linearizing around a fixed basic state we have taken no account of the way in which the wave action attempts to change the atmospheric basic state; the heat flux represents, in part, the interaction of the wave with the mean flow, and not necessarily the actual heat transport which would result were the system allowed to come to a consistent equilibrium. Lastly, several theories of atmospheric equilibration hold that the heat flux adjusts in order to maintain a dynamics-driven critical meridional temperature gradient in midlatitudes (e.g. Stone, 1978). Thus the additional heat transport due to the presence of the great continental ice sheets might conceivably not change the total poleward heat transport, but instead lead to a reduction in the ocean or the transient eddy heat fluxes.

3.3 Testing of model parameter choices

We have had to make several choices for different parameters controlling the stationary wave behavior. In this section we examine the sensitivity of the output to those choices and discuss how any differences might affect the interaction between the stationary wave and the ice sheets. We will concentrate on changes to the low level temperatures and winds because of their influence on the mass balance over the ice sheet.

3.3.1 Basic state surface velocity

Figure 3.15 shows the model response for a range of surface wind values. We have kept the forcing wind, $\overline{U}_f$, constant at $5ms^{-1}$. The main effect of changing the surface wind is to change the balance of the terms on the LHS of the lower boundary condition (Equation (3.19). The larger the surface wind, the larger the role of the first term on the LHS of Equation (3.15) in balancing the topographic forcing. This leads to a slight decrease in v' and there is also a phase shift of the high pressure ridge to the west. Again the effect is small for the range of surface winds we have considered.

Also worth noting is that the wavelength of the far field response increases slightly with increasing surface wind. This is consistent with the wavenumber of the external

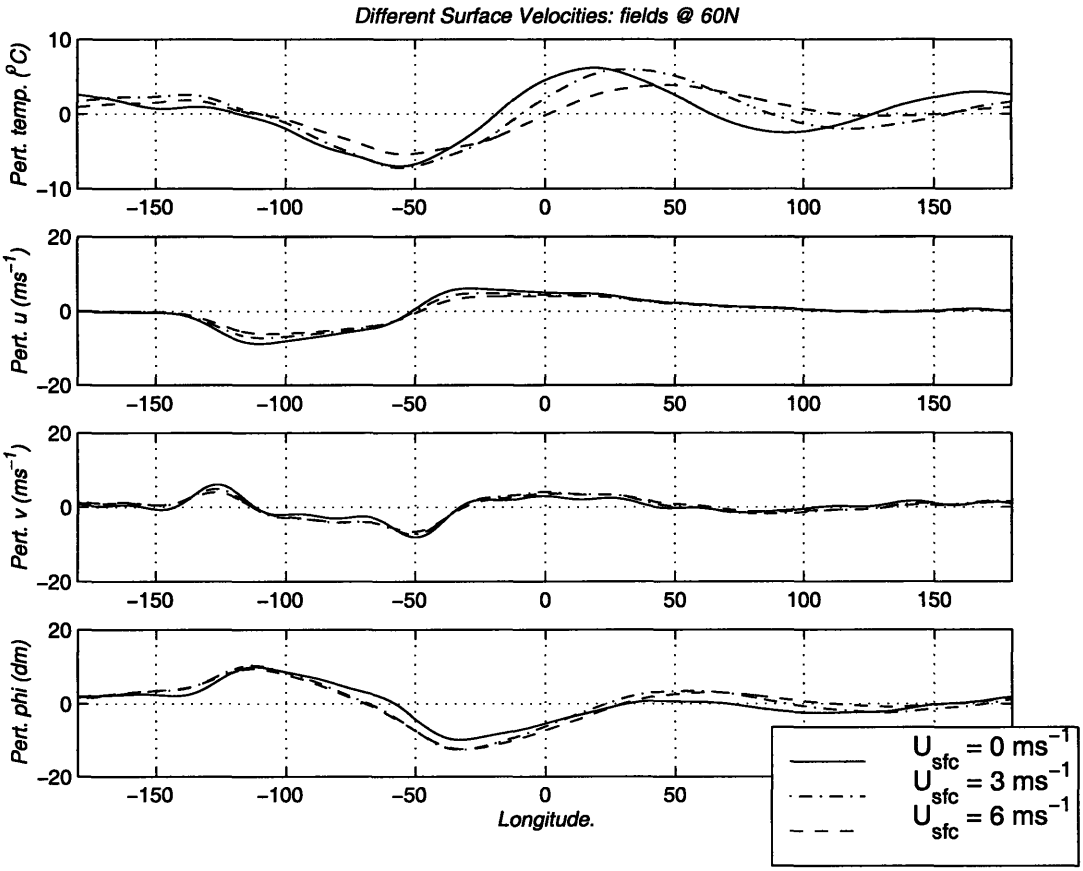

Figure 3.15: Sensitivity of atmospheric response to basic state surface velocity. Fields are at $1km$. The middle value is the standard basic state. The test ice sheet lies between $130W$ and $50W$. Panels are as for Figure 3.7.

Rossby wave decreasing as the mean tropospheric wind increases (Equation (3.24)).

3.3.2 Basic state shear

We can also look at the response to a range of vertical shears in the basic state. Again to limit the number of things which are changing in the model, $\overline{U}_f$ is kept at $5ms^{-1}$. Figure 3.16 shows the response to a range of shears which are equivalent to tropopause jet strengths of between 13 and 33 ms^{-1}. The differences are quite striking. In the case of decreased shear, v' must increase in order that the same magnitude of topographic forcing is balanced. A larger v' means a larger amplitude ridge over the ice sheet. It is also phase shifted further west. A decreased shear also means that the mean tropospheric wind decreases and therefore, as explained in Section 3.1.2, the wavelength of the external Rossby wave decreases.

For the ranges of shears shown in Figure 3.16 the far field response differs widely. There are two reasons for this. If the wavelength of the external mode changes then, first, the phase of the stationary wave at any given location changes, and secondly, the projection of the external mode onto the topographic forcing is different. As seen in Figure 3.5 the topographic forcing varies quite strongly as a function of wavenumber.

The characteristic sawtooth shape of the ice age cycles means that the ice sheets are at, or close to, maximum size for at least a full precessional cycle before their collapse. The climate forcing varies significantly over one precessional cycle of the earth's orbit and so the relevant basic state must also be expected to vary. The above results suggest that the stationary wave response to those ice sheets, and especially the remote response, should also vary strongly over that cycle, despite the fact that the ice sheets themselves might not be changing much.

3.3.3 Lapse rate

High latitudes are generally characterized by more stable air and hence higher static stability. But we are also interested in ice sheets which exist in midlatitudes. The quasigeostrophic scaling does not allow for a variation in N^2 with latitude, and so we must adopt a compromise value. The range of lapse rates shown in Figure 3.17

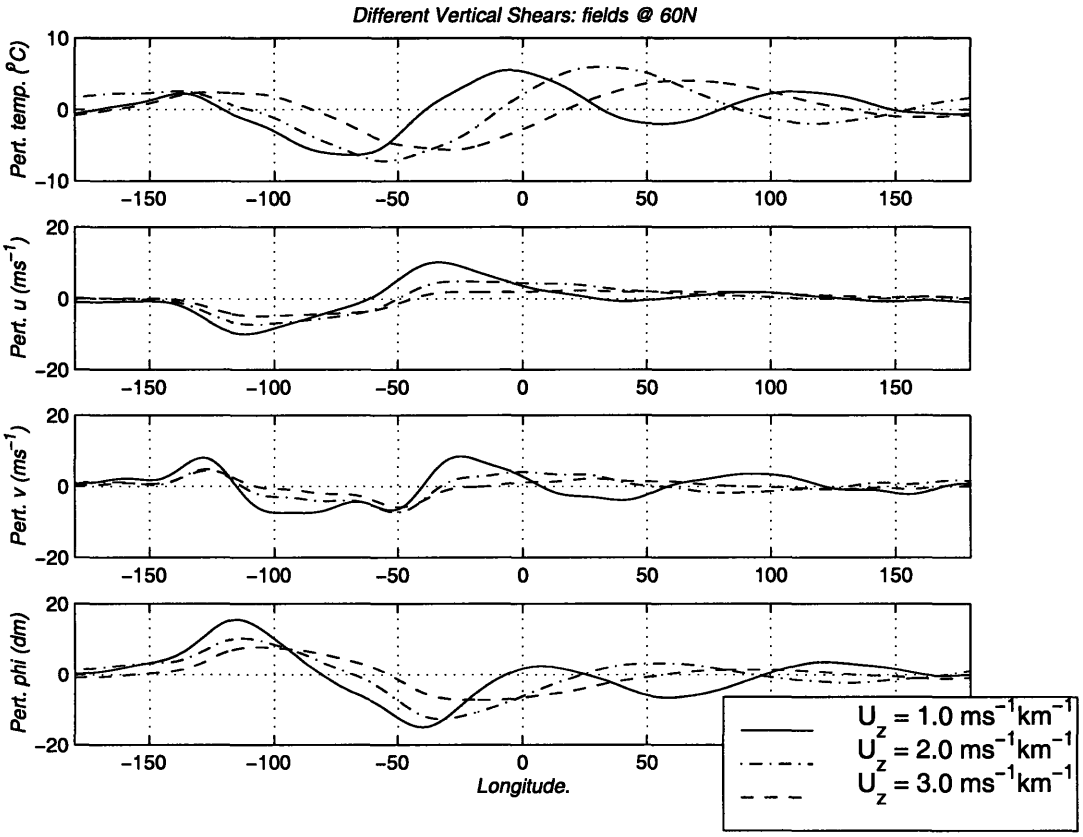

Figure 3.16: Sensitivity of atmospheric response to basic state wind shear. Fields are at $1km$. The middle value is the standard basic state. The test ice sheet lies between $130W$ and $50W$. Panels are as for Figure 3.7.

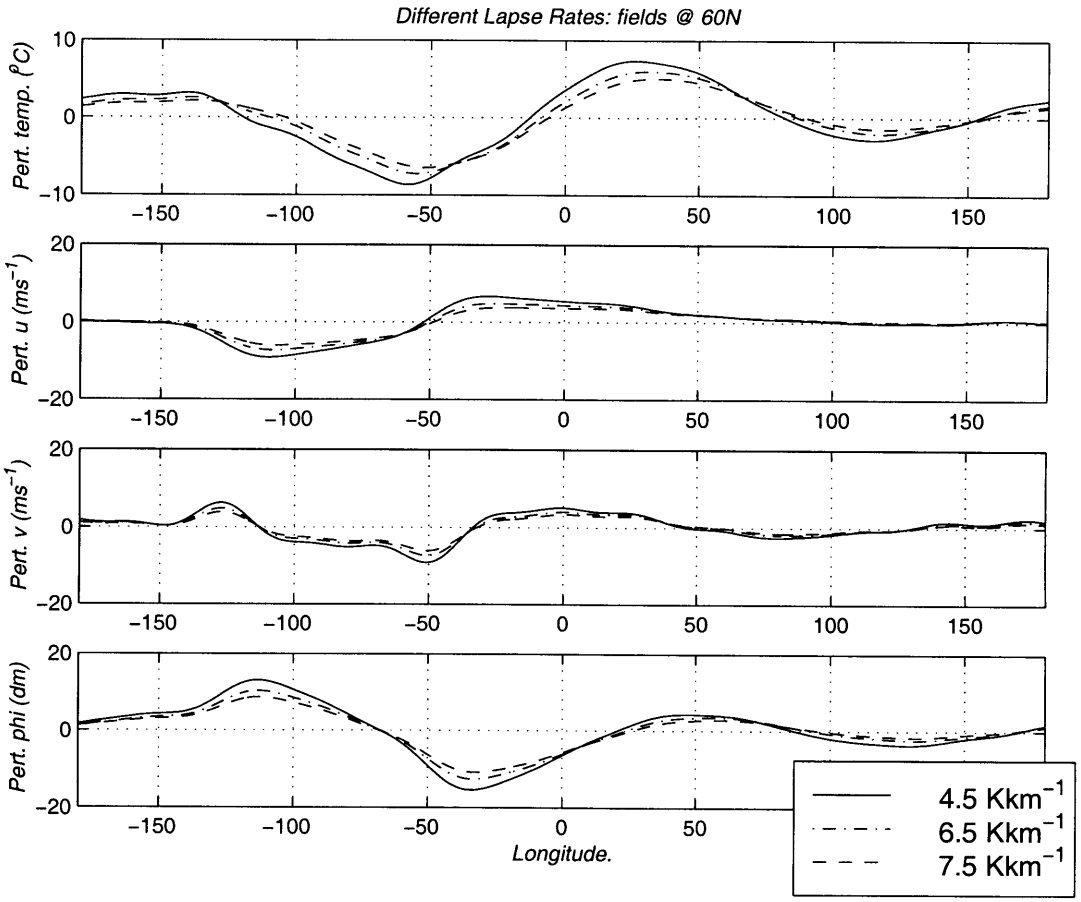

Figure 3.17: Sensitivity of atmospheric response to basic state lapse rate. Fields are at $1km$. The middle value is the standard basic state. The test ice sheet lies between $130W$ and $50W$. Panels are as for Figure 3.7.

corresponds to a range in N of between $0.86 \times 10^{-2} s^{-1}$ and $1.4 \times 10^{-2} s^{-1}$. The changes in the stationary wave response are not large, and the main effect of varying N is to change the size of the topographic forcing in the lower boundary condition (Equation (3.19). An increased N^2 leads to a decrease in the value of the PV gradient (Equation (3.13)). Hence from Equation (3.24) the wavelength of the external Rossby wave should increase. Figure 3.17 shows that this happens but the effect is again quite small.

3.3.4 Latitude of β, f_0 calculation

The standard case takes β and f_0 as calculated at a latitude of $60N$. We are interested in ice sheets which exist from $70N$ down to around $40N$. We would therefore like to

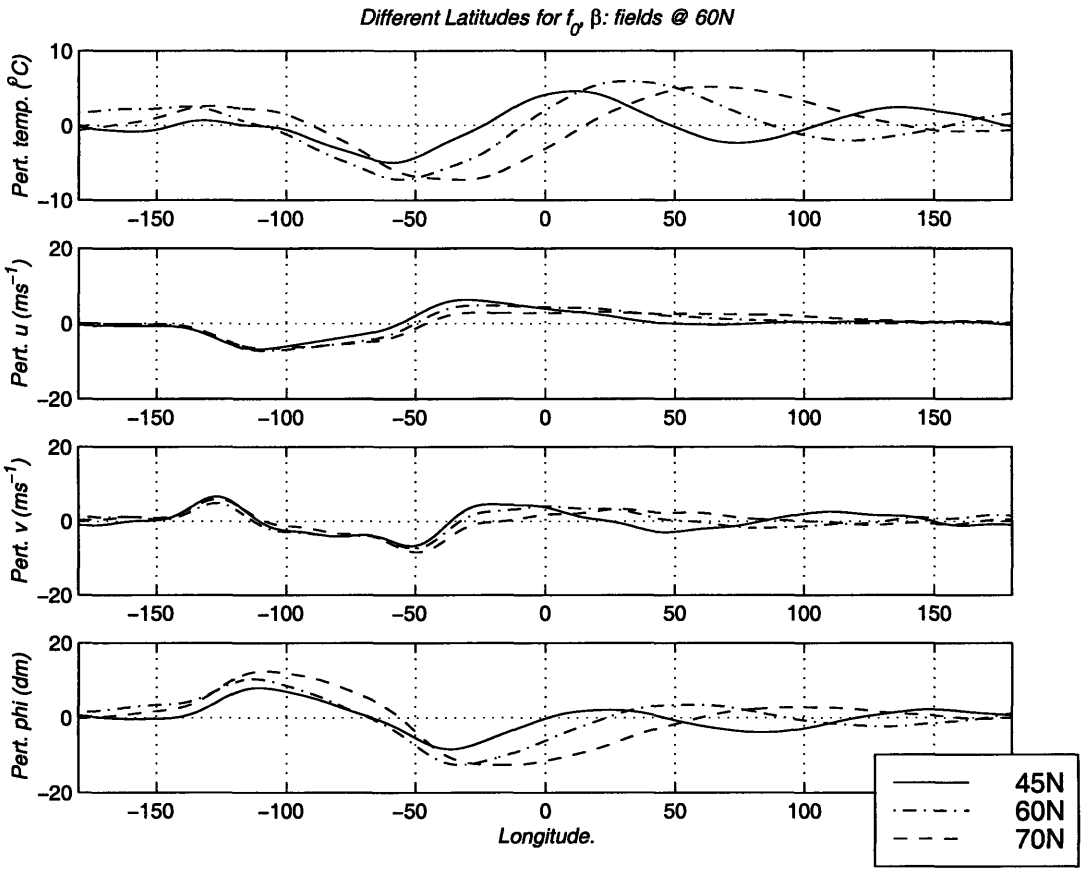

Figure 3.18: Sensitivity of atmospheric response to latitude taken for β and f_0. Fields are at $1km$. The middle value is the standard case. The test ice sheet lies between $130W$ and $50W$. Panels are as for Figure 3.7.

know what difference it makes to the atmospheric response to take different values for β and f_0. Figure 3.18 shows the stationary wave response for the calculation of β and f_0 at three different latitudes, 45N, 60N, and 70N. To facilitate an easier comparison, we have kept the length of the channel equal to that of a longitude circle at $60N$. Hence the forcing magnitude does not change as a function of wavenumber between the different cases.

Figure 3.18 shows that, close to the ice sheet, u' and v' are not affected much by the calculations at different latitudes. This is because the low level velocities are largely determined by the forcing topography, which we have kept fixed in this comparison. There are changes in the far field response, however, and again the difference in the response is due to changes in the basic state PV gradient. Calculating β and f_0 at $45N$ gives a lower troposphere PV gradient of $3.7 \times 10^{-11} s^{-1}$. Calculating the same at $70N$

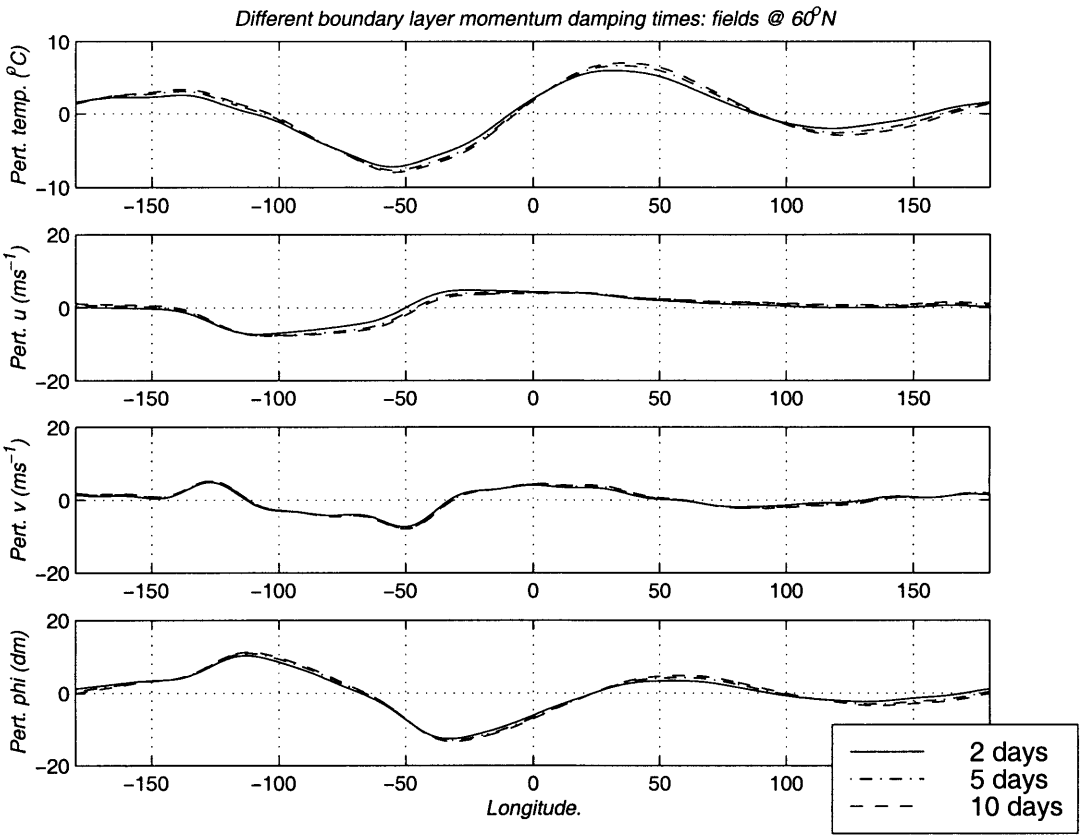

Figure 3.19: Sensitivity of atmospheric response to boundary layer momentum damping time. Fields are at $1km$. The middle value is the standard case. The test ice sheet lies between $130W$ and $50W$. Panels are as for Figure 3.7.

gives a lower troposphere PV gradient of $4.5 \times 10^{-11} s^{-1}$. From Equation (3.24) therefore, calculating β and f_0 at higher latitudes leads to an increase in the wavelength of the external Rossby wave.

3.3.5 Boundary layer damping times

The atmospheric response proves to be insensitive to the boundary layer momentum damping time over a wide range of values, shown in Figure 3.19. Figure 3.20 shows the results for the same range of values of the thermal damping time. While the u', v', and ϕ' fields are not changed very much, the temperature field depends strongly on the value of τ_r used in the boundary layer.

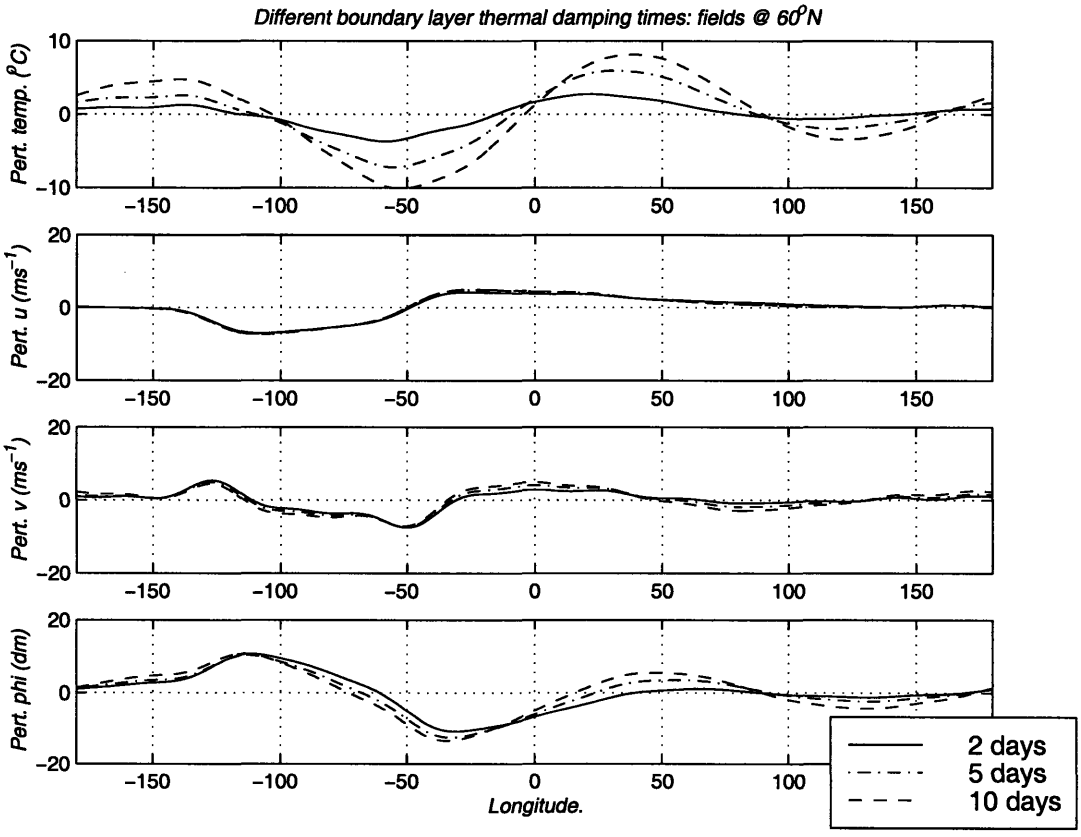

Figure 3.20: Sensitivity of atmospheric response to boundary layer thermal damping time. Fields are at $1km$. The middle value is the standard case. The test ice sheet lies between $130W$ and $50W$. Panels are as for Figure 3.7.

The reason for this behavior can be seen from the canonical form of the wave equation developed in Section 3.1.1. Equation (3.21) made the two assumptions; that N^2 and τ_r were both constant. If we are considering the solution only in the boundary layer, then these assumptions hold for our basic state profiles. λ is a function of both τ_m and τ_r but near the surface the dependence on τ_r is stronger at low wavenumbers. This is because $\overline{U}$ is small and therefore the $\overline{q}_y/\overline{U}$ dominates over the other terms inside the square brackets in Equation (3.21). The physics of what is happening can be seen from Equation (3.20). For low wavenumbers and close to the surface, the PV equation is a balance between the stretching term (the term containing the vertical derivatives of geopotential), which is damped by the thermal damping time, and the advection of the planetary vorticity gradients by the perturbation winds (the $\overline{q}_y/\overline{U}\phi_{kl}$ term). The momentum damping, τ_m, only acts on the term originating from advection of the relative vorticity by the basic state (the $(k^2+l^2)\phi_{kl}$ term). This only plays a significant role in the balance, for high wavenumbers, or higher up in the atmosphere where $\overline{U}$ is larger.

The WKB solution to Equation (3.20) confirms the reasoning above. Strictly speaking, the scaling appropriate to Equation (3.21) is beyond the domain of validity for WKB theory (e.g. Bender and Orzag, 1978). However the theory often performs well even if the scaling justifications do not apply to the equation concerned, and it provides a useful tool to show the qualitative behavior of the solution (see Held, 1983, for example). The WKB solution to Equation (3.21) has the form

$$\phi_{kl} \sim e^{(z/2H)} \frac{A}{\sqrt{\lambda}} exp\left(-i\int^{z'} \lambda dz'\right) \tag{3.28}$$

where we have substituted back for the real geopotenitial ϕ_{kl}. z' is a dummy integration variable, and A is a constant such that the lower boundary condition is satisfied. Since the temperature is proportional to the vertical gradient of the geopotential, we have

$$T'_{kl} \sim \frac{\partial \phi_{kl}}{\partial z} \sim Ae^{z/2H} exp\left(\int^{z'} \lambda dz'\right)\left\{\frac{1}{2H\sqrt{\lambda}} - \frac{1}{\lambda}\frac{d\sqrt{\lambda}}{dz} - i\sqrt{\lambda}\right\}. \tag{3.29}$$

Figure 3.21 shows the results from calculating the magnitude of amplitude factor for the temperature (the term inside the curly brackets of Equation (3.29)) for different combinations of damping times (2.5 days or 5 days) and using the standard case basic state profiles at the surface. We show the results as a function of zonal wavenumber,

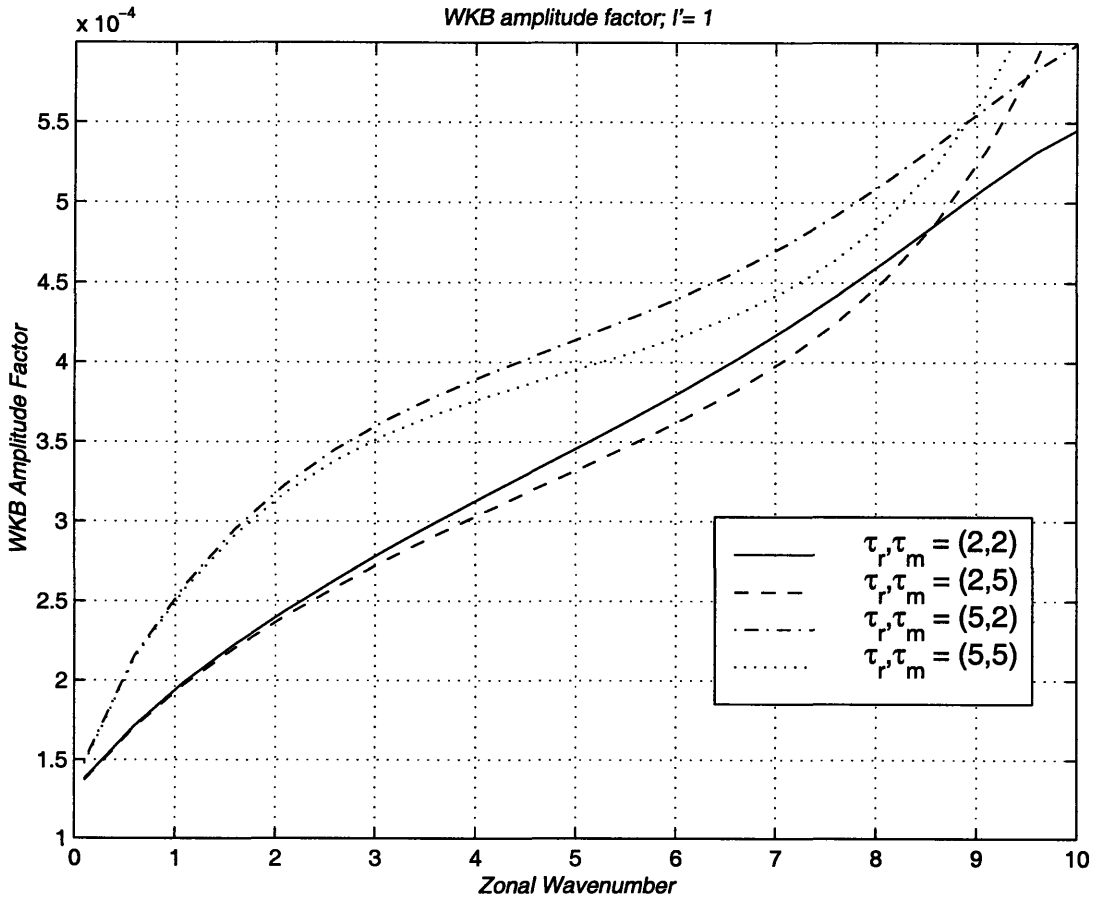

Figure 3.21: WKB amplitude factors (as defined in the text) for temperature, as a function of zonal wavenmuber ($l' = 1$) for various boundary layer momentum and thermal damping time scales (units in *days*). Units of amplitude factor are arbitrary.

keeping the meridional wavenumber fixed at $l' = 1$. For $l' = 1$ the overall atmospheric response is largest at zonal wavenumbers 2, 3, and 4 (Figure 3.3). For this range of zonal wavenumbers, the momentum damping time makes virtually no difference to the solution amplitude, and all sensitivity is to the thermal damping time. It is only at higher wavenumbers ($k' > 6$) that momentum damping has as large an effect as the thermal. For these higher wavenumbers however, both the topographic forcing and the atmospheric response are small, and so they contribute little to the total response.

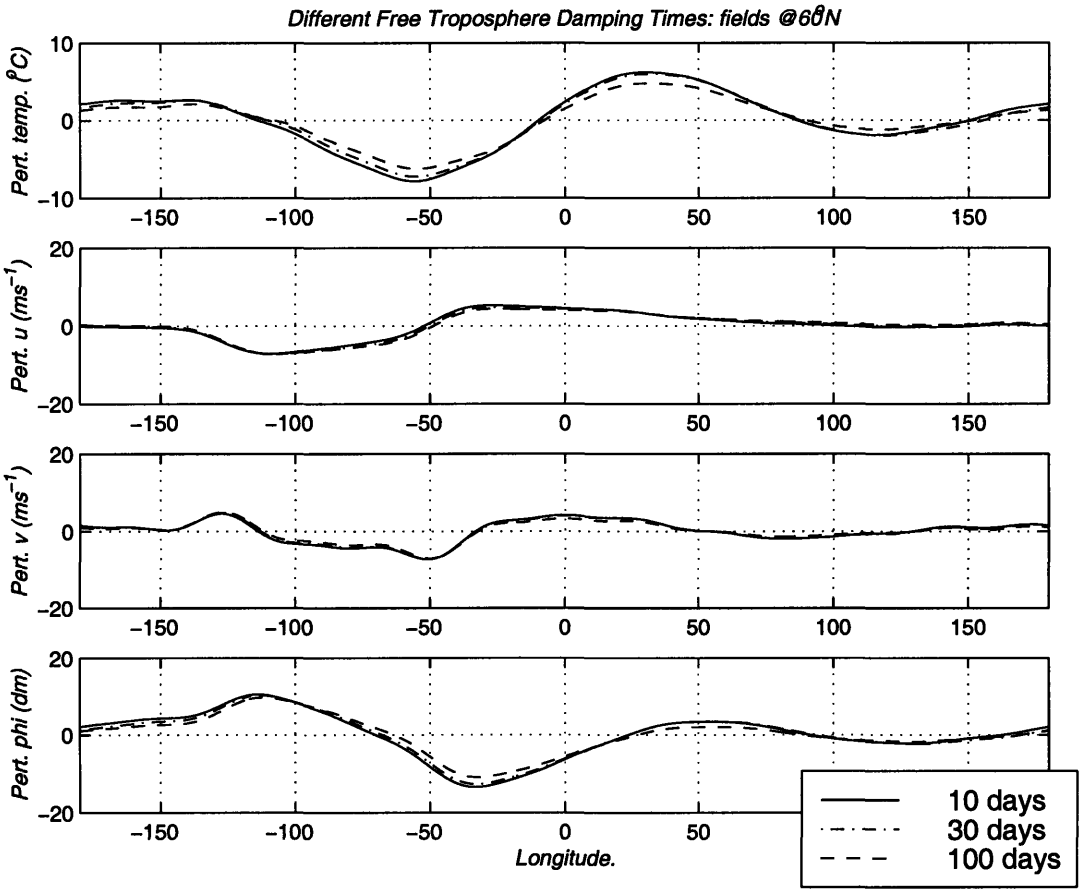

Figure 3.22: Sensitivity of atmospheric response to free troposphere damping times, momentum and thermal. Fields are at $1km$. The middle value is the standard basic state. The test ice sheet lies between $130W$ and $50W$. Panels are as for Figure 3.7.

3.3.6 Free atmosphere damping times

Neither the thermal or momentum free tropospheric damping times have a significant effect on the low level response. In Figure 3.22 we show the results for varying both the thermal and momentum damping times over a wide range of values. The boundary layer thermal and momentum damping times damping times were kept at 2 and $5days$ respectively.

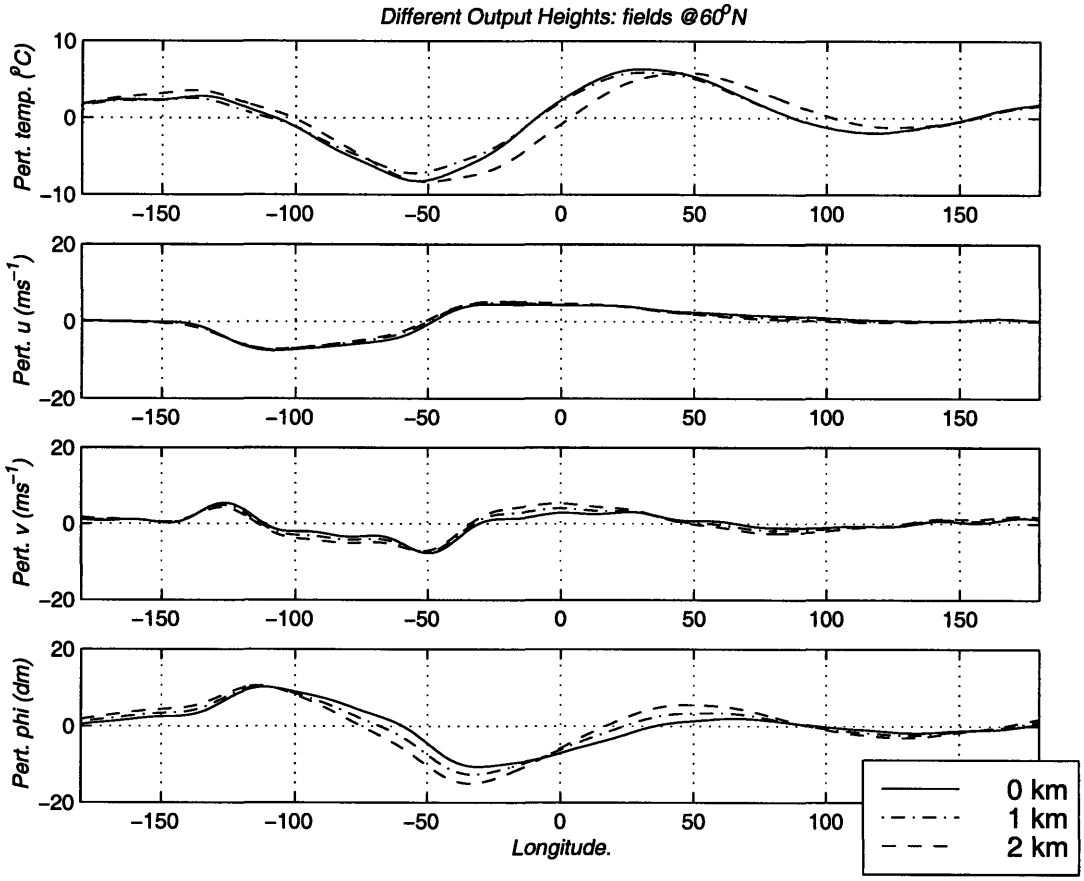

Figure 3.23: Sensitivity of atmospheric response to model output height. Standard basic state used. The middle value is the standard. The test ice sheet lies between $130W$ and $50W$. Panels are as for Figure 3.7.

3.3.7 Output fields at different heights close to the surface

We have chosen to show the perturbation fields in the preceeding sections at a height of $1km$. Figure 3.23 shows the fields output from the model levels at the surface, at $1km$ and at $2km$. Within the boundary layer the fields do not vary much with height. $2km$ is in the transition zone between the boundary layer damping and the free troposphere damping. As noted already, the temperature begins to change at that level because of the change in $d\phi'/dz$ (Figure 3.4).

The atmospheric model couples to the ice sheet model via the low level winds and temperatures (which are inputs into the mass balance parameterizations). Figure 3.4 shows that we can assume that over the depth of a typical ice sheet $(2 - 3km)$, the

perturbation fields are constant with height. We can therefore use the output from the atmospheric model at just one level (we choose $1km$). This removes the need to interpolate onto the ice sheet surface from different atmospheric levels when calculating the mass balance.

3.3.8 Different numbers of wavenumbers

For computational speed we would like to limit the number of wavenumbers used in building up the stationary wave fields. Since the atmospheric response to forcing drops off rapidly with increasing wavenumber (Figure 3.3), we should be able to retain a small set of wavenumbers and still capture all important details of that response. We found using 15 zonal wavenmubers and 25 meridional wavenumbers was sufficient. The reason we need to keep more meridional wavenumbers is because, relative to the size of the channel, the ice sheet is smaller in the y direction than in the x direction. The far field response could be captured accurately using keeping fewer wavenumbers (since most of the response is the external Rossby wave), but the details of the flow close to the ice sheet required the larger number of wavenumbers that we have retained.

3.3.9 Different cut-off thresholds

To speed up computation a little, we have used a cut-off threshold on the topographic forcing. We only calculate the atmospheric response at wavenumbers where the topographic forcing is greater than 5% of the maximum forcing. If the threshold was increased to 10%, then some of the detail began to be lost compared to the solution using all the wavenumbers.

3.4 Sensible heating

Observations shows that the surface of an ice sheet is generally colder than the air lying immediately above it (Paterson, 1994). There is on average, therefore, a net cooling of the layer of air above the snow or ice. An important question is what is the size of the flow that is induced in the atmosphere by this net cooling. In a simulation of the

climate existing over the Laurentide ice sheet at the last glacial maximum, Cook and Held (1988) concluded that the flow due to the topographic forcing dominated over the effects of the sensible and latent heat fluxes. The diabatic cooling of the atmosphere over the Laurentide maximized at $1Kday^{-1}$, averaged over the lower troposphere. Their simulation, however, was for a winter climate, when the topographic effects would be largest, so it is not clear whether the dominance of the topographic forcing holds year-round in an ice age climate.

We can use our model to look at the size of the response to an imposed diabatic heating profile. We concentrate on the sensible heat flux because although latent heating is an important part of the surface energy budget where ice is melting, the ablating regions are restricted to the ice sheet margins. The forcing on the atmospheric flow is therefore small compared to the sensible heating. If diabatic heating is retained in the development of the quasi-geostrophic equations, Equation (3.11) becomes

$$\overline{U}\frac{\partial q'}{\partial x} + v'\overline{q}_y + \frac{1}{\tau_m}\frac{{\nabla_h}^2\phi'}{f_0} + f_0 e^{z/H}\frac{\partial}{\partial z}\left(\frac{e^{-z/H}}{N^2}\frac{1}{\tau_r}\frac{\partial\phi'}{\partial z}\right) = \frac{f_0^2 R}{Hc_p}\frac{\partial}{\partial z}\left\{\frac{e^{-z/H}\dot{Q}}{N^2}\right\}, \qquad (3.30)$$

and the lower boundary condition Equation (3.15) can be rewritten as

$$\overline{U}\frac{\partial}{\partial x}\left(\frac{\partial\phi'}{\partial z}\right) - \frac{\partial\phi'}{\partial x}\left(\frac{\partial\overline{U}}{\partial z}\right) + \frac{1}{\tau_r}\frac{\partial\phi'}{\partial x} = -N^2\overline{U}\frac{\partial z_s}{\partial x} + \frac{R}{c_p H}\dot{Q} \qquad (3.31)$$

where $\dot{Q}$ is the rate of heating per unit mass. If it is assumed that the sensible heat flux is mixed quickly within the boundary layer, then the sensbile heating and $\dot{Q}$ are related by Equation (3.25).

Measurements and modeling from glaciers and ice sheets (e.g. Ohmura et al., 1994; Brun et al., 1989) suggest that the time averaged sensible heat flux over such a surface is between 10 and $20Wm^{-2}$. It can however reach much higher values at any given moment, depending on the prevailing meteorological conditions (for example, Ohmura et al. measured sensible heat fluxes of up to $60Wm^{-2}$ on Greenland).

We consider the response to a $15Wm^{-2}$ cooling imposed over the area of the test ice sheet. The topographic forcing is set to zero. Figure 3.24 shows that this produces a small cooling over the ice sheet (reaching a maximum of about $\sim 2.5^oC$ over the eastern

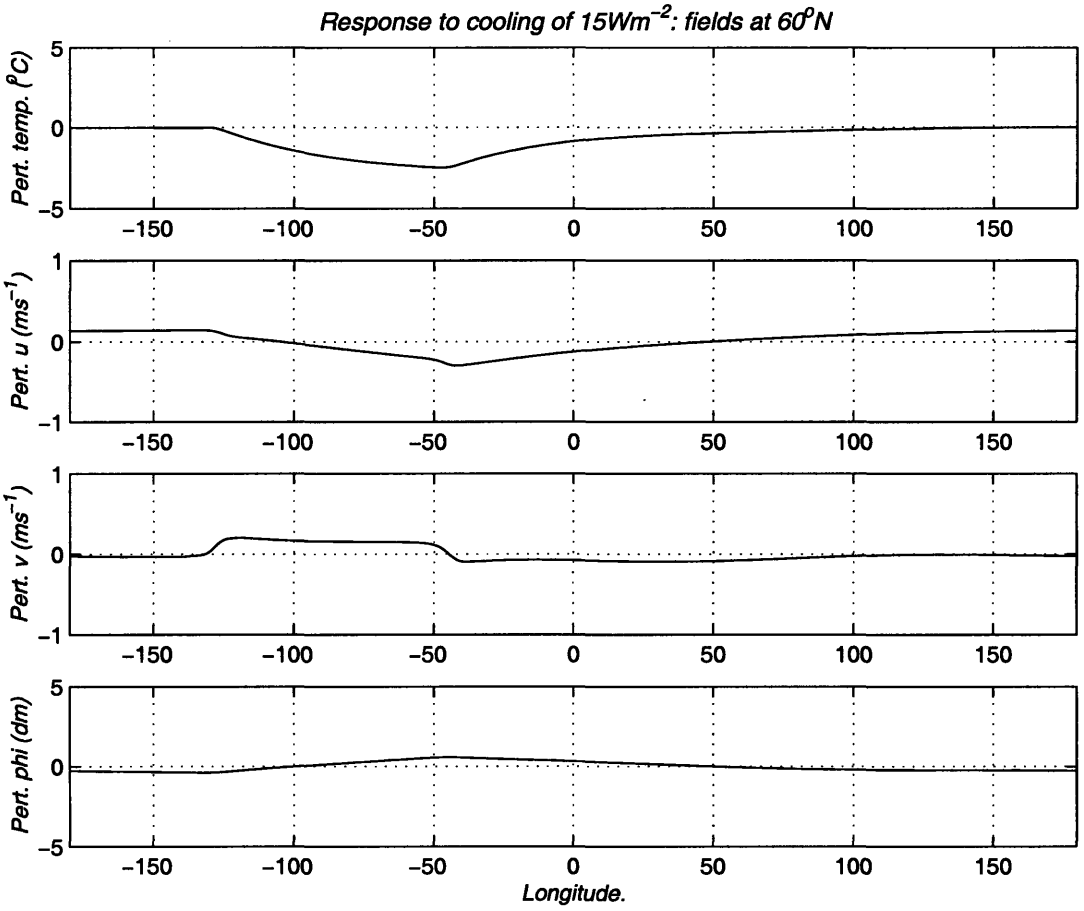

Figure 3.24: Response to imposed cooling of $15Wm^{-2}$ over region of test ice sheet. Topographic forcing is set to zero. Fields are output at $z = 0$. The test ice sheet lies between $130W$ and $50W$. Panels are as for Figure 3.7. Note, though, the changed axes limits.

slopes) and a weak response in the wind and geopotential fields. The temperature perturbation found here compares with summer measurements over Greenland (Steffen, K. et al., 1996) where the mean difference between land and air temperature is less than 1^oC. Stronger temperature inversions can exist over Antarctica (up to 20^oC (Schwerdtfeger, 1970)). The difference is likely due to the fact that the air mass over Antarctica is much more stationary than that over Greenland.

Both the temperature and geopotential perturbation associated with this imposed cooling are much smaller than the solutions for topographic forcing (e.g. Figure 3.7). This is consistent with the results of Cook and Held (1988), and means that the high pressure region over the ice sheets, which is common to all GCM simulations of the LGM

climate, is topographic in origin. For the high pressure to be a result of diabatic cooling, a much larger cooling would be required than that which is supported by observations in today's climate.

The time scale for the boundary layer damping depends on the depth of the boundary layer chosen (i.e. Equation (3.25)). For a given sensible heating, if the chosen depth of the boundary layer is decreased, then the thermal damping time must decrease proportionately. For the same $15Wm^{-2}$, a calculation was made with a $200m$ boundary layer depth and a $0.5day$ damping time scale, and holding the free tropospheric damping times fixed at the standard values. The magnitude of the cooling over the ice sheet increases to 3^oC, and the phase of the response shifts so that the cold temperature perturbation sits directly over the region of imposed cooling. The geopotential and wind response remain small. The atmospheric response decreases quickly above the top of the boundary layer, consistent with the result that for surface heating, the amplitude of the response decreases exponentially with a characteristic scale equal to the depth of the heating (Pedlosky, 1992).

Summary

In this chapter we have described the linear quasigeostrophic stationary wave model we have used to represent the atmospheric response to an evolving ice sheet. We have shown the characteristic response we expect to a steeply sided ice sheet; an asymmetric high pressure ridge sits over the western slopes of the ice sheet with tight pressure gradients to the west and weaker ones spreading over most of the ice sheet to the east. Balanced with this are northerly winds over the majority of the ice sheet. These winds bring cold air from the north, leaving the ice sheet generally colder than it would be in the zonally averaged climate.

The model we are using has some important limitations. We have chosen to use a model without meridional variation in the basic state. While this likely does not affect the immediate response over the ice sheet itself, the downstream propagation of the stationary waves will be changed. In the real atmosphere, the presence of the zero wind line in the tropics means that there is a singularity there in the refractive index of the basic state. Stationary wave activity is refracted towards the lower latitudes as

it propagates away from the source. This behavior is missing from our model, and it means that the far field model response, away from the ice sheet, will be different from the response in a model with meridional variation. We are also not able to look at the circumstances under which high latitude stationary waves might be confined meridionally by the atmospheric basic state (Held 1983). Held suggests that the variation of the effectiveness of meridional trapping (which is sensitive to changes in the basic state) might be a cause of stationary wave variability. A spherical coordinate model with full meridional variation in the basic state could look at these questions in more detail.

For ice sheets of the size we are interested in, the assumption of linearity in our model is also open to question, and we expect the nonlinear calculations to modify the response somewhat. Previous works suggests that the linear calculation overestimates the size of the stationary wave by up to a factor of two, and that the center of the high pressure ridge is shifted to the northwest.

We have also examined the sensitivities of the model response to different, but still plausible, basic states. The stationary wave amplitude is linearly proportional to the forcing wind, $\overline{U}_f$, which is an arbitrary choice, and the low level temperatures are also sensitive to the choice of thermal damping time, which is not well constrained by measurements of sensible heat fluxes over ice (Section 3.1.3). We have taken values for these parameters which give results consistent with observations of today's climate, but Figure 3.20 suggests that the amplitude of the stationary wave temperatures over the ice may be uncertain by a factor of two. The far field response depends on the wavelength of the external Rossby wave, which is sensitive to parameters which alter the basic state PV gradients. The phase of the stationary wave remote from the forcing topography can be reversed, leading to a local temperature change of perhaps 5^oC (Figure 3.16). We therefore expect that the remote stationary wave response can change significantly over a $20kyr$ precessional cycle of the earth's orbit.

The pattern of atmospheric response to the ice sheet is robust. This gives confidence that the physics of the interaction between the ice sheet and the atmospheric flow will be qualitatively well represented in our model. The sources of uncertainty we have found in the magnitude give an indication of the range of possible behavior of the coupled atmosphere-ice sheet system during the ice ages. In the next chapter we review the physics of ice sheet modeling and introduce ablation and melting parameterizations which will enable the coupling of an ice sheet to the stationary wave it induces.

Chapter 4

Ice sheets, accumlation, ablation, and the seasonal cycle

In Chapter 2 ice flow was treated using the perfectly plastic material approximation; the ice adjusts instantaneously to changes in its mass balance. In actuality ice behaves as a viscous fluid, slowly spreading under its own weight. The flow of ice may be modeled in a more sophisticated manner by integrating the appropriate equations of motion. We first review these equations, and then introduce the shallow ice approximation which takes advantage of the aspect ratio of an ice sheet. This scaling analysis greatly simplifies the equations. The numerical ice sheet model used in this thesis is the SICOPOLIS code of Greve (1995). While this code has an ability to comprehensively model the thermodynamic behavior of ice sheets, we will use the code in isothermal mode; that is, the temperature within the ice is set to a constant everywhere. We will show that the general shape of an ice sheet is unchanged by making the isothermal approximation, and so we argue that retaining the temperature dependence is an unnecessary complication for our purposes.

Simplicity is also a motivation in choosing representations of ablation and precipitation. Melting occurs at the edge of ice sheets and during the summer. This is the important property of ablation as far as this thesis is concerned, and the full physics involved in melting is not needed to capture it. Similarly, for the precipitation parameterization, we will emphasize the role of topography. Snowfall accumulates preferentially on the upwind slopes of the ice sheet creating an east-west gradient in accumulation.

However, the parameterization we develop does not account for the location of moisture sources nor does it include increased precipitation in regions of enhanced baroclinicity. We will discuss the consequences of these assumptions in later chapters.

This chapter also shows results from an integration of the ice sheet model in a zonally averaged climate. An analysis of the mass budget is made, and the equilibrium ice sheet is discussed in the context of the simpler modeling study in Chapter 2. Lastly we look at the stationary wave response for seasonal changes in the basic state, and consider the effect of the seasonal cycle on the ablation and accumulation budgets.

4.1 Ice sheet modeling

An ice sheet may be modeled as an isotropic, incompressible, nonlinear, viscous, heat conducting fluid (e.g. Hutter, 1983). Stresses exist within the ice sheet due to the weight of the overlying ice. The ice responds to these stresses by slow deformation (creep flow). The response of the ice is highly nonlinear however; the strain rate increases roughly as the third power of the applied stress. The flow is also strongly temperature dependent, which means that factors such as frictional heating within the ice and geothermal heating from below also affect the dynamics of the ice sheet.

Ice behaves according to laws of conservation of momentum, mass, and energy. The following discussion is based largely on Calov and Huttter (1996), and Abe-Ouchi (1993). Incompressibility gives

$$\nabla \cdot \vec{\nu} = 0. \tag{4.1}$$

where $\vec{\nu}$ is the ice velocity. The assumption of incompressibility neglects the processes that occur in the uppermost $50m$ as the snow and firn is gradually compressed into ice (Paterson, 1994).

The flow of ice can be approximated by Stokes flow, since accelerations within the ice are negligible. In this case, Newton's second law of motion becomes

$$0 = -\nabla p + \nabla \cdot \boldsymbol{t}' + \rho_I \vec{g}. \tag{4.2}$$

Here p is the isotropic pressure, $\boldsymbol{t}'$ is the deviatoric stress tensor (the full Cauchy stress tensor minus the isotropic pressure), and ρ_I is the density of ice (taken to be $910 kgm^{-3}$). The thermodynamic equation can be expressed as

$$\rho_I C_I \frac{\partial T_I}{\partial t} = -\nabla \cdot (\kappa \nabla T_I) + tr(\boldsymbol{t}'\boldsymbol{D}) - \delta L \dot{m} \tag{4.3}$$

T_I is the ice temperature, C_I is the specific heat capacity, which is temperature dependent ($C_I = 146.3 + 7.253T[K] Jkg^{-1}K^{-1}$). Likewise, κ, the thermal conductivity, has some temperature dependence ($\kappa = 9.828 exp(-0.0057T[K])$ (Ritz, 1988). $\boldsymbol{D}$ is the strain rate tensor, and $tr(\boldsymbol{t}'\boldsymbol{D})$ is the pressure work term, and represents frictional heating within the ice. L is the latent heat of melting for ice, δ is a switch representing whether melting is occurring or not, and $\dot{m}$ is the volumetric melting rate.

To close the equations, a constitutive relation (or flow law) is required to relate the strain rates to the applied stresses.

$$\boldsymbol{D} = A(T_I')f(t_s')\boldsymbol{t}' \tag{4.4}$$

t_s' is the second invariant of the deviatoric stress tensor ($t_s' = \frac{1}{2}tr(\boldsymbol{t}'^2)$). T_I' is the homologous temperature which is the actual temperature minus the melting temperature. The melting temperature for ice decreases with increasing pressure due to the Claussius-Clapeyron relation.

The usual constitutive relation used in ice modeling is Glenn's Flow Law (Paterson, 1994).

$$f(t_s') = (t_s')^{\frac{n-1}{2}} \tag{4.5}$$

t_s' is effectively a measure of the magnitude of the stress acting on an element within the ice sheet. The value of n is an empirical fit to laboratory measurements and to field data. The usual value taken for ice sheet modeling is $n = 3$. No qualitatively different behavior has been found in ice sheet modeling for other values of n.

Warmer ice flows faster, and to account for this temperature dependence, an Arhenius-type law is used:

$$A(T_I') = EA_0 e^{\frac{-Q}{R(T_I'+T_0)}} \tag{4.6}$$

where $T_0 = 273K$, Q is an activation energy with an experimentally determined value of about $139kJmol^{-1}$ for temperatures at or above -10^oC. The constant, A_0, is chosen such that $A(T_I' = -10^oC) = 5.2 \times 10^{-25}s^{-1}Pa^{-3}$ (Greve, 1995). Modeled thermomechanical ice sheets show that for Greenland, a reasonable range of temperatures is from around -40^oC at the upper surface, increasing up to pressure melting temperature at the base, typically around -5^oC. (Calov and Hutter, 1996; Abe-Ouchi, 1993). E is an enhancement factor introduced to account for other factors within the ice which change its flow properties, such as aerosol (dust) loading and ice crystal orientation. Ice formed during glacial climates is observed to be less viscous than ice formed during interglacials (e.g. Paterson, 1994), and a value of $E = 3$ is commonly used during glacial climates to account for this (e.g. Greve, 1995). We have used $E = 3$ for all simulations. Since the overall structure of the ice sheet is not affected by the value of E, the choice is relatively unimportant for our purposes.

Equations (4.5) and (4.6) imply that, since both the stress and the temperature increase with depth, the largest flow of ice will occur near the bottom of the ice sheet.

4.1.1 Shallow ice approximation

The equations in the previous section can be simplified by using the shallow ice approximation (formalized in Hutter, 1983; Morland 1984), which takes advantage of the fact that the horizontal length scales in ice sheets are typically very much larger than vertical length scales. Therefore variations in quantities in the horizontal direction may be neglected compared to variations in the vertical. Using this assumption, scale analysis yields the shallow ice equations. The momentum balance reduces to:

$$\sigma_{zz} = -\rho_I g(h_s - z) \tag{4.7}$$

$$\sigma_{xz} = -\rho_I g(h_s - z)\frac{\partial h_s}{\partial x},\ \sigma_{yz} = -\rho_I g(h_s - z)\frac{\partial h_s}{\partial y} \tag{4.8}$$

The σs are the individual elements in the stress tensor, $\boldsymbol{t}$, and h_s is the height of the top surface of the ice sheet. Equation (4.7) is the hydrostatic balance: the force in the vertical direction on the vertical surface is equal to the weight of the overlying ice (i.e. the pressure head). The physical meaning of Equation (4.8) is that there is a force balance between the horizontal shear stresses within the ice and the horizontal variations in the overlying pressure head. Equation (4.8) results in a steeply sided ice sheet: a large stress (i.e. σ_{xz}) at the bottom of an ice sheet is a consequence of either a large depth (i.e. large $(h_s - z)$) or steeply sloping topography. This is essentially the same argument as maintaining the yield stress in perfectly plastic approximation made in Chapter 2.

The relations in Equation (4.8) are combined with the flow law and the thermodynamic equation to give the velocity and temperature fields within the ice sheet.

$$\vec{\nu_h}(x, y, z, t) = \vec{\nu_h}(b) + C(z, t, \|\nabla_h h_s\|)\nabla_h h_s \tag{4.9}$$

where $\vec{\nu_h}$ is the horizontal velocity field and h_b is the bottom surface velocity.

$$C(z, t, \|\nabla_h h_s\|) = -2(\rho_I g)^n \|\nabla_h h_s\|^{n-1} \int_{h_b}^{z} A(T_I'(z'))(h_s - z)^n dz' \tag{4.10}$$

and

$$\|\nabla_h h_s\| = \sqrt{(\frac{\partial h_s}{\partial x})^2 + (\frac{\partial h_s}{\partial y})^2}. \tag{4.11}$$

The thermodynamic equation becomes

$$\frac{\partial T_I}{\partial t} = \kappa \frac{\partial^2 T_I}{\partial z^2} - \vec{\nu} \cdot \nabla T_I + EA(T_I'(z'))\frac{2(\rho_I g)^{n+1}}{\rho_I C_I}(h_s - z)^{n+1}\|\nabla_h h_s\|^{n+1} \tag{4.12}$$

Equation (4.9) is the only place where the ice temperature couples to the ice velocity. In this thesis, we use the SICOPOLIS model in isothermal mode; the temperature is set to a constant, -10^oC, and the melting temperature is held fixed at 0^oC. The isothermal approximation can give a good approximation to the flow if the temperature chosen

is representative of a layer where the ice flow is largest, namely in the lowest layers of the ice sheet. We are only concerned here with the overall shape of the ice sheet and this is not changed by using the isothermal approximation. Under the isothermal approximation, Equations (4.9) and (4.10) can be integrated analytically in the vertical to yield an equation for the height of the ice sheet surface as a function of horizontal position.

After developing the accumulation and ablation parameterizations in the sections below, we will show the effect of using a different isothermal temperature and also of using the full thermomechanically coupled ice sheet calculations that the SICOPOLIS code is capable of.

4.1.2 Ice sheet boundary conditions

We require boundary conditions for the ice sheet. Since our runs are isothermal, we will discuss only the mechanical boundary conditions. At the upper surface, the ice is assumed to be stress free. The appropriate lower boundary condition for ice sheets has been analyzed in recent modeling efforts. Calov and Hutter (1996) argue, based on comparison of modeling results with observations for Greenland, that a no-slip boundary condition is correct for a cold ice (i.e. frozen) base, but that a basal sliding law (e.g. Paterson, 1994) should be used in those regions where the ice is temperate (a mix of water and ice). In their work, the use of a sliding law changed the shape of some of the slopes overlying areas where the base was temperate, consistent with observations. Ritz et al. (1995) however find that over a large range of the sliding law coefficient (including zero sliding), the changes in area, altitude and volume of the Greenland ice sheet were relatively small. Since the basic shape of the ice sheet is unchanged by the lower boundary condition employed, we choose to use a no-slip boundary condition.

As mentioned in Chapter 2, a continental scale ice sheet is heavy enough to depress the underlying bedrock. The process of bedrock adjustment is represented in the SICOPOLIS code by a relaxation to isostatic equilibrium. Isostatic equilibrium is the state governed by Archimedes' principle; each column of the ice sheet is considered to displace an amount of bedrock whose weight is equal the weight of the ice column. However, the bedrock cannot respond instantly to changes in loading; it takes several thousand years to come to equilibrium. The lower ice sheet boundary, h_b, is therefore

described by the following equation.

$$\frac{\partial h_b}{\partial t} = -\frac{1}{\tau_{iso}}\left(h_b - h_0 + \frac{\rho_I}{\rho_M}(h_s - h_b)\right) \tag{4.13}$$

$h_0(x, y)$ is the relaxed state of the bedrock topography in the absence of ice sheets. τ_{iso}, the relaxation time scale, is taken to be $3000kyr$. The ratio of ice density to bedrock density, ρ_M, is taken to be 1:3 (e.g. Paterson, 1994).

Calving (shedding of icebergs) into the ocean is assumed to occur if the ice sheet encounters the continent's edge. This is modeled simply by setting the height of the ice sheet equal to zero at the water's edge. Parameterizing calving in this way has given good approximations to ice sheet extent and topography over Greenland in todays' climate, as well as giving estimates of calving budgets which are in agreement with observations (Bugnion, 1999). The presence of floating ice shelves, such as seen around Antarctica, obviously cannot be modeled by treating calving in this manner. Ice shelves are, however, generally found in inlets or bays where there is support for the floating ice from three sides. For most of the thesis, we are considering idealized rectangular continents, so the development of ice shelves is unlikely.

4.2 Ablation parameterization

The surface of an ice sheet can be characterized in one of three ways (Paterson, 1994): dry snow, firn (which is wetted snow that has survived one summer of melting), and exposed and/or superimposed ice, where there is so much melting that the snow layers are saturated, essentially creating a continuous body of ice. Most of a large ice sheet is too cold (because of its height) for any melting. Where it does occur, the melting of snow and ice involves many different climate variables. Shortwave and longwave radiation radiation, air and surface temperature, cloudiness, surface albedo, atmospheric humidity, surface wind speeds and shear are all factors which affect the amount of melting. Also, snow melting at the surface initially turns into melt-water which percolates down into the snow-pack before refreezing and releasing latent heat to the surrounding firn. It is only after the firn has become saturated with meltwater that there is run-off of melt-water from the ice sheet. The surface of melting ice has a

very different albedo from fresh snow (about 40% for clean ice compared to about 85% for dry snow, Paterson, 1994), so as soon as melting starts the energy budget changes radically. A complete calculation of the energy balance at the ice sheet surface requires the input of many atmospheric fields and is computationally expensive to perform, so simplified representations of melting have been developed. These contain parameters whose values can be taken from a combination of theory and tuning to observations. These ablations parameterizations have been used in long time scale integrations of climate models. Pollard (1980) created a formulation (referred to in Chapter 2) linearly dependent both on the local temperature and on the direct insolation. He used a best fit to measurements taken from glaciers, although the spread in the measurements was large.

We use the positive degree day (PDD) approach to parameterize ablation (Braithwaite and Oleson, 1989; Reeh, 1989). The amount of PDDs in a year is equal to the integral of the positive temperatures over that year. These accumulated positive temperatures can be regarded as a melting potential which acts first to melt the current year's snowfall and then, if there are remaining PDDs, to melt the underlying ice. The SICOPOLIS model uses the amended PDD melting model of Calov and Hutter (1996), which takes into account the different albedos of ice and snow, and also allows for percolation downwards and refreezing of melted snow within the snow pack.

Following Calov and Hutter (1996), the PDD model is expressible as follows: if the annual temperature variation of the surface temperature, T_s, at any given point is assumed to have a sinusoidal variation

$$T_s(x, y, z, t) = T_0 + T_a sin(2\pi t[yr]) \tag{4.14}$$

then the PDDs are given by

$$PDDs = \left\{ \begin{array}{ll} \Delta T_0 & \text{if } T_a \leq T_0 \\ \frac{\Delta}{\pi}\left(T_0 arccos(-T_0/T_a) + \sqrt{T_a^2 + T_0^2}\right) & \text{if } -T_a < T_0 < T_a \\ 0 & \text{if } -T_a \geq T_0 \end{array} \right\} \tag{4.15}$$

where Δ is the interval of the year over which the temperatures are positive. Reeh (1990)

has an alternative formulation including a normal distribution of temperature variations added to the temperature profile in Equation (4.14). The melting for a given year is then calculated as follows: Initially the year's accumulation is melted at a rate β_1 per PDD. This meltwater is assumed to percolate down into the snow pack and refreeze. Up to 60% of the years accumulation is melted in this way, at which point the firn is assumed to become saturated. If there are still remaining PDDs they are then used to melt the superimposed ice (refrozen snow melt) as well as the underlying ice at a rate β_2 per PDD. The meltwater produced here is assumed to run off the ice sheet. The different values of β reflect the different albedos of snow and ice. We take $\beta_1 = 1.2\ m^oC^{-1}yr^{-1}$ and $\beta_2 = 2.8m^oC^{-1}yr^{-1}$. As an indication of sensitivity to these choices, Ritz et al. (1996), modeling the Greenland ice sheet, looked at a range of values for β_1 of between 1.1 and 1.9 $m^oC^{-1}yr^{-1}$, and for β_2 of between between 2.9 and 5.8 $m^oC^{-1}yr^{-1}$. The effect across this substantial range of values was to change the ice sheet area and volume by about 10%, although these results are dependent to a degree on the geometry of the ice sheet they were simulating (Greenland).

As noted in the introduction to this chapter, the choice of melting model is not especially important for the purpose of this thesis. All the melting models have the property of concentrating the melting at the edge of the ice sheet and during the summer. Since all we are looking for is the general form of the ice sheet, the representation of the physics by which this melting is achieved is largely irrelevant. It is sufficient that the parameter values for the model chosen are taken to be within a reasonable range, as judged by observations from today's climate.

4.3 Accumulation parameterization

In the last section we discussed the parameterization of ablation on an ice sheet. The atmosphere also affects the mass balance of the ice sheet via the accumulation of precipitation (in the form of snow) at its surface. In actuality precipitation is affected by numerous and complex climate processes, however, ice sheet modelers generally employ only very simplified representations. One commonly used concept for the mass balance over an ice sheet is that of the equilibrium line altitude (ELA). The ELA is the latitude-dependent height, above which there is net accumulation over the year, and below which there is net melting. In very simple versions the net accumulation and ablation are

simply constants (Weertman, 1976). Other treatments allow for a height dependence of the accumulation and/or ablation (Oerlemans, 1980). Ice is then added to the ice sheet at locations above the ELA and subtracted from the ice sheet below the ELA. Climate forcing can then be simulated by raising or lowering the ELA, but there is no inclusion of a seasonal cycle. While an ELA-based parameterization can usefully examine the response of ice to a changing mass balance, it does not take into account that the presence of an ice sheet changes the meteorological conditions which give rise to precipitation. Since the precipitation is subsequently incorporated into the main body of the ice, it seems likely its distribution should have important consequences for the ice sheet's shape, area and volume.

Sanberg and Oerlemans (1983) recognized that during the evolution of an ice sheet, the changing topography would significantly affect the the distribution of precipitation over that ice sheet. If the atmospheric flow is upslope, then adiabatic cooling of the air results in its becoming saturated, causing enhanced precipitation. Conversely if the flow is downslope, the air is adiabatically warmed and able to hold more moisture, so precipitation becomes less likely. The phenomenon of enhanced precipitation on the windward slopes and decreased precipitation on the leeward slopes is well known and observed in today's climate. For example, the western slopes of the Rockies experience much higher annual rainfall than the eastern slopes ('the rain shadow'). Smith (1979) classifies topographically induced precipitation into three groups. The first is the mechanism already mentioned; the air becomes saturated via direct adiabatic cooling due to topographic uplift, clouds form, and provided the mountain is of large enough scale that the clouds are not advected beyond the slopes, precipitation occurs there. The second type of enhanced precipitation is caused by the formation of low level clouds over hills. Large scale precipitation is enhanced where it falls through these 'seeder' clouds. Lastly, if the air is lifted above its level of free convection (LFC), it becomes unstable and convective precipitation ensues.

For an ice sheet developing in the midlatitude westerlies, we expect that precipitation would be concentrated on the western edge where the upslope winds are largest. If it is sufficiently cold (which we expect), it falls as snow and is subsequently incorporated into the ice sheet. As that ice sheet edge moves, the locus of the high precipitation will move with it. Sanberg and Oerlemans (1983) found that if they accounted for the effects of upslope precipitation, the resulting simulated Fennoscandian ice sheet had a much greater westward extent than did the ice sheet simulated without the upslope

effects. Their results also demonstrate that the enhanced upslope precipitation creates a tendency for ice sheets to migrate in the prevailing upwind direction.

Because of the difficulty of creating a comprehensive moisture scheme that is sufficiently fast for long model integrations, a lot of modeling of the Pleistocene ice sheets has been limited to fixing the precipitation at today's patterns (e.g. Greve, 1997; Peltier and Tarasov, 1997). The amount of precipitation is adjusted from today's value using the modeled local temperature at the given model time (typically, the precipitation is adjusted by the ratio of the surface saturated vapor pressure in the modeled climate to the current climate). Sanberg and Oerlemans' work suggests that it is important to keep track of the changing precipitation patterns, especially during the growth of an ice sheet. Moreover, given that the topography was so different during a full glacial climate, it is very unlikely that the the precipitation patterns in today's climate would be appropriate for glacial climates.

GCM 'snapshot' simulations of the last glacial maximum show substantial changes in the precipitation rate (e.g. Manabe and Broccoli, 1985; Kutzbach and Guetter, 1986). While precipitation rate in northern mid- and high- latitudes is generally lower, due to the colder glacial conditions, one common feature to GCM simulations is an increased precipitation rate over the North Atlantic region due to changes in the position and baroclinicity of the storm track. In the simulations of Manabe and Broccoli (1985), the North Atlantic storm track is located further south than in today's climate and also extends further west. As a consequence, the southeastern slopes of the ice sheet experiences an increase in annual precipitation of about $30 cm yr^{-1}$ compared to the current climate. Others changes in precipitation have also been modeled: the LGM simulation of Hall et al. (1996) shows an increase in annual precipitation over the northwestern Laurentide of up to $1.2 m yr^{-1}$ compared to the present day.

In parameterizing the precipitation rate in this work, we cannot account for all the factors which contribute to the distribution in reality, but we can hope to isolate the processes important for ice sheet development. In particular, we expect that the overall shape and volume of the ice sheet is determined more by the integrated accumulation over the interior of the ice sheet than by the local accumulation maxima and minima around the edge of the ice sheet. This is simply because the integrated interior accumulation is larger by far then the integrated accumulation around the margins.

One of the main questions in this thesis is how the east-west gradient in accumulation

affects the ice sheet's configuration, and whether the flow due to the stationary wave is enough to cause to winds to deviate significantly from westerly. With that in mind, we want a precipitation rate parameterization which emphasizes the topographic affects of precipitation and includes the prevailing wind direction. Also, since colder air holds less moisture, precipitation should decrease with latitude and with the height of the surface.

A parameterization of the precipitation rate, P, which has the above properties, and which is similar to that of Sanberg and Oerlemans (1983), is the following:

$$P = max[0, (\gamma_0 + \gamma_1 w) e_{sat}(T_s)] \tag{4.16}$$

γ_0 and γ_1 are constants. w is the vertical velocity mechanically forced by the horizontal velocity fields flowing up or down a sloping surface.

$$w = \vec{u}(z_s) \cdot \nabla z_s \tag{4.17}$$

$\vec{u}$ is the velocity vector as output by the stationary wave model. This allows for the direction of the upslope/downslope flow to change if the induced stationary wave fields are strong enough to change the direction of the prevailing winds.

$e_{sat}(T_s)$ is the saturation vapor pressure at the surface, which is a function only of the surface temperature, T_s. If T_s is less than or equal to 0^oC the precipitation is considered to fall as snow. A good approximation for $e_{sat}(T_s)$ is

$$e_{sat} = e_0 e^{\frac{aT[^oC]}{b+T[^oC]}} \tag{4.18}$$

with $e_0 = 611.2mb$, $a = 17.67$, and $b = 243.5^oC$ (Emanuel, 1994)

The constant γ_0 gives the background precipitation rate—what the precipitation rate would be in the absence of the ice sheet. The slope term, with coefficient γ_1, creates increased precipitation if the flow is upslope and decreased precipitation if the flow is downslope.

The above parameterization is based on that of Sanberg and Oerlemans (1983), who took

$$P = (\gamma_0' + \gamma_1' Sl)W \tag{4.19}$$

where W is the column water vapor and Sl is the slope in the direction of the wind. In their precipitation model, Sanberg and Oerlemans take the wind to be purely westerly, and so the Sl was always just $\partial z_s/\partial x$. They also set Sl equal to zero if the flow was downslope. The full precipitation model of Sanberg and Oerlemans is prognostic in W, with parameterizations for evaporation over different surface types, and diffusion and advection terms representing moisture mixing and transport respectively. Letreguilly and Ritz (1993) have a parameterization which closely follows Sanberg and Oerlemans' precipitation model, but use the relative humidity on the right hand side (RHS) of Equation (4.19) instead of the column water vapor. In Appendix A there is a derivation of the formulation in Equation (4.16) starting from the moisture budget equation. This derivation shows that it is the surface vapor pressure (closely related to the column water vapor) which determines the topographic precipitation more directly than the relative humidity.

We take the value of γ_0 to be $2.5\times10^{-11}m^2skg^{-1}$. This means that with the slope term set to zero, and for a yearly temperature variation of $T_s = 10^oC+10^oCsin(2\pi t[yr])$, integrating Equation (4.16) gives the total precipitation as $1.1m$. For $T_s = 10^oCsin(2\pi t[yr])$, the precipitation is $54cm$ of which $16cm$ water equivalent (w.e.) falls as snow.

The value for γ_1 is taken to be $5.9\times10^{-9}ms^2kg^{-1}$. There are a couple of justifications for this value. First, in Appendix A it is shown that this is the value obtained by deriving Equation (4.16) from the steady state moisture budget equation. Secondly, Sanberg and Oerlemans chose to tune γ_1' to match current precipitation rates over northwestern Europe. Relating their parameterization to Equation (4.16), and assuming a relative humidity of 70% and a surface wind speed of $4ms^{-1}$, their tuned value is equivalent to a γ_1 of $6.0\times10^{-9}ms^2kg^{-1}$.

Because the value of γ_1 arrived at from a derivation of Equation (4.16) starting from the moisture budget and the value γ_1 taken from a tuning to observations agree so closely, we can be confident that Equation (4.16) will give physically plausible values for the upslope precipitation.

Figure 4.1 shows the precipitation rate as a function of vertical velocity for a fixed surface temperature of 0^oC. If the average atmospheric flow at a given location is

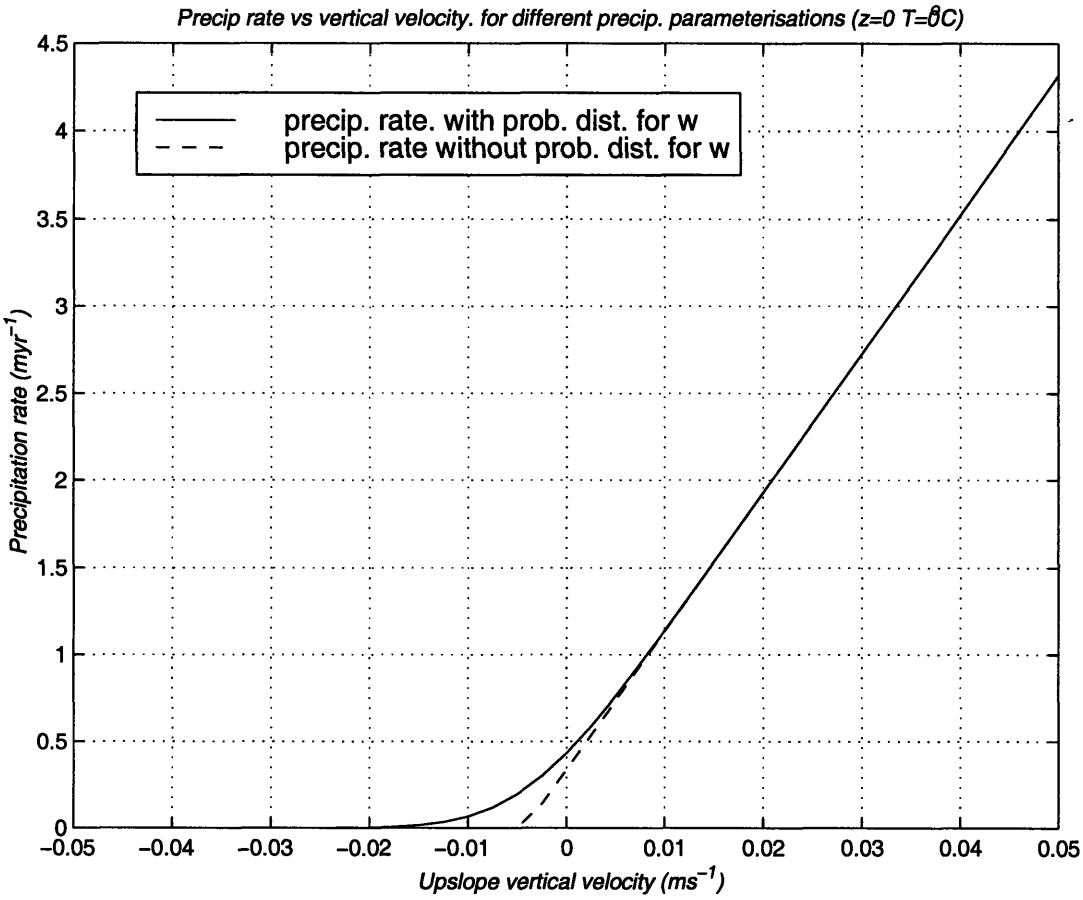

Figure 4.1: Precipitation rate as a function of vertical velocity. The dashed line is the curve given by Equation (4.16) for $T_s = 0^oC$. The solid line is the curve generated if a distribution of vertical velocities is allowed.

strongly downslope, Equation (4.16) gives zero precipitation rate, which is not very physical. In reality we would expect there would always be some synoptic weather systems which would be strong enough to change the flow direction temporarily, thereby generating upslope flow and precipitation. Such systems also contain dynamics (fronts, deep convection etc.) generating precipitation in the interior of the atmosphere. A way of introducing this variability is to allow for a distribution of vertical velocities centered on the topographically forced upslope velocity w. To do this, we define the fraction of the time that the vertical velocity is between w' and $w' + dw'$ to be

$$f(w')dw' = \frac{e^{-\alpha^2(w'-w)^2}dw'}{N} \tag{4.20}$$

α is the inverse of the halfwidth of the velocity distribution. We take α^{-1} to be $1cms^{-1}$ which is typical for the variability in vertical velocities for synoptic scale motions. N is a normalization factor to ensure that $\int_{-\infty}^{\infty} f(w')dw' = 1$. The precipitation is then the integral over the time for which w' gives a positive precipitation rate. This integral may be done so long as the time scale over which the full distribution of vertical velocities is realized is short, compared to the time scale over which the stationary wave can be considered to be in steady state. Since the relevant time scales are synoptic (a few days) and seasonal respectively, this assumption is a reasonable one. Appendix B shows how the integral can be reduced to an expression involving error functions, for which there are very accurate asymptotic expansions. The precipitation rate function which is produced by treating the vertical velocities in this way is also shown in Figure 4.1. The annual accumulation is then given by the integration of the precipitation rate over the fraction of the year for which T_s is below zero.

The distribution of vertical velocities in Equation (4.20) is reasonable for large scale motions but there are other scales of vertical motion associated with, for example, fronts and convection which $f(w')dw'$ does not represent. Treating the precipitation rate in the above manner does, however, remove the rather unphysical hard edge to the precipitation rate curve of Equation (4.16) when the flow becomes sufficiently downslope.

The precipitation rate parameterization that we are using focuses on the topographic effects on precipitation. It does not account for the increase in precipitation due to the enhanced storm tracks in LGM GCM simulations. The results presented in Chapter 6 will be used to discuss what the effect of this might be on the ice sheet.

4.4 Zonally symmetric climate forcing

Having developed the accumulation and ablation parameterizations in the previous sections, these parameterizations are now used to demonstrate the behavior of the ice sheet model in a zonally averaged climate. We will allow the ice sheet to evolve to equilibrium in a specified atmospheric basic state, and look at the balance of terms in the mass budget of the steady state ice sheet. There have been several approximations made in our ice sheet model, and so we also need to consider the effects that these approximations have on the equilibrium profile of the ice sheet.

The ice sheet is allowed to evolve on a rectangular continent bounded by an ocean at approximately $40N$, $70N$, $130W$, and $50W$. The model grid spacing is $40km$, which gives a 122 (east-west) by 86 (north-south) model grid. The continent bedrock is assumed to lie at sea level when there is no ice loading.

We take the ice sheet as existing in a zonally symmetric climate. The surface temperature at any point is given by

$$T_s(x, y, z_s(x, y), t) = \overline{T}_y(y - y_{fz}) + \Gamma z_s(x, y) + T_a(y)sin(2\pi t) \tag{4.21}$$

$\overline{T}_y$ is the meridional temperature gradient ($-6.6^oC/1000km$), y_{fz} is the y coordinate of the annually averaged 0^oC isotherm, which we take to lie at $45N$. Γ is the atmospheric lapse rate (-6.5^oCkm^{-1}). $T_a(y)$ is the amplitude of the annual temperature cycle, which we take to be 10^oC at a latitude of $45N$. An adjustment has to be made for the fact we have assumed uniform vertical shear in the channel. This is equivalent, via the thermal wind relation, to assuming uniform meridional temperature gradient across the channel. If the meridional temperature gradient is weaker in summer than in winter, then the amplitude of the annual temperature cycle must increase with latitude. We therefore take the following

$$T_a(y) = 10^oC + (y - y_{fz})\frac{\overline{T}_y|_{sum} - \overline{T}_y|_{win}}{2} \tag{4.22}$$

In taking $\overline{T}_y|_{sum} - \overline{T}_y|_{win} = 2.6^oC/1000km$, for example, Equation (4.22) gives a change in the amplitude of the annual cycle from 10^oC at $40N$ to 15.5^oC at 70^oN. The effect on the results of making this adjustment is small, but it facilitates a direct comparison with a 4-stage seasonal cycle introduced in Section 4.5

4.4.1 Equilibrium ice sheet

In Chapter 5 we will examine the effects of the atmospheric feedbacks on the ice sheet. First though, we isolated the the ice dynamics by switching off the feedbacks. We do not calculate the atmospheric stationary wave, and the slope parameter, γ_1, in Equation (4.16) is set to zero. The climate felt by the ice sheet is zonally symmetric; the only variation in the spatial distribution precipitation is because of the decrease of

$e_{sat}(T_s)$ with height and latitude (Equation 4.18).

In Figure 4.2a we show the ice sheet that is in equilibrium with this climate. The ice sheet model was integrated for $60kyr$, after which time it is in steady state. The ice sheet has a volume of $21 \times 10^6 km^3$ and covers an area of $7.5 \times 10^6 km^2$. It reaches a maximum height of $2.8km$, and the maximum thickness of the ice is $3.8km$. The horizontal mass flux of ice is also shown in Figure 4.2a. The maximum mass flux occurs in the center of the southern margin and is equivalent to $3.2myr^{-1}$; that is, in the absence of ablation the flux from the interior would increase the height at the margin by $3.2myr^{-1}$ This is equivalent to $5.2km^3$ of ice per $40km$ grid square.

4.4.2 Mass balance of an ice sheet

The average accumulation is $10.7cmyr^{-1}$, equal to a total of $802km^3$ of ice over the whole ice sheet. The calving of ice into the ocean amounts to $467km^3$ of ice per year. In equilibrium the mass budget must add up to zero, and the remainder of the years accumulation (42%) is accounted for by melting, occurring in a thin stip at the southern margin of the ice sheet.

Figure 4.2 highlights several important features about ice sheets. In an active ice sheet the balance is that of snowfall accumulating in the interior and gradually flowing to the ice sheet margin, where it either calves into the ocean or melts in summer. A typical flow velocity for the ice sheet is about $100myr^{-1}$, so snow accumulating in the middle of an ice sheet does not reach the coast for at least $10kyr$. At the southern margin of the ice sheet in Figure 4.2, the annually averaged temperature is about -7^oC. The amplitude of the annual cycle is about 12^oC. Therefore melting occurs for about three months during the summer. The amount of melting decreases fast away from the margin because the temperature rapidly decreases with ice sheet height. In steady state, the southward flux of ice at the southern margin equals the summer melting (the local accumulation is only a small part of the budget). Figure 4.2d shows that the melting increases rapidly southwards (the gradient is about 0.7 myr^{-1} per 1^o of latitude. The number of positive degree days (PDDs) increases southwards both because the temperature is increasing and because the length of the melting season increases. This strong latitudinal gradient in melting means that even if the accumulation in the interior were to double then (assuming the same proportion of calving to melting) the mass flux would double, and

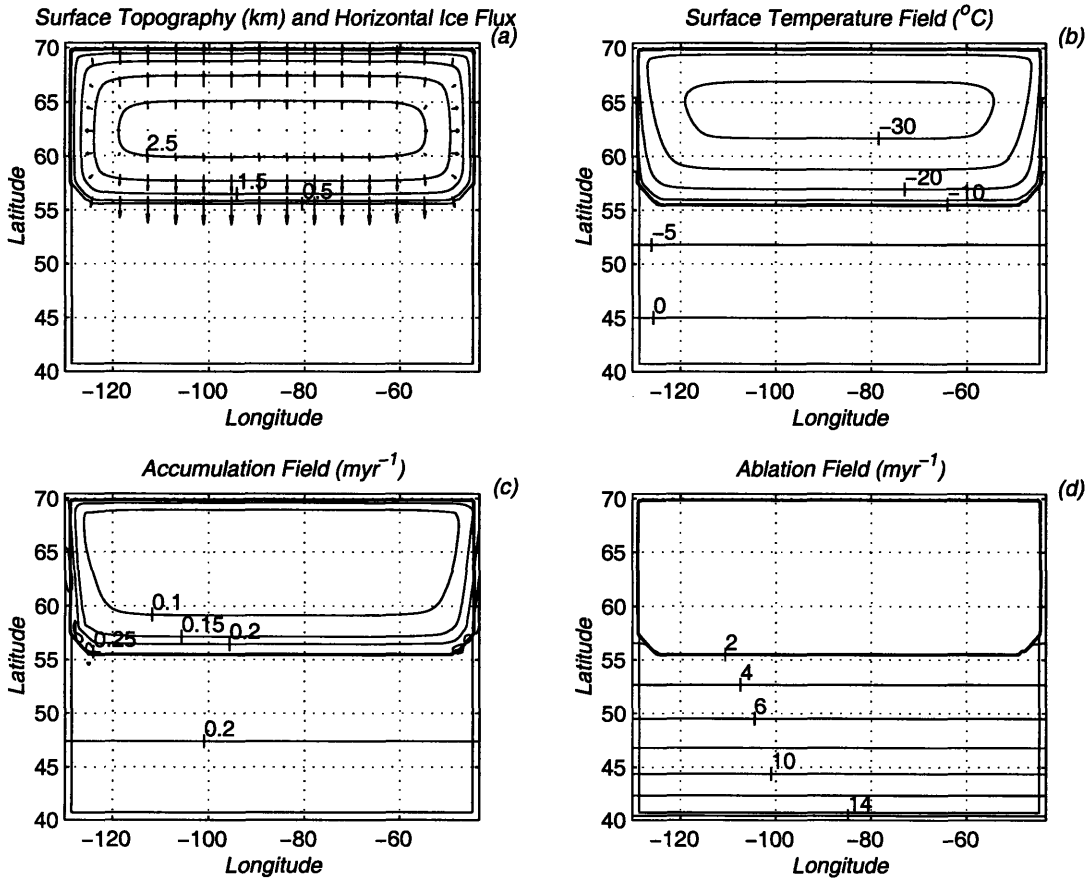

Figure 4.2: Ice sheet fields for ice sheet in equilibrium with the zonally averaged climate described in the text. (a) surface height (km) and horizontal mass flux. The largest vector represents a mass flux of $1.2 \times 10^5 myr^{-1}$, (b) annually averaged surface temperaturse field, (c) snowfall accumulation rate (myr^{-1}), and (d) ablation rate (myr^{-1}). In figures (b), (c), and (d) the bold line is the margin of the ice sheet.

the ice sheet would only push down about another 6 or 7 degrees of latitude. A doubling of precipitation over the whole ice sheet represents a uniform temperature increase (via the Claussius-Clapeyron equation) of about 10^oC. This is a substantial temperature difference and we would hope to be able to model glacial climates to better accuracy than this. The relative insensitivity of the ice margin to accumulation totals gives some hope therefore for being able to model the ice sheets (or at least their area) over glacial climates.

4.4.3 Ice sheet modeling assumptions

We have chosen to use an isothermal ice sheet model rather than allow for temperature dependence in the flow law. We have also used a no-slip boundary condition instead of a sliding law, and we have not accounted for the existence of temperate ice in the lowest layers of the ice sheet. The full SICOPOLIS code has treatments of all of these factors. The details are described in Greve (1995). We can examine the difference that our modeling assumptions make to the equilibrium ice sheet profiles. Figure 4.3 shows the profile of an ice sheet where the isothermal temperature was set at -5^oC instead of the -10^oC that we took in the standard run. The margin of the ice sheet is virtually unchanged, but using the warmer temperature means less viscous ice and so the ice builds up less in the interior before flowing to the margins. The height of the ice sheet is reduced compared to the standard case ($\sim 2500m$ compared to $\sim 2750m$). Also shown in Figure 4.3 is an ice sheet integrated using the full polythermal ice sheet code (except with no geothermal heating from below) (Greve, 1995). Including the temperate ice and allowing for basal sliding again has the effect of reducing the ice sheet height slightly (to $\sim 2450m$), but again the margin is very similar to the standard case.

An important conclusion to be drawn from Figure 4.3 it that it is the summer temperature which is the dominant factor controlling the southern margin of the ice sheet. The volume can change depending on the ice sheet viscosity, but the strong latitudinal gradient in ablation means that the ice is unable to push into areas where the summer temperature is much above zero. A feature of the results in Chapter 5 will be that the southern margin usually lies somewhere between the 0^oC and the 5^oC summer isotherm at the $z = 0km$ level.

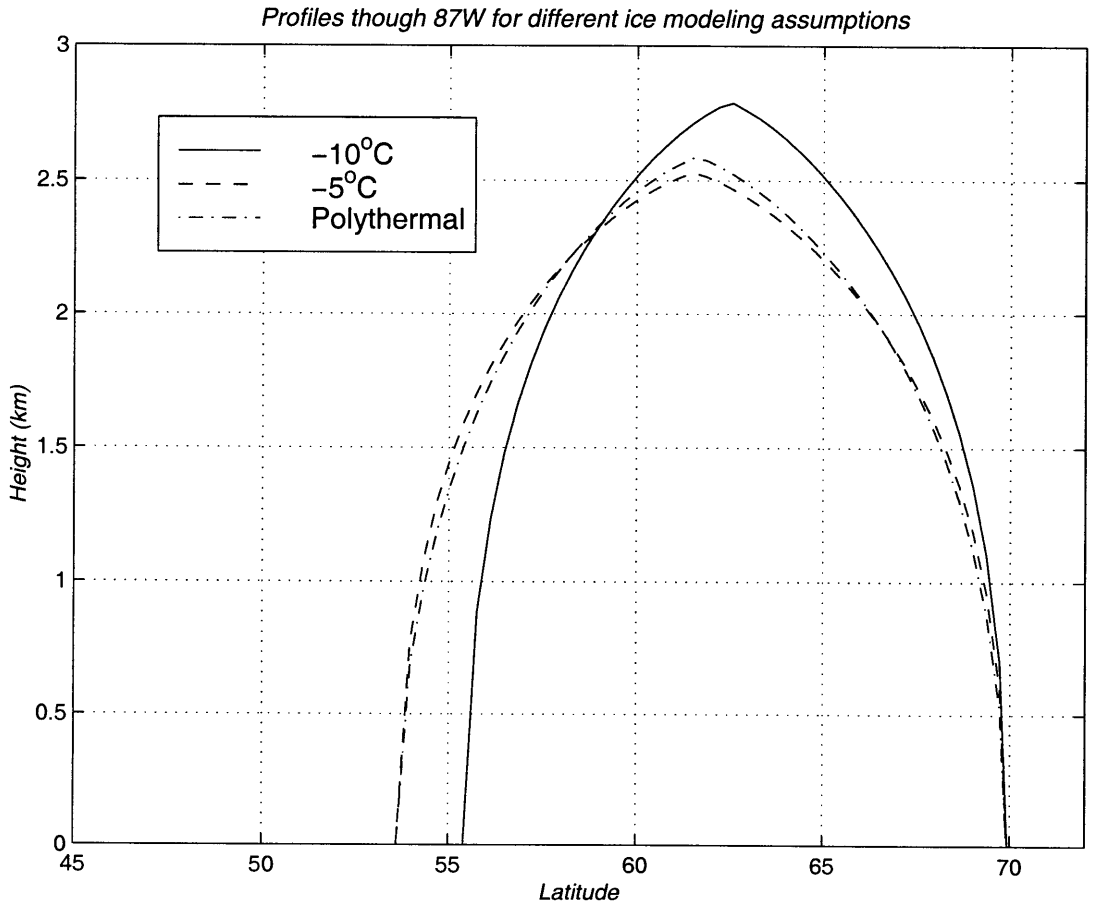

Figure 4.3: Profiles for different modeling assumptions for the temperature dependency of the flow. Details of the different assumptions are in the text.

4.5 Seasonal cycle

In Chapter 5 we will assume that the temperature over the ice sheet can be described by the following relation

$$T_s(x,y,z_s(x,y),t) = \overline{T}_y(y - y_{fz}) + \Gamma z_s(x,y) + T_a(y)sin(2\pi t[yr]) + T'(x,y) \qquad (4.23)$$

where $T'(x,y)$ is the temperature perturbation at $z = 1km$ as output by the stationary wave model using the standard basic state introduced in chapter 3. The above relation accounts (in a simplified way) for the temperature variation over the seasonal cycle but it does not account for seasonal variations in the vertical wind and temperature structure which would change the amplitude of the atmospheric response to topographic forcing. The variation in the vertical structure in today's climate at $60N$ is actually quite small. The jet is weaker in summer than in winter (a maximum of $20ms^{-1}$ compared to $40ms^{-1}$) but it is centered at a higher latitude ($45N$ compared to $30N$) (Peixoto and Oort, 1992). The net effect of this is the the strength of the jet at $50N$ is between 15 and $20ms^{-1}$ year round. However, the differing strength of the jet in winter and summer does mean that each season has different meridional variation in the atmospheric refractive index. Downstream of the topographic feature this can have a significant influence on the stationary wave propagation (Nigam and Lindzen, 1989).

GCM simulations of the LGM have looked at the seasonal cycle. In Manabe and Broccoli (1985), which uses a seasonal simulation and a static mixed layer ocean, the changes from the present climate are much more dramatic in winter than in summer. There is an increase in the winter meridional temperature gradient between $30N$ and $60N$ of $3.0°C/1000km$ (this change is equivalent to about 40% of the observed annual mean temperature gradient). By contrast, in summer the changes in the midlatitude temperature gradient is less than half of this. Kutzbach and Guetter (1986) use a GCM forced by reconstructed CLIMAP sea surface temperatures (SSTs) (CLIMAP members, 1981), and look at perpetual January and July simulations. They also show much stronger cooling in winter than in summer when compared to the current climate.

All GCM simulations show a high pressure ridge sitting somewhere over the ice sheet in both summer and winter. The flow associated with ridge is generally more pronounced

in winter than in summer. The different simulations differ, though, in the strength of the surface high pressure ridge. Kutzbach and Guetter have a ridge with a strength of about $1030mb$ in both summer and winter, although the ridge is more extensive in winter. To compare to the numbers we have modeled for the test ice sheet in Chapter 3, $1030mb$ is equivalent to a geopotential perturbation of about $170gpm$. Hall et al. (1996) using a GCM also forced by CLIMAP SSTs and with a full seasonal cycle find a ridge with a strength of $1030mb$ in summer and an extremely intense ridge of $1064mb$ in winter. Gates (1976) performed a July simulation using a two level model forced by CLIMAP SSTs, and obtained a ridge with a strength of about $1040mb$. A more recent simulation by Vettoretti et al. (1999) shows a weaker summer high of 1020mb. Taken as a whole, the simulations show generally increased meridional temperature gradients and suggest that changes from the current climate are larger in winter than in summer.

We need to address how changes in the seasonal cycle might affect the stationary wave pattern. In this section we create a 4-stage seasonal cycle (where each stage represents a season), each with a different basic state and therefore a different stationary wave pattern. This is compared to using the annually averaged basic state. Because the GCMs indicate increased seasonality in glacial climates we have chosen a considerably larger seasonal variation in the basic state structure than exists in today's climate. Figure 4.4 shows the basic states which we take. The fall/spring basic state is the same as the standard basic state in Chapter 3. The surface velocity doubles between summer and winter ($2ms^{-1}$ to $4ms^{-1}$), and the vertical wind shear increases by two thirds ($1.5ms^{-1}km^{-1}$ to $2.5 \times 10^{-3}s^{-1}$). The lapse rate is left unchanged. This causes the tropospheric PV gradients change from about 3.1β in summer to 4.5β in winter. We have chosen the basic states so that the fall/spring basic state is also the same as the annual average.

Figure 4.5 shows the stationary wave response to the different seasonal basic states at $60N$. The topographic forcing is the same test ice sheet used in Chapter 3. The maximum temperature perturbation change at $60N$ is -4.9^oC in summer and about -8.5^oC in winter. In the fall and spring it is -7.2^oC. The ridge in the geopotential over the ice sheet is $80gpm$ in summer and $135gpm$ in winter. While the overall shapes of the perturbation fields are qualitatively the same in the different seasons, one difference is the lack of a warm temperature perturbation on the western slopes of the ice sheet in summer. This is likely due to the lower surface wind, which means that the advection of warm temperature perturbations from the west cannot as effectively balance the

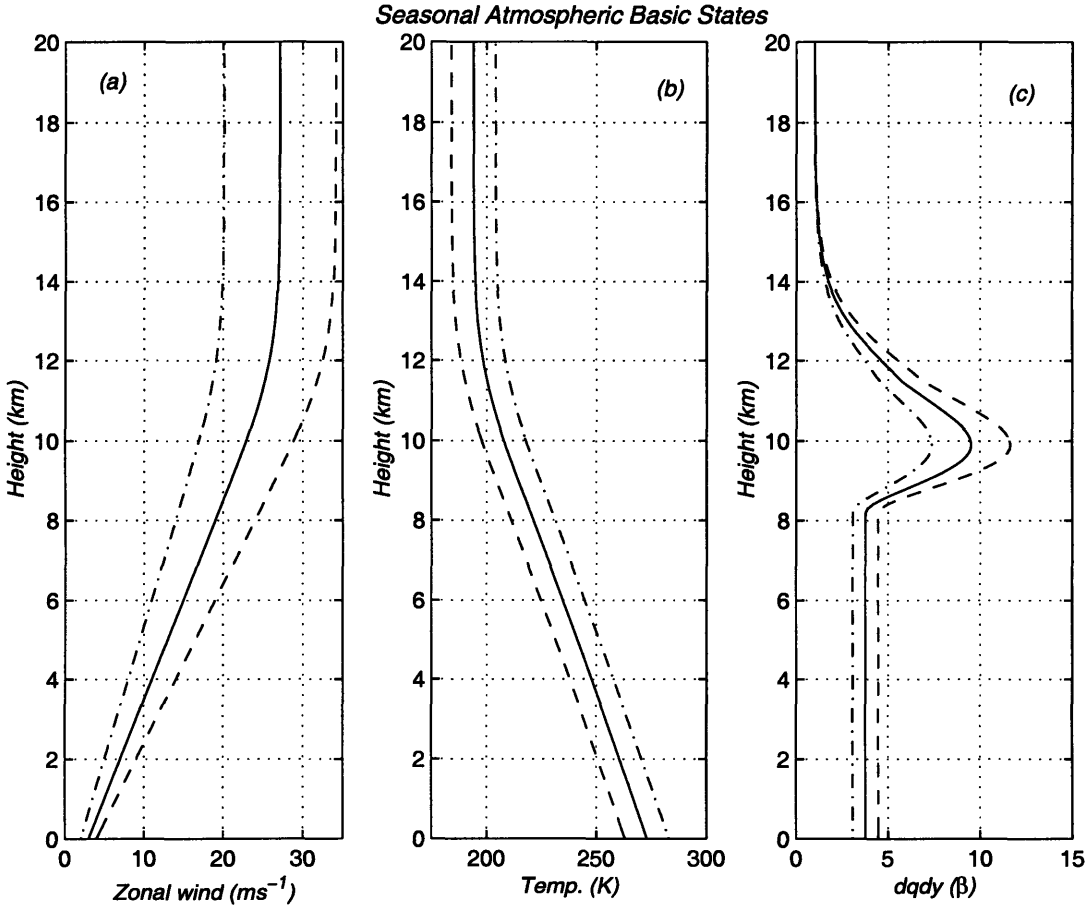

Figure 4.4: Seasonal atmospheric basic states. The solid line is the basic state used for the fall and spring seasons. The dashed is the winter basic state. The dot-dashed line in the summer basic state. (a) zonal winds in ms^{-1}, (b) Temperature (K), and (c) PV gradients in units of beta ($= 1.13 \times 10^{-11} m^{-1} s^{-1}$).

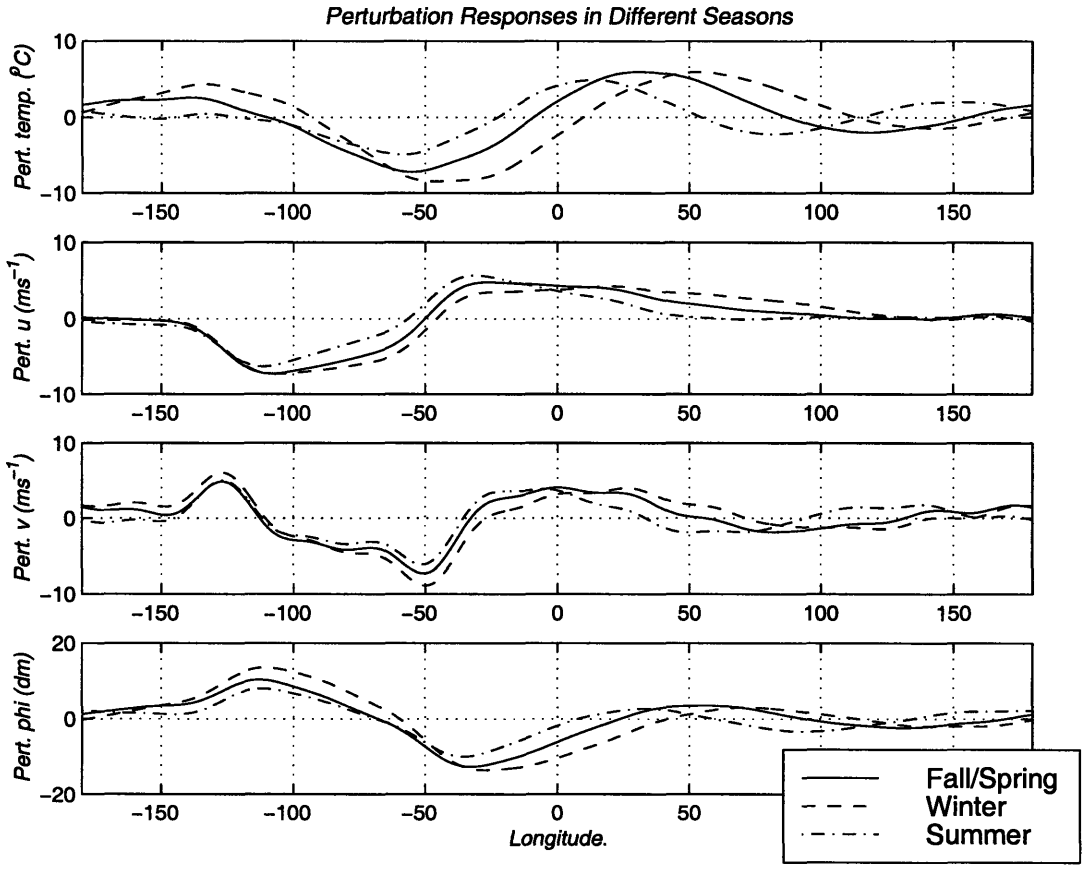

Figure 4.5: Stationary wave perturbation responses to the seasonal basic states. The test ice sheet lies between about $130W$ and $50W$. Panels are as for Figure 3.7.

cooling due to the ascent up the ice sheet. It is also noteworthy that the phase of the remote response differs between the seasons; higher PV gradients in winter result in a shorter wavelength response, consistent with Equation (3.24). This phase difference is such that between $50E$ and $100E$ the temperature difference between the summer and winter temperature perturbations is about $7°C$. The phase of the response output by the channel model cannot be taken to be that which would apply in the real climate, but Figure 4.5 does show that the remote response to the Laurentide ice sheet was likely different in different seasons.

4.5.1 Precipitation

We calculate the precipitation rate over the test ice sheet for each season and in-

cluding the slope parameter, γ_1, in Equation (4.16). Figure 4.6 shows the precipitation rates at 60N in each of the different seasons. The precipitation rate maximizes on the western edge of the ice sheet where the atmospheric slow is strongly upslope. In the interior of the ice sheet, the flow at 60N is largely downslope which, combined with the reduction in precipitation rate with height, means that the precipitation rate decreases to less than $10 cm yr^{-1}$. Also evident in Figure 4.6 is the increased moisture supply in summer. Figure 4.6 shows a comparison of the annually averaged precipitation rate of the four seasons with the precipitation rate calculated using Equation (4.23) for the temperature variation. It is clear that Equation (4.23) can do a good job of accounting for annual accumulation over the seasonal cycle.

4.5.2 Ablation

Since the summer temperatures determine the melting, it seems most appropriate to use the summer basic state to calculate the stationary wave used to determine the ablation patterns. Local to the ice sheet, the basic pattern does not change between seasons, but the amplitude is weaker in summer. We have used an exaggerated seasonal cycle in the basic state, based on LGM GCM simulations. The summer basic state in Figure 4.4 is also weaker than that suggested by both the models and the paleodata. In Chapter 5 therefore, we use the temperature perturbations generated by the standard basic state (same as Fall/Spring in Figure 4.5), but we will also show the results for a variety of basic states to give an idea of the range of possible responses. Given our limited knowledge of the LGM basic state and its seasonal variation a full treatment of the seasonal cycle would be subject to as much uncertainty as our approach.

Summary

Chapters 3 and 4 have introduced the necessary components to model the interaction between ice sheets and stationary waves. In particular, in this chapter, the use of an isothermal ice sheet model has been justified: the overall shape of the ice sheet is unchanged by using a temperature dependent flow law. We have also shown that we expect a significant redistribution of the patterns of precipitation as an ice sheet evolves.

The precipitation rate parameterization developed emphasizes the effect of topography on the accumulation.

In a zonally averaged climate, the two dimensional ice sheet model reproduces the picture given by the one dimensional approach in Chapter 2; the southern margin of the ice cannot exist at latitudes where the summer temperature rises much above 0^oC because the melting rate is a strong function of latitude.

In the simplified ice sheet geometry used in this chapter, the patterns of melting and accumulation do not change between seasons, although the magnitude does. The relevant season for melting is summer, and so we should focus on the temperature patterns for that season. As regards the accumulation, the topographic effects dominate the distribution.

In the next chapter we couple the stationary wave model developed in Chapter 3 to the ice sheet model we have presented here, using the accumulation and ablation parameterizations developed in this chapter. The coupled model enables us to study how the two components interact with each other during the evolution of an ice sheet.

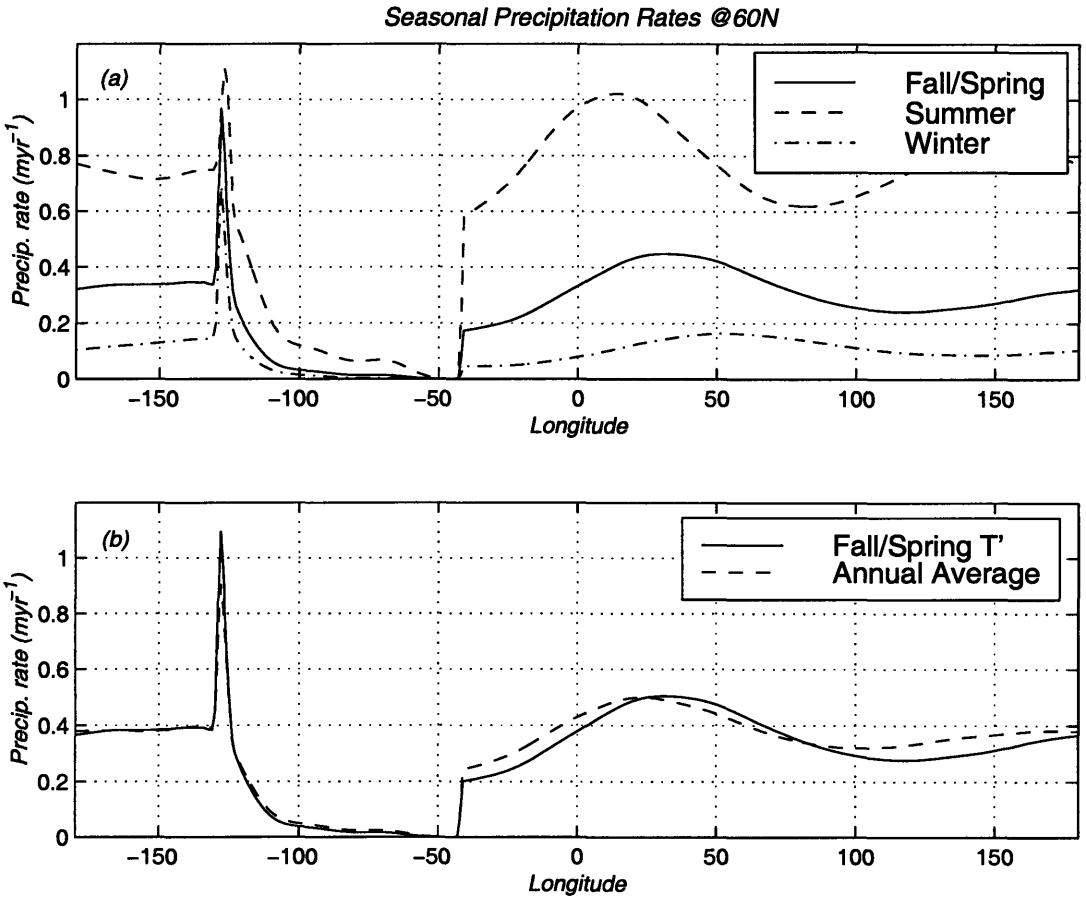

Figure 4.6: Precipitation rates at 60N over test ice sheet. (a) seasonal precipitation rates myr^{-1} (b) comparison of annually averaged precipitation rate (dashed line) to that calculated using Equation (4.23) and the Fall/Spring basic state (solid line). The slope parameter, γ_1 (Equation (4.16)) is included, giving high totals on the western slopes and decreased precipitation on the eastern. The test ice sheet lies between about $130W$ and $50W$.

Chapter 5

Results for an idealized geometry

In this chapter we will present the main results from modeling studies using the idealized framework established in Chapters 3 and 4. The purpose of using a simplified geometry (rectangular continent, flat surface topography, etc.) is to isolate the interaction between the atmosphere and the ice sheet. We will show that there are two main feedbacks in this interaction: topographically influenced precipitation, and cold temperatures in the lee of the ice sheet induced by the stationary wave. To more clearly illustrate the behavior the ice sheet, we show the equilibrium integrations resulting from including each feedback separately, and then combine them to understand how the two mechanisms compete against each other to create the final configuration of the ice sheet. Because of the (unavoidable) simplifications made in the modeling, we cannot have absolute confidence about the magnitude of the feedbacks, and we therefore integrate the model for a plausible range of atmospheric basic states. Doing this changes the details of the ice sheet's response, but the mechanisms of the interaction remain robust. It is important to stress that the ice sheets shown here are in equilibrium with the climate and the stationary waves (subject to our modeling assumptions). This distinguishes these results from GCM 'snapshot' simulations and from EBM simulations which, while in equilibrium, do not account for the atmospheric dynamics.

The stationary wave pattern over an ice sheet is not due solely to the ice sheet itself; other features of the climate also generate stationary waves to which the ice sheet will respond. Therefore we consider the effect of including a background stationary wave in our model integration. During an ice age climate we expect there to be three

main sources for the topographically induced stationary wave pattern: the Tibetan plateau, the Laurentide and the Fennoscandian. In this section we include an idealized representation of the Tibetan plateau which generates a stationary wave consistent with that observed in today's climate. Its effect over the evolving ice sheet (representative of the Laurentide) is mainly felt through the changes in the temperature pattern; changes due to the winds are negligible.

The simple modeling approach of Chapter 2 suggested that the stationary wave would have quite a strong effect on the growth and decay of the ice sheets creating them. We therefore look at the time evolution of the ice sheets. During the growth phase of an ice sheet, its area is largely controlled by where the climate is cold enough for ice to exist, rather than by ice dynamics. There is some additional areal increase after the ice has had enough time to build up sufficiently that the flux of ice from the interior is able to push the margin southwards. We also consider the more realistic case of the ice sheet initiating on high ground and then growing in response to a cooling climate.

The retreat of the ice sheet is investigated. Starting from the equilibrium ice sheets, we raise the atmospheric basic state temperature. The simple modeling approach suggested the stationary wave might lead to an accelerated melt-back of ice because at any given latitude the ice is maintained, at least in part, by the stationary wave that it creates. While the retreat of the ice sheet is speeded up, the effect is not as dramatic as the simple model suggested. This would seem to be due to the response time for ice in the interior of the ice sheet to react to melting at the margin; in the ice flow resolving model of Chapter 4 this process takes several thousand years, whereas the perfectly plastic ice approximation in the simple model assumes the response is instantaneous.

Lastly in this chapter, we look at how periodic forcing on the atmospheric basic state is reflected in oscillations of the ice sheet. Milankovitch insolation cycles (see Chapter 1) cause changes in the atmospheric basic state. This will alter the atmosphere's response to topography, especially downstream of the source. In the model we have constructed, we can consider plausible changes to the basic state temperature, the basic state vertical shear, and the size of the background stationary wave. These integrations show the largest effect on the ice sheet is due to the direct forcing of the temperature. Periodic variations in the atmospheric wind shear affect the ice volume mainly through changes to the area, and there is also some small effect on the overall shape of the ice sheet. Periodic variations in the background stationary wave have only a minor impact on the

ice sheet.

5.1 Equilibrium ice sheets

The basic question asked in this section is as follows: starting from a zonally averaged climate what is the equilibrium ice sheet that evolves in concert with the atmospheric stationary wave that it creates? We specify a climate (the zonally averaged atmospheric basic state) and integrate the ice sheet model to equilibrium.

In Chapter 4 we showed the equilibrium ice sheet in a fixed zonally symmetric climate. The precipitation was adjusted for the height of the ice sheet but did not take account of whether the flow was upslope or not (i.e. γ_1 in Equation (4.16) is set to zero). Figure 5.1 replots this ice sheet. The associated climate fields were previously shown in Figure 4.2. The steady state ice sheet is sustained by a balance between accumulation in the interior, and calving or melting at the margins. In particular, the southern margin is located where the southward flux of ice equals the summer melting—the accumulation at the margin is only a small part of the mass budget there. For the ice sheet in Figure 5.1, the accumulation in the interior minimizes on the summit (due to the Claussius-Clapeyron relation (Equation (4.18)), at around $5cmyr^{-1}$. The average accumulation over the ice is $10.7cmyr^{-1}$, which compares to $18.7cmyr^{-1}$ for Antarctica and $34.0cmyr^{-1}$ for Greenland in today's climate (Ohmura and Wild, 1996).

5.1.1 Precipitation feedback

We can isolate the effect of the topographically induced precipitation on the ice sheet by setting γ_1 to its standard value ($5.9 \times 10^{-11} m^2 skg^{-1}$) and by not including the stationary wave (ϕ' set to zero). The prevailing wind is therefore purely westerly. The model is integrated to equilibrium, and the resulting ice sheet is shown in Figure 5.2. Focusing on the height contours, the main difference from Figure 5.2 seems to be that the ice on the eastern flank does not make it as far south as for the ice sheet which evolves in the zonally symmetric climate. The ice mass flux vectors though, show that the internal dynamics within the ice sheet are very different in the two integrations. When the topographic precipitation is included (Figure 5.2, the convergence of ice maximizes

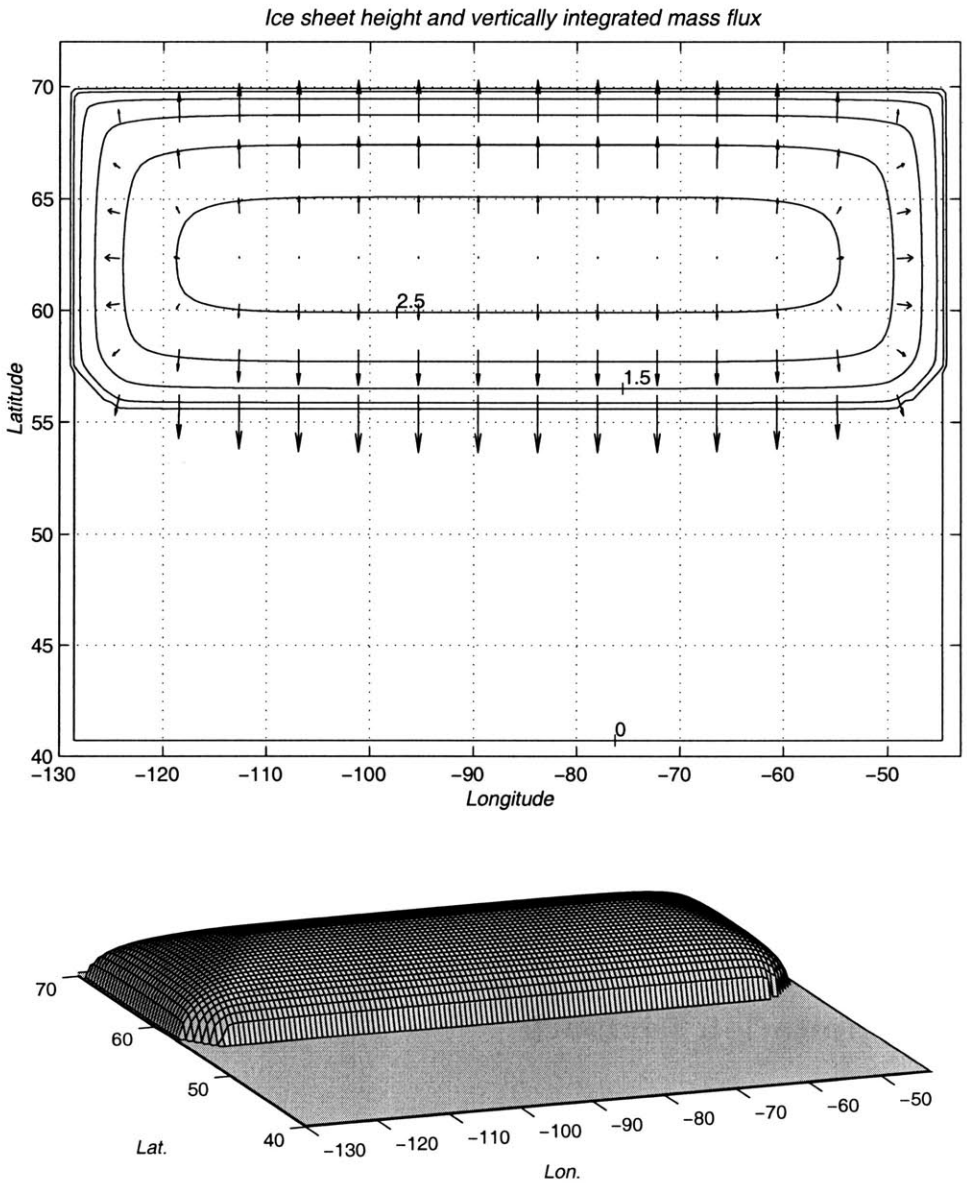

Figure 5.1: Contours, vertically integrated mass fluxes, and 3-D view of equilibrium ice sheet for zonally symmetric climate. The upper panel shows height contours (every $0.5km$) and mass flux vectors. The largest vector plotted corresponds to $1.2 \times 10^5 m^2 yr^{-1}$, which would raise the height of the ice in a $40km^2$ grid box by $3.2myr^{-1}$. The largest flux of ice (not plotted because of resolution) is $1.3 \times 10^5 m^2 yr^{-1}$.

at $13myr^{-1}$ at the western margin. This convergence is balanced by calving into the ocean. In general, Figure 5.2 shows the flux of ice in the western half of the ice sheet is much larger than on the eastern half.

This difference is caused by the precipitation distribution which is shown in Figure 5.3. There is a strong enhancement of precipitation on the western flank (associated with the upslope flow there). In equilibrium this must imply a high mass flux of ice towards the ice sheet boundary. The precipitation maximizes locally at $3.03myr^{-1}$, and the direction of the ice flux is such that this accumulation maximum turns into ice which flows almost due west, where it calves into the ocean upon meeting the western continental boundary. In contrast, the eastern slopes are starved of accumulation, and there is a substantial area over which the precipitation rate is less than $5cmyr^{-1}$. This very weak interior accumulation means only a small flux of ice southward at the southern margin. The amplitude of the seasonal cycle (from Equation (4.22) at the southern margin on the eastern flank (at $62N$) is about 13^oC. Figure 5.3 shows therefore that the temperature just barely makes it above freezing there: very little summer melting is required to balance the flux of ice from the interior.

5.1.2 Stationary wave feedback

We can also separately examine the effect of the stationary wave on the ice sheet by again setting $\gamma_1 = 0$ in Equation (4.16), and allowing the topography (as it evolves) to force a stationary wave. In this case then, the precipitation is adjusted only for the surface temperature, and the ice sheet evolves in a climate (i.e. the surface temperature) determined in part by the stationary wave that it induces in the atmospheric flow. The equilibrium ice sheet that results is shown in Figure 5.4. There is again a dramatic difference from Figure 5.1. The maximum height of the ice exceeds $3km$, and the southern margin reaches down to about $43N$—almost $1500km$ further south than the ice sheet in Figure 5.1. On the western flank there is a slight warming, and the southern margin only makes it down to about $62N$—about $800km$ further north than the margin in Figure 5.1. Vettoretti et al. (1999) have shown that the difference between GCM and EBM simulations of the LGM are consistent with this effect.

The ice mass flux is increased compared to the zonally symmetric case, caused largely by the increased ice depth. The relevant climate forcings for the ice sheet are shown

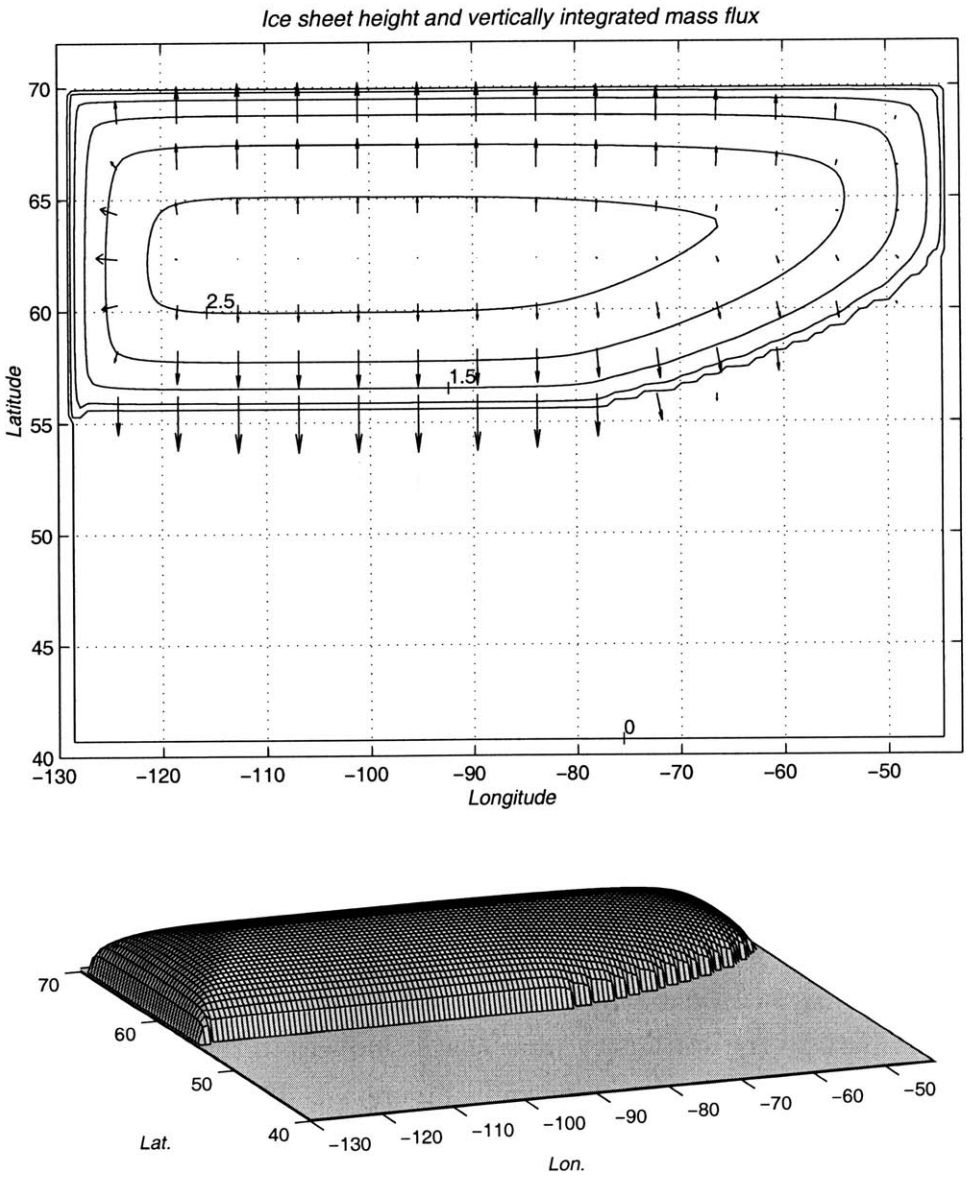

Figure 5.2: Equilibrium ice sheet for an integration including the topographic precipitation feedback. Otherwise as for Fig. 5.1. The largest vector plotted corresponds to an ice flux of $1.2 \times 10^5 m^2 yr^{-1}$. The largest flux of ice (not plotted because of resolution) is $5.2 \times 10^5 m^2 yr^{-1}$.

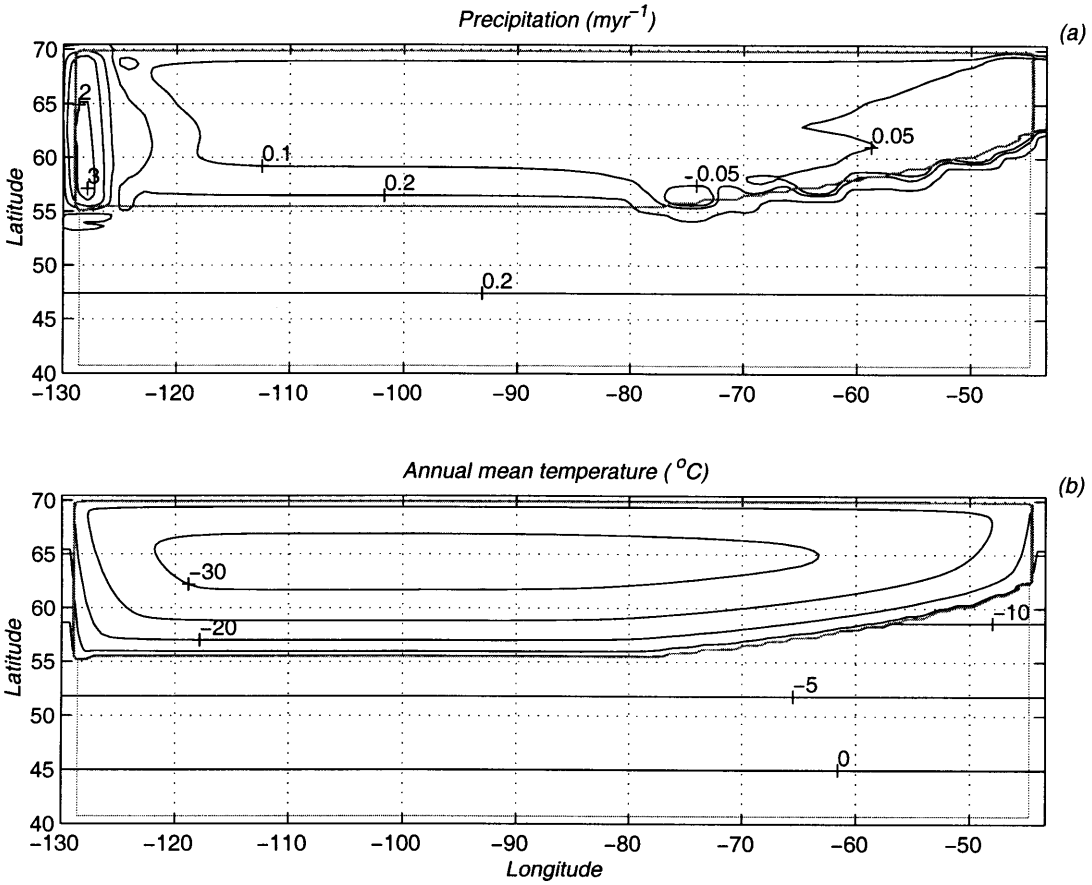

Figure 5.3: (a) Accumulation rate (myr^{-1}); contour intervals are (0.05, 0.1, 0.2, 0.5, 1, 2, 3, 4), and (b) annually averaged surface temperatures (^oC), for the ice sheet shown in Figure 5.2. The outline of the ice sheet is shown as a thick, faint line.

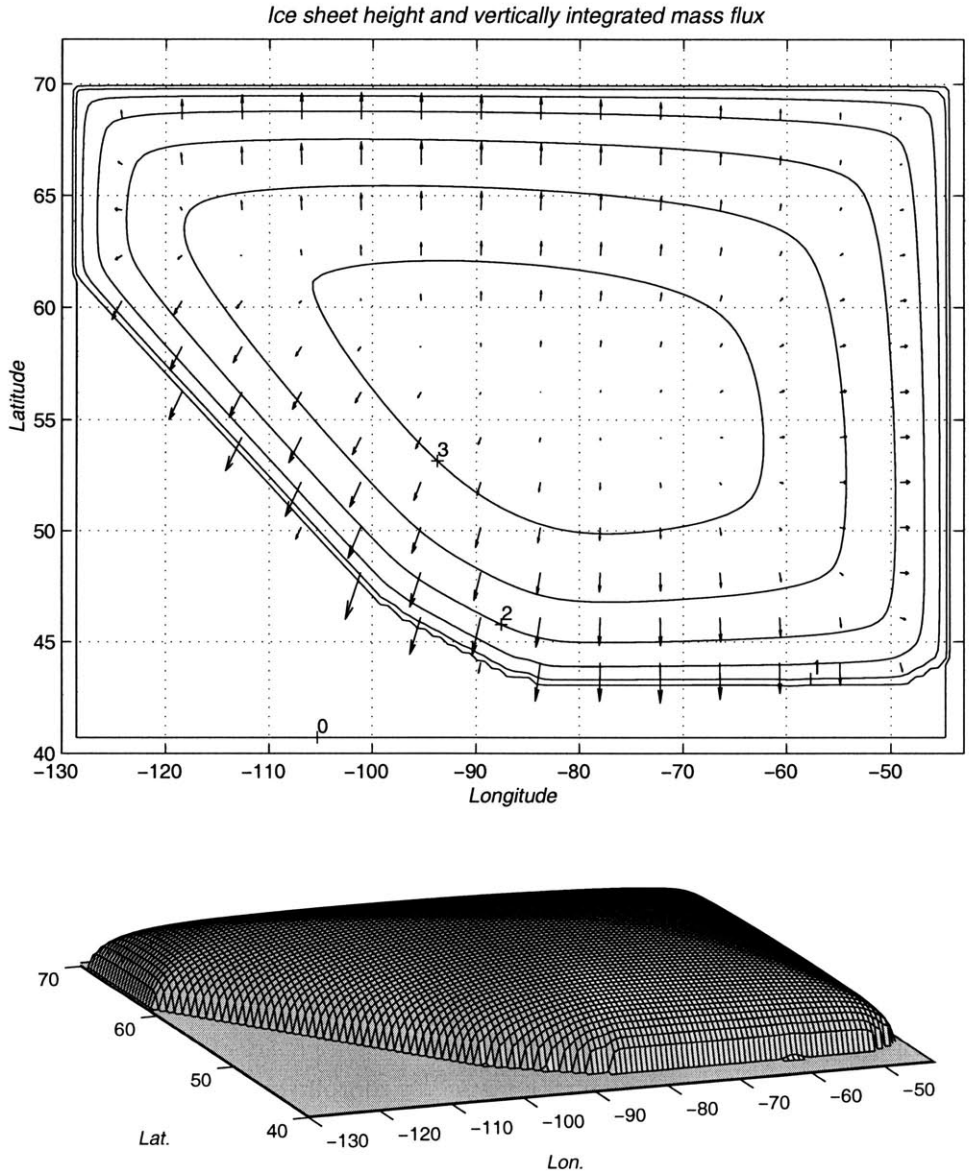

Figure 5.4: Equilibrium ice sheet for an integration including the stationary wave feedback. Otherwise as for Figure 5.1. The largest vector plotted corresponds to an ice flux of $2.0 \times 10^5 m^2 yr^{-1}$, which is also the largest flux.

in Figure 5.5. The $1km$ winds show an anticyclonic circulation over the ice sheet, as expected from Chapter 3. This brings cold northerly winds down over the ice sheet, particularly in the east, ensuring the ice there does not melt. The annually averaged temperatures are shown in Figure 5.5b. Almost everywhere the southern margin lies at a temperature of between -3^oC and -5^oC. The exception is the extreme western part of the margin which does not make it above -5^oC. This means the maximum summer temperature is about 5^oC. Thus with a sinusoidal variation in temperature, the melting season extends into fall and spring, occupying about half the year.

The ice sheet in Figure 5.4 is the most directly relatable to the simplified modeling in Chapter 2. We therefore show, in Figure 5.6, north-south cross-sections though the ice sheet at longitudes in sectors which correspond to the WTR and CTT feedbacks in Chapter 2 (Figure 2.6). An important difference is that the stationary wave created by the ice sheet in Figure 5.4 is a property of the whole ice sheet and not merely the height in any given sector, as was assumed in Chapter 2. Nonetheless, Figure 5.6 confirms the strong feedback which operates when the ice sheet induces a temperature perturbation at its southern margin.

5.1.3 Combined feedbacks

The stationary wave and the topographic precipitation feedbacks are now combined, and the resulting equilibrium ice sheet is shown in Figure 5.7. In some ways the inclusion of both feedbacks has restored the ice sheet to looking more like that which evolved in the zonally symmetric climate; the extension of the ice in the southeast is less than for the ice sheet in Figure 5.4, and the southern margin in the west lies close to the same latitude as the ice sheet forced by the zonally averaged climate (Figure 5.1). The mass flux within the ice sheet, however, again shows a very different picture. The mass convergence reaches a maximum value of $18myr^{-1}$ (compared to $3.1myr^{-1}$ for the ice sheet in Figure 5.1. The effects of the precipitation feedback are evident, with a very active western half of the ice sheet (high mass flux), and a quiescent eastern half (low mass flux). The ice sheet also develops a slight double-domed structure. The ice margin in Figure 5.7 is surprisingly zonal given the different processes that are acting on the western margins. This is a coincidence, and for different atmospheric basic states, or more realistic geography, we would not expect the margin to be as zonal.

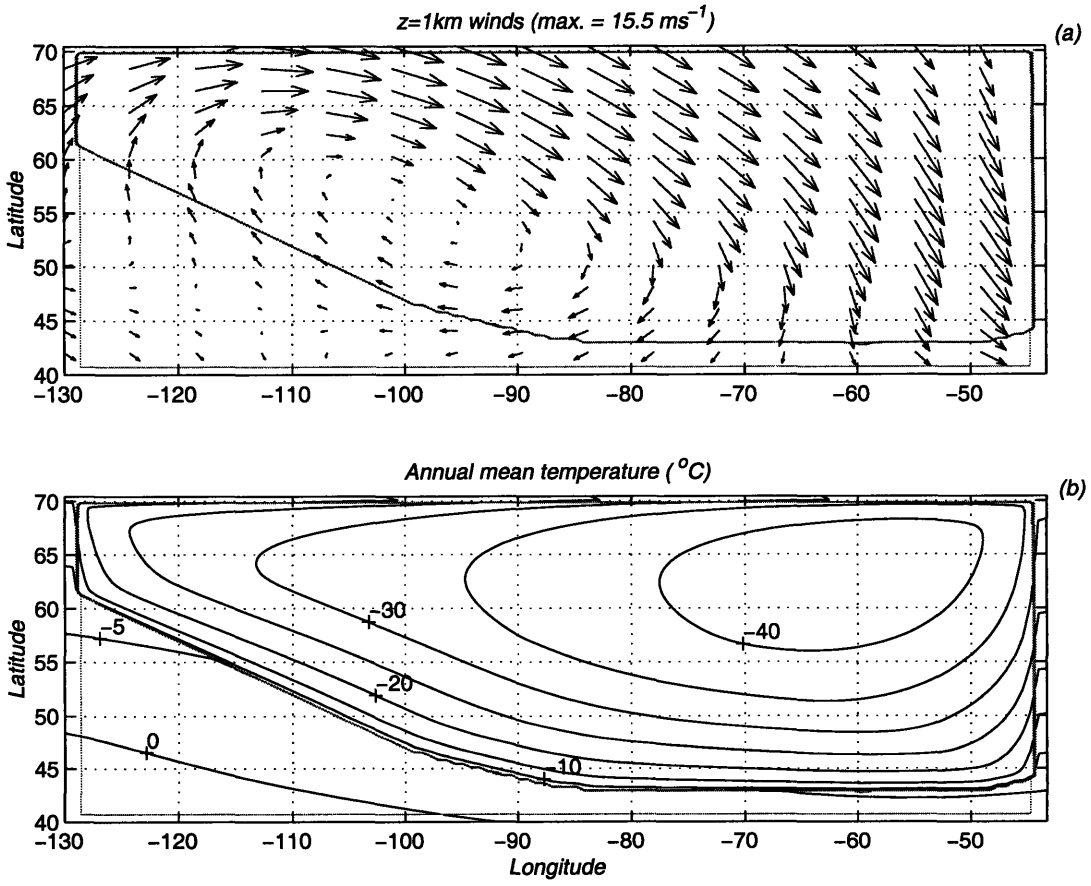

Figure 5.5: (a) wind vectors at $1km$ (maximum $15.5ms^{-1}$), and (b) annually averaged surface temperatures (^{o}C), for the ice sheet shown in Fig. 5.4. The outline of the ice sheet is shown as a thick, faint line.

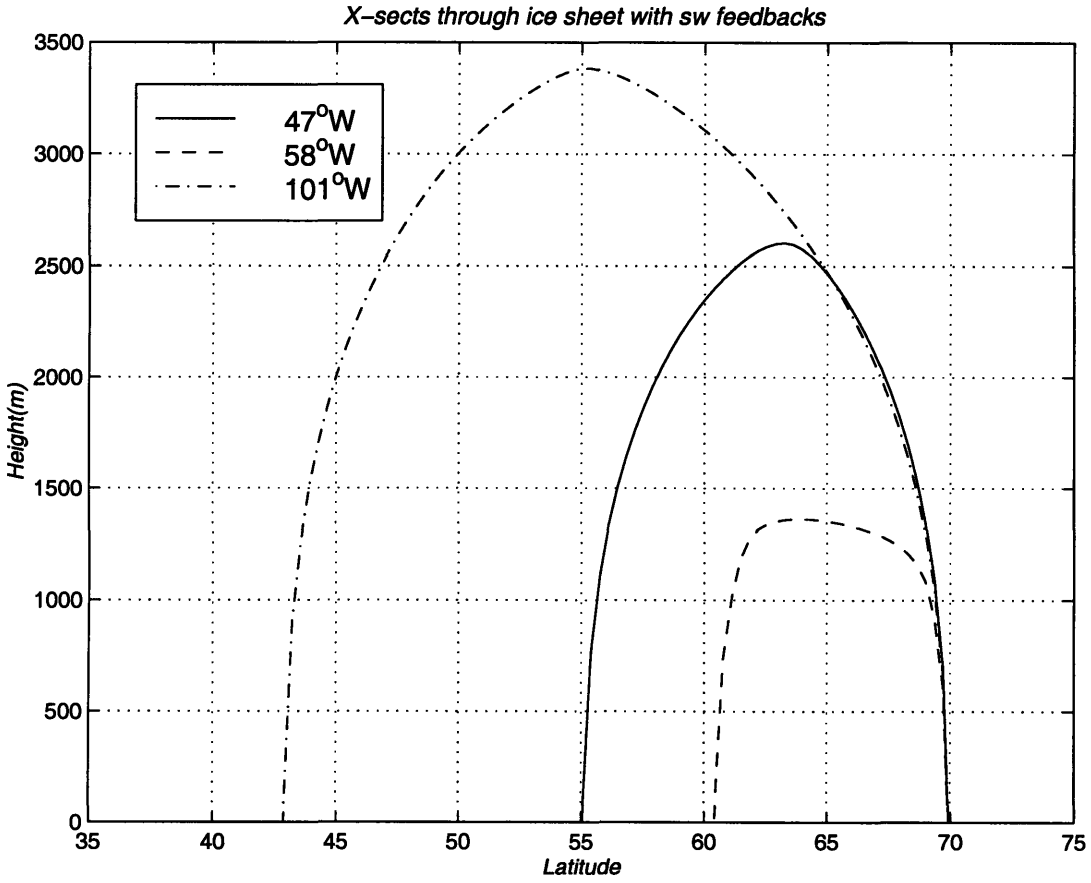

Figure 5.6: North-south cross-sections though the ice sheet shown in Figure 5.4. The longitudes chosen correspond to sectors in which the feedbacks invoked in Chapter 2 operate: $127W$; WTR feedback, $113W$; no feedback, $113W$, CTT feedback. This plot corresponds to Figure 2.6.

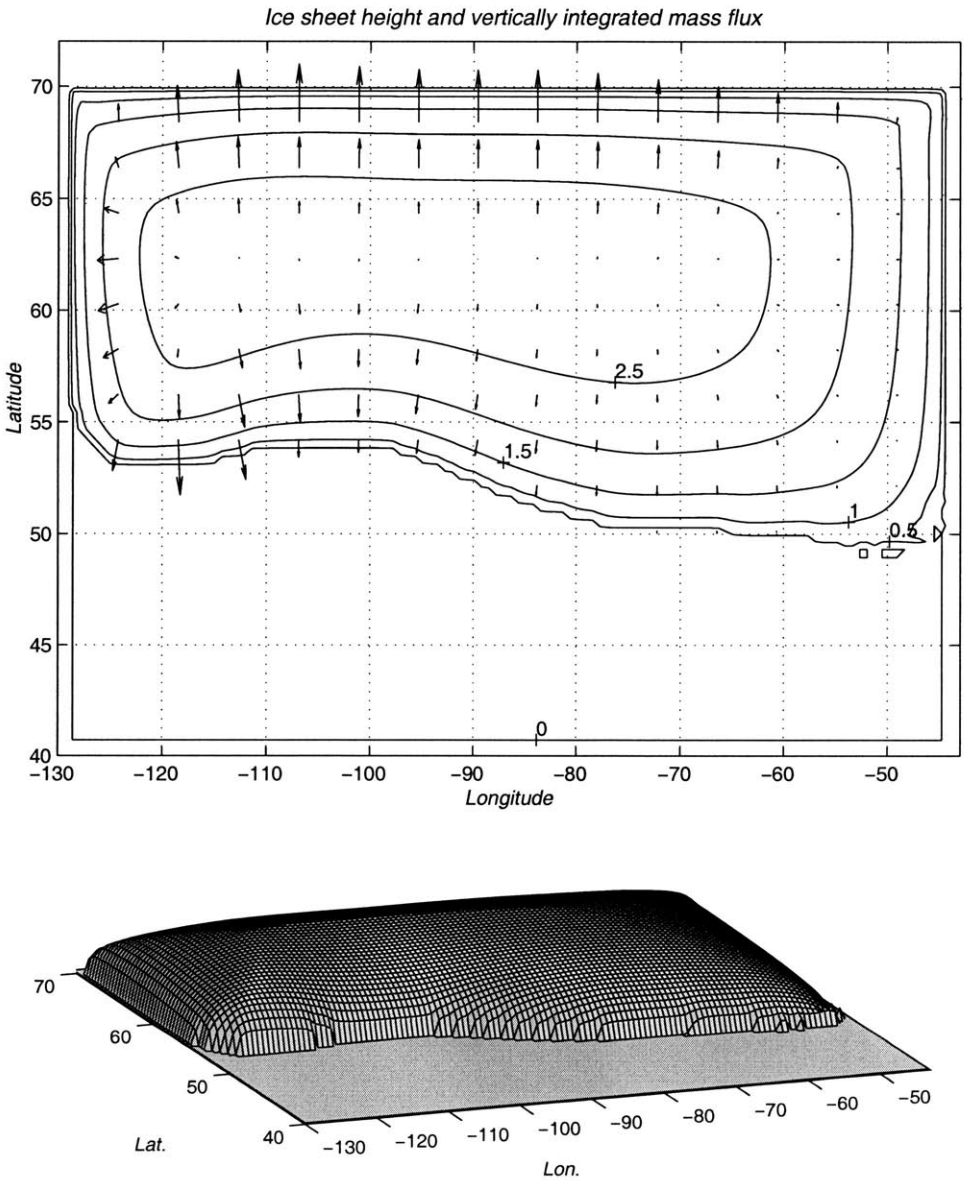

Figure 5.7: Equilibrium ice sheet for integration including the both the stationary wave and the topographic precipitation feedbacks. Otherwise as for Figure 5.1. The largest vector plotted corresponds to an ice flux of $1.4 \times 10^5 m^2 yr^{-1}$. The largest flux of ice (not plotted because of resolution) is $8 \times 10^5 m^2 yr^{-1}$.

Stat. wave.	Top. precip.	Volume ($10^6 km^3$)	Area ($10^6 km^2$)	Max. height (km)
NO	NO	21.7	7.7	2.8
NO	YES	19.3	7.1	2.8
YES	NO	38.7	12.0	3.5
YES	YES	26.0	9.4	2.9

Table 5.1: Details of equilibrium ice sheets for different combinations of allowed feedbacks. The first column refers to whether the atmospheric stationary wave was calculated. The second column refers to whether the effects of topographically influenced precipitation were included.

Figure 5.8a shows the precipitation over the ice sheet. The upslope direction is now affected by the perturbation winds associated with the stationary wave, and this has several consequences. On the western flank of the ice sheet the anticyclonic atmospheric circulation turns the upslope flow to southwesterly. This means there is some enhancement of precipitation over the southern margin there, with up to $50 cm yr^{-1}$ of accumulation. The result is ice on the western flank pushing further south than in either of the ice sheets shown in Figures 5.2 and 5.4. The maximum summer temperature is about $5^o C$ (Figure 5.8b), and therefore melting takes place for about half the year. Over the rest of the ice sheet, the anticyclonic circulation means that northerlies predominate. This implies enhanced precipitation over the northern flank; the accumulation there forms ice which quickly flows north and calves into the ocean; it does not contribute much to the overall structure of the ice sheet. What is more important is the large area of extremely low accumulation ($< 5 cm yr^{-1}$) that now extends over most of the ice sheet; this is due to the prevailing winds there being downslope. This low accumulation rate means that ice flows outwards only very sluggishly. The southern margin of the ice sheet barely makes it above freezing in the summer, meaning a very short melt season. The weak mass flux also prevents the ice sheet from pushing further south which, if it happened, would increase the area over which accumulation occurs, increase the size of the stationary wave, and cause an even greater cooling of the climate at the southern margin, thereby allowing for further extension of the ice sheet southwards. The ice margin in Figure 5.7 compares to the ice margin in Figure 5.4 in which the precipitation was not controlled by downslope winds.

Some of the important characteristics of the four different equilibrium ice sheets are summarized in Table 5.1. What we have seen from these integrations is that the

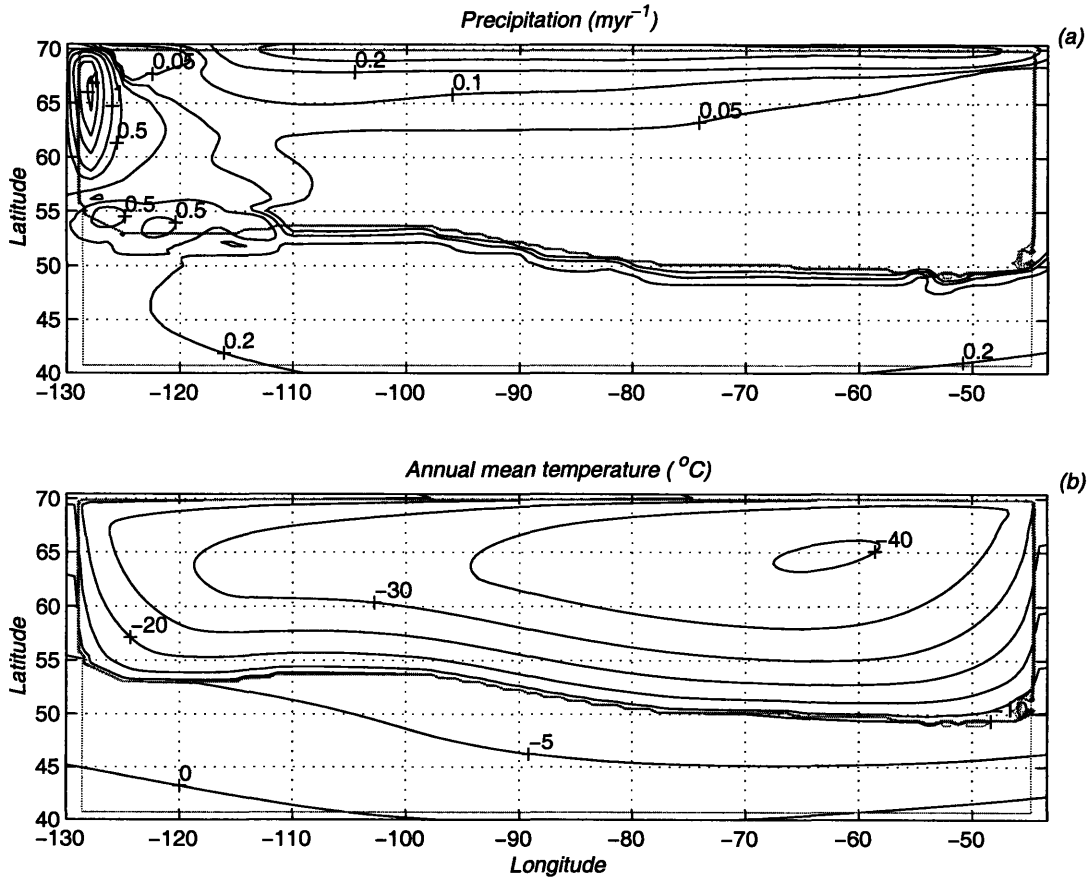

Figure 5.8: a) Accumulation rate (myr^{-1}); contour intervals are (0.05, 0.1, 0.2, 0.5, 1, 2, 3, 4), and (b) annually averaged surface temperatures (^oC), for the ice sheet shown in Figure 5.7. The outline of the ice sheet is shown as a thick, faint line.

topographic precipitation has a tendency to create an ice sheet aligned along a southwest-northeast axis. On the other hand the stationary wave creates the complimentary tendency; an ice sheet aligned along a northwest-southeast axis. When both feedbacks are included the equilibrium configuration of the ice sheet is a consequence of these competing processes and therefore depends on the relative strength of the feedbacks.

5.2 Results for different basic states

The results discussed above were produced using one particular atmospheric basic state — the standard basic state of chapter 3. However the correct basic state to use for the LGM is not known. Moreover, as noted in Chapter 3, we do not expect that basic state to remain constant over the time scales associated with Milankovitch cycles. We therefore need to consider the ice sheet's response for the plausible range of basic states. GCM and EBM simulations, together with current observations, provide some guide as to what range is reasonable. Some of the various GCM simulations are reviewed in more detail in Chapter 4, but generally, they show enhanced meridional temperature gradients in glacial climates, with the difference from today's climate being larger in winter than in summer. Since we have shown that the ice margin is largely controlled by the patterns of melting, which occurs predominantly in the summer, we ought to choose a basic state which we believe to be relevant for the summer season.

The basic state we have used so far in this chapter gives a jet strength of $23ms^{-1}$ at $10km$, which is slightly larger than the jet strength at high mid-latitudes in today's climate. A reasonable lower bound for the jet strength is that for summer in today's climate. We therefore define a 'weak' basic state to be the same as the summer basic state given in Chapter 4 ($10km$ jet strength of $17ms^{-1}$). A reasonable upper bound might be the midlatitude winter jet strength in today's climate; none of the GCM runs show a glacial summer jet strength at high mid-latitudes greater than this. So we define a 'strong' basic state at the same as the winter basic state in Chapter 4 ($10km$ jet strength of $29ms^{-1}$). Largely because the ice sheet behaves diffusively, we do not expect the coupled ice sheet–stationary wave system to have different regimes, so we don't expect qualitatively different behavior for parameters outside these bounds. This would not necessarily be the case if the physics of rapid ice sheet collapse, such as basal sliding,

had been included as a possibility in the ice sheet model.

In the linear model there is some arbitrariness in picking the strength of the forcing wind ($\overline{U}_f$ in Equation (3.19)). We have chosen to use the $1km$ basic state wind, which for the weak, standard, and strong basic states means a $\overline{U}_f$ of 3.5, 5.0, and 6.5 ms^{-1} respectively. The strong basic state will therefore generate the largest stationary wave. Figure 5.9 shows the equilibrium ice sheets which evolved in the weak and strong basic states. Both the stationary wave and precipitation feedbacks are included in these integrations. The shapes of the ice sheets are similar to Figure 5.7. The main affect is that the southeastern extension of the eastern flank of the ice sheet is proportional to the magnitude of the stationary wave; the larger the stationary wave, the larger the extension. It is somewhat surprising that the western lobe of the ice sheet remains largely unchanged for the range of the basic states shown. The weaker basic state means warmer temperatures at these latitudes, and so one might expect some retreat of the margin. However there is an eastward phase shift of the atmospheric response compared to the standard basic state. This moves the high pressure further over the ice sheet and brings stronger southerlies over the southwest of the ice sheet, causing local enhancement of the precipitation, which appears to be enough to compensate for the slightly increased temperatures. For the strong basic state, the westward shift of the response compared to the standard case reduces the precipitation and therefore tends to offset the tendency to advance because of the reduced temperatures there. The behavior of this lobe illustrates how the different aspects of the atmospheric response can play off against each other to create the final ice sheet's configuration.

5.3 Background stationary wave

The ice sheets of the Pleistocene did not evolve in isolation from each other. The stationary waves that topographic obstacles of their size create would have extended around the northern hemisphere. The stationary waves therefore provided a mechanism by which the ice sheets could have interacted with each other. The Tibetan Plateau also generates a significant planetary scale pattern, and would have also exerted an influence on the evolution of the ice sheets; it is this particular interaction we explore in this section. In Chapter 6 we will look at the stationary wave that the reconstructed topography of the LGM generates, but here we will stick with the simplified model

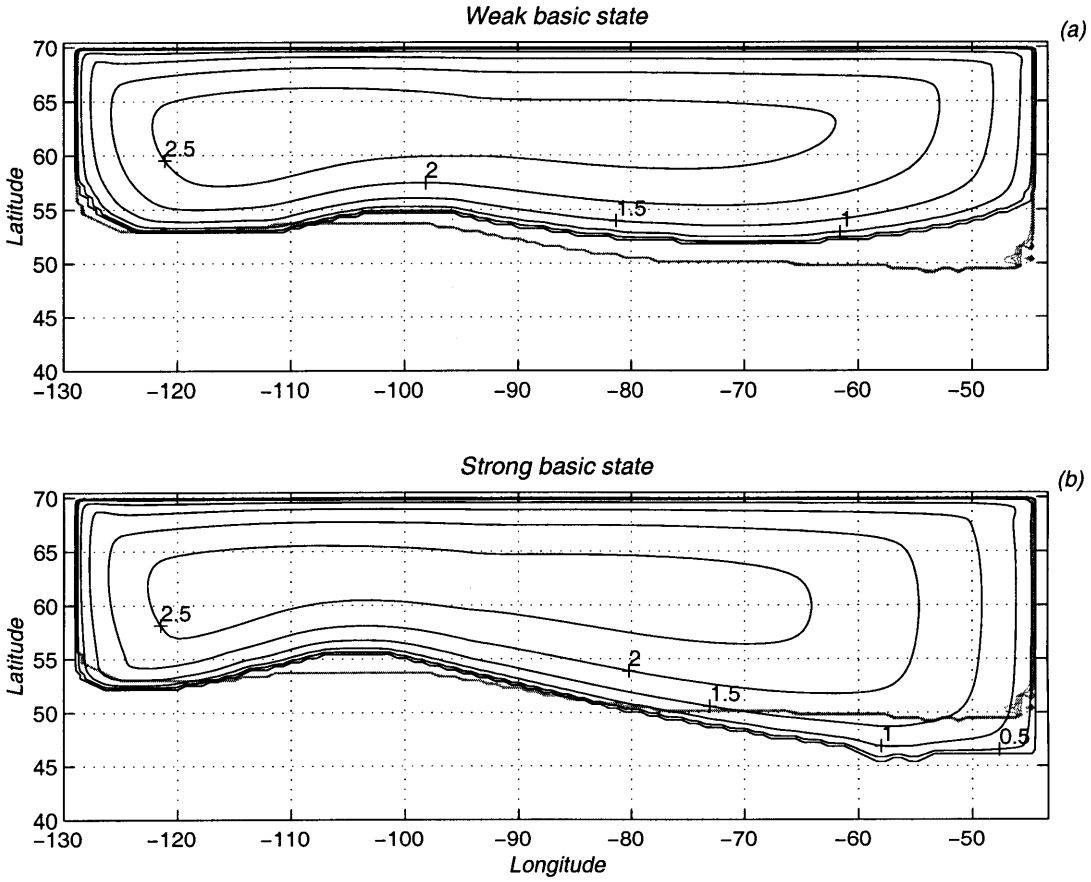

Figure 5.9: Equilibrium ice sheets using the (a) weak and (b) strong basic states. The outline of the equilibrium ice sheet for the standard basic state (i.e. Figure 5.7) is shown as a thick, faint line. Contours every $0.5km$.

geometry. The point here is not to produce a simulation of the stationary wave due to the Tibetan Plateau, but rather to see how the ice sheet responds to a plausible 'background' stationary wave (i.e. one not created by the ice sheet itself).

Our representation of the Tibetan plateau produces a trough of about $50gpm$ over the rectangular continent (Figure 5.10a). This is a slightly smaller trough than Charney and Eliassen (1949) attribute to the real eastern hemisphere topography, but the phase is approximately the same. The magnitude of the trough is similar to that obtained in other winter simulation models with more complicated geometry (e.g. Trenberth and Chen, 1988), but the pattern is simpler. Consistent with the geopotential heights, the low level temperatures are negative, minimizing at about -3^oC at $100W$ and $65N$ (Figure 5.10b). The low level perturbation background winds over the continent are around $1ms^{-1}$, and are therefore much smaller than typical winds induced locally by the ice sheet (see Figure 3.6 for example).

Figure 5.11 displays the equilibrium ice sheet resulting from an integration including this background stationary wave. Essentially, the differences from Figure 5.7 can be explained by the temperature perturbation associated with the background stationary wave. The southern margin at $90W$ is about 4.5^o further south. Using the meridional temperature gradient this converts to a cooling of 3.3^oC. The perturbation due to the background stationary wave alone is about -2.5^oC (Figure 5.10). A further extension of the ice occurs because as the ice sheet grows, there is then a larger area over which to accumulate, leading to an increased flux southwards.

5.4 Growth phase of ice sheet

Up to this point, we have looked at the configuration of ice sheets that have been integrated to equilibrium with the climate. We now consider their time dependent behavior. The simplified model of Chapter 2 suggested that the stationary wave feedback would act to change the growth rate by controlling the temperature at the ice sheet's southern margin. In this section we investigate the extent to which this holds true in the more complicated three-dimensional model. Figure 5.12 shows the time evolution of the four ice sheets shown in Figures 5.1 to 5.8 (i.e. various combinations of feedbacks). For each of these runs the zonally averaged climate was specified and constant in time.

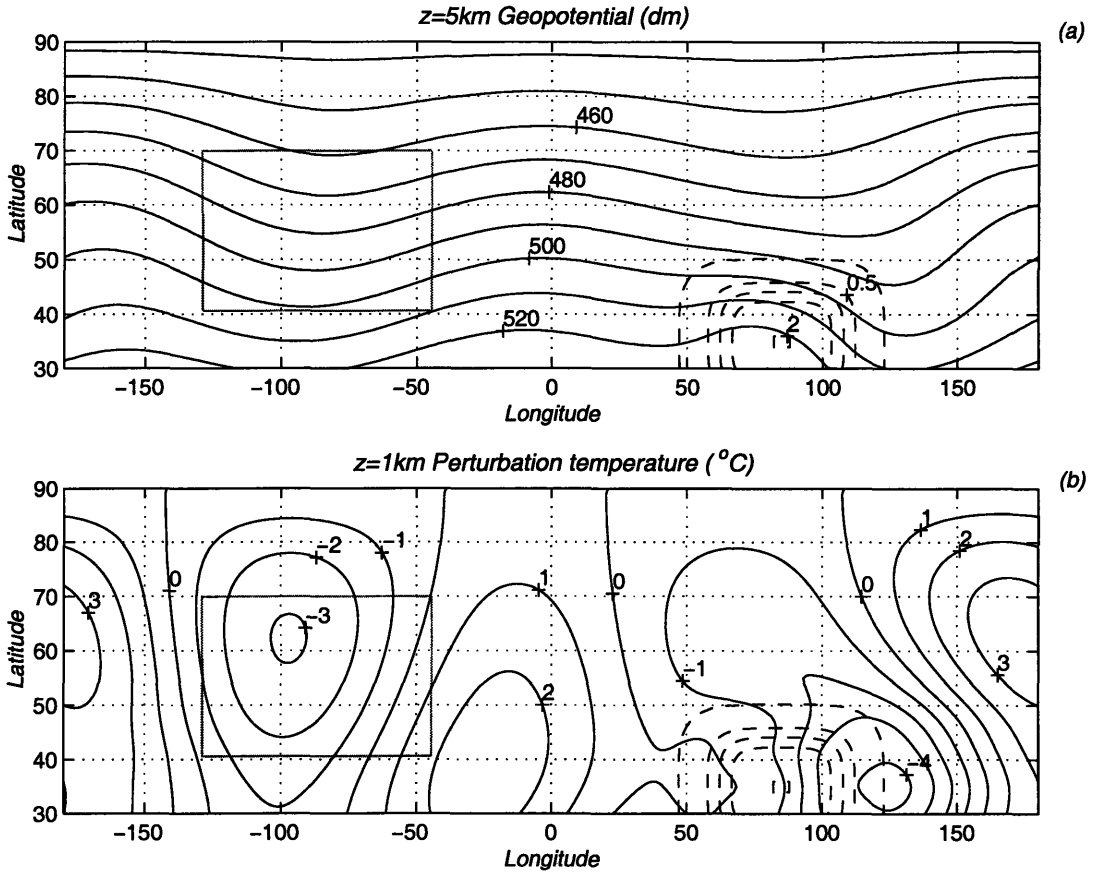

Figure 5.10: Background stationary wave. (a) Geopotential heights (dm) at $z = 5km$, and (b) perturbation temperatures (^oC) at $z = 1km$ (lower panel), generated by representation of the Tibetan Plateau with a maximum height $2km$ (dashed contours). The outline of the rectangular continent is also shown by the thick, faint contour.

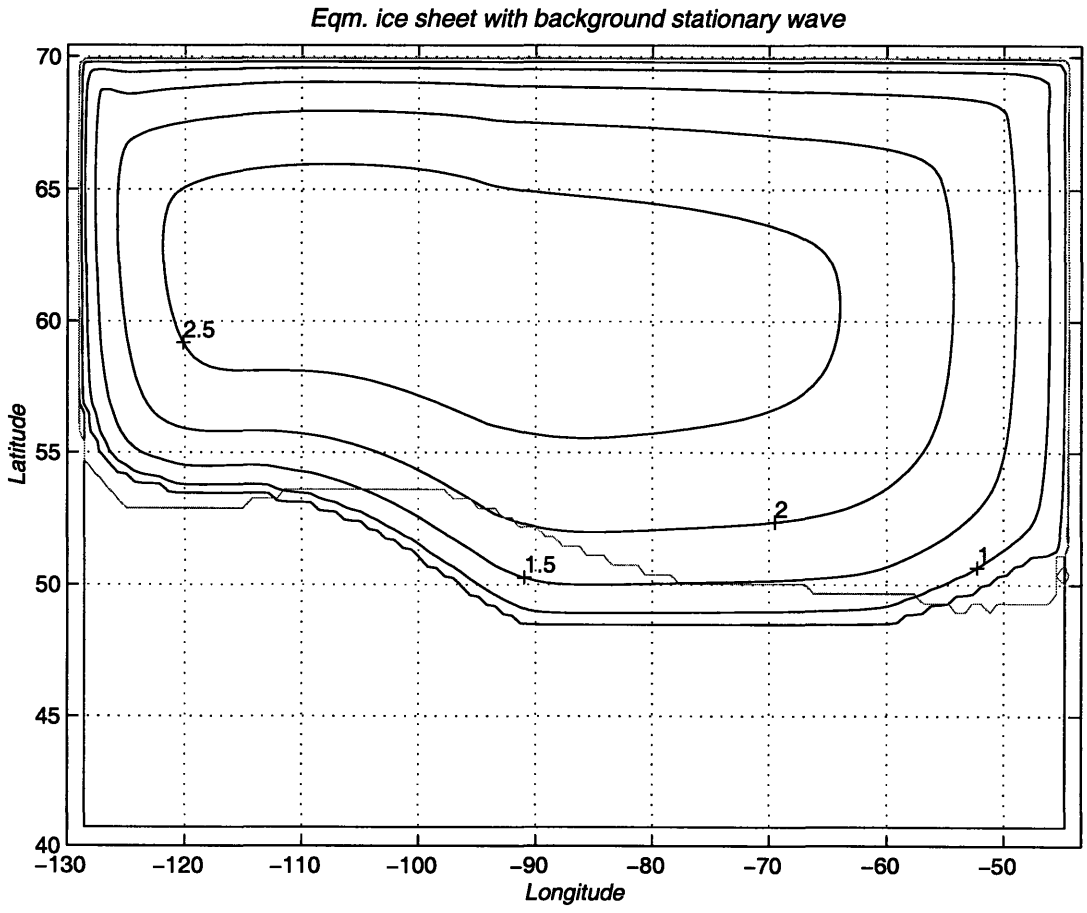

Figure 5.11: Equilibrium ice sheet for an integration including a background stationary wave. The faint contour is the outline of the ice sheet shown in Figure 5.7 (i.e. no background stationary wave).

The integrations were started with an ice free continent. Since the summer zero degree isotherm at sea level lies at $55N$, ice immediately begins to accumulate northwards of this line, and thus the area starts off at a finite value. The ice volume however builds up from zero. The area of the ice sheet increases only very slowly beyond its initial value: several thousand years are required for the ice to build up enough in the interior to create a southwards mass flux at the southern margin which significantly exceeds the melting rate there. For the case of a fixed zonally averaged climate, the ice sheet takes about $60kyr$ to reach equilibrium. Including the precipitation feedback alone does not change much the time taken to attain the equilibrium state. Equilibrium is taken to have been reached when the ice sheet stops changing in size significantly (i.e. a few percent of its asymptotic value); for our purposes we do not need to use any more precise definition.

The results in Chapter 2 suggested that the growth rate of an ice sheet would be increased if the CTT feedback (cold perturbation temperatures) acted over most of the ice sheet. In Chapter 3 the predominance of the CTT feedback was demonstrated to be robust, at least for this simplified geometry, and Figure 5.4 confirms the effect. Figure 5.12 shows that with the stationary wave feedback alone, the growth rate (of the volume or the area of the ice sheet) exceeds the growth rate for an ice sheet evolving without climate feedbacks. The mechanism of this increased growth rate is essentially that described in Chapter 2: including the stationary wave feedback increases the area of the ice sheet, and so it simply increases the area over which falling snow is incorporated into the ice sheet. A larger amount of time is now required to reach equilibrium, which is achieved after about $140kyr$.

The simplified model of Chapter 2 assumed that the precipitation rate remained constant throughout the evolution of the ice sheet. But when both feedbacks are incorporated in the three-dimensional model, a large area of the ice sheet experiences prevailing downslope winds and so the precipitation is sharply reduced there (Figure 5.8). This then limits the rate at which the ice can grow. In fact, Figure 5.12 shows that the precipitation effect almost exactly compensates for the increased area for the first few thousand years, so that the growth rate is the same as for the cases without either feedback.

When both feedbacks are included, the time to reach equilibrium is increased dramatically; even after $200kyr$, the area of the ice sheet is still increasing, albeit slowly (the ice sheet area reaches 90% of its equilibrium value after about $140kyr$). The slow

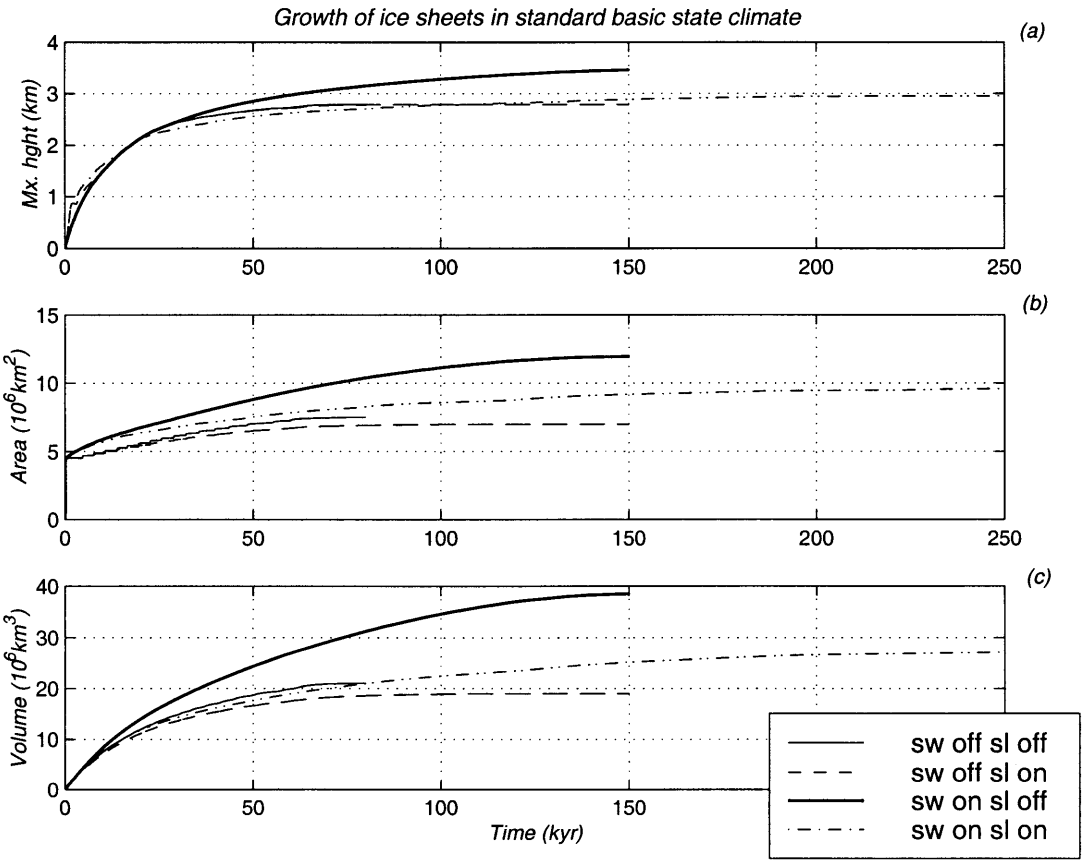

Figure 5.12: Time evolution to equilibrium for ice sheets integrated using different combinations of the feedbacks. (a) maximum surface height (km), (b) basal area ($10^6 km^2$), and (c) volume ($10^6 km^3$). The legend shows which feedbacks were included in each integration. SW refers to the stationary wave feedback. SL (for slope) refers to the topographic precipitation. Each integration is only plotted until the ice sheet attains equilibrium.

equilibration appears to be because the ice sheet has to play catch up towards a climate which it itself is creating: a change in the ice sheet causes a redistribution of the melting and accumulation patterns, which then changes what the ice sheet's equilibrium configuration will be.

For all of the ice sheets in Figure 5.12, the equilibration time is longer than the two main Milankovitch cycles (precession; $19kyr$ and $23kyr$, and obliquity; $41kyr$). Moreover, the integrations in this thesis only include simplified ice physics. Accounting for the temperature dependence of the ice flow and allowing for polythermal ice (a mixture of ice and water at melting point) at the base greatly increases the time to reach full dynamical equilibrium. Although the shape does not change significantly, the temperature field within the ice continues to evolve (R. Greve, personal communication). Therefore the ice sheets could not have been in equilibrium with the climate at any time during the glacial cycles. This is also well established by previous work (e.g. Calov and Hutter, 1996).

5.4.1 Growth from isolated plateau with gradual climate cooling

The ice sheets in Figure 5.12 evolved in an instantaneously imposed glacial climate. A more realistic scenario for the evolution of an ice sheet, of course, is a gradual cooling of the climate. It is almost certain that ice sheets first initiate on high terrain, but the ruggedness of the terrain is an issue in whether a mass of ice that starts off as a glacier eventually becomes an ice cap or an ice sheet. If there are high mountains, initiation is more likely, but if there are also deep neighboring valleys with high melt rates then it may be much harder to extend the initial glacier. Once an ice cap is sufficiently large its high albedo can play a role in cooling the surrounding region, further extending the ice area, although the presence of clouds diminishes the albedo effect. This is a feedback which we do not account for in looking at the growth of the ice sheet: the climate cooling is an externally imposed forcing. An additional important factor for growth, as we shall show in this section, is the maxima in the accumulation tracking the upwind slopes as the ice sheet evolves.

Bearing the above in mind, a small plateau ($1km$ high) is placed in the central northern region of the rectangular continent (Figure 5.13, first panel). The temperature

is initially raised from the standard basic state value such that permanent year round accumulation occurs only on the high ground of the plateau. We take a warming of 8.5^oC. The climate is then cooled linearly over the initial $15kyr$ back to the standard basic state climate. The first few thousand years of ice sheet growth are controlled by the upslope precipitation. Accumulation rates on the western slopes exceed $1myr^{-1}$ and mean that the ice there builds up quickly. The ice mass flux is always in the downslope direction and so the ice sheet spreads westward. The western edge of the ice sheet has both high accumulation rates and a westward flux of ice from the interior, causing the moving western margin to quickly build up height. This creates a lower surface temperature on the ice which protects it from melting, even though Figure 5.13 shows that for the first $10kyr$ or so, the climate is too warm to support an ice sheet east of the plateau.

At $8kyr$ the ice has built up enough that a small atmospheric stationary wave is created. That this is so can be seem by observing that the westward progressing edge of the ice sheet begins to turn slightly to the south. The developing anticyclonic atmospheric circulation creates prevailing winds over the ice sheet with a small southerly component to them. The upslope precipitation therefore gradually moves towards the southwestern flank of the ice sheet.

It is only at around $10kyr$ that the rest of the climate cools down sufficiently to allow year round accumulation at sea level. After this, the ice sheet begins to form east of the plateau. Up to this time there is a flux of ice eastward from the plateau, but it is so small that it is easily melted by even a small positive summer temperature. Even for temperatures only slightly above freezing, the PDD model gives melt rates of several meters a year and a much larger ice flux would be required to overcome this. It is not plausible, either, that precipitation rates would be large enough in the lee of the topography for the accumulation to exceed the melting. After $10kyr$, however, the growth of the ice sheet is controlled mainly by the remaining climate cooling and also by the growing stationary wave. The ice sheet continues to evolve slowly, albeit at a gradually diminishing rate, for about another $200kyr$.

We conclude two things from this section about the initial growth of the ice sheet. The first is that the early evolution is dominated by the upslope precipitation, which was also noted by Sanberg and Oerlemans (1983). The windward edge of the ice sheet grows quickly towards the upwind direction. This rapid and roughly westward march

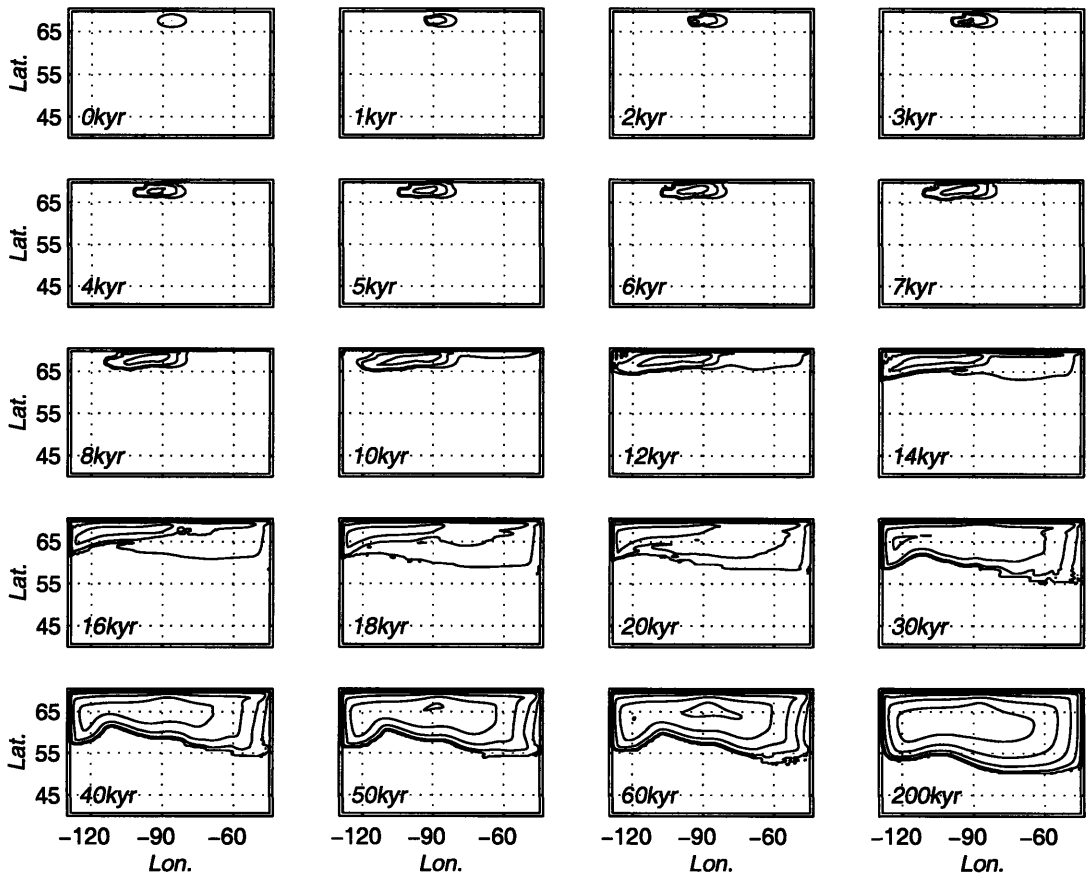

Figure 5.13: Time sequence (not evenly spaced) for an ice sheet initiated on a small plateau. The climate is cooled by 8.5^oC over the first $15kyr$ towards the standard basic state climate. Height contours are every $0.5km$. The time is indicated in the lower left corner of each panel.

stops only when the ice sheet encounters the continental margin, whereupon it begins to calve into the ocean. For the Fennoscandian, which almost certainly initiated on the high ground over Scandinavia, the ice would have quickly encountered the North Sea, and so the upslope effect would have been important only in the very earliest stages of its growth cycle. For the Laurentide, however, which may have initiated over Keewatin and Quebec (Clark et al., 1993), upslope precipitation likely played a very important role in the early westward expansion of the ice sheet.

The second conclusion is that once the western ice margin has reached the ocean (or perhaps an insurmountable mountain range like the Rockies), further expansion of the ice is driven predominantly by decreasing summer temperatures rather than by outward spreading of ice from within the interior of the ice sheet. The land-based margin of the ice sheet tends to track a summer isotherm which is only a few degrees above freezing. This is not to say that the ice sheet does not affect where that isotherm lies—the albedo feedback and the stationary wave feedback certainly act to cool the climate around the ice sheet—we just emphasize that the extension of the ice is not caused by the internal ice dynamics, but rather by climatic cooling.

5.5 Decay phase of an ice sheet

The results from the simple model in Chapter 2 suggested that if cold temperatures dominate over the most of the ice sheet, then the stationary wave feedback tends to increase the rate at which ice melts if the climate is warmed. The reason for this is that the ice at the margin is maintained there partly by the atmospheric stationary wave induced by the ice sheet. Therefore a reduced ice sheet reduces the stationary wave, warming the margin and leading to an enhanced melt rate. This section considers the extent to which the above holds true in the more complex model. We again choose to show results for the different combinations of the feedbacks to highlight the role that each has in the ice sheet's evolution. Starting from each of the equilibrium ice sheets shown in Figures 5.1 to 5.8, we impose an instantaneous warming of 5^oC at $1.5kyr$ into the integration. The ice sheet model dynamics are fully spun up, so there is no initial adjustment to a dynamical balance. As a warming is imposed, some areas of land are left below sea level because the bedrock, which was set initially at $z = 0$ has been depressed by the overlying ice. In these integrations, we do not allow the sea to inundate these

areas. Nor do we account for the fact that there might be pro-glacial lakes contained by the depressed bedrock in front of the retreating ice, into which the calving of ice might be an additional effective mechanism for ice wastage. We are instead isolating the interaction between the atmosphere and the ice sheet. Moreover the fact that the model starts off with a flat continent at sea level is unrealistic and means that there is nothing to prevent the sea from inundating in front of the retreating ice. Although calving ahead of a retreating ice sheet is very difficult to model, it has been shown as potentially a very effective mechanism for ice wastage (Pollard, 1982).

Figure 5.14 shows time evolution in the ice sheets, plotted as a percentage change from initial size in order to make a better comparison with the results in Chapter 2. When the warming is first imposed, there is an initial increase in the maximum height of the ice sheet. This is because the first effect to take hold is an increase in the precipitation rate in the warmer climate (Equation (4.16)). After about $5kyr$ though, the rapidly collapsing margins increase the ice flux away from the interior, and the ice subsides.

The area and volume of the ice sheet both begin to decrease as soon as the warming is imposed. Figure 5.14 shows that including the stationary wave effect alone does indeed increase the melt rate. However including both the stationary wave and precipitation feedbacks produces a decay rate about the same as for when neither feedback is included. As for the case of ice sheet growth, the stationary wave feedback acts to change the decay in the manner suggested by the simple model in Chapter 2, but including the precipitation feedback almost exactly cancels the change in the decay rate. The reason here, though, is different from the case of ice sheet growth. Snapshots of the melting ice sheets are shown in Figure 5.15. Without the precipitation feedback, the ice retreats almost uniformly along its whole margin, meaning that any ice on the western flank is gone after about $8kyr$. But when the precipitation feedback is included, the high precipitation rates in the west (Figure 5.8) mean that the ice dome there can be sustained. This dome contributes significantly to forcing the stationary wave over the rest of the ice sheet, and therefore it maintains lower temperatures over the ice. The effect is quite small—the ice sheet temperature is lowered by around 2^oC—but it is enough to reduce the melt rate back to what it was with no feedbacks. Figure 5.14 also shows the results when just the precipitation feedback is used in the integration. In this case, the shallow slopes on the eastern flank make the ice sheet more vulnerable, since for a given temperature increase, more of the ice sheet becomes exposed to melting.

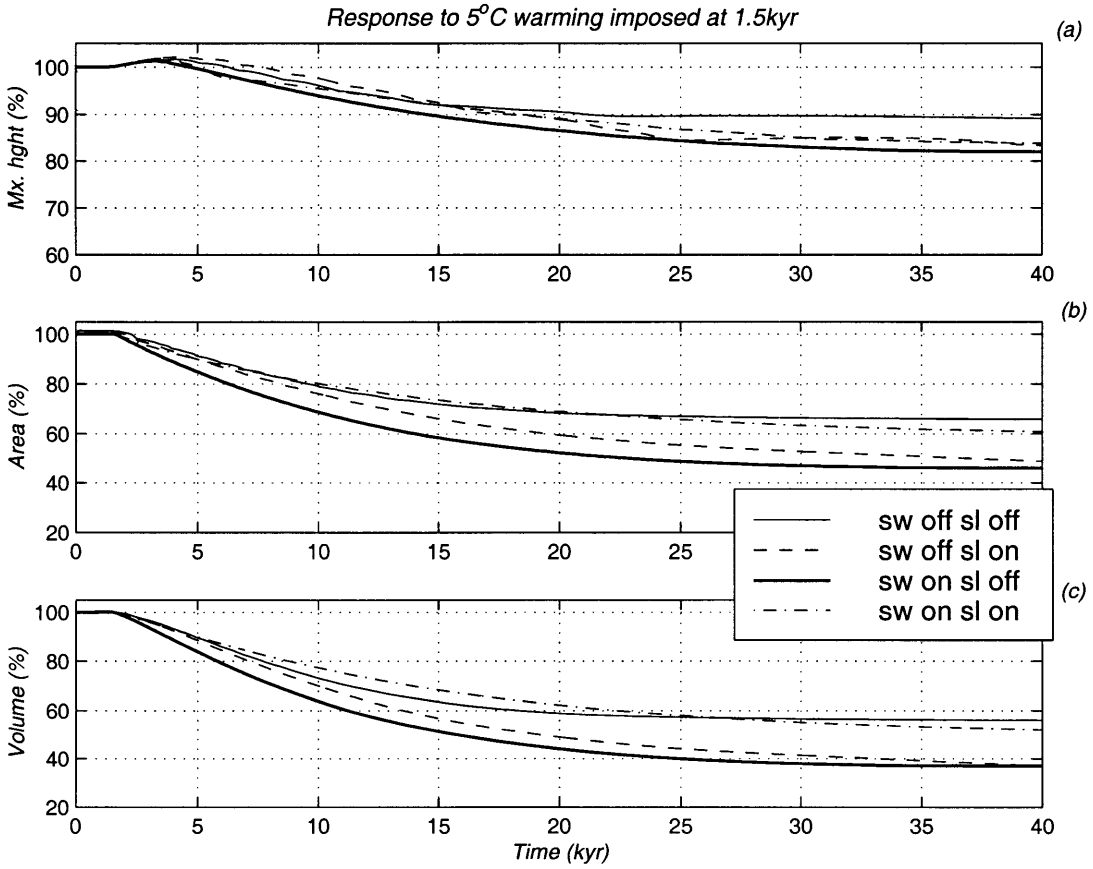

Figure 5.14: Response of ice sheets integrated using different combinations of the feedbacks to a 5^oC warming imposed at $1.5kyr$. Conventions as for Figure 5.12.

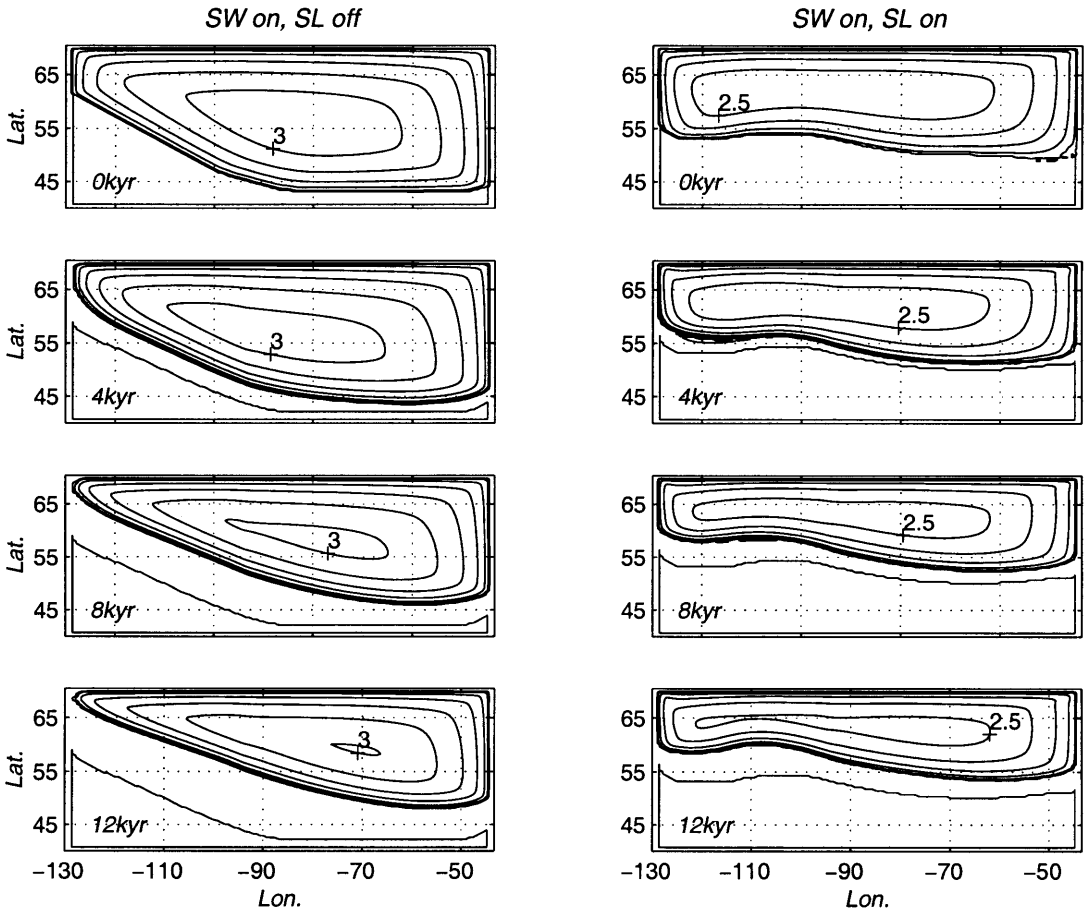

Figure 5.15: Time sequence of retreat for two of the ice sheets plotted in Figure 5.14. The panels on the left are for the integration where only the stationary wave feedback was included. The panels on the right are for the integration where both the topographic precipitation and the stationary wave feedbacks were allowed. The bedrock surface in front of the retreating ice sheets is below the $z = 0$ level. Contours every $0.5km$. The time is indicated in the lower left corner of each panel.

The above results are less dramatic than Chapter 2 suggested would be the case. There, the inclusion of the CTT feedback in the simple model caused a dramatic increase in the melt rate of the ice. We have shown that some of the difference can be attributed to the more complicated situation which applies in three dimensions. The behavior of the ice sheet at one longitude is dependent on what the rest of the ice sheet is doing. A second reason is the perfectly plastic approximation assumed the ice sheet redistributed its volume instantaneously: the ice profile adjusted to wastage at the margin by immediately pushing more ice southwards into melting regions. In reality this happens only by the flow of ice which takes place over thousand of years, and therefore the feedbacks are less effective.

5.6 Periodic forcing of the basic state

In this section we look at how the periodic changes in the earth's orbit might change the interaction between the ice sheets and the stationary waves. As reviewed in the introduction, the relevant orbital cycles leading to changes in the incident insolation are the precession (with periods of $19kyr$ and $23kyr$), the obliquity ($41kyr$), and the eccentricity (95, 125 and $400kyr$), which although it does not itself directly change insolation significantly, modulates the amplitude of the precessional cycle. The magnitude of the insolation forcing varies with season, but it has generally been assumed that it is most important to consider the high latitude northern summers. This conclusion is based on the importance of the summer melting season to the ice sheet mass balance. This was emphasized and analyzed in chapter 4. Both the magnitude of the direct forcing felt by the ice sheet and its phasing relative to the orbital cycles depend on many factors and feedbacks in the climate system. The model presented in this thesis is too simple to include all the potential factors and so we limit discussion to those best addressed by the model. We expect variations in the insolation to affect the atmospheric basic state, and so we consider separately forcing in three of its important elements. The first element is the direct forcing of the basic state temperature—changing the temperature at all latitudes by the same amount. Secondly, we impose periodic variations in the atmospheric vertical wind shear (equivalent to meridional temperature gradient), to which the stationary wave pattern was shown to be quite sensitive to in Chapter 3. Lastly, a sizable fraction of the stationary wave in today's winter climate is due to the presence of

the Tibetan Plateau. The magnitude of the stationary wave generated is sensitive to the proximity of the atmospheric basic state jet to the plateau which we expect, in turn, to be sensitive to orbital configuration (Lindzen and Pan, 1994). While in today's climate this is a winter phenomenon, we also consider the possibility that in glacial climates the summer background stationary wave undergoes periodic variations.

For each of the above cases we consider forcing periods of $20kyr$ and $40kyr$, representative of the dominant oscillation periods in the insolation. Because the equilibration time for the ice sheets is much longer than these periods, we expect that the amplitude of the ice sheet's response will differ for these two periods. The magnitude of the periodic forcings we choose are large, but plausible. Thus we hope to place bounds on the magnitude of the response, again noting we are limiting the set of feedbacks which we allow in the system.

We emphasize that we are considering each of the forcings in isolation and do not attempt to assess how they have operated in combination in the real climate. Nor do we allow for other presumably important feedbacks which would come into play as the ice sheets undergo changes in size. Among these feedbacks are the ice-albedo feedback, calving into pro-glacial lakes, and changes in poleward heat transport and ocean circulation. To account for these different factors comprehensively would require careful consideration of the sensitivity to orbital forcing of the different components of the climate system, and an understanding of how they act in combination.

Having isolated a potentially important aspect of the interaction between the ice sheets and the climate (the stationary waves), the purpose of this section is to try to understand how that interaction works for the case of time dependent forcing.

5.6.1 Varying basic state temperature

The basic state temperature was changed by a sinusoidally varying perturbation with an amplitude of 5^oC. This is slightly larger than the maximum temperature forcing that Short et al. (1990) calculate as associated with direct orbital forcing, and which applies in the interior of the continents. We noted in the Chapter 1 that EBMs do not have the dynamics necessary to address how the atmosphere redistributes this insolation forcing, and here we mean to use it only as a rough reference. The temperature increment was applied at all levels and latitudes in the atmosphere meaning that the atmospheric

refractive index, which depends only on gradients of temperature, was not affected. Any change in the atmospheric stationary wave pattern was therefore due to changes in the size of the ice sheet, and not to changes in the basic state.

Oscillation periods of both $20kyr$ and $40kyr$ were looked at. Starting from equilibrium conditions (with both precipitation and stationary wave feedbacks included), the model was integrated forward $200kyr$ under the influence of this variable forcing. As for the previous section we again prevent the inundation of the sea behind retreating ice sheets. Figure 5.16 shows the last $100kyr$ of both runs. The $40kyr$ forcing produces an oscillation in the volume of $\sim \pm 15\%$ and of about $\sim \pm 10\%$ in the area. The maximum height varies by $\sim \pm 5\%$.

There are several things to note about Figure 5.16. First, the time mean values of the various fields are different from their equilibrium values when integrated under steady climate forcing. This is due to the asymmetry in the growth and decay process. Nonlinearities mean that the even if the mean of the forcing is zero, the mean of the response is not necessarily zero. For instance, starting from equilibrium with steady forcing and then cooling, ice will begin to accumulate at the front of the ice sheet where temperatures are now cold enough to sustain year round ice. Because the growth and decay processes are different, the warming of the climate is not an exact reverse of the cooling. Indeed, as the climate begins to warm again the interior accumulation increases because of the increase in saturation vapor pressure with temperature. If the melt-back is not complete by the time the climate begins to cool and the ice sheet renews its growth again, then the average volume over the cycle will be larger than the equilibrium volume was under steady forcing. This 'ratchet effect', where the ice volume increases every cycle, will continue until the southern margin lies sufficiently far south that the melting during the warm part of the cycle becomes large enough to exactly offset the net accumulation over the cycle. This physics is also reflected in the mean values of the various fields shown in Figure 5.16, which are different for $20kyr$ forcing and for $40kyr$ forcing: different oscillation periods means a different amount of the oscillatory forcing projects onto the mean of the response. However, the shape of the oscillations are the same, from which we conclude that the same physics applies at each stage of the cycle for both forcing periods.

Another point from Figure 5.16 is that the amplitude of the response to $40kyr$ forcing is larger than for $20kyr$ forcing. This implies that the adjustment time of the ice sheet to

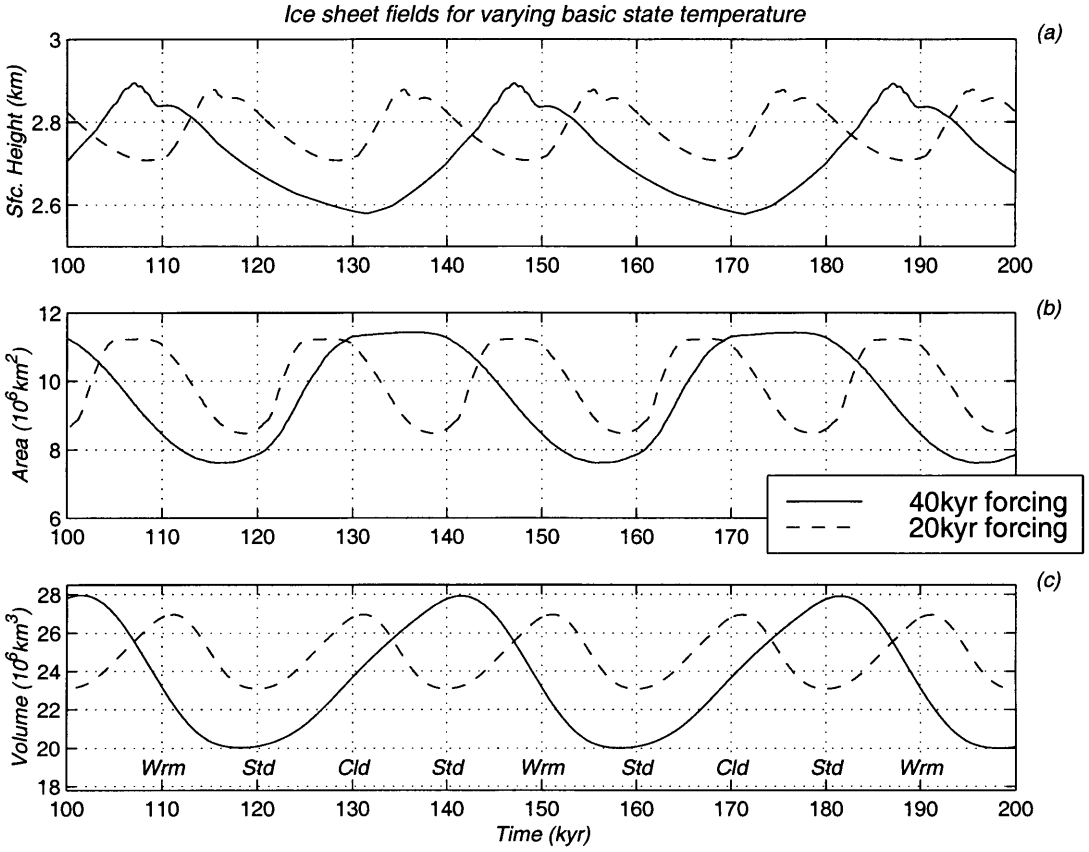

Figure 5.16: Time series of ice sheet fields for sinusoidal $20kyr$ and $40kyr$ forcings on basic state temperature. (a) Maximum surface height (km), (b) basal area ($10^6 km^2$), and (c) volume ($10^6 km^3$). The integration was started at $t = 0kyr$ from equilibrium with the standard basic state. The last $100kyr$ of a $200kyr$ run are plotted. The text at the bottom of (c) gives the phase of the $40kyr$ forcing. At points marked Wrm (Cld) it is 5^oC warmer (colder) than the standard basic state (Std).

the size of forcing we have chosen is considerably larger than $20kyr$. Were the adjustment time much shorter than $20kyr$, the ice sheet could be considered to be in equilibrium at each time step, and the amplitude of the response would be the same at $20kyr$ as at $40kyr$.

Figure 5.17 shows ice sheet during one $40kyr$ forcing cycle. For this integration, the perturbation forcing at $160kyr$ is zero. The tendency of the forcing is such that after $160kyr$ the climate is cooling (at $170kyr$ it is 5^oC colder, and at $190kyr$ it is 5^oC warmer). From both Figure 5.16 and Figure 5.17, it is seen that the area that the ice sheet covers follows closely the cooling climate. Maximum areal extent of the ice sheet is reached when the climate is coldest at $170kyr$. Even though the air column holds less moisture in the colder climate, the accumulation over the whole ice sheet (and therefore the volume) increases because of the larger ice sheet area at this time. Integrated accumulation over the ice sheet increases from $1120km^3yr^{-1}$ at $160kyr$ to $1280km^3yr^{-1}$ at $170kyr$ despite the fact that the mean accumulation over the ice sheet has dropped from $0.143myr^{-1}$ to $0.118myr^{-1}$ during the same time.

The small scale features which develop as the ice sheet grows are due to the precipitation parameterization that was used, which tends to enhance local details. The fact that these features persist is another indication that the ice dynamics does not have enough time to come into equilibrium with the changing forcing of the basic state. If the ice sheet were in equilibrium with the forcing climate we would expect the shape to be as smooth as in Figure 5.7. After $170kyr$, the climate is beginning to warm again. Ice has now accumulated so that the surface of the ice sheet is at a higher elevation than the surface was when the ice first formed there. In order to melt the ice, the climate must warm to a higher temperature than that which allowed the ice to form there in the first place. The area of the ice sheet thus remains approximately constant between about $170kyr$ and $180kyr$. During this time ice accumulates in the interior, and because the area of the ice sheet is relatively large, the volume continues to grow.

The volume begins to decrease 1 to $2kyr$ after the ice sheet begins to recede from its maximum area. This lag is likely due to the increasing accumulation in the interior as the temperature warms. After this point though, the melting more than offsets the increasing accumulation. The interior accumulation causes the maximum height to continue to increase until around $187kyr$ (about $5kyr$ after the volume begins to decrease). At this time the western slopes of the ice sheet undergo strong wastage and

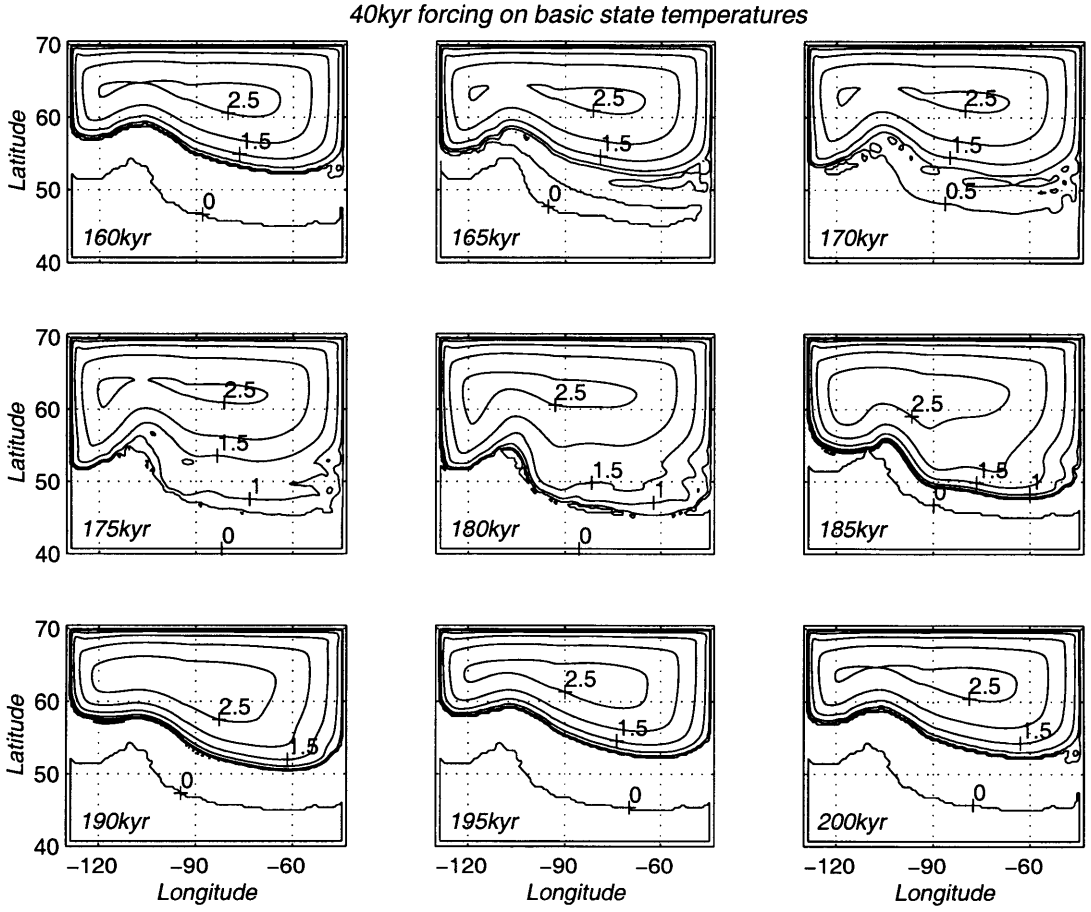

Figure 5.17: Time sequence for one cycle of the $40kyr$ sinusoidal forcing of the basic state temperature. Refer to Figure 5.16 for the phase and magnitude of the forcing. Contours every $0.5km$. In front the retreating ice sheet the bedrock is often below the $z = 0$ level.

the peak of the western dome drops quickly to below the height of the eastern dome, which lies further into the interior of the ice sheet (Figure 5.16). The height of the eastern dome continues to increase until around $190kyr$. This causes the slight double peak in top panel of Figure 5.16. At $190kyr$ the climate forcing is at its warmest and the ice sheet volume is decreasing rapidly. At this point, the average melting, where it occurs, is $1.8myr^{-1}$. The presence of bedrock depression in front of the receding ice sheet is because the ice retreats faster than the rebound time restores the bedrock to isostatic equilibrium.

Because the ice melt-back is more rapid compared to the ice growth, the cycle in ice sheet volume has a saw-toothed shape to it. The growth phase is nearly twice as long as the decay phase of the cycle. This is a less exaggerated (although cleaner) sawtooth than the $100kyr$ cycle from observations of the late Pleistocene ice ages. These have about a $80kyr$ growth time, and a $20kyr$ decay time (Figure 1.2). Bedrock depression has often been invoked as contributing to the saw-toothed shape of the ice age cycles (Pollard, 1982). As ice builds up, the underlying bedrock is depressed. If the ice then begins to retreat faster than the bedrock is restored to equilibrium, the retreating margin at any given latitude is at a lower height than the ice there first formed at, and due to the atmospheric lapse rate it is therefore at a warmer temperature. This then reinforces the melt-back. It is possible here to calculate the respective contributions of the imposed warming and the bedrock depression to creating the shape of the ice sheet cycle. Consider Figure 5.17. At the location of the ice margin when the ice sheet has its smallest area, the ice builds up to about $2km$ in height when the ice sheet is at its thickest during the cycle, which implies the bedrock has been be depressed by about $1km$ (Equation (4.13), and assuming isostatic equilibrium). Using the atmospheric lapse rate (-6.5^oCkm^{-1}), this means that the most the bedrock depression could contribute is 6.5^oC, and that only at the point of greatest retreat at the end of the retreat phase. The contribution to the warming is actually less than this because the relaxation time of the bedrock ($3kyr$) is sufficiently fast for some rebound to occur as the ice sheet retreats. On the other hand, the hottest imposed climate contributes 10^oC of warming (compared to the coldest climate), and it occurs during the period of greatest retreat for the ice sheet volume (Figure 5.16). Therefore, the imposed climate change contributes more to the retreat of the ice sheet than does the bedrock depression. It means also that the saw-toothed shape of the cycle, at least in these integrations, is controlled mainly by the asymmetry in the accumulation and melting processes and not by the bedrock depression. This

conclusion depends to an extent on the processes and parameters we have used in the model: if the real ice sheets were more unstable to small warmings than our model is, then a faster or more complete retreat of ice would mean the bedrock depression could have a more significant influence on the retreat.

Figure 5.16 highlights the differences in the phasing of the ice volume and the area of the ice sheet. For an ice sheet like the one we are considering which can spread equatorward on a continent in response to a cooling climate, the dominant factor is the area over which the ice can exist: more ice area simply allows more snow to accumulate. However the relative phase of the ice volume or area relative to the temperature forcing will depend on the details of the ice and climate physics and the geometry assumed. For instance, consider an ice sheet like that on Antarctica, where it is too cold for significant melting, and where ice wastage occurs almost entirely via calving. Assuming these conditions did not change over a forcing cycle, the area would remain roughly constant and the volume would track the temperature forcing with a lag dictated by the length of time for changes in interior accumulation to be reflected in changes in the calving rate at the margin. We have moreover assumed an ice sheet with frozen bed. If changes in the surface temperature are communicated to the bed and are large enough to change the bottom boundary condition (cold or temperate ice), then substantial changes in the ice volume might occur. This last process is mitigated by a couple of factors. Firstly, runs with the full thermodynamic calculation do not show a large change in volume (Figure 4.3), albeit for a conservative sliding law. Secondly, the thermal equilibration time is long compared to the periods of the forcing we are considering, and thus by the time the temperature signal was communicated to the bed, it would be strongly damped.

5.6.2 Varying basic state shear

The response to reasonable variations in the atmospheric shear is much smaller than the response to the temperature forcing, with changes essentially confined to local details of the ice sheet. The standard case basic state has a shear of $2.0 \times 10^{-3} s^{-1}$. To this was added a sinusoidal perturbation of amplitude $0.5 \times 10^{-3} s^{-1}$. This gives a variation in the $10km$ jet strength between 18 and $28 ms^{-1}$. Again, both $20kyr$ and $40kyr$ forcing periods were considered. The forcing velocity, $\overline{U}_f$, was held fixed at $5 ms^{-1}$.

The thermal wind relation (Equation (3.8)) means the vertical wind shear is propor-

tional to the meridional temperature gradient. The forcing we use therefore implies a change in $\overline{T}_y$ of $\pm 1.65^o C/1000km$. Because of this relationship, changing the shear also changes the zonal mean temperature at different latitudes, but the temperature at one point can be kept fixed. The point of varying the shear is to look at changes to the stationary wave pattern, so we would like the zonal mean temperature at the margin to change as little as possible. The temperature at $45N$ was kept fixed. Consequently, the direct temperature forcing at the margin is at most $\pm 1.5^o C$.

Figure 5.18 shows the periodic oscillations, for the last $200kyr$ of a $300kyr$ integration. The longer integration was needed for the oscillation to come to equilibrium with the forcing. The variations in the ice sheet are much smaller than for the direct temperature forcing. For the $40kyr$ forcing, the area and volume both oscillate by $\sim \pm 3\%$, and the maximum surface height by $\sim \pm 1\%$. As for the direct temperature forcing, the $20kyr$ and $40kyr$ periods produce different means and amplitudes. The sequence of contour plots, Figure 5.19, shows that the main difference in the ice sheet occurs on the southeastern edge, which extends during periods of high shear and retreats during periods of weak shear. The significant effect of the varying vertical wind shear for the ice sheet is that stronger shear produces increased cooling over the southeast, allowing ice to accumulate there. As the shear weakens the climate is warmed locally there and the ice retreats. The pattern in the volume is the same as for the periodic temperature forcing: the volume increases when the area is either increasing or stays high and, with a slight phase lag, it decreases sharply when the area decreases.

5.6.3 Varying background stationary wave

The changes associated with periodic variations in the background stationary wave are very minor. To create these variations, the height of the topography forcing the background stationary wave introduced in Section 5.3 was varied (rather unphysically) between 0 and $2km$, again with periods of 20 and $40kyr$. Figure 5.20 shows the time series for the ice sheet response. The last $200kyr$ of a $300kyr$ integration is shown. The ice sheet has not yet come into equilibrium with the periodic forcing, so there is still a slight linear trend in the fields.

The amplitudes of oscillations in all fields are all about $\pm 1\%$. The background stationary wave was shown to have only a small effect on the equilibrium ice sheet size

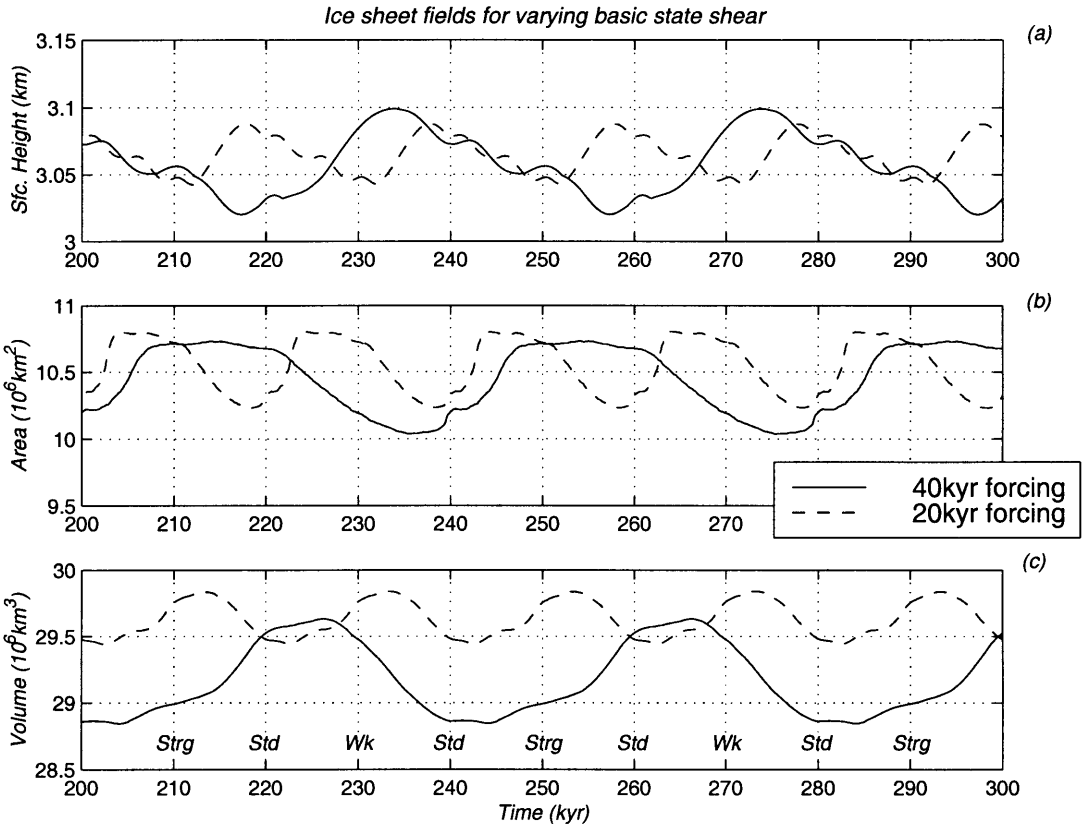

Figure 5.18: Time series of ice sheet fields for sinusoidal $20kyr$ and $40kyr$ forcings on basic state wind shear. Panels are as for Figure 5.16. The last $200kyr$ of a $300kyr$ run are plotted. The text at the bottom of (c) gives the phase of the $40kyr$ forcing. At points marked $Strg$ (Wk) The shear is $0.5 \times 10^{-3} s^{-1}$ greater (smaller) than the standard basic state (Std).

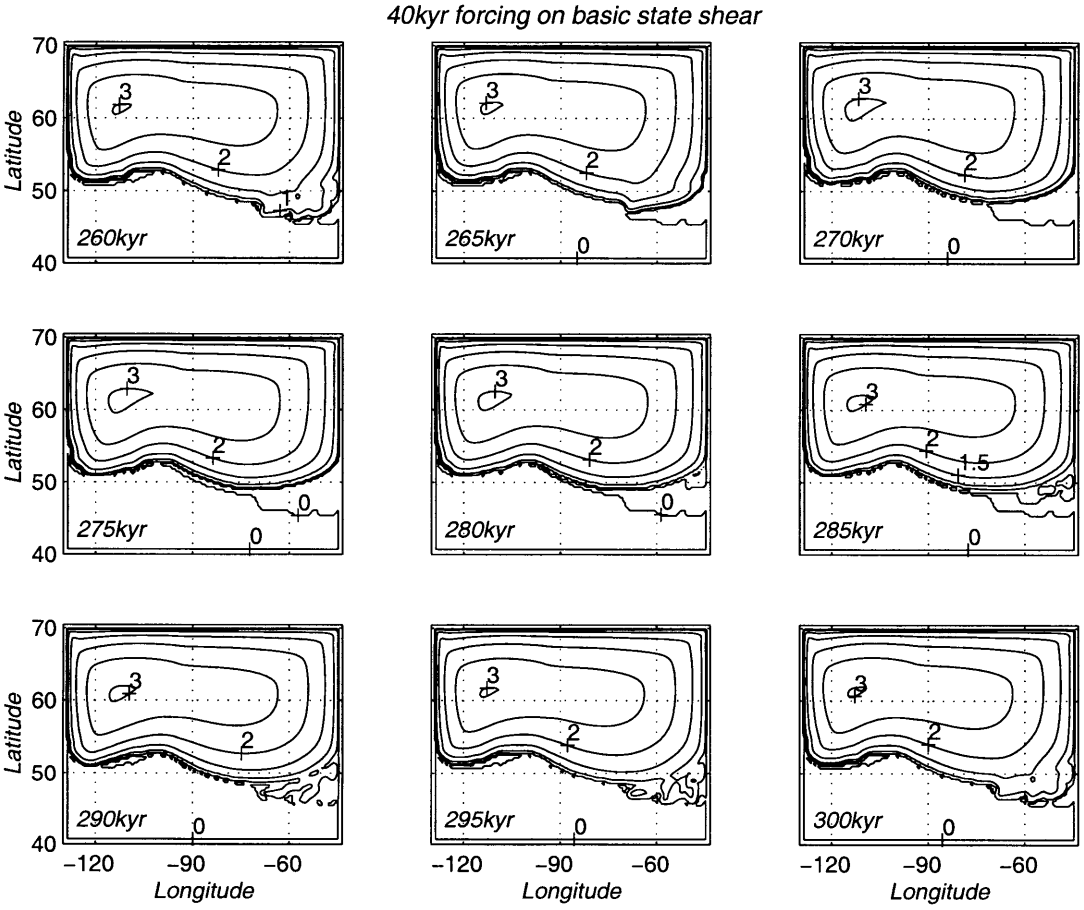

Figure 5.19: Time sequence for one cycle of the $40kyr$ sinusoidal forcing of the basic state wind shear. Refer to Figure 5.18 for the phase and magnitude of the forcing. Contours every $0.5km$. Most of the changes occur on the south eastern slopes. In front the retreating ice sheet the bedrock is often below the $z = 0$ level.

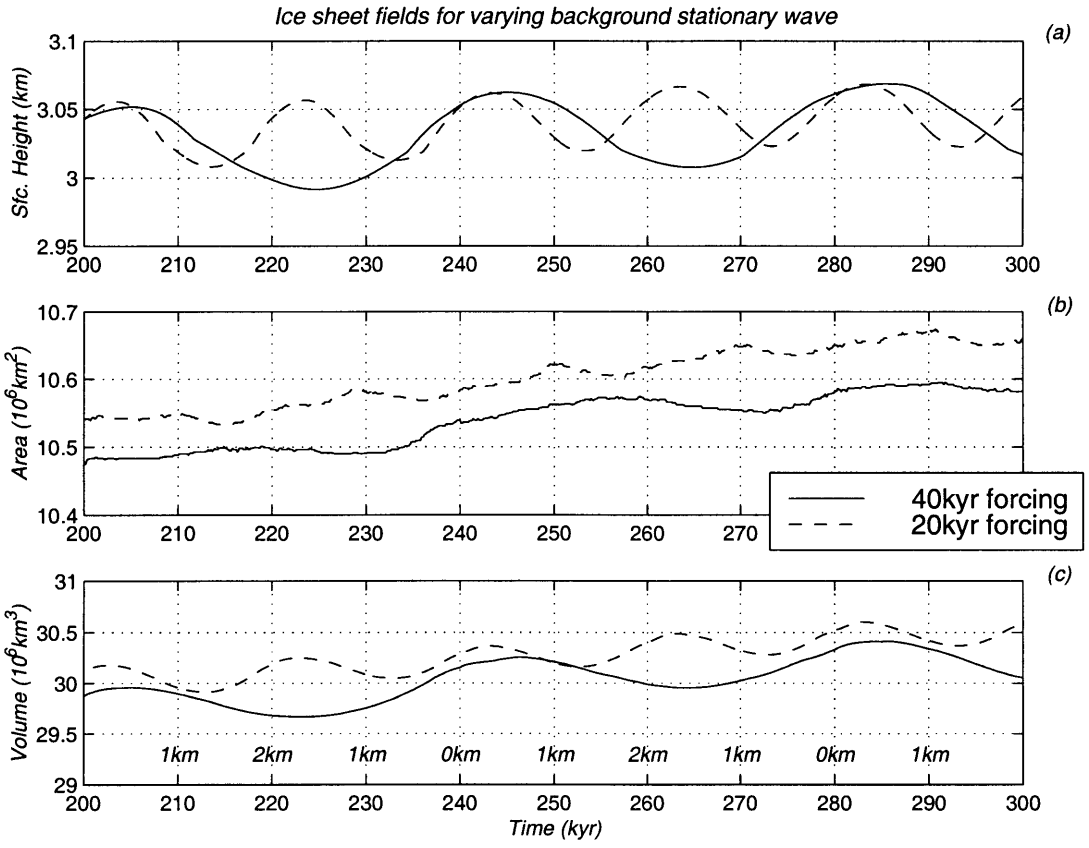

Figure 5.20: Time series of ice sheet fields for sinusoidal $20kyr$ and $40kyr$ forcings of the background stationary wave. Panels are as for Figure 5.16. The last $200kyr$ of a $300kyr$ integration are plotted. The text at the bottom of (c) gives the phase of the $40kyr$ forcing. The height of the topography forcing the background stationary wave is indicated. See text for details.

in Section 5.3. This fact, and the long equilibration time compared to the period of the forcing means we should have expected that the fractional changes in all of the ice sheet fields would be small. The background stationary wave creates a temperature perturbation at the margin of 2.5^oC at most (Figure 5.10). The total range for the direct temperature forcing was 10^oC, which also applied acros the whole ice sheet. It seems that the background stationary wave (and variations to it during glacial climates) would have to be similarly large to have a significant effect on the shape of the ice sheet over orbital time scales. We show in Chapter 6 that while the stationary wave due to the Tibetan Plateau is unlikely to have exerted such a large effect over the Laurentide ice sheet, the Laurentide itself may have created a stationary wave with sufficient amplitude downstream to have influenced the evolution of the Fennoscandian.

5.6.4 Ice sheet response to beating of precessional frequencies

It is often proposed that a likely explanation for the dominant $100kyr$ cycle in the ice ages of the last $850kyr$ is that the climate system responds to the beating between the two main frequencies ($19kyr$ and $23kyr$) in the precessional component of the insolation. The beat frequency of these two components is $109kyr$. Since the ice sheet evolution is nonlinear, we expect that some of the power in the beat envelope will be picked up by the ice sheet. The question is whether it might dominate the response. The model in this thesis was not developed with the purpose of simulating the $100kyr$ cycle, and as a result does not have some of the physics often invoked to create rapid ice sheet decay (calving into pro-glacial lakes, dust loading, snow ageing, basal melting etc.). Nonetheless we can look at how it responds to forcing by two component frequencies which combined have a much longer beat frequency. Starting from the ice sheet in Figure 5.7 a $\pm 5^oC$ forcing was imposed on the teperature at periods of $19kyr$ and $23kyr$. Figure 5.21 shows the ice sheet response over a run of $300kyr$. It can been seen that the ice sheet's area and volume responds in a weakly nonlinear way: the amplitude of their response is closely related to the amplitude of the forcing. Individual cycles have the same shape as those in Figure 5.16. On a time scale of $20kyr$ and in a growth phase of the cycle, the ice area is governed by where the climate cooling is sufficient to allow year-round snow. In the decay phase, it is determined by whether the warming is enough to overcome the ice sheet's elevation. The volume lags the ice sheet area as in Section 5.6.1. Where there is increased ice cover, snow can accumulate.

The maximum ice sheet height responds quite differently however. Its response is dominated by roughly $100kyr$ variability, and suggests that different processes govern its response.The maximum height occurs in the interior of the ice sheet, and as such it is controlled both by accumulation there, and by the interiors response to what is happening at the margin. Figure 5.21 shows that when the ice margin is not oscillating rapidly (quiescent forcing), the height can gradually increase. During high forcing however, the margin fluctuates greatly and as a result the ice interior gradually subsides—every time the margin extends, the interior height is pulled down a little but more. The response of the maximum height here contrasts with that in Figure 5.16, where the forcing was a pure sinusoid. That case produced a response with the same periodicity as the forcing. It is thus the interaction between the different forcing periods that generates the longer frequencies in the response here.

The behavior of the ice sheet height illustrates that nonlinearities will tend to extract power from a modulating envelope, and also that different aspects of the system can respond at different periods. The deep sea cores record ice volume though, which in this model responds quasi-linearly to the forcing. The main possible way in which the ice sheet height can contribute to the flow is via the thermomechanical behavior of the ice. Frictional heating within the ice is proportional to the stress, and the stress increases with increasing ice depth. If the frictional heating became sufficient to produce a temperate base where it had been frozen before, then the ice dynamics might be dramatically affected. It is not clear without modeling the heating whether it would be suffient to melt the base, or how the phase of the change would be related to the observed ice volume.

Summary

This chapter has presented some of the main results of this thesis. We have shown that a powerful feedback operates when the presence of an ice sheet influences the atmospheric circulation. The interaction between the ice sheet and the atmosphere is mediated via two main processes. First, changes in atmospheric circulation alter the prevailing winds. This then changes the time-mean temperature patterns, altering where ice melts during the summer season. The circulation is such that northerlies extend over most of the ice sheet, bringing colder temperatures than would otherwise exist over the

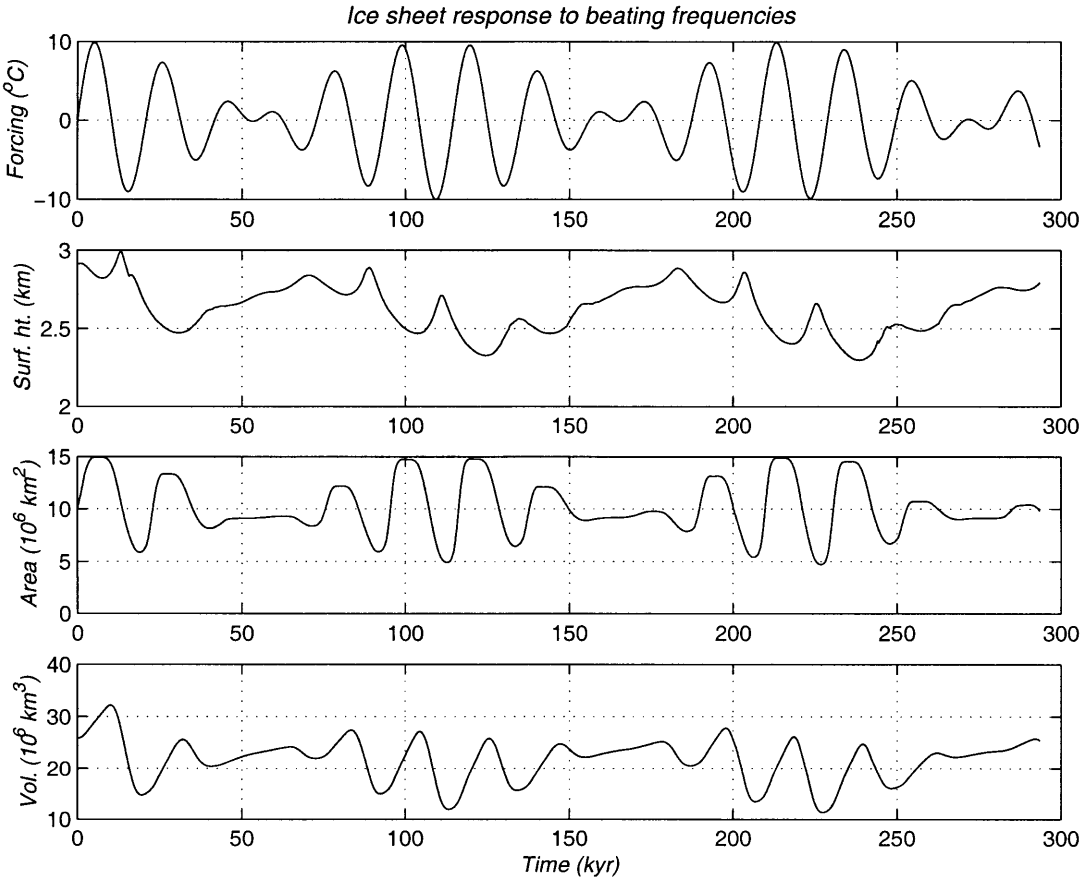

Figure 5.21: Forcing and response of ice sheet to forcing of basic state temperature using calculated precessional frequencies, for a $300kyr$ model integration. (a) the frocing is the sum of two sinusoids with periods of $19kyr$ and $23kyr$, (b) maximum surface height (km), (c) ice sheet area ($10^6 km^2$), and (d) ice sheet volume ($10^6 km^3$).

eastern slopes. Secondly, precipitation is focussed on the upwind slopes on the western flank of an ice sheet. This high accumulation leads to a strong southward mass flux pushing the ice to lower latitudes. Also, accumulation rates are strongly reduced by extended areas of prevailing downslope winds. In combination these two processes act to create the final configuration of the ice sheet. Exactly what that configuration is depends on the relative strength of the feedbacks, which in turn depends on our model parameterizations. The mechanism of the interaction is however robust to a reasonable range of parameters and atmospheric basic states.

These processes also affect the time evolution of the ice sheet. For an ice sheet initiating on a small plateau, the early growth is dominated by the upslope precipitation which pushes the ice westwards. Once the ice sheet has reached sufficient size to create a sizable change in the atmospheric circulation, further growth of the ice is controlled mainly by climate cooling and changes in the temperature patterns caused by the stationary waves.

If a sudden warming is imposed on the ice sheet, then the feedbacks act to change the decay rate of the ice sheet. The amount of the change is however less than that suggested by the results in Chapter 2, largely because of the long response time for ice in the interior to react to changes at the margin, where the feedbacks are most effective.

We also considered periodic forcing to the climate basic state on time scales appropriate to the earth's orbital variations. Direct forcing of the temperature has the largest effect. The saw-tooth shaped response to sinusoidal variation of the basic state temperature is due to the differences between melting and accumulation rates over the ice sheet. For a land based ice sheet, and for reasonable variations in the temperature, the controlling factor for its growth or decay is whether the temperatures permit year-round accumulation of snow or not. Periodic variations in the atmospheric vertical wind shear created only small changes to the overall ice sheet, but changed some local details on the southeastern flanks. Oscillations in the background stationary wave we chose had very little impact on the ice sheet. The ice area and volume respond quasi-linearly to forcing at realistic precessional frequencies. The maximum height responds to the beat frequency, which is close to $100kyr$.

The stationary wave model we are using is a very simple one and the scalings used in the linear and quasigeostrophic scalings cannot be rigorously justified for the high, steep-sided plateaus appropriate to ice sheets. The shape of the ice sheet is however

determined more by the large scale atmospheric response (i.e. prevailing northerlies over most of the ice sheet), than by details of the flow around the margins. We can have some confidence in the large scale response. The model produces a plausible looking stationary wave of roughly the right size and phase, as judged both by observations in the current climate (Figure 1.4) and from GCM simulations. This was considered in more detail in Chapter 3.

The precipitation is more uncertain. Much of the coastal accumulation over Antarctica is generated by weather systems impinging on the sides of the ice sheet and being deflected around the steep sides (Bromwich, 1988), rather than being forced over the ice sheet as is assumed in this model's parameterization. This would reduce the average rate of convergence of water vapor in the air column and reduce the upslope precipitation maxima. Runs in which this reduction was imposed did not significantly change the final equilibrium shape of the ice sheet because the local precipitation maximum on the western flank forms ice which quickly flows into the ocean. However, the rate of the westward propagation of the ice sheet initiated on the small plateau does depend on the precipitation maximum allowed in the model. A more complete precipitation parameterization ought therefore to include an accounting for the possibility of storms being at least partially deflected around the ice sheet.

Chapter 6

Application to Pleistocene climates

The results up to this point have only been for an idealized geography. This chapter tries to establish the extent to which the conclusions from earlier chapters can be applied to the real climate system, especially as relating to full glacial climates and glacial inception. The chapter is organized into two distinct halves. The first half looks at the stationary waves produced in the channel model using the current topography and also the reconstructed topography of the Last Glacial Maximum (LGM). We will show, in agreement with other work, that the atmospheric response to the Tibetan Plateau is much more global in extent than the response to the Rockies: some part of the stationary wave over North America is due to the Tibetan Plateau, whereas almost none of the response over Tibet is due to the Rockies. The global scale of the Tibetan Plateau stationary wave means that there is the potential that changes to it will affect remote climates. Within the limitations of the stationary wave model we can say that it is possible that the Tibetan Plateau may have played a role in the initiation of the Laurentide, and that once established the Laurentide was the dominant source of planetary scale stationary waves.

The second half focuses on the evolution of ice sheets over the North America. It explores how the feedbacks between the ice sheet and the atmosphere, demonstrated in earlier chapters, behave for the actual coastline and surface elevation of North America. In particular we find that the observed lack of ice over Alaska and the extension of ice over New England at the LGM may be attributable to the interaction of the ice sheet with the atmospheric stationary waves.

6.1 Stationary waves for interglacial topography

The topography of the northern hemisphere is currently dominated by the Tibetan Plateau in the east and the Rockies in the west. This is also true of all of the interglacial climates during the Pleistocene. The only significant changes to the earth's topography over this period have come from the waxing and waning of the great continental ice sheets. The current topography can thus be used to explore how the stationary waves might have varied during interglacial climates. This also leads to the question of whether these variations might have affected where and when the ice sheets nucleated.

First, we compare the current observed stationary wave pattern with that obtained by forcing the stationary wave model of Chapter 3 with the current northern hemisphere topography. The results presented below concentrate on the east-west differences in the stationary wave perturbation fields. The measure used for this is the range, defined as the maximum minus the minimum of the perturbation field in the region of interest. Observations of the current winter climate (Figure 1.3) show that the high-low pattern straddling the Tibetan Plateau has a total range of about $250gpm$ at $500mb$. Over the Rockies, on the other hand, the range is slightly larger — about $300gpm$. The geopotential heights have a much tighter structure over the Tibetan Plateau than over the Rockies, caused by the smaller scale of the Tibetan Plateau (Figure 1.1b). The range of the temperature perturbations (lower panel of Figure 1.4) is about the same over the two mountain complexes (a little over 10^oC). It should also be kept in mind that Figure 1.4 is a January average, and so there is also a direct thermally forced component to zonal temperature perturbations.

Figure 6.1 shows the response of the stationary wave model to the current northern hemisphere topography. The model has the standard basic state and parameters from Chapter 3, with the exception that the 0^oC isotherm was taken to lie at $70N$. The topography is taken from the present day $1^o \times 1^o$ data set of Peltier (1994). The model produces a stationary wave pattern which has similar large scale features to observations, but there are some important differences. The range of the high-low pattern in the model is equivalent to about $300gpm$ at $500mb$ over Tibet, compared to $250gpm$ over the Rockies — the reverse of the observations. In the channel model the lack of meridional variation in the basic state means the jet impinges directly on the Tibetan Plateau rather than only over the northern flank of the plateau, as in reality. This might account in

part for the reversal in the relative amplitudes between model and observations, but there are also many other likely contributing factors, such as the assumption of linearity and the omission of thermal forcing in the model.

Another notable difference is the pattern of propagation away from the Rockies. In observations, the temperature pattern downstream of the Rockies lies along an axis running east-northeast (Figure 1.4), whereas the modeled pattern apparently propagates east-southeast. This difference in the model response is either due to the absence of thermal forcing which, if included, would lead to a superposition of different wave-trains, or it is due to different downstream propagation characteristics owing to the simplified model basic state and the channel geometry.

Even given these differences, Figure 6.1 shows that the model produces a qualitatively correct picture of the global stationary wave pattern, despite the simplifying model assumptions and the neglection of thermal forcing. The fact that the model reproduces about the right amplitude for the stationary wave is essentially an artifact of a tuned parameter set. As reviewed in Chapter 1, different researchers have come to different conclusions about the relative contributions of thermal and topographic forcing to the total observed response. The modeling ambiguity arises out of the fact that most of the thermal response is due to the release of latent heat in the interior of the atmosphere. In midlatitudes the largest contribution to this forcing comes from within the atmospheric storm tracks and its effect is such that the patterns due to topographic and thermal forcing tend to overlay each other. In trying to reproduce the observations using a stationary wave model which neglects thermal forcing, it might be argued that we are implicitly including the contribution from latent heating in storm tracks. We are however neglecting the feedbacks which might change the relationship between the responses to the two forcings in a changed climate state.

6.1.1 Separation of topography into eastern and western hemispheres

It is useful to consider the atmospheric response to each of the major mountain complexes separately. Since it is only the Rockies in the western hemisphere, and the Tibetan Plateau in the eastern, which contribute significantly to the global stationary wave pattern, we can examine their respective effects by splitting the northern hemi-

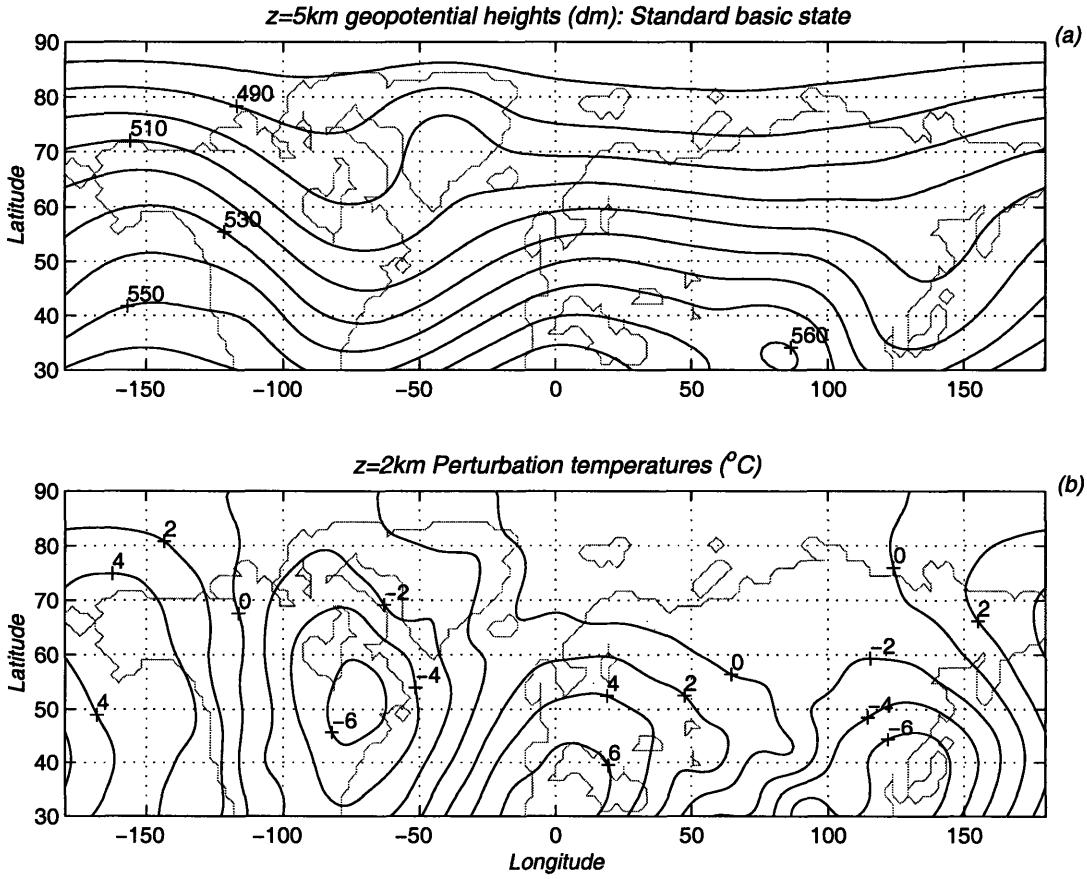

Figure 6.1: Stationary wave model output for current topography and standard basic state. (a) $z = 5km$ geopotential heights (dm), and (b) $z = 2km$ perturbation temperatures (^oC).

sphere topography into western and eastern halves. In Chapter 5 the results suggested that the main effect on the ice sheet evolution is via the stationary wave temperatures. Therefore the results in this section are presented using the $z = 1km$ temperatures. Given both the simplicity of our model and the uncertainty about the appropriate basic state for the atmosphere, we need to consider the range of phases and amplitudes of the atmospheric response that might be possible during a transition to glaciation, and also during a full glacial climate. Therefore we will show the response for a range of atmospheric basic states. As in Chapter 5, the strong and weak basic states in the results below are the same as the winter and summer basic states, respectively, introduced in Chapter 4.

Concentrating on the response over North America, the Tibetan Plateau alone generates a high-low pattern with a total range of roughly $150gpm$ at $500mb$ (not shown). Associated with this circulation are cold perturbation temperatures extending across most of North America (Figure 6.2). The Rockies alone (western topography) generate a local pattern which is quite similar to this (Figure 6.3), though it is of slightly shorter scale (i.e. noisier). Since we are considering a region close to the Rockies, the response to the small scale details has not yet dissipated. Damping acts most strongly on shorter scales, and it is only downstream of the topography that the larger scales come to dominate the atmospheric response. The range of the induced temperature perturbations over North America due to the western and eastern topography are approximately equal (about 5^oC for the standard basic state), but maximize in slightly different locations.

6.1.2 Initiation of the Laurentide

Using the current topography, we can also consider the question of whether the stationary waves in the atmosphere can play a role in the nucleation of ice sheets. GCM simulations of the last interglacial using the appropriate orbital configuration have had some difficulty in reproducing the start of glaciation (e.g. Phillipps and Held, 1994; Dong and Valdes, 1995). If plausible changes to the atmospheric basic state change the stationary wave significantly, then are the temperatures, either locally or remotely from the source, affected such that nucleation at any given location is more or less likely? Based on the results of Chapter 5 we can assume that changes in the wind fields associated with stationary waves are unlikely to affect nucleation. We expect therefore

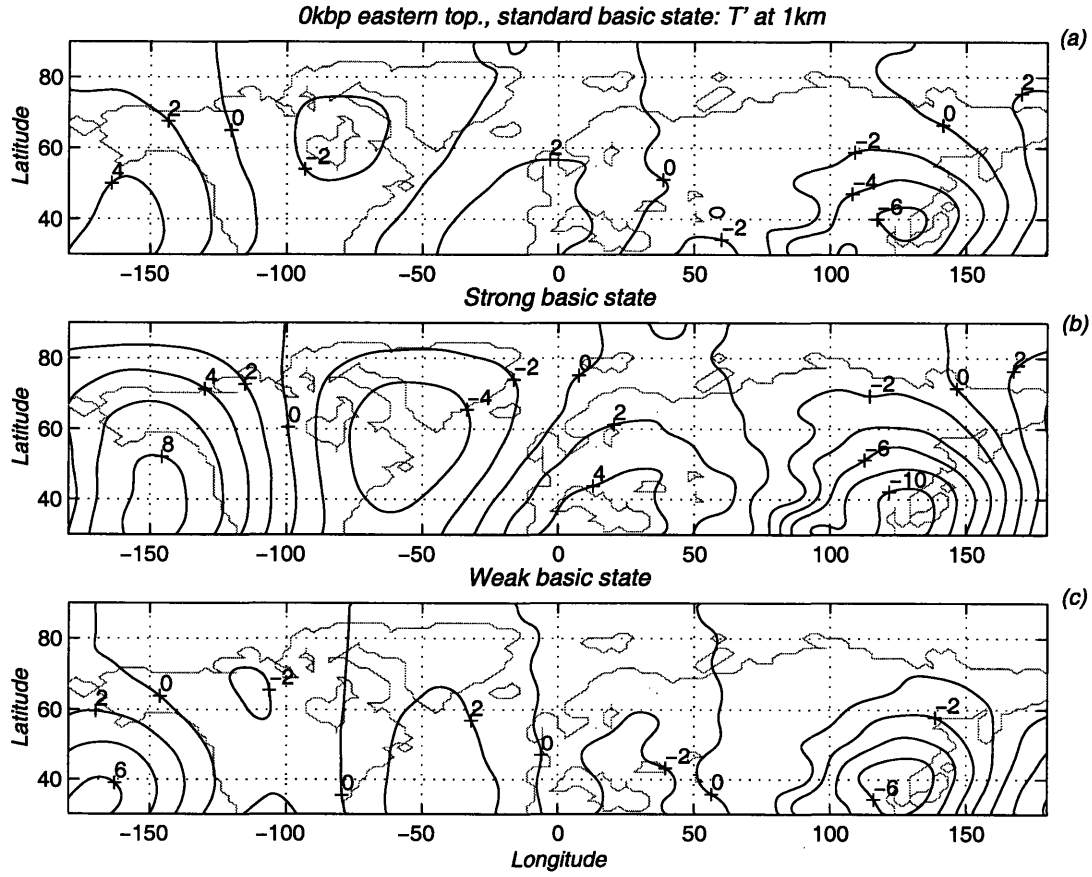

Figure 6.2: Stationary wave model output for current eastern topography only using different basic states. Fields are the $1km$ temperature perturbation. (a) standard basic state, (b) strong basic state, and (c) weak basic state.

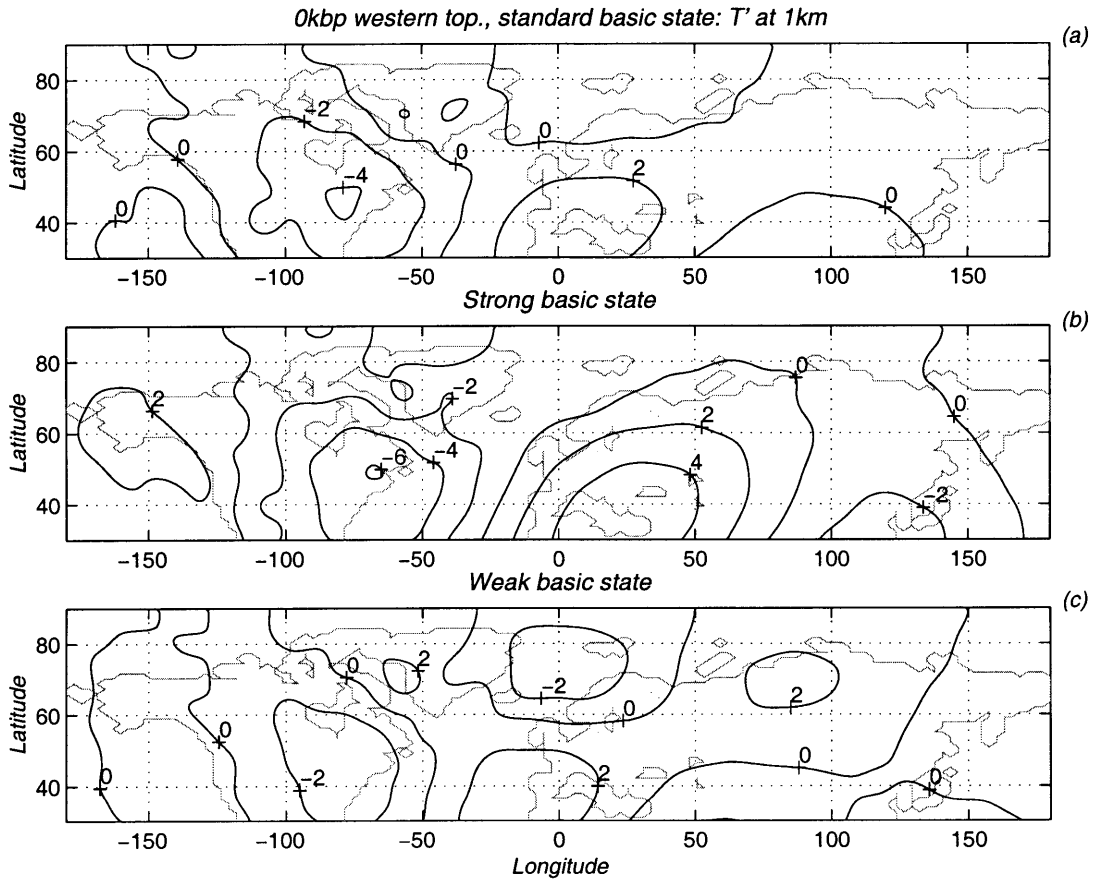

Figure 6.3: As for Figure 6.2 but for current western topography only.

that the crucial factor in determining whether an ice sheet nucleates or not is whether there is any significant melting during the summer.

Geological evidence suggests that the Laurentide first initiated over Keewatin, Quebec, and Baffin island just after 120 kbp (Clark et al., 1993). Despite being at a similar latitude (and with similar surface elevation), the western portions of the Laurentide did not come into being until after 100kbp. This suggests that there was a strong east–west gradient in the summer temperatures across North America at these latitudes. That is, year-round snow cover was possible in the east, but not in the west. It is interesting to ask whether the topographically forced stationary waves could have contributed to this pattern. We consider a range of atmospheric basic states (which is equivalent to the forcing climate in our model), because if an interglacial climate persists for $20kyr$, the climate experiences a full precessional cycle in insolation forcing and the climate is likely to change as a result. This means that glacial inception at any given location may occur preferentially at different phases of the orbital forcing. Since we are concerned with interglacial summer climates in the Pleistocene, where the zonal mean baroclinicity is likely not very different from today's values, we will concentrate on a range of basic states bounded by the weak and standard basic states already introduced.

There are two sources of topographic stationary waves to consider. The first is the Rockies, generating a local response. Figure 6.3a and Figure 6.3c show that that there is a cooling in the lee of the Rockies of about 3^oC relative to the upwind side, and centered over Hudson Bay. The shape of the response does not change between Figures 6.3a and 6.3c because we are looking at a region local to the source. The Rockies therefore create a temperature pattern consistent with initiation in the east and moreover we do not expect this pattern to change much over an orbital cycle. The second source is the Tibetan Plateau. As already noted, the summer stationary wave pattern is sharply diminished compared to winter because the summer subtropical jet moves northwards away from the plateau. Nonetheless, we don't want to exclude the possibility a different orbital configuration might put the subtropical jet closer to the Plateau. Figure 6.2a is probably an upper bound on the possible amplitude of the summer response. The phase of the response over North America is uncertain because it is so remote from the source, but Figure 6.2a suggests that there is the potential for the Tibet Plateau to supply an east–west temperature difference of up to 4^oC, which would vary over an orbital cycle.

Our simple model cannot fully answer the question of glacial inception, but it does

suggest that the role of the stationary waves (and their variation) should be accounted for in a more complete treatment of the issue.

6.2 Stationary waves for LGM topography

The topography appropriate to the LGM has been reconstructed by Peltier (1994). We separate this LGM topography into western and eastern halves and the examine the atmospheric response using the same basic states as in Section 6.1. This isolates the stationary waves due to the Laurentide, the Fennoscandian and the Tibetan Plateau. Figure 6.4 shows the $z = 0$ geopotential heights for the total, western and eastern topography. A perturbation of $10gpm$ is equivalent to a perturbation in the mean sea level pressure (*pmsl*) of about $1mb$. For the standard basic state, the perturbation ϕ' over the Laurentide has a maximum value of $150gpm$ (Figure 6.4a), equivalent to a total *pmsl* of about $1030mb$. This is about the same as most GCM simulations of the LGM (e.g. Manabe and Broccoli, 1985; Kutzbach and Guetter, 1986), but there is some disagreement between the GCMs about the exact location of the surface high over the ice sheet. A difference from the present work is that these GCM simulations used the CLIMAP reconstruction (CLIMAP project members, 1976) for the Laurentide which gives somewhat larger ice sheets.

Contrasting Figure 6.4b and Figure 6.4c shows that the Laurentide ice sheet was the largest source of stationary waves on the planet. Compared to the Tibetan Plateau, the larger spatial scale of the Laurentide projects onto wavenumbers with a larger response. In summer the dominance is likely more marked than it is in our channel model simulations, since in today's climate at least, the jet moves away northwards from the Tibetan plateau in summer, whereas as the Laurentide would have sat year-round in the middle of the westerlies.

Figures 6.5 and 6.6 are the equivalent of Figures 6.2 and 6.3, but for $21kbp$. We again consider the stationary wave response for the same range of atmospheric basic states. We focus first on the effect of the Laurentide (Figure 6.6). Taking the standard basic state results, temperatures are warmed by 3^oC over Alaska, and cooled by 10^oC over Hudson Bay. Note that this local effect is much larger than the (remote) effect due to the Tibetan Plateau (Figure 6.2) over the same region. Cook and Held (1988) show

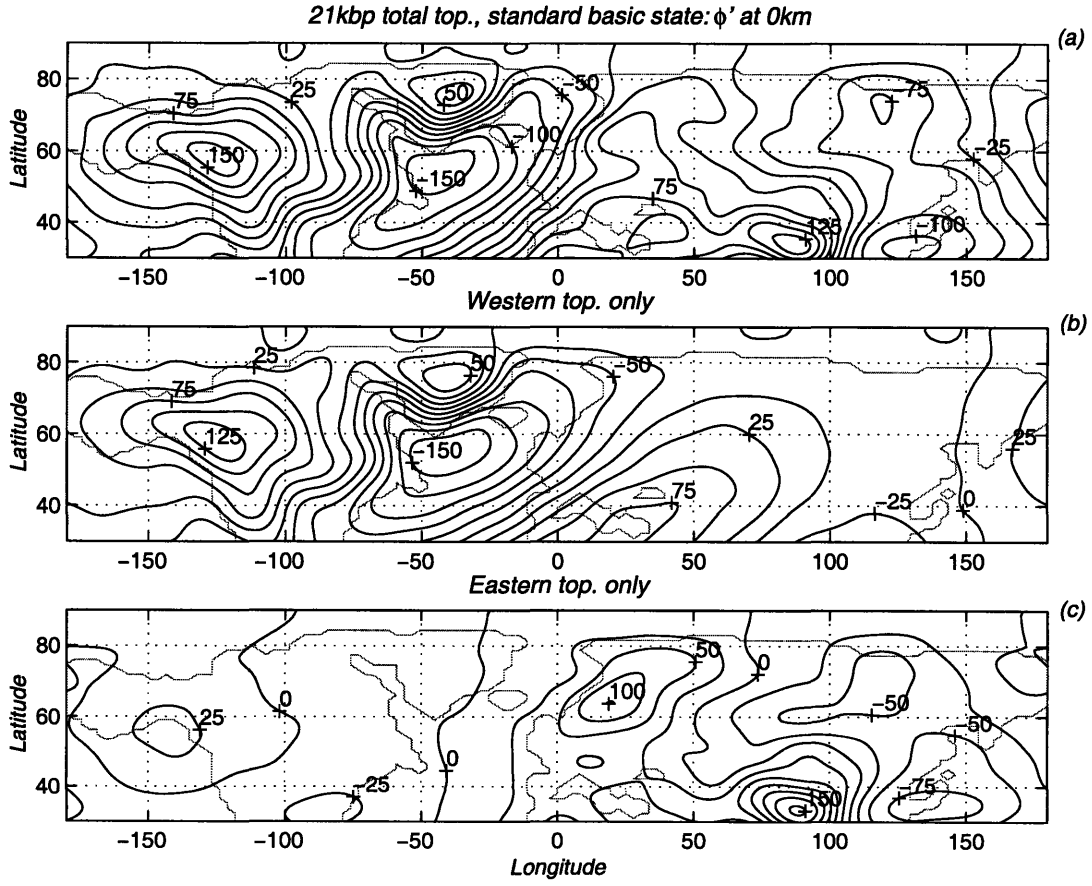

Figure 6.4: $z = 0$ geopotential heights produced by $21kbp$ topography. Standard basic state used. (a) total topography, (b) western topography only, (c) eastern topography only. A value of $10gpm$ is equivalent to $1mb$.

the temperature fields from their GCM simulation (using the CLIMAP reconstructed topography). Their cold temperature perturbation in the lee of the ice sheet is a little bigger, but their results show a significantly larger warm temperature perturbation to the west (up to 10^oC warming over the central Laurentide in their linearized simulation).

It is also notable that the largest perturbation temperatures caused by the Laurentide occur downstream. This means a very strong warming over northern Europe. Depending on the atmospheric basic state used, the location of the maximum temperature varies by about 40^o of longitude, but the qualitative effect is robust. In the case of the standard basic state the warming is equal to between 4^oC and 8^oC over northwestern Europe. This warming would tend to inhibit the southward growth of the Fennoscandian and might partially account for the fact that the Fennoscandian only penetrated down to about $55N$ whereas the Laurentide existed as far south as $40N$.

Figure 6.5 shows the effect of $21kbp$ eastern topography only. The difference between Figures 6.5 and 6.2 is due solely to the presence of the Fennoscandian. The Fennoscandian was smaller than the Laurentide in both height and extent and so the atmospheric response to its presence is correspondingly less. Locally, the Fennoscandian creates a warm-cold temperature pattern with a total range of $\sim 4^oC$. Note that this is smaller than the 4 to 8^oC warming over the region that the model suggests resulted from the presence of the Laurentide 3000 miles to the west. Conversely, the effect of the stationary wave induced by the Fennoscandian over North America is negligible.

The results of this section demonstrate that the stationary wave pattern in the northern hemisphere during the last glacial maximum was dominated by the presence of the Laurentide ice sheet. Our LGM results indicate that the induced stationary wave was larger than that due to the Tibetan Plateau. The Laurentide results in large warm temperature perturbations over Europe, creating a strong constraint on the southward extension of the Fennoscandian. The perturbation temperatures due to the Laurentide are larger than those due to the Fennoscandian, even over the Fennoscandian itself.

The results also suggest that the variation in radiative forcing over a Milankovitch cycle would result in a varying atmospheric response remote from the Tibetan Plateau and that the stationary waves might play a significant role in preconditioning different locations for glacial inception.

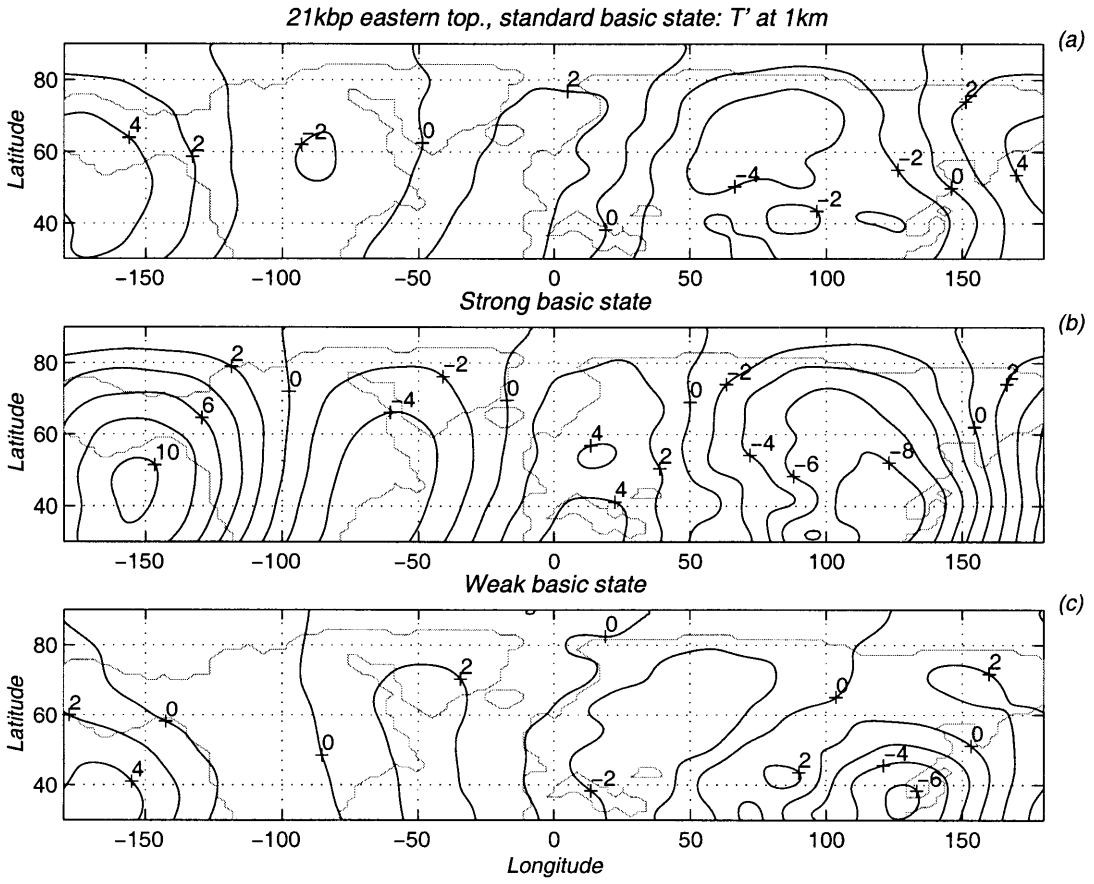

Figure 6.5: As for Figure 6.2 but for $21kbp$ eastern topography only.

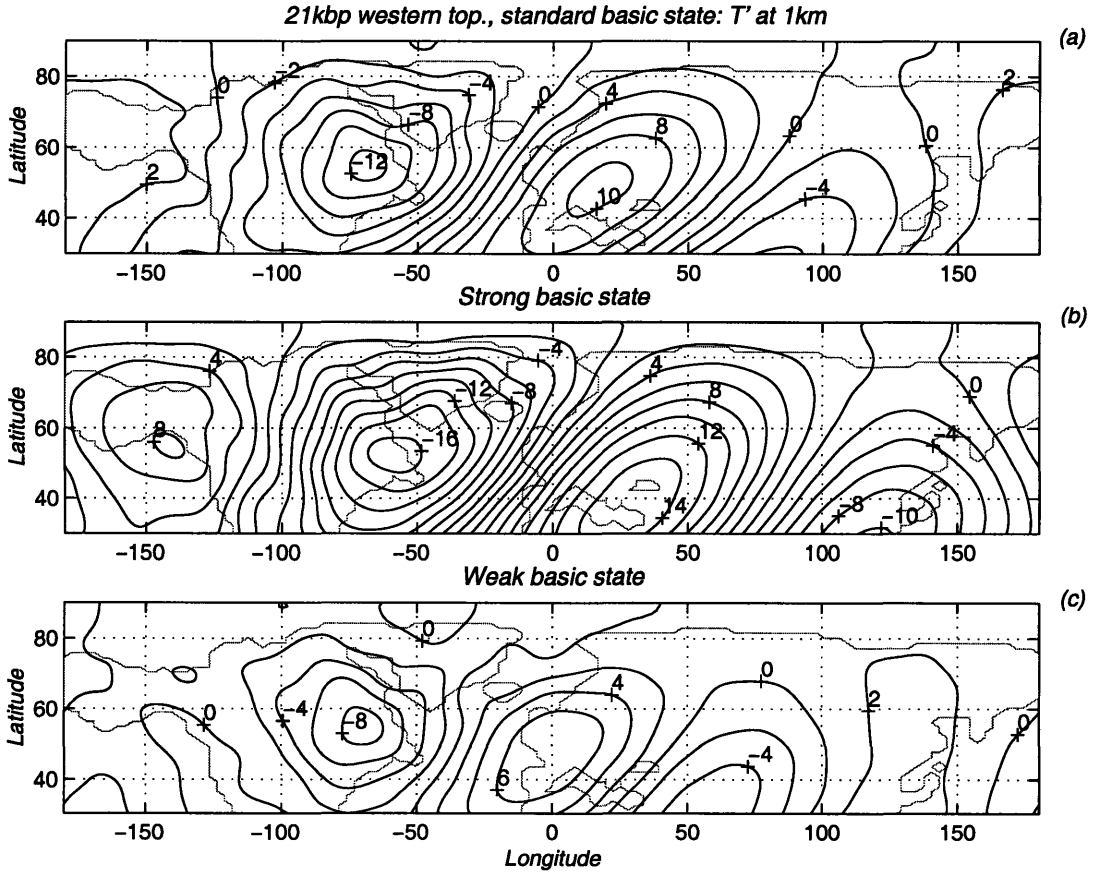

Figure 6.6: As for Figure 6.2 but for $21kbp$ western topography only.

6.3 Evolution of North American ice sheets

Chapter 5 presented integrations of the ice sheet model on a flat, rectangular continent in order to isolate the interaction between an ice sheet and the atmosphere. This left out an important factor in the configuration of an ice sheet—the geography of the continent upon which it sits. Coastal outlines delimit an ice sheet's margin and also affect the internal ice flow, which must accommodate the large mass divergence which calving into the ocean produces. Surface elevation is also important: the ice surface over Greenland partly reflects the features of the bedrock topography underneath (e.g. Calov and Hutter, 1996)

In the model integrations below, we use North America (with some minor, convenient modifications) as a template. There are two reasons for choosing North America rather than Eurasia. First the Laurentide was the largest body of ice in the northern hemisphere at the LGM, and some of its main features remain to be explained. One of these is that despite being 20^o north of New England where there was ice cover, Alaska remained largely ice free at the LGM. It has been suggested this might have been due to the variable topography in Alaska (e.g. Dong and Valdes, 1997), or the advection of heat from the warm waters of the Kuroshio current (Peltier and Marshall, 1995). Neither of these mechanisms has been successfully isolated and modeled. Fabre et al. (1997) took temperatures and accumulation patterns from a GCM, run to equilibrium under LGM boundary conditions and insolation values. They treated the LGM simulation minus the $0kbp$ simulation as a perturbation to the current observed climate, and used the resulting fields as input for an ice sheet model for the Northern hemisphere. The ice sheet which resulted did not extend over Alaska. However, it was not diagnosed whether this was a consequence of low accumulation or high melting in their GCM output. Another problem is that Laurentide simulations tend not to produce a sufficiently far southward extension of ice over New England (Tarasov and Peltier, 1997). This would suggest that the climate (and in particular, summer temperatures) produced by the models is too zonal, and we want to see what role the topographic stationary waves play in the zonal asymmetry. The second reason for choosing North America is that the results from the first half of this chapter suggest that once established, the Laurentide itself was the dominant source of stationary waves over North America, whereas the pattern over the Fennoscandian was likely a complicated superposition from different sources.

The pattern of temperatures suggested by the Laurentide margins (i.e. no ice in Alaska, extension over New England) is suggestive of that produced by a topographic stationary wave. This section explores the extent to which the coupled ice-sheet/stationary-wave model can explain the shape of the Laurentide. The results presented should be regarded as an exercise in the tuning of the model parameters, but we discuss the robustness of the response and the effects of the parameterizations we have chosen.

The ice sheet model had to be adapted to look at the North American continent. Computational limitations required that the grid size be increased from $40km$ to $60km$. Figure 6.7 shows the bedrock topography used which was taken from the data set of Peltier (1994). The ice sheet is allowed to develop within a 'mask' indicated in Figure 6.7. This mask is taken from a combination of the northern outline of the Laurentide from simulations by Tarasov and Peltier (1994), and the current coastline elsewhere. In the following model integrations we do not account for changing global sea level. This means that using the current topography leaves some areas within the mask below sea level, especially in the northeast of Canada, where it is known to have been glaciated at the LGM. Where this occurs, the height of the bedrock is reset at $10m$. This involves an adjustment of $200m$ at most (in central Hudson Bay), and generally much less. It is smaller therefore than the depth of any ice sheet over the area. We also need a western boundary for our ice sheet model, and we use the modern coastline of Alaska even though there was a land bridge between Alaska and Asia at the LGM. In addition, some changes were made to the standard basic state climate. The latitude of the annually averaged 0^oC isotherm of the basic state climate was shifted from $45N$ to $52N$. The $z = 0$ basic state wind was reduced from $3ms^{-1}$ to $0ms^{-1}$, and the basic state shear was increased from $2.0ms^{-1}$ to $2.8ms^{-1}$. This gives a $10km$ jet strength of $28ms^{-1}$ and a meridional temperature gradient of $-9.2^oC/1000km$. These changes were made to tune the climate forcing for the stationary wave response. The reasons for this will be explained in detail below. Lastly, the assumed amplitude of the annual temperature cycle, which was made latitude dependent only for ease of comparison in Chapter 4, was instead set to a constant value of 10^oC. Otherwise all parameters are kept at the same standard values stated in Chapters 3 and 4.

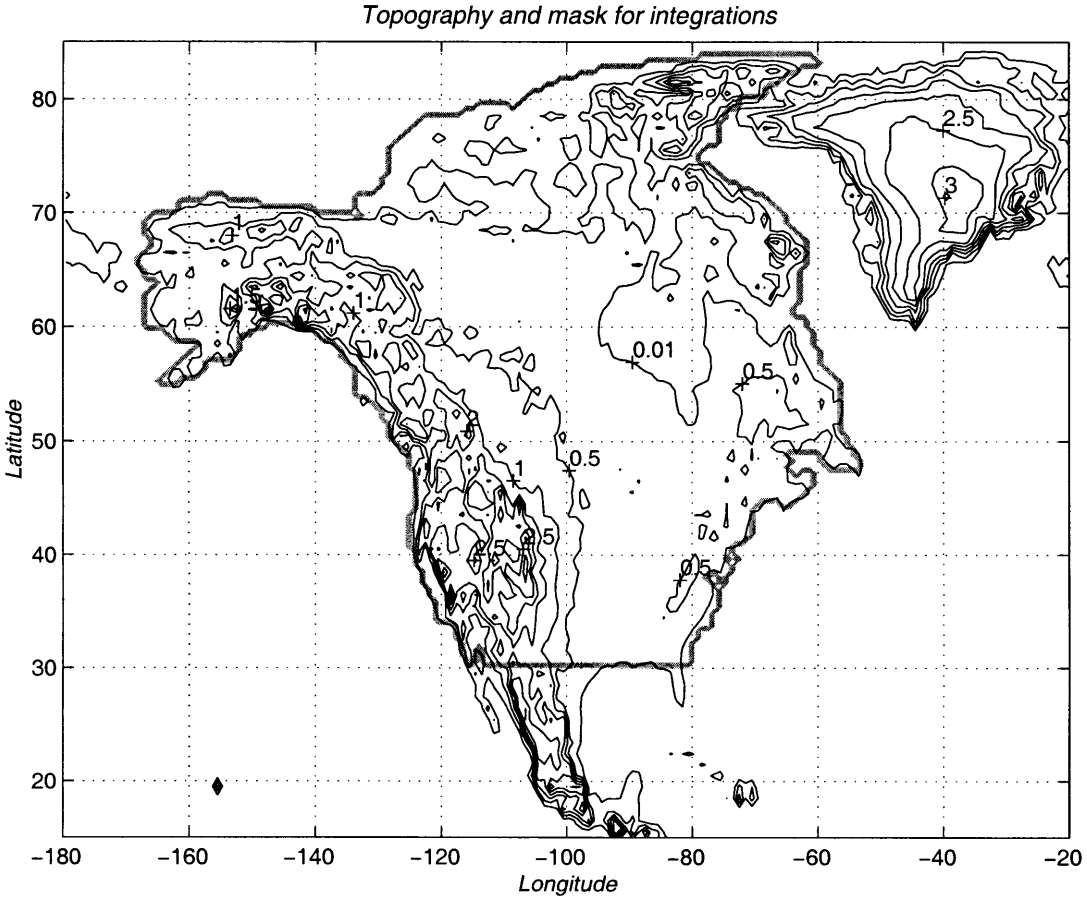

Figure 6.7: Bedrock topography (km) and mask for North America. The ice is allowed to evolve within the mask (denoted by the thick, faint contour. Some adjustments have been made from modern topography, which are described in the text.

6.3.1 Zonally symmetric forcing

Figure 6.8 shows the ice sheet which evolves when forced by a zonally symmetric climate. Neither the stationary wave feedback nor the precipitation feedback are included in this integration. The precipitation is adjusted only for the height of the surface (i.e. Equation 4.16 with $\gamma_1 = 0$). The resulting ice sheet is itself nearly zonal. The surface elevation on the western half of the ice sheet's southern margin is higher (and therefore colder) than on the eastern half, so it might be expected that ice could exist further south on the western side. That this is not so is because the mass flux of ice is dependent on both the slope and the depth of ice (this can be derived readily from Equation 4.11). The forcing climate is zonally symmetric so the east-west spreading of ice will tend to equalize the height of the surface. This means that the depth of ice sheet on the west is less than on the east, again because of the difference in the underlying bedrock elevation. There is consequently a smaller southward flux of ice on the western side of the ice sheet than on the east. This means a colder summer temperature on the west can melt enough ice to balance the southward flux from the interior. This compensates for the surface elevation, keeping the margin relatively zonal.

6.3.2 Stationary wave feedback

We now put the stationary wave feedback back into the model integration. We still leave out the topographic precipitation feedback ($\gamma_1 = 0$ in Equation 4.16). In the results presented below, we only calculated the stationary wave due to the western hemisphere topography north of the equator (the Rockies, the ice sheet, and to a lesser extent Greenland). While it is possible that other sources of stationary wave play a role in the early phase of the ice sheets development, we showed in Chapter 5 that their phase and amplitude are subject to large uncertainty. Moreover we also demonstrated that once established on a continental scale, the ice sheet itself dominates the local atmospheric response. Therefore, in considering established continental-scale ice sheets, we can neglect the background stationary wave. In the model integrations, the ice sheet and bedrock topography within the mask is interpolated onto the channel grid every $50yr$. For points outside the mask, the current western hemisphere topography (down to the equator) is left unchanged. The calculated stationary wave is used to diagnose the accumulation and ablation fields, which are then taken as input for the ice sheet

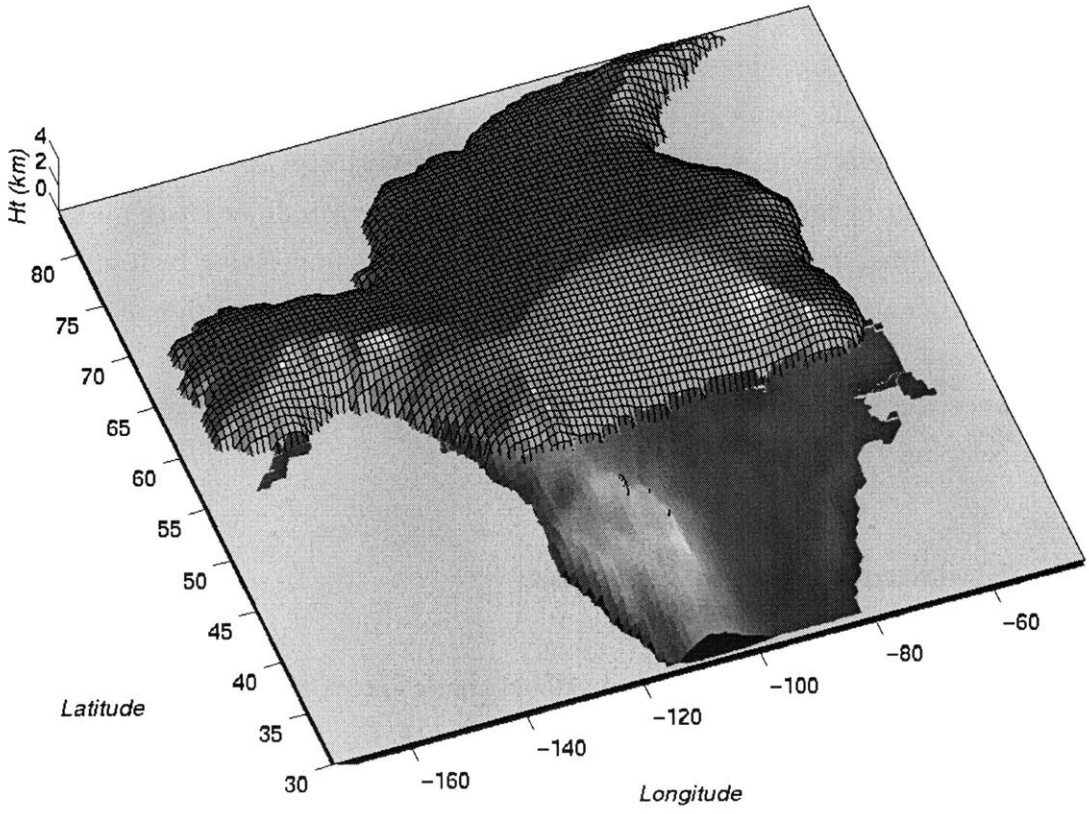

Figure 6.8: Three-dimensional view of equilibrium ice sheet forced by a zonally symmetric climate. The model parameters used are given in the text.

model for the next $50yr$. The forcing velocity, $\overline{U}_f$ (Equation 3.19), was kept at $5ms^{-1}$.

Figure 6.9 shows the equilibrium ice sheet which evolved in an integration including the stationary wave feedback. The basic state used was the same as that for Figure 6.8. As for the more simplified geometry (Chapter 5), the evolved ice sheet generates an anticyclonic atmospheric circulation over the ice sheet bringing warm temperatures in the west and cold in the east. The warm perturbation temperatures ahead of the ice sheet are sufficient to largely deglaciate Alaska, with remaining ice being confined to the high ground of the Brooks Range. Another significant point from Figure 6.9 is the extension of ice over over New England. The prevailing northerlies, generating cold temperatures in the lee of the ice sheet (as in Chapter 5), mean the eastern ice margin in Figure 6.9 is about $1400km$ further south than that in Figure 6.8. Both of the above features are observed in the Laurentide and they suggest that the stationary wave feedback may have contributed significantly to the ice sheet's shape.

The presence of ice caps on the Alaskan peninsula is well documented in observations (e.g. Climap, 1981), whereas Figure 6.9 has none. This discrepancy is likely due to the $1^o \times 1^o$ topographic data set used which is far too coarse to capture any of the mountain peaks on the penisula (see Figure 6.7), many of which actually rise above $2.0km$.

The basic state used in the integrations in Figures 6.8 and 6.9 was changed from the standard basic state. By reducing the surface wind velocity, the phase of the atmospheric response was moved eastward and improved the simulation a little. From Equation (3.15), if $\overline{U}$ decreases v' must increase in order to balance the forcing, so the phase of ϕ' shifts eastward. However, the major change made to the basic state was increasing the basic state shear (equivalently, the meridional temperature gradient). This had to be done because a common feature of the integrations was a small ice cap which developed over the southern Rockies. Once it formed it generally grew, established itself over a large area, and finally merged with the main ice sheet. The meridional temperature gradient needed ($-9.2^oC/1000km$) to prevent this happening is probably too large for summer midlatitudes, even in a glacial climate. A straightforward calculation shows why it is necessary in our model. Figure 6.10 shows two cross sections through the initial bedrock topography at $40N$ and $48N$. In this region, the Rockies increase in height southwards. Taking into account just the atmospheric lapse rate the peak topography at $40N$ would be 8.2^oC colder than the peak at $48N$. If the peak at $48N$ can just sustain ice year round (summer temperature just below freezing), then for our model

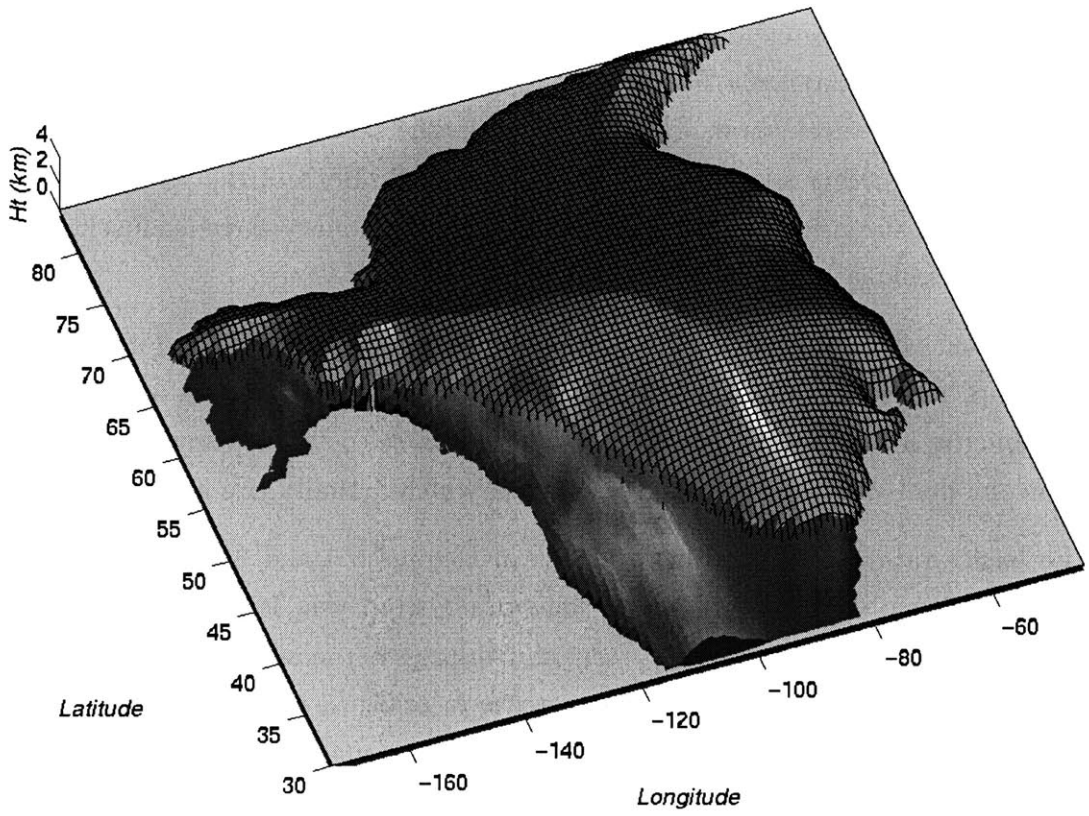

Figure 6.9: Three dimensional view of equilibrium ice sheet for integration including the stationary wave feedback. Otherwise parameters are as for Figure 6.8.

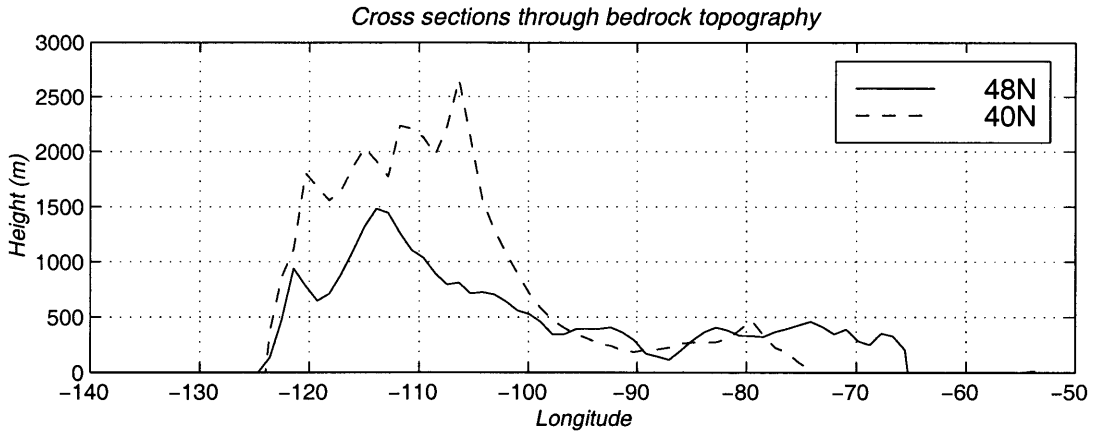

Figure 6.10: Cross section through model equilibrium bedrock topography at two latitudes. Note the much higher topography to the south.

assumptions a meridional temperature gradient of at least $-9.1^oC/1000km$ is required to prevent ice from forming at $40N$.

Since the southern Rockies ice cap did not merge with the main ice sheet at the LGM, it must be that some of the simplifying model assumptions lead to ice that initiates on high ground surviving to become more extensive. One factor which we have left out is variability in the temperature—the annual cycle in temperature is represented by a smooth sinusoid. Small scale ice features will persist if there is more local accumulation than melting. As such they are vulnerable to episodes of unusual warmth which, with the associated high melt rates, might be enough to remove all the previous accumulation. Large ice sheets are however a balance between melting or calving at their margin, and the flux of ice accumulating in their interiors. They are therefore more able to survive a few instances of high melting at their margin than are small ice features. Short time scale variability within a season and also interannual variability would reduce the chances of an ice cap persisting for long enough to become established. As already mentioned, the topographic resolution smooths over individual peaks and valleys. Moreover, the shallow ice approximation is valid only for large bodies of ice and cannot be used to represent mountain glaciers, for example. Therefore the behavior of ice forming on mountain peaks is not well captured by the ice sheet model. Mountain glaciers survive in a quasi-steady state in the Rockies today: relatively rapid flow rates into deep valleys prevent the ice from building up indefinitely.

Aside from the development of the Rockies ice cap, the qualitative effect of deglacia-

tion in Alaska and extension of ice over New England were robust for a range of parameters, with the magnitude of the effect related directly to the amplitude of the stationary wave.

6.3.3 Current precipitation patterns

Because it is difficult to parameterize snow accumulation in simple models, some LGM simulation attempts have used current precipitation patterns adjusted by the local temperature changes between the current climate and the modeled LGM (e.g. Tarasov and Peltier, 1997). Using NCEP reanalysis data for current precipitation and current mean annual temperature (Kalnay, E. et al., 1996), we performed a similar experiment. The data was taken from a relatively coarse grid of $\sim 2^o \times 2^o$. The precipitation rate at any given location was taken to be equal to the current precipitation rate multiplied by the saturation vapor pressure for the modeled annually averaged surface temperature (taking into account the height of the ice sheet), and divided by the saturation vapor pressure for today's annually averaged surface temperature. The precipitation was assumed to fall as snow for the fraction of the year the modeled climate was below zero. This is obviously an unreasonable treatment of the physics of precipitation, but it does at least retain the patterns in today's climate and is thus a useful comparison. The resulting ice sheet is shown in Figure 6.11, and is extremely similar to that of Figure 6.9 The forcing precipitation field for the ice sheets in Figures 6.9 and 6.11 are shown in Figure 6.12. Despite the very different patterns in the accumulation, a remarkably similar looking ice sheet has evolved. The temperatures forcing the ablation fields in the two integrations are the same (apart from very minor differences due to the small changes in the ice sheets). The close correspondence of the two ice sheets demonstrates the dominant importance of summer temperatures in creating the final configuration of the ice sheet. This also suggests that the southeastward extension of the Atlantic storm track that many GCM simulations indicate, would have had relatively little impact on the Laurentide. Consistent with this, Tarasov and Peltier (1997) were unable to obtain the southeastward extension of the ice sheet over New England even with a factor of 2 increase in the local precipitation. The ice sheet will only respond significantly to large changes in accumulation in the interior. The results in Chapter 4 showed that accumulation at the margin is a relatively minor part of the mass balance there; the dominant terms are the flux of ice from the interior, and the melting.

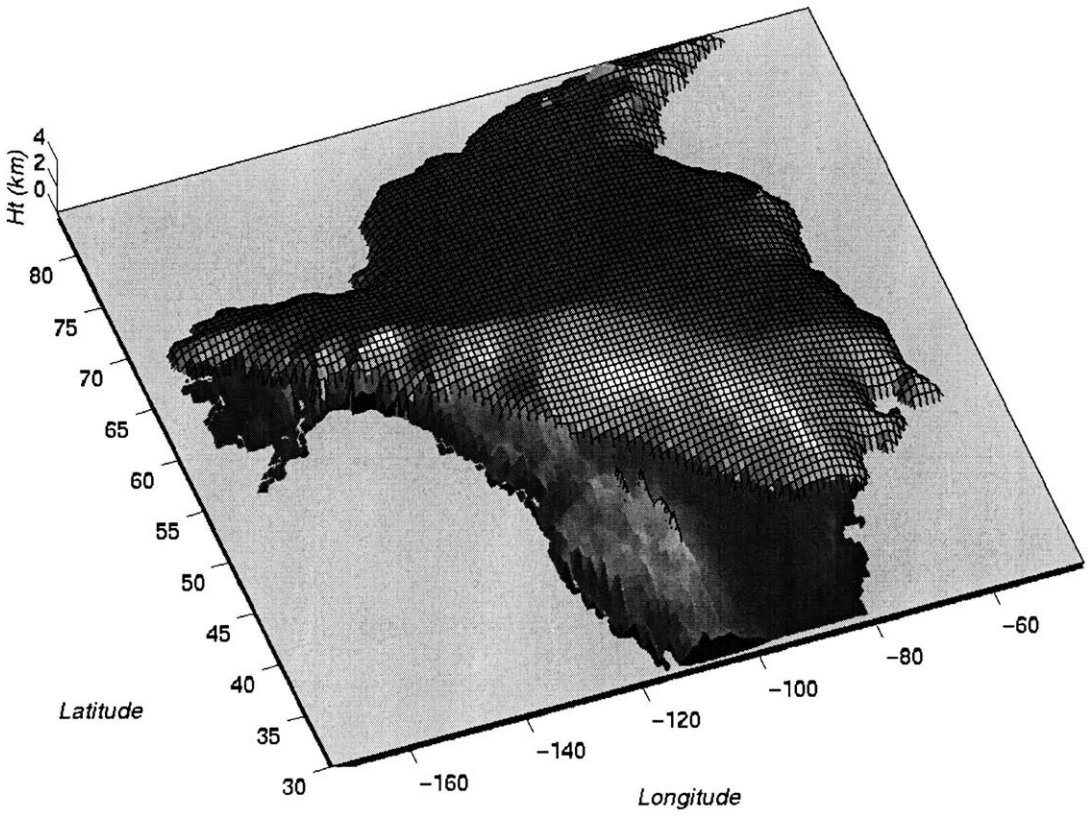

Figure 6.11: Three dimensional view of equilibrium ice sheet for integration including the stationary wave feedback. Accumulation is derived from current data, adjusted for temperature changes at the surface. The details of this are described in the text. Otherwise model parameters are the same as Figure 6.9.

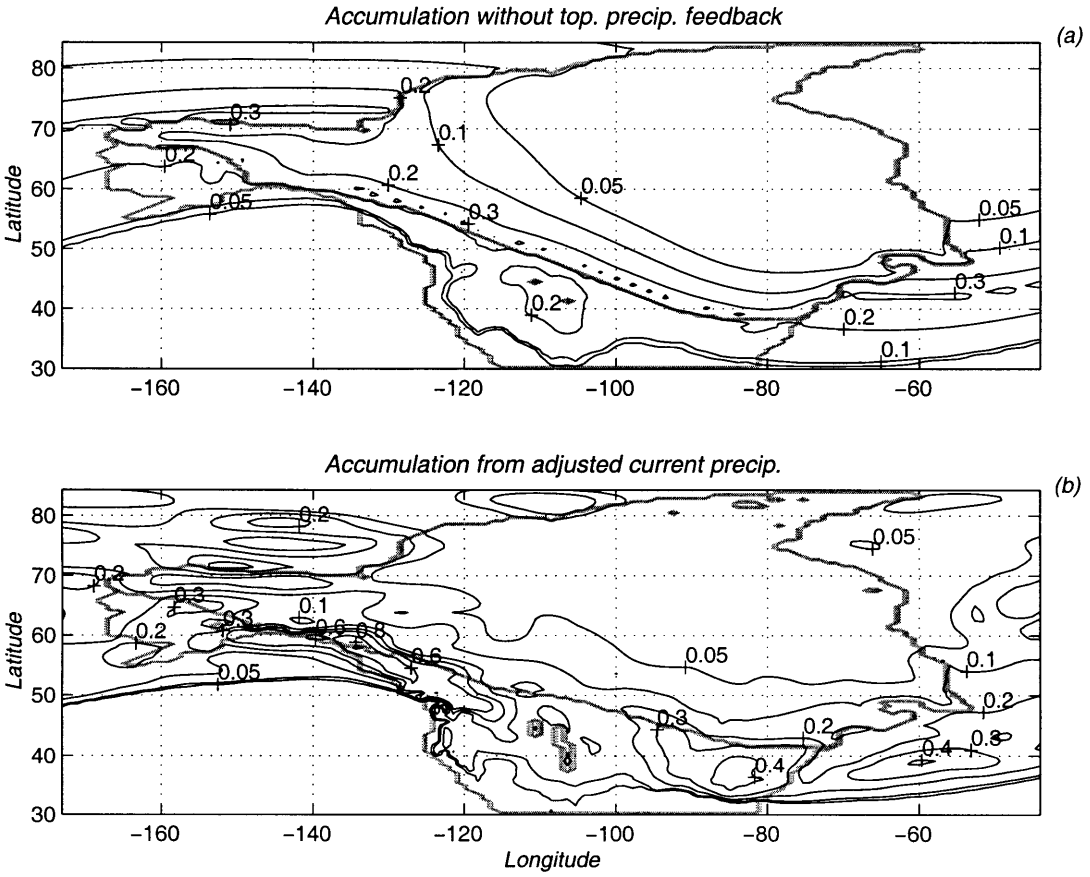

Figure 6.12: Accumulation fields for ice sheet shown in Figures 6.9 and 6.11. (a) is the model parameterization, (b) is based on current precipitation patterns. Contours are plotted at (0.05,0.1,0.2,0.3,0.4,0.6,0.8)myr^{-1}. The continental and ice sheets margins are plotted with a thick faint line. These different patterns produce a very similar ice sheet.

Using current precipitation patterns however does not take into account that the precipitation maxima will follow the windward ice sheet margin. The next section shows that in a region with highly variable topography like Alaska, topographic precipitation might play a major role in establishing the presence of an ice sheet.

6.3.4 Combined feedbacks

We now include the topographic precipitation feedback in the ice sheet integration (i.e. include γ_1 in Equation (4.16)). Figure 6.13 shows the resulting ice sheet. The extension of the ice into New England remains the same, the ice cap over the southern Rockies has grown and merged with the main ice sheet, and the ice sheet has extended down into central Alaska. The last two features are not observed in the climate record.

Once ice begins to develop on the Brooks range, it quickly develops steep sides. The prevailing winds are southwesterly and so the upslope flow results in high precipitation rates, exceeding $2myr^{-1}$. This high accumulation is enough to further build up the ice sheet and create enough southward mass flux that the ice pushes down into central Alaska. Only the southern portion experiences warm enough temperatures for the melting to exceed the southward flux of ice. The accumulation and temperature fields which are in equilibrium with the ice sheet are plotted in Figure 6.14. The accumulation maximizes at around $2myr^{-1}$ where the upslope flow is greatest. The stationary wave creates an east-west temperature difference of between 20 and 25^oC. The high pressure over the ice sheet has a *pmsl* of $1041mb$, which is higher than for most GCM simulations of the LGM. The large stationary wave is needed because of the strong meridional temperature gradient: in order for central Alaska and New England to have the same model temperature, the stationary wave must have a range across the continent of 25^oC. For the standard basic state temperature gradient the range required is only 2/3 of this value.

The precipitation scheme has several limitations which might contribute to the production of ice over Alaska, some of which have already been mentioned. As previously noted, the flow is assumed to go over the ice sheet rather than around the steep sides. Any deflection around the sides would reduce the rate of moisture convergence within the air column, and therefore the precipitation rate too. There also is an implicit assumption of constant relative humidity (see Appendix A1) so the scheme does not account

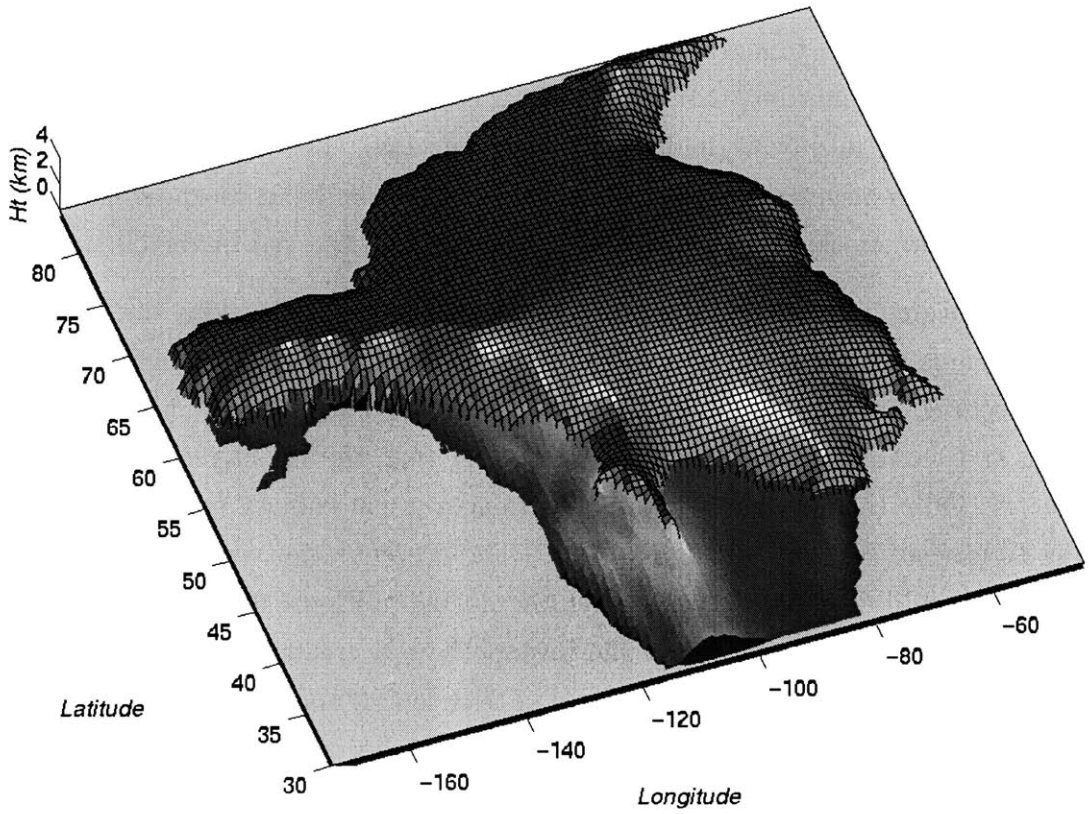

Figure 6.13: Three dimensional view of equilibrium ice sheet for integration including both the stationary and precipitation feedbacks. Otherwise model parameters are the same as Figure 6.8.

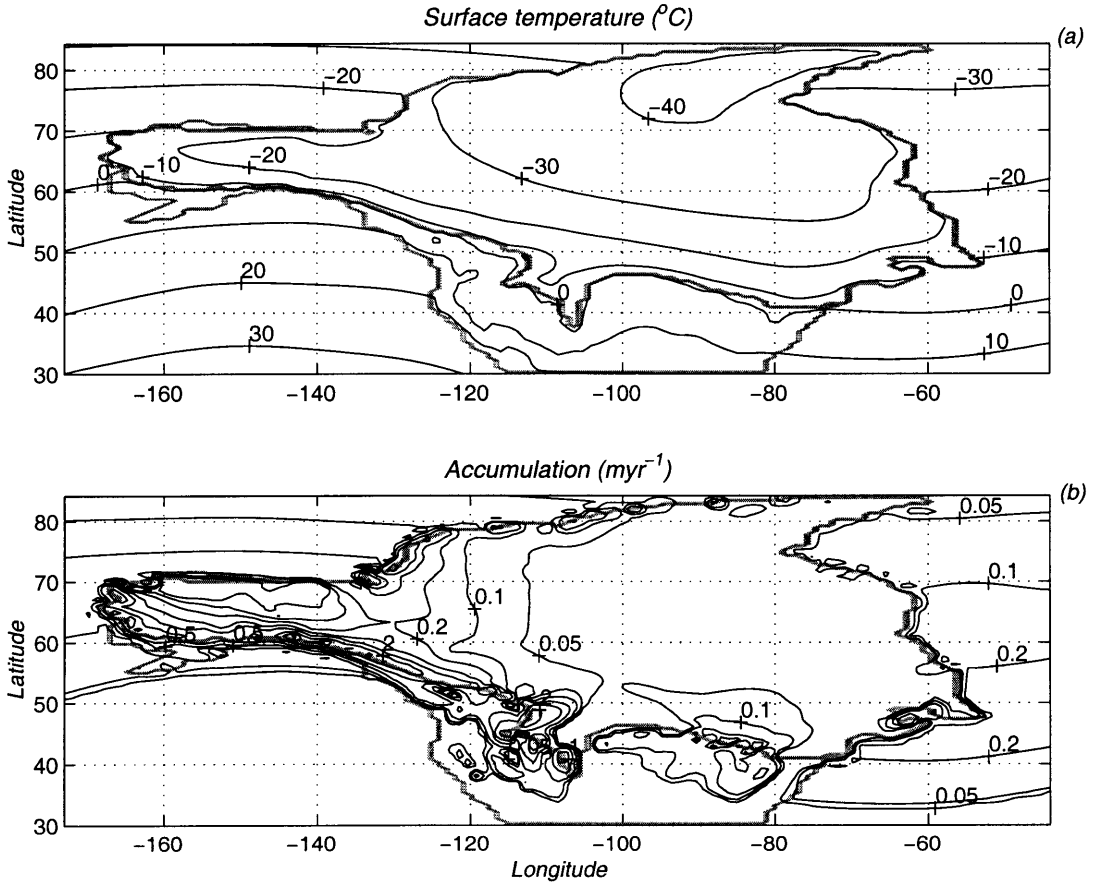

Figure 6.14: Climate fields forcing the ice sheet shown in Figure 6.13. (a) Surface temperature (^oC), and (b) accumulation. The accumulation contours are (0.05,0.1,0.2,0.5,1,2)myr^1.

for evaporation, or the distance from the moisture source. This means that, even well inland, precipitation rates can exceed $2myr^{-1}$, which is not observed in today's midlatitude climates.

It is possible to remove the ice from Alaska by increasing the size of the stationary wave: taking $\overline{U}_f = 7.5ms^{-1}$ produces the ice sheet shown in Figure 6.15, which leaves only residual ice over the Brooks range and the Wrangell mountains. Such a stationary wave though is unrealistically large and, moreover, creates prohibitively warm temperatures for the existence of ice over the northern Rockies, where it was observed to have been at the LGM. The lack of ice over Alaska in this integration is also partly a function of geography. The calving of the ice into the Beaufort sea (north of Alaska) provides a sink for the westward ice flux, where for the simple rectangular geometry in Chapter 5, that ice would flow to the western coastal boundary. It seems therefore that the likely explanation for the lack of ice over Alaska is that the Laurentide ice sheet, developing first in eastern North America, generated a stationary wave pattern which kept summer temperatures above freezing in the Aleutian lowlands, and that the complicated topography in the higher regions prevented the development of extended ice coverage.

Paleo-reconstructions show that the Gulf of Alaska remained free of sea-ice (e.g Crowley and North, 1991). This would have had two consequences which our simple model does not address. First the seasonality (i.e. the amplitude of annual temperature cycle) in Alaska and western North America would have been less than in the continental interior (as it is in today's climate). The model simply assumes that over land, the seasonality is uniform. Secondly, warmer ocean air (and always above 0^oC) would have been brought up over Alaksa by the southerly flow, possibly contributing to the lack of lowland ice. This warm advection was insufficient, however, to prevent year-round snow cover developing over Alaska in the GCM ice sheet inititation experiment of Dong and Valdes (1995), probably because of the higher elevation of the land.

Summary

The results of this chapter have shown that the stationary waves probably played an important role during the Pleistocene ice ages. In interglacial climates the atmospheric flow in the lee of the Rockies creates a cooling of several degrees, consistent with the

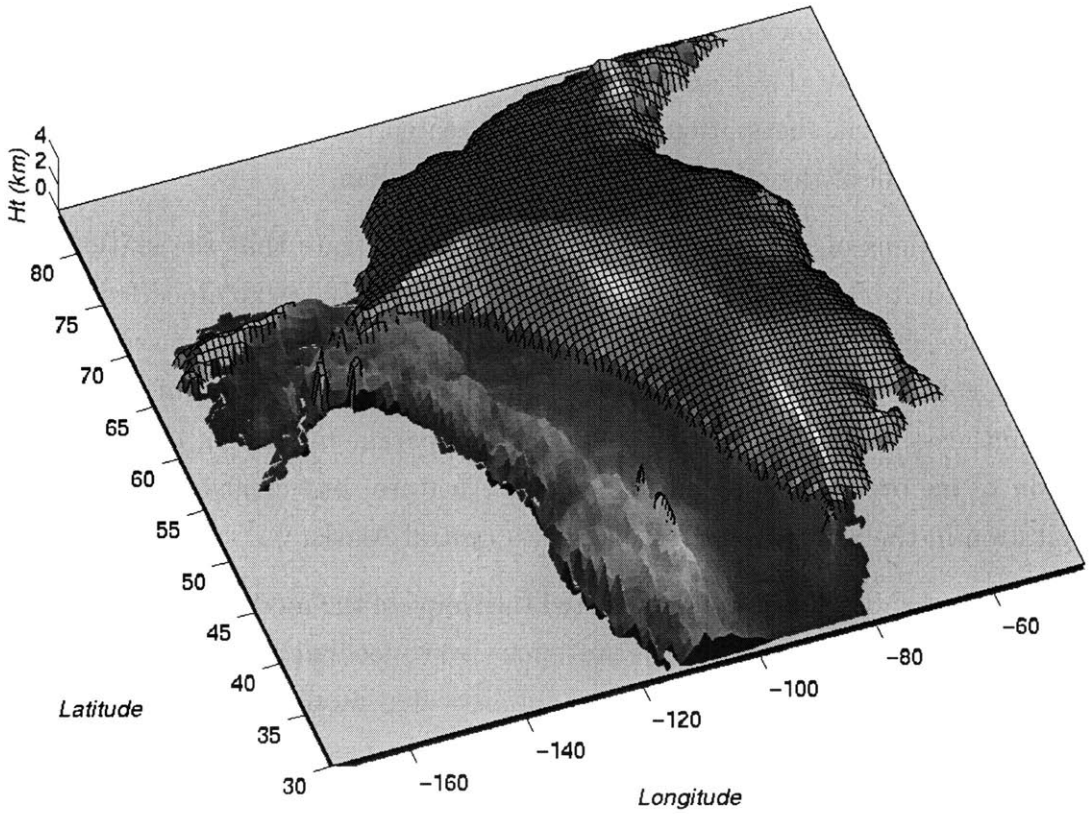

Figure 6.15: Three dimensional view of equilibrium ice sheet for integration with both feedbacks included and strong stationary wave forcing ($\overline{U}_f = 7.5ms^{-1}$). Otherwise model parameters are the same as Figure 6.8.

nucleation of ice over Keewatin and Quebec. This temperature pattern will not change due to Milankovitch forcing because it is local to the forcing topography. The results relating the Tibetan Plateau are more suspect, because we are using a simplified model. They suggest, though, that the stationary wave due to the Tibetan Plateau could create an east-west temperature difference across North America of several degrees centigrade. We expect that this would vary over a Milankovitch cycle because the phase of the response remote from the forcing is sensitive to the atmospheric basic state.

The model results show that, at the LGM, the stationary waves due to the Laurentide were larger than those due to either the Tibetan Plateau or the Fennoscandian. It is also likely that, via the stationary waves it created, the Laurentide exerted strong downstream control of the climate over the Fennoscandian.

The integrations of the ice sheet model also demonstrate that the stationary wave feedback has the potential to account for several previously unexplained features of the Laurentide ice sheet. Warm temperatures induced over Alaska help keep it ice free. Conversely cold temperatures over New England cause an extension of the Laurentide in the southeast. The topographic precipitation parameterization we use leaves the extension of ice over New England as a robust feature, but creates sufficient upslope precipitation in the west to push ice back into central Alaska.

The feedbacks we have discussed affected the shape of the model Laurentide ice sheet, but in order to conclude whether the stationary wave feedback was in fact sufficient to create the observed configuration, a more sophisticated model than ours is required: a fully nonlinear stationary wave model should be used to assess the extent to which the linear calculations hold, particularly with regard to the pattern of the prevailing flow around the edges of the ice sheet; the temperature forcing should include representations of intraseasonal and interannual variability; a precipitation scheme which takes into account the distance from the moisture source and changes in relative humidity would be able to account for inland precipitation; and a higher resolution ice sheet model would help examine the initiation and growth of permanent ice in regions of highly variable topography.

We did not look at the Fennoscandian ice sheet, partly because it was not clear that the atmospheric flow around it would be as straightforward as for the Laurentide. Since the Fennoscandian was smaller than the Laurentide, the amplitude of the stationary wave it generated was less, but the tendency on the ice sheet's shape would have been the

same. In modeling the extent of the Fennoscandian it is likely also important to account for the variation in the amplitude of the seasonal cycle across the Asian continent, which is larger than for North America, and assumed constant in the model. The results of this thesis would suggest that the reason Siberia remained largely ice free is not that the accumulation was low, but that the summer temperatures exceeded 0^oC, thereby melting any winter accumulation.

Chapter 7

Summary and discussion

Before reviewing and discussing the results of this thesis, we first restate several relevant features of the great continental ice sheets that have dominated the northern hemisphere landscape during the ice ages of the Pleistocene. The ice sheets have a length scale equal to that of the continents (i.e. 3000 to $4000km$), and a typical depth of about 3 to $4km$. This vertical scale is dependent to an extent on the assumptions made about the ice physics. Ice sheets are also characterized by steep sides, typically rising to $1km$ in height within $100km$ of the margin. Because of the atmospheric lapse rate, the surface temperature decreases quickly with elevation, and therefore melting is confined to a narrow zone around the margin. Over thousands of years, ice behaves as a viscous fluid, slowly spreading under its own weight; the accumulation of snowfall in the interior is balanced by the flow of ice towards the ice sheet's margins. The coastal boundaries have been basically fixed during the Pleistocene (apart from sea level changes), so we have focused particularly on what controls the land-based margins.

We have shown that an ice sheet's area and volume are quite insensitive to the details of the accumulation distribution in its interior. The flow of ice is essentially diffusive in character, and the details of the accumulation patterns are smoothed over as the ice flows to the margin. As confirmation of this, we showed in Chapter 6 that an ice sheet that evolved from a precipitation distribution based on observed patterns in today's climate was very similar to an ice sheet that evolved from a precipitation parameterization based purely on the modeled surface temperature (Figures 6.9 and 6.11). Precipitation is perhaps the hardest atmospheric field to model and so this insensitivity to accumulation

distribution gives hope for the successful modeling the ice age ice sheets.

At their margins, large ice sheets typically have a convergence of ice flux amounting to several meters per year. This is much larger than typical accumulation rates, which therefore do not play a large role in the mass budget at the margin. A land-based margin is thus located where there is an approximate balance between the convergence of ice flux from within the interior and summer melting occurring in a narrow zone at the margin. The exception to this is where the prevailing winds are upslope. Observations from today's climate show that where this happens, precipitation rates of 2 to $3myr^{-1}$ are possible. Here then, the precipitation on the windward margins can become a significant part of the mass budget, leading to an increased ice flux in the windward direction. Chapter 5 showed that the effect of upslope precipitation was sufficient to push the margin several hundred kilometers south of where it would otherwise lie (Figure 5.7).

Since it is the melting at the margin that mainly balances the ice flux from the interior, the pattern of summer temperatures is crucial to determining the location of an ice sheet's land margins. We have argued in this thesis that the temperature patterns around an ice sheet are controlled to a significant degree by the time averaged atmospheric response to the presence of an ice sheet. The induced circulation is mainly due to the ice sheet's topography, which generates a high pressure, anticyclonic circulation centered over the western slopes. Associated with this circulation are warm perturbation temperatures on, and to the west of, the western slopes, and cold perturbation temperatures over the rest of the ice sheet. For an ice sheet the scale of the Laurentide, the magnitude of the cold temperature perturbation is of order 10^oC, equivalent to a climate about $1500km$ further north. It represents a local climate forcing as significant as Milankovitch insolation cycles. This result stresses that east-west temperature changes due to the reorganization of the atmospheric circulation can be as important in a glacial climate as north-south changes.

Chapter 5 showed that to a rough approximation, and for an idealized continental geometry, the land-based ice sheet margin lies within a narrow range of summer isotherms stretching across the continent (between about 0 and 5^oC in our model, but this depends on model details). Compared to an ice sheet forced by a zonally symmetric climate, the pattern of temperatures produced by the induced atmospheric circulation leads to a northward retreat of the western margins, and a southward extension of the rest of the ice sheet (Figure 5.4). When the effects of topographically influenced precipitation are

included, this picture changes somewhat. The anticyclonic circulation generates heavy precipitation on the southwestern flank of the ice sheet, pushing the ice southward there. Over the remainder of the ice sheet, the prevailing winds are largely downslope, and the descent of air there suppresses precipitation. This reduces the interior accumulation and also therefore, the southward flux of ice.

One of the main conclusions from Chapter 5 was that for the simplified geometry and ice physics that we assumed, the above processes are the determining factors controlling the ice sheet's configuration. The two feedbacks have competing effects, and their relative strengths cannot be comprehensively determined using the simple model developed in this thesis, but we showed that the qualitative nature of the interaction was robust for a wide range of model parameters.

The internal ice dynamics are affected strongly by the precipitation rates. Where the prevailing winds are upslope (generally on the western and northern flanks), the resulting high accumulation at the surface must be balanced by a large ice flow within the ice sheet towards the margins. Low accumulation due to prevailing downslope winds on the eastern flank reduce the ice flow to a small fraction of that in the western half of the ice sheet (Figures 5.2 and 5.7).

In considering the time evolution of an ice sheet, it was demonstrated that for an ice sheet initiating away from the western continental coastline, the effect of the precipitation maximum tracking the upwind slopes of the evolving ice sheet causes rapid westward progression of the ice. Subsequent to the ice reaching the west coast, a further expansion of the ice depends more on the cooling of the climate, than on the interior accumulation creating an ice flux which pushes the margin southwards (Figure 5.13).

In model experiments in which periodic climate forcing on Milankovitch time scales was imposed over the ice sheet, we determined that the ice responds more to direct forcing of the temperature than to changes in the atmospheric stationary waves, either caused by the ice sheet itself, or due to other sources. Sinusoidal forcing of the climate temperature produces a saw tooth shaped response in the ice sheet. The saw tooth is not as extreme as that observed in the global ice volume record, and is due primarily to the asymmetry between the mechanisms of melting and accumulation rather than to the effects of bedrock depression (Section 5.6). A combination of sinusoidal forcings at the precessional frequencies in the insolation (19 and $23kyr$) produced a quasi-linear response on the volume and area of the ice sheet. However the height of ice the ice sheet

acted as a strong rectifier of the forcing, and responded mainly at the beat frequency ($109kyr$).

Applying the simple modeling approach to the reconstructed topography of the LGM, we conclude that the Laurentide was the largest source of atmospheric stationary waves on the planet, and that it likely exerted a strong influence on the climate over the Fennoscandian because of the downstream propagation of its atmospheric stationary wave pattern (Figures 6.4 and 6.6). Integrations of the coupled ice sheet and stationary wave model over North America show that the interaction between the Laurentide and the atmospheric stationary wave it generated has the potential to explain the lack of ice over Alaska and the extension of ice over New England at the LGM (Figure 6.9). Both of these features have not been explained to date. While we can say that the interaction had the tendency to create the observed shape of the Laurentide, we cannot conclude that it was, by itself, sufficient to do so, both because of the uncertainties in our model parameterizations, and also our lack of detailed knowledge about the glacial atmosphere.

Some potentially important physics was left out of the model we developed in Chapters 3 and 4. The model was not constructed to simulate any particular climate cycle or state, but rather to try to model for the first time how atmospheric dynamics interacts with ice sheets on time scales appropriate to the ice ages. The reduced modeling approach was used to explore potential mechanisms and to indicate the possible range of the interactions. We have tried to account for the simplicity of the model in weighting the conclusions of this thesis. We next turn to the omitted physics and how it might be used in further work to assess the interaction in a more comprehensive approach.

The ice sheet model did not account for the temperature dependence of ice flow. This excludes the effects of frictional heating within the ice. If this heating is sufficient to raise the base temperature to melting point, then the resulting mix of ice and water (temperate ice) means the ice sheet is no longer grounded on the bedrock, and it becomes free to slide. A temperate base allows for the existence of ice streams (fast flowing regions), and has been invoked as an explanation for the massive discharges of icebergs observed in the paleoclimate record (MacAyeal, 1993). Whether the base is frozen or not can reflect the climate at the upper surface of the ice sheet. Higher accumulation leads to a stronger downward flux of ice into the ice sheet, giving less time for the temperature to rise above the melting point at the base. Similarly, a colder surface temperature means colder ice is drawn down into the interior, making a frozen base more likely. A frozen

bed leads to different erosion of the underlying bed than a temperate base, and these differences are seen in the geologic record of the last ice age (e.g. Martini, 1997). The picture is complicated by the nature of the underlying bed (e.g. soft till versus hard rock), but it would be interesting to explore the full thermomechanical behavior of the ice sheet model of Greve (1995). The point would be to see whether the lower boundary condition resulting from the model integration (i.e. temperate or frozen) could be tested against the geologic record, and perhaps combined with it to give a prediction of the climate which existed above the ice sheets.

At the surface of the ice sheet, we assumed that the ice temperature was approximately the same as that of the atmosphere directly above it. This seems reasonable for seasonal averages in observations over Greenland (Steffen et al., 1996). However the surface temperature is actually determined by a combination of direct radiation fluxes, exchange of sensible and latent heat with the atmosphere, and thermal conduction within the snow pack and ice. These fluxes are, in turn, dependent on atmospheric variables such as temperature, cloudiness, wind speed, and relative humidity. Surface energy balance models which try to take account of these factors are being applied to ice sheets (Bugnion, 1999). The melting and ablating of ice are also dependent on the surface energy balance, but for the purpose of looking at a continental scale ice sheet, an ablation parameterization dependent only on temperature is probably sufficient to capture the large scale picture. However, one of the main sensitivities in the stationary wave model was to the thermal damping time scale. To determine what that should be requires an accounting of the exchange of sensible heat between the atmosphere and the ice surface.

The stationary wave model used in this thesis was linear, quasigeostrophic, and had a channel geometry. While we concluded that this was sufficient to give a qualitatively correct atmospheric response to the ice sheet topography, the details of the flow, particularly around the steep sides of the ice sheet would likely change if a high resolution, nonlinear, primitive equation model were used instead. Nonlinear models have shown that for topography greater than a certain size, the atmospheric response saturates (stops increasing with the size of the topography) (Trenberth and Chen, 1988). This effect might have an impact on the later stages of the ice sheet's growth. Also, the lack of realistic meridional variation and spherical geometry in a channel model is a big constraint on modeling the downstream propagation of the stationary wave. We have shown it is likely that the Laurentide exerted a strong influence on the climate over

the Fennoscandian because of the downstream propagation its stationary wave pattern (Figure 6.6). However, a spherical coordinate model with realistic meridional variation would be better able to assess the robustness of this effect, and how it would be likely to change across a range of atmospheric basic states. The results of this thesis tell us that the important fields to concentrate on with such a model would be the low level summer temperatures. The damping used in our model is a very simplified representation of the atmospheric boundary layer. A more comprehensive treatment would include a non-quasigeostrophic balance at low levels, and different heat and momentum transfer over land, ocean, and ice.

We used a very simplified precipitation parameterization, which suffered from several potentially important simplifications. The relative humidity was, in effect, assumed to be constant, and no account was taken of where the moisture originated from. Moreover, the topographic precipitation was taken as proportional to the prevailing upslope wind. We included a distribution of vertical velocities to represent qualitatively the variations associated with individual storms, but this did not allow for the storms to be deflected around the steep ice sheet sides. Additionally, the low resolution of the model precipitation grid ($1^o \times 1^o$) cannot represent microclimates within mountain ranges, something which probably matters for ice sheet initiation. Changes in storm track location and extent are likely not that important because, as we reviewed above, the ice sheet is quite insensitive to the details of the interior accumulation distribution. It would be useful however to look at the role of topographic precipitation further. A two-dimensional isothermal shallow ice model representing an east-west segment through an ice sheet would provide no practical constraint on model resolution, while retaining the physics of ice flow. Such an approach could look at the effect of varying the topographic precipitation effects (i.e. γ_1 in Equation (4.16)), and also investigate the role of topographic resolution in ice sheet initiation. In such a model it would also be relatively easy to include a moisture scheme which had representations of relative humidity and evaporation along the lines of Sanberg and Oerlemans (1983).

Finally, we address the climate prescribed in the model. The zonal mean climate was imposed as a forcing, and therefore does not reflect the many feedbacks which act to change it during a glacial period. For example, the development of the northern hemisphere ice sheets was accompanied by an extension of sea ice, and the resulting increase in albedo at high latitudes acted to cool the climate further. Moreover, we showed in Chapter 3 that the stationary wave associated with large ice sheets can potentially affect

the poleward heat transport significantly, although we would need to account for the wave-mean flow interaction in the atmosphere to study this more. A further simplification was made in the imposition of a purely sinusoidal annual temperature cycle. In reality, many individual weather events produce a distribution of temperatures around the average. This is important because of the very nonlinear behavior of the ice mass budget as the temperature passes through $0°C$. Melting increases strongly with temperature, so only a few warm events are required to melt weeks of slow accumulation. It would also be worthwhile to include realistic interannual variability in temperature. One abnormally warm summer might be sufficient to melt the previous few years' accumulation, and such an effect would obviously have important consequences for ice sheet initiation.

A recent simulation of a northern hemisphere ice sheets forced by climate output from a low resolution GCM simulation of the LGM produced a reasonable match with the reconstructed LGM ice sheets (Fabre et al., 1997). Even though the model was used in anomaly mode (i.e. to represent deviations from the current climate), it would be useful to diagnose how the climate fields from the GCM acted to produce the mass budget over the ice sheet. Such a study would be capable of seeing how the feedbacks proposed in this thesis act in a more complicated atmospheric model.

We have shown that the great continental ice sheets must have caused a significant change in the atmospheric circulation, and that these changes acted over time to control the shape of the ice sheet. The inclusion of the physical processes discussed above would refine the interaction, and help constrain further how the mechanisms presented actually played out in a glacial climate.

Appendix A

Moisture budget

In this appendix we will show how the steady state moisture budget equation can be reduced to the precipitation rate parameterization introduced in Chapter 4. The purpose of doing this is to see what implicit assumptions have been made in the precipitation parameterization, and to get an idea of the extent to which the neglected terms might affect the amount and distribution of the precipitation.

The time mean equation for conservation of water vapor can be written as

$$P = E - \nabla \cdot \vec{Q}_{sw} - \nabla \cdot \overline{\vec{Q}_{tr}} \tag{A.1}$$

where P is precipitation, E is evaporation, $\vec{Q}_{sw}$ is the steady state flux of water vapor due to the stationary wave fields, and $\overline{\vec{Q}_{tr}}$ is the time averaged convergence of transient water vapor flux. If the units of precipitation rate are ms^{-1}, then $\vec{Q}_{sw}$ can be expressed as

$$\nabla \cdot \vec{Q}_{sw} = \frac{1}{\rho_w} \nabla \cdot \int_{z_s(x,y)}^{\infty} \rho q \vec{u} dz \tag{A.2}$$

where ρ_w is the density of water, ρ is the atmospheric density, q is the specific humidity, and $\vec{u}$ is the velocity field obtained for the stationary wave model. $z_s(x, y)$ is the surface height. To a good approximation $q = \epsilon \mathcal{H} e_{sat}/p$ where $\epsilon = 0.622$, $\mathcal{H}$ is the relative humidity, p is pressure, and e_{sat} is the saturation vapor pressure. After a little manipulation, and using the ideal law $p = \rho RT$, Equation (A.2) is expressible as

$$\nabla \cdot \vec{Q}_{sw} = \frac{\epsilon \mathcal{H}}{\rho_w g H} \nabla \cdot \int_{z_s(x,y)}^{\infty} \vec{u} e_{sat} dz \tag{A.3}$$

Both the scale height, H $(= RT/g)$, and $\mathcal{H}$ have been taken as constant, which enables them to be taken outside the integral and the divergence operator. Taking H and $\mathcal{H}$ as constant is equivalent to saying that most of the variation in column water vapor is due to the exponential temperature dependence of the saturation vapor pressure. Time-mean climatological values of $\mathcal{H}$ at the surface vary between about 40% to 70% (Peixoto and Oort, 1992). Over the Antarctic ice sheet, the time averaged relative humidity stays within this range (Schwerdtfeger, 1970).

Liebniz's theorem (e.g. Abramowitz and Stegun, 1965) gives the relationship for differentiating under the integral when the limits are a function of the differentiating variable. For a general function $f(x,t)$ it can be shown that

$$\frac{\partial}{\partial t} \int_{u(x)}^{v(x)} f(x,t) dt = f(x,v) \frac{\partial v}{\partial x} - f(x,u) \frac{\partial u}{\partial x} + \int_u^v \frac{\partial f}{\partial x} dt \tag{A.4}$$

We apply Liebniz's rule to Equation (A.3) and make the further assumption that the vapor pressure at high altitudes is negligible. We substitute the resulting expression into Equation (A.1).

$$P = E - \nabla \cdot \overline{\vec{Q}_{tr}} + \underbrace{\frac{\epsilon \mathcal{H}}{\rho_w g H} \left(\vec{u}(z_s) \cdot \nabla z_s\right) e_{sat}}_{\text{term I}} - \underbrace{\frac{\epsilon \mathcal{H}}{\rho_w g H} \int_{z_s}^{\infty} \nabla \cdot (e_{sat} \vec{u}) dz}_{\text{term II}} \tag{A.5}$$

Terms I and II in Equation (A.5) are the stationary wave moisture divergence.

Term I is directly relatable to the upslope term in the moisture parameterization in Chapter 4. The coefficients in Equation (A.5) suggest that, for $\mathcal{H} = 0.7$ and $H = 7.5km$, the constant, γ_1, in Equation 4.16 should be $5.9 \times 10^{-9} m^2 s k g^{-1}$. This is the value we take. Term II, which is neglected in the precipitation rate parameterization, represents the moisture convergence due to the stationary wave fields themselves, as opposed to the topographically forced convergence.

We use the standard case stationary waves and test ice sheet described in Chapter 3

to look at the relative magnitudes of terms I and II. The results are shown in Figure A.1. Over the ice sheet, most of the moisture convergence is associated with term I. This gives support to the neglecting of term II in Equation (4.16). Away from the ice sheet the moisture convergence due to the stationary wave fields is fairly small ($\sim 10 cmyr^{-1}$).

The precipitation rate parameterization we use subsumes the evaporation and the divergence of transients (see Equation (A.5) into one term $\gamma_0 e_{sat}(T_s)$. This is a strong simplification, as it takes no account of the moisture sources, nor of any zonal asymmetries in the convergence of transients due to the presence of the stationary waves themselves. The atmospheric storm tracks in today's climate, for example, are locations of increased moisture convergence compared to the zonal average (Peixoto and Oort, 1992). The consequence of not accounting for these effects will be discussed further in Chapter 4.

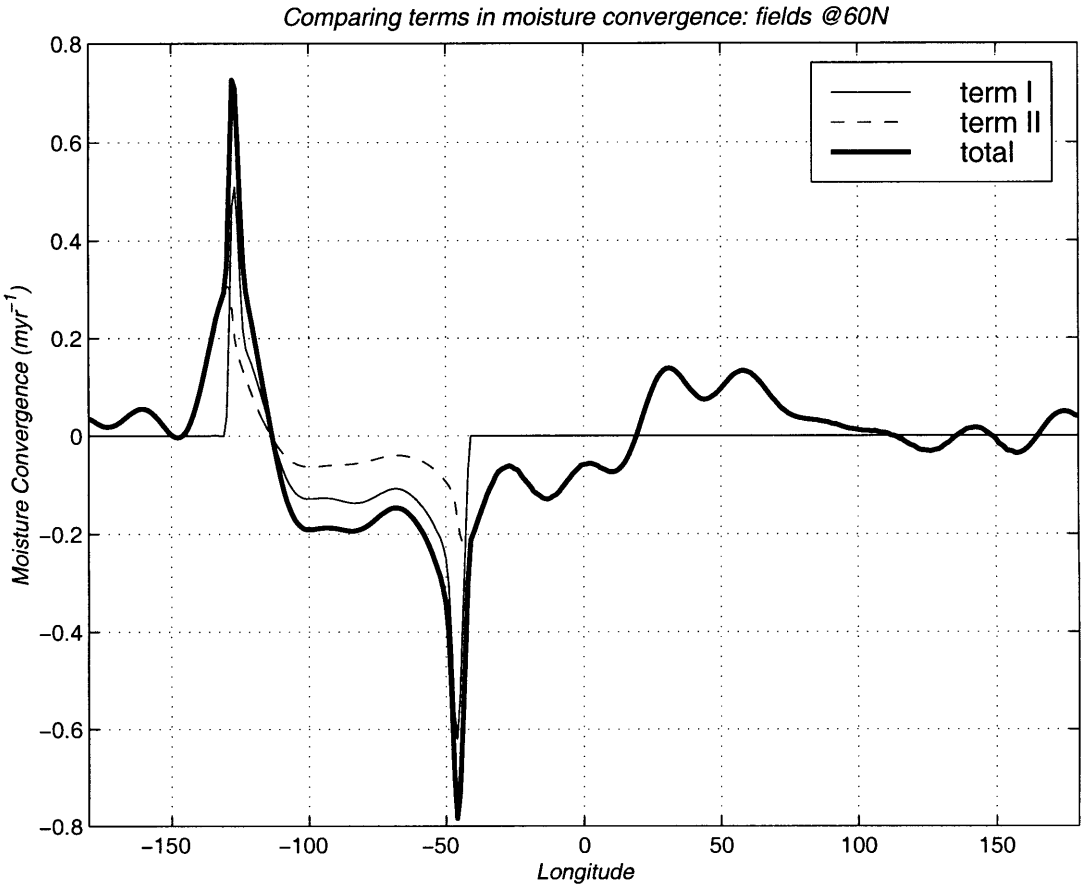

Figure A.1: Stationary wave moisture convergence associated with standard case test stationary wave of Chapter 3, as a function of longitude (total). Also shown are the separate terms which together comprise the total convergence. Term I is the mechanical convergence forced by the topography, and term II is the convergence within the stationary wave fields. These are defined in the text. The test ice sheet lies approximately between $150W$ and $50W$.

Appendix B

Moisture integral

In this appendix we show the calculation of the precipitation rate using a distribution of vertical velocities described in Section 4.3. The precipitation rate for fixed T_s is the integral of Equation 4.16 over the fraction of time for which the vertical velocity is large enough to give precipitation:

$$P = e_{sat}(T_s) \int_{-\gamma_0/\gamma_1}^{\infty} (\gamma_0 + \gamma_1 w') f(w') dw' \tag{B.1}$$

with

$$f(w')dw' = \frac{e^{-\alpha^2(w'-w)^2} dw'}{N} \tag{B.2}$$

From the normalization requirement that $\int_{-\infty}^{\infty} f(w')dw' = 1$, we get, using standard integrals, that $N = \sqrt{\pi}/\alpha$.

If we substitute a dummy variable $x = w' - w$, then Equations (B.1) and (B.2) become

$$P = \frac{\gamma_1 e_{sat}}{N} \int_{-x_0}^{\infty} (x_0 + x) e^{-\alpha^2 x^2} dx \tag{B.3}$$

where $x_0 = \gamma_0/\gamma_1 + w$. Equation (B.3) can be rewritten as

$$P = \frac{\gamma_1 e_{sat}}{N} \left\{ x_0 \int_0^{\infty} e^{-\alpha^2 x^2} dx + \frac{x_0^2}{|x_0|} \int_0^{|x_0|} e^{-\alpha^2 x^2} dx + \int_{-x_0}^{\infty} x e^{-\alpha^2 x^2} dx \right\} \tag{B.4}$$

The modulus of $|x_0|$ in the second term on the RHS of Equation (B.4) accounts for the possibility that x_0 might be negative. The above integrals have standard analytic solutions, which means Equation (B.4) can be written as

$$P = \frac{\gamma_1 e_{sat}}{N} \left\{ x_0 \frac{\sqrt{\pi}}{2\alpha} + \frac{x_0^2}{|x_0|} \frac{\sqrt{\pi}}{2\alpha} erf(\alpha |x_0|) - \frac{1}{2\alpha^2} \left| e^{-alf^2 x^2} \right|_{-x_0}^{\infty} \right\} \tag{B.5}$$

$erf(\alpha x_0)$ is the error function. Abramowitz and Stegun (1965) give the following very accurate asymptotic series expansion for the error function.

$$erf(y) = 1 - (a_1 t + a_2 t^2 + a_3 t^3) e^{-y^2} \tag{B.6}$$

where $t = 1/(1+py)$, and a_1, a_2, a_3, and p are all constants. Equation (B.5) can therefore be directly calculated to give the precipitation rate for a given T_s.

References

Abe-Ouchi, A., 1993: Ice sheet response to climate changes. PhD thesis, ETH, Zurich, Switzerland.

Abramowitz, M., and I. A. Stegun, 1965: *Handbook of Mathematical Functions with Formulas, Graphs, and Mathematical Tables.* Dover publications, New York, pp 1046.

Anderson, D. M., and R. S. Webb, 1994: Ice age tropics revisited. *Science*, **367**, 23-24.

Andrews, D. G., J. R. Holton, and C. B. Leovy, 1987: *Middle Atmosphere Dynamics*, Academic Press, New York. pp 489.

Bader, H. P., and P. Weilenmann, 1992: Modeling temperature distribution, energy and mass flow in a (phase changing) snowpack. I. Model and case studies. *Cold regions Science and Technology*, **20**, 157-181.

Bender, C. M. and S. A. Orzag, 1978: *Advanced Mathematical Methods for Scientists and Engineers.* McGraw-Hill, New York, 593pp.

Berger, A. L., 1978: Long term variations of daily insolation and quaternary climate changes. *J. Atmos. Sci.*, **35**, 2362-2367.

Berger, A., H. Gallee, T. Fichefet, I. Marsiat and C. Tricot, 1990: Testing the astronomical theory with a coupled climate-ice sheet model. *Paleo*^{3}, **89**, 125-141.

Braithwaite, R. J. and O. B. Oleson, 1989: Calculation of glacier ablation from air temperature, West Greenland. In *Glacier Fluctuation and Climate Change.* Oerlemans J. (ed). Kluwer Academic, Dordrecht, Netherlands, pp219-233.

Bromwich, D. H., 1988: Snowfall in high southern latitudes. *Rev. Geophys.*, **26**, 149-168.

Brun, E., E. Martin, V. Simon, C. Gendre, and C. Coleou, 1989: An energy and mass model of snow cover suitable for operational avalanche forecasting. *J. Glaciol.*, **35**, 333-342.

Bugnion, V, 1999: Model Estimates of the Mass Balance of the Greenland and Antarctic Ice Sheets. To be submitted.

Calov, R., and K. Hutter, 1996: The thermomechanical response of the Greenland ice sheet to various climate scenarios. *Climate Dyn.*, **12**, 243-260.

Charney, J. G. and A. Eliassen, 1949: A numerical method for predicting the perturbations of the middle latitudes westerlies, *Tellus*, **1**, 38-54.

Clark, P. U., and coworkers, 1993: Initiation and development of the Laurentide and Cordilleran ice sheets following the last interglaciation. *Quat. Sci. Rev.*, **12**, 79-114.

CLIMAP Project, 1981: Seasonal reconstructions of the earth's surface at the last glacial maximum. Geol. Soc. Am. Map Chart Ser., MC-36.

CLIMAP project members, 1976: The surface of the ice age earth. *Science*, **191**, 1131-1137.

Cook, K. H. and I. M. Held, 1988: Stationary waves of the ice age climate. *J. Climate*,**1**, 87-89.

Cook, K. H. and I. M. Held, 1992: The stationary wave response to large-scale orography in a general circulation model and a linear model. *J. Atmos. Sci.*, **49**, 525-538.

Crowley, T. J., and G. R. North, 1991: *Paleoclimatology*, OUP, Oxford, UK. pp 339.

Dong, B., and P. J. Valdes, 1995: Sensitivity studies of northern hemisphere glaciation using an atmospheric general circulation model. *J. Climate*, **8**, 2471-2496

Emanuel, K., 1994: *Atmospheric Convection.* OUP, Oxford, UK. pp 580.

Fabre, A., C. Ritz, and G. Ramstein, 1997: Modeling of last glacial maximum ice sheets using different accumulation parameterizations. *Ann. Glac.*, **24**, 223-228.

Gallee, H., J. P. vanYpersele, T. Fichefet, I. Marsiat, C. Tricot, and A. Berger, 1992: Simulations of the last glacial cycle by a coupled, sectorially averaged climate-ice sheet model 2. response to CO_2 variations. *J. Geophys. Res.*, **97**, 15713-15740.

Gates, W. L., 1976: The numerical simulation of ice age climate with a global general circulation model. *J. Atmos. Sci.*, **33**, 1844-1873.

Greve, R., 1995: Thermomechaninsches verhalten polythermer eis-schilde—theorie, analytic, numerik. PhD dissertation, Institut fur Mechanik, Technische Hochschule Dannstadt, pp 226.

Greve, R., 1997: Application of a polythermal three-dimensional ice sheet model to the Greenland ice sheet: response to steady state and transient climate scenarios. *J. Atmos. Sci.*, **10**, 901-918.

Hall, N. M. J., P. J. Valdes, and B. Dong, 1996: The maintenance of the last great ice sheets: A UGAMP GCM study. *J. Atmos. Sci.*, **9**, 1004-1019.

Held, I. M. 1983, Stationary and quasi-stationary eddies in the extratropical troposphere: theory. In *Large Scale Dynamical Processes in the Atmosphere*, B. J. Hoskins and R. P. Pierce, Eds.,127-168. Academic Press, New York.

Holton, J. R., 1979: *An introduction to Dynamic Meteorology.* Academic Press, New York. pp 511.

Hoskins B. J., and D. J. Karoly, 1981: The steady linear response of a spherical atmosphere to thermal and orographic forcing. *J. Atmos. Sci.*, **38**, 1179-1196.

Hutter, K., 1983: *Theoretical Glaciology; Material Science of Ice and the Mechanics of Glaciers and Ice Sheets.* D. Reidel, Boston. pp 510.

Imbrie, J., E. A. Boyle, S. C. Clemens, A. Duffy, W. R. Howard, G. Kukla, J. Kutzbach, D. G. Martinson, A. McIntyre, A. C. Mix, B. Molfino, J. J. Morley, L. C. Peterson, N. G. Pisias, W. L. Prell, M. E. Raymo, N. J. Shackleton, and J. R. Toggweiler, 1992: On the structure and origin of major glaciation cycles: 1. linear responses to milankovitch forcing. *Paleoceanography*, **7**, 701-738.

Imbrie, J., E. A. Boyle, S. C. Clemens, A. Duffy, W. R. Howard, G. Kukla, J. Kutzbach, D. G. Martinson, A. McIntyre, A. C. Mix, B. Molfino, J. J. Morley, L. C. Peterson, N. G. Pisias, W. L. Prell, M. E. Raymo, N. J. Shackleton, and J. R. Toggweiler, 1993: On the structure and origin of major glaciation cycles: 2. The 100,000 yr cycle. *Paleoceanography*, **8**, 699-735.

Imbrie, J., and J. K. Imbrie, 1980: Modeling the climatic response to orbital changes. *Science*, **207**, 947-953.

Milankovitch, M., 1941: Canon of insolation and the ice age problem (in Yugoslavian). K. Serb. Acad. Beorg. Spec. Publ. 132. (English translation by Israel Program for Scientific Translations, Jerusalem, 1969)

Jacqmin, M., and R. S. Lindzen, 1985: The causation and sensitivity of the northern winter planetary waves. *J. Atmos. Sci.*, **42**, 724-745

Kalnay, E. et al., 1996: The NCEP/NCAR 40-year reanalysis project. *Bulletin of the American Meteorology Society*, **77**, 437-471.

Kuhn, M. 1979: The computation of heat transfer coefficients from energy balance gradients on a glacier. *J. Glaciol.*, **22**, 263-272

Kutzbach, J. E. and P. J. Guetter, 1986: The influence of changing orbital parameters and surface boundary conditions on climate simulations for the past 18,000 years. *J. Atmos. Sci.*, **43**, 1726-1759.

Letreguilly, A., and C. Ritz, 1993. Modeling of the Fennoscandian ice sheet In *Ice in the Climate System*, 21-46. Peltier, W. R. (ed). NATO ASI Series I: Global Environmental Change 12. Springer-Verlag, Berlin.

Lindemann, M., and J. Oerlemans, 1987: Northern hemisphere stationary waves: a strong feedback mechanism. *J. Climatol.*, **7**, 109-117.

Lindzen, R. S. and B. Farrell, 1980: A simple approximation for the maximum growth rate of baroclinic eddies. *J. Atmos. Sci.*, **37**, 1648-1654.

Lindzen, R. S., 1994: The effect of concentrated PV gradients on stationary waves. *J. Atmos. Sci.*, **51**, 3455-3466.

Lindzen, R. S. and G. H. Roe, 1997: The effect of concentrated PV gradients on stationary waves: correction. *J. Atmos. Sci.*, **54**, 1815-1818.

Manabe, S., and Broccoli, A. J., 1985: The influence of continental ice sheets of an ice age. *J. Geophys. Res.*, **90**, 2167-2190.

Martini, I. P., 1997: *Late glacial and postglacial environmental changes*, OUP, Oxford, UK. pp 343.

Morland, L. W., 1984: Thermo-mechanical balances of ice sheet flows. *J. Geophys. Astrophys. Fluid Dyn.*, **29**, 237-266.

Niehaus, M. C. W., 1980: Instability of non-zonal baroclinic flows. *J. Atmos. Sci.*, **37**, 1447-1463.

Nigam, S., and R. S. Lindzen, 1989: The sensitivity of stationary waves to variations in the basic state zonal flow. *J. Atmos. Sci.*, **46**, 1746-1768.

Oerlemans, J., 1980: Model experiments on the 100,000-yr glacial cycle. *Nature*, **287**, 430-432.

. Oerlemans, J., and N. C. Hoogdendoorn, 1989: Mass-balance gradients and climate change. *J. Glaciol*, **35**, 399-405.

Ohmura, A., T. Konzelmann, M. Rotach, J. Forrer, M. Wild, A. Abe-Ouchi, H. Toritani, 1994: Energy balance for the Greenland ice sheet by observation and model computation. In *Snow and Ice Covers: Interaction with the Atmosphere and Ecosystems.* IAHS Publ. no. 223.

Ohmura, A., and N. Reeh, 1991: New precipitation and accumulation maps for Greenland. *J. Glaciology*, **43**, 140-145.

Ohmura, A., M. Wild, and L. Bengtsson, 1996: A possible change in the mass balance of Greenland and Antarctic ice sheets in the coming century. *J. Climate*, **9**, 2124-2315.

Paterson, W. S. B., 1994: *The Physics of Glaciers.* 3rd Edition. Pergammon Press, Oxford, UK. pp 480.

Pedlosky, J., 1992: *Geophysical Fluid Dynamics.* Springer-Verlag, New York. pp 710.

Peixoto, J. P. and A. H. Oort, 1992: *Physics of Climate.* American Institute of Physics, New York. pp 520.

Peltier, W. R., and S. Marshall, 1995: Coupled energy-balance/ice-sheet model simulations of the glacial cycle: a possible connection between terminations and terrigenous dust. *J. Geophys. Res.*, **100**, 14269-14289.

Phillipps, P. J., and I. M. Held, 1994: The response to orbital perturbations in an atmospheric model coupled to a slab qocean. *J. Climate*, **7**, 767-782

Pollard, D., 1978: An investigation of the astronomical theory of the ice ages using a simple climate-ice sheet model. *Nature*, **272**, 233-235.

Pollard, D., 1980: A simple parameterization for ice sheet ablation rate. *Tellus*, **32**, 384-388.

Pollard, D., 1982: A simple model yields realistic 100kyr glacial cycles. *Nature*, **296**, 334-338.

Pollard, 1983: A coupled climate model applied to the Quaternary ice ages. *J. Geophys. Res.*, **88**, 7705-7718.

Press, W. H., B. P. Flannery, S. A. Teukolsky, and W. T. Vetterling. *Numerical Recipes* (Cambridge University Press, Cambridge, England 1990).

Raymo, M. E., W. F. Ruddiman, J. Blackman, B. M. Clement, and D. G. Martinson, 1989: Late Pliocene variation in northern hemisphere ice sheets and north atlantic deep water circulation. *Paleoceanography.*, **4**, 413-446.

Reeh, N., 1900: Parameterization of melt rate and surface temperature on the Greenland ice sheet. *Polarforschung*, **59**, 113-128.

Ritz, C., 1987: Time dependent boundary conditions for calculation of temperature fields in ice sheets. In *The physical basis of ice sheet modeling.* Washington, E. D. & J.S. Walder (eds). IAHS publication No. 170.

Ritz, C., A. Fabre, and A. Letreguilly, 1996: Sensitivity of a Greenland ice sheet model to ice flow and ablation parameters: consequences for the evolution through the last climate cycle. *Climate Dyn.*, **13**, 11-24

Roe, G. H., and M. R. Allen, 1999: Competing explanations for the 100,000-yr ice age cycle. To be submitted.

Sanberg, J. A. M. and J. Oerlemans, 1983: Modeling of Pleistocene European ice sheets: the effect of upslope precipitation. *Geol. Mijnbouw*, **62**, 267-273.

Schwerdtfeger, W., 1970: The Climate of Antarctica. In *World survey of climatology, Vol. 14*, Orvig, S. (ed). Elsevier, Amsterdam, Netherlands.

Shackleton, N. J., and N. D. Opdyke, 1973: Oxygen isotope and paleomagnetic stratigraphy of equatorial Pacific core V28-238: Oxygen isotope temperature and ice volumes on a 10^5 year and 10^6 year scale. *Quart. Res.*, **3**, 39-55.

Short, D. A., J. G. Mengel, T. J. Crowley, W. T. Hyde, and G. R. North, 1990: Filtering of Milankovitch cycle by earth's geography. *Quat. Res.*, **35**, 157-173.

Simons, M., and B. Hager, 1997. Localization of the gravity field and the signature of glacial rebound. *Nature*, **390**, 500-503.

Smith, R. B., 1979: In *Advances in Geophysics, Vol. 21*, 87-230. Saltzman, B. (ed). Academic Press, New York.

Steffen, K., J. E. Box, and W. Abdalati, 1996: Greenland climate network. In Colbeck, S. C. (ed) CRREL, 96-27. Special report on glaciers, ice sheets and volcanoes, trib. to M. Meir.

Stone, P., 1978: Baroclinic adjustment. *J. Atmos. Sci.*, **35**, 561-571.

Suarez, M. J., and I. M. Held, 1979: The sensitivity of an energy balance climate model to variations in the orbital parameters. *J. Geophys. Res.*, **84**, 4825-4836.

Swanson, K., and R. T. Pierrehumbert, 1996: Lower tropospheric heat transport in the Pacific storm track. *J. Atmos. Sci.*, **54**, 1533-1543.

Tarasov, L. and W. R. Peltier, 1997: Terminating the 100kyr ice age cycle. *J. Geophys. Res.*, **102**, 21655-21693.

Trenberth, K. E., and S. Chen, 1988: Planetary waves kinematically forced by Himalayan orography. *J. Atmos. Sci.*, **45**, 2934-2948.

Valdes, P. J., and B. J. Hoskins, 1989: Linear stationary wave simulations of the time-mean climatological flow. *J. Atmos. Sci.*, **46**, 2509-2527.

Vettoretti, G., W. R. Peltier, and N. A. McFarlane, 1999: Global water balance and atmopsheric transport at the last glacial maximum: climate simulations with the CCCma atmospheric general circulation model. *To appear in Can. J. of Earth Sci.*

Weertman, 1963: Rate of growth or shrinkage of non-equilibrium ice sheets. *J. Glaciol.*, **38**, 145-158.

Weertman, J., 1976: Milankovitch solar radiation variations and ice age ice sheet sizes. *Science*, **261**, 17-20.